

IN-SITU OPTICAL MICROSCOPY, POTENTIOSTATIC
AND POTENTIODYNAMIC STUDIES OF 316L
STAINLESS STEEL AND OTHER METALS IN SULFURIC
ACID SOLUTIONS WITH NICKEL, CHLORIDE AND SULFATES

RANDAL J. POWER





Library and
Archives Canada

Bibliothèque et
Archives Canada

Published Heritage
Branch

Direction du
Patrimoine de l'édition

395 Wellington Street
Ottawa ON K1A 0N4
Canada

395, rue Wellington
Ottawa ON K1A 0N4
Canada

Your file Votre référence

ISBN: 978-0-494-33446-1

Our file Notre référence

ISBN: 978-0-494-33446-1

NOTICE:

The author has granted a non-exclusive license allowing Library and Archives Canada to reproduce, publish, archive, preserve, conserve, communicate to the public by telecommunication or on the Internet, loan, distribute and sell theses worldwide, for commercial or non-commercial purposes, in microform, paper, electronic and/or any other formats.

The author retains copyright ownership and moral rights in this thesis. Neither the thesis nor substantial extracts from it may be printed or otherwise reproduced without the author's permission.

AVIS:

L'auteur a accordé une licence non exclusive permettant à la Bibliothèque et Archives Canada de reproduire, publier, archiver, sauvegarder, conserver, transmettre au public par télécommunication ou par l'Internet, prêter, distribuer et vendre des thèses partout dans le monde, à des fins commerciales ou autres, sur support microforme, papier, électronique et/ou autres formats.

L'auteur conserve la propriété du droit d'auteur et des droits moraux qui protègent cette thèse. Ni la thèse ni des extraits substantiels de celle-ci ne doivent être imprimés ou autrement reproduits sans son autorisation.

In compliance with the Canadian Privacy Act some supporting forms may have been removed from this thesis.

Conformément à la loi canadienne sur la protection de la vie privée, quelques formulaires secondaires ont été enlevés de cette thèse.

While these forms may be included in the document page count, their removal does not represent any loss of content from the thesis.

Bien que ces formulaires aient inclus dans la pagination, il n'y aura aucun contenu manquant.


Canada

**In-Situ Optical Microscopy, Potentiostatic
and Potentiodynamic Studies of 316L
Stainless Steel and Other Metals in Sulfuric
Acid Solutions with Nickel, Chloride and
Sulfates**

By

© Randal J. Power

B.Eng., Memorial University of Newfoundland, 2005

Supervised by

Dr. John Shirokoff

Dr. John Molgaard

**A thesis submitted to the School of Graduate Studies in partial fulfillment of the
requirements for the degree of
Masters of Engineering**

Faculty of Engineering and Applied Science, Memorial University of Newfoundland

April 30, 2007

ABSTRACT

The corrosion patterns of 316L stainless steel is examined using a custom developed corrosion test cell which allows for in-situ analysis of a sample surface using a conventional microscope and off the shelf digital photography equipment.

Laboratory prepared solutions of 3.5% NaCl, 3.39M sulfuric acid with 0.25M nickel sulfate and a variety of 1M sulfuric acid, nickel sulfate and nickel chloride based solutions were tested under aerated and deaerated conditions. The results illustrate the wide variety of corrosion behaviors possible for 316L stainless steel under potentiostatic and potentiodynamic test conditions. Analysis of these samples provides both a detailed visual account of the corrosion process in addition to standard electrochemical analysis regarding pitting potentials, corrosion potential, corrosion rate, etc.

Polarization data and analysis regarding the corrosion patterns observed is presented including in-situ images of grain boundary etching, surface layer changes and pitting. Detailed images and analysis of chromium carbide and sulfide inclusion behaviors in sulfuric acid were performed showing the tendency of sulfide inclusions to dissolve and act as nucleation sites for pits.

Experimental hydrometallurgical process fluids were also tested, confirming the ability of in-situ optical microscopy to successfully image and providing valuable insights into the corrosion processes taking place.

Titanium, aluminum, magnesium and electronic materials were tested in predominantly 3.5% NaCl solution to confirm the feasibility of imaging different metals undergoing corrosion.

Key Words: in-situ optical microscopy, pitting potential, corrosion potential, pit, sulfuric acid, nickel chloride, nickel sulfate, NaCl, saltwater, oxygen, argon, potentiodynamic, potentiostatic, austenitic stainless steel, 316L, sulfide inclusion, carbide inclusion.

ACKNOWLEDGEMENTS

A great deal of appreciation and thanks is extended to Dr. John Shirokoff and Dr. John Molgaard for their instruction and guidance throughout my graduate studies. A note of thanks is also extended to Mr. Paul Bishop for his assistance with machining various components and Mr. Michael Shaffer for his assistance with the scanning electron microscope testing.

I would also like to extend thanks to those people who have helped and guided me throughout the years of my education, particularly my grandmother Philomena Chafe, my mother Carolyn Green and my aunt Joanne Chafe. Great things are rarely achieved without the contributions of many.

The authors would like to thank the Atlantic Canada Opportunities Agency (ACOA), Memorial University of Newfoundland (MUN), and Inco Ltd. For financial support given to the Inco Innovation Centre (IIC) project. Also, the financial support of the Natural Sciences and Engineering Research Council of Canada (NSERC) is gratefully acknowledged.

TABLE OF CONTENTS

ABSTRACT.....	ii
ACKNOWLEDGEMENTS.....	iv
LIST OF TABLES.....	xi
LIST OF FIGURES.....	xii
LIST OF EQUATIONS.....	xvii
NOMENCLATURE.....	xviii
1 INTRODUCTION.....	1
2 OBJECTIVES.....	3
3 LITERATURE REVIEW.....	4
3.1 General Theory of Corrosion.....	4
3.1.1 Open Circuit or Corrosion Potential.....	8
3.1.2 Natural Exposure Tests vs. Accelerated Tests.....	12
3.1.3 General Structure of Polarization Plots for Passivating Metals.....	14
3.1.3.1 Active Region.....	14
3.1.3.2 Passive Region.....	15
3.1.3.3 Transpassive Region.....	15
3.1.3.4 Secondary Passivity.....	16
3.1.4 Passivation Principles.....	16
3.1.5 Pitting Principles.....	18
3.1.5.1 Pitting Potential Principles.....	19
3.1.6 Stages of Pitting.....	22
3.1.6.1 Pit Nucleation.....	22
3.1.6.2 Pitting Initiation Theories.....	24
3.1.6.3 Pit Propagation.....	25
3.1.6.4 Metastable Pitting.....	27
3.1.6.5 Stable Pitting.....	27
3.1.6.6 Pit Repassivation.....	28
3.1.6.7 Transpassive Pitting Characteristics.....	28
3.1.7 Factors Effecting Pitting.....	30
3.1.7.1 Metallurgical.....	30
3.1.7.1.1 Metal Type.....	30
3.1.7.1.2 Precipitates and Metallic Inclusions.....	31
3.1.7.1.3 Surface Condition.....	32
3.1.7.1.4 Heat Treatment.....	33
3.1.7.2 Electrochemical Reactions.....	34
3.1.7.3 Composition of Solution.....	34
3.1.7.4 Mass Transport.....	37
3.1.7.5 Temperature.....	37
3.1.7.6 Pit Electrolyte Composition.....	38
3.1.8 Methods of Electrochemical Testing and Chemical Effects that Influence their Results.....	39

3.1.8.1	Potentiokinetic Testing	39
3.1.8.2	Potentiostatic Testing.....	40
3.1.8.3	Pitting Potential Interpretation and Limitations on Test Results	42
3.1.8.4	Cyclic Polarization.....	43
3.1.8.5	Tests Based on Stochastic Theory of Pitting	44
3.1.8.6	Chemical Reactions	44
3.1.8.7	Explanation of Eh-pH Diagrams.....	45
3.1.8.8	Liquid Junction Potential (LJP)	47
3.1.8.9	Electrode/Electrolyte Interface	48
3.1.8.9.1	Limiting Current	48
3.1.8.9.2	Flow rate	48
3.1.9	Crevice Corrosion	50
3.1.10	Sample Mass Loss Due to Corrosion.....	51
3.2	Solution Chemistry and Effects	53
3.2.1	Volume Effects on Solution Composition	53
3.2.2	Sulfuric Acid Solution	54
3.2.2.1	Specified Acid Solution Composition for Baseline Analyses	54
3.2.2.2	Acid Concentration Effects.....	54
3.2.2.3	Chloride Concentration Effects.....	56
3.2.2.4	Sulfate Concentration Effects	56
3.2.2.5	Iron, Nickel and Other Ion Effects.....	57
3.2.2.6	Aeration.....	58
3.2.3	Seawater Solution	59
3.2.3.1	Specified Salt Solution Composition	59
3.2.3.2	Chloride Concentration Effects.....	59
3.2.3.3	Aeration.....	60
3.2.4	Surface Analysis Equipment.....	61
3.2.4.1	Scanning Electron Microscope (SEM)	61
3.2.4.2	Energy Dispersive Spectroscopy (EDS)	61
3.2.4.3	Optical Microscopy.....	62
3.2.4.4	Metallograph	64
3.2.5	Surface Analysis Techniques	65
3.2.5.1	Analysis Methods Regarding Pit Morphology	65
3.2.5.2	Low Magnification Surface Analysis	67
3.3	Sample Material Properties.....	68
3.3.1	Stainless Steel Specific Information	68
3.3.1.1	Effect of Different Alloying Elements.....	70
3.3.1.2	Eh-pH Diagrams for Sulfuric Acid and Salt Solution	72
3.3.1.3	Surface Feature and Inclusion Types, Shapes, and Effects	76
3.3.1.3.1	Chromium and Iron Carbides.....	77
3.3.1.3.2	Sulfide Inclusions.....	78
3.3.1.3.3	Smaller Nucleation Sites.....	79
3.3.1.3.4	Mechanical Defects.....	80
3.3.1.4	Common Pit Structures	80

3.3.2	Titanium Specific Information.....	83
3.3.2.1	Eh-pH Diagrams for Sulfuric Acid and Salt Solution	84
3.3.2.2	Oxide Types	85
3.3.3	Aluminum Specific Information	86
3.3.3.1	Oxide Types	86
3.3.4	Visual Analysis Techniques and Applications	87
3.3.4.1	Raman Spectroscopy and Microscopy	87
3.3.4.2	SPM and AFM Systems	87
3.3.4.3	Electrochemical Droplet cells	88
3.3.4.4	XANES	89
3.3.4.5	Contrast Enhanced Microscopy and Elliptical Microscopy for Surface Imaging (EMSI)	89
3.3.5	Areas of Technical Interest in the Scientific Community.....	91
4	Experimentation Materials and Equipment	94
4.1	Experimental Metals	94
4.1.1	Stainless Steel	94
4.1.2	Titanium.....	94
4.1.3	Aluminum	94
4.1.4	Magnesium.....	95
4.2	Experimental Solutions.....	96
4.2.1	Sulfuric Acid Based Solutions	96
4.2.1.1	Aeration.....	96
4.2.1.2	Base Solution	96
4.2.1.3	Various Mixes of Solution	96
4.2.2	Artificial Seawater Salt Solution	98
4.2.2.1	Aeration.....	98
4.2.2.2	Solution Composition	98
4.3	Experimental Equipment	99
4.3.1	Test Cell (refer to other section)	99
4.3.2	Image and Video Capture Equipment.....	99
4.3.3	Potentiostat.....	99
4.3.4	Reference Electrode	99
4.3.5	pH Meter	100
4.3.6	Mechanical Polisher.....	100
4.3.7	Constant Temperature Bath	100
4.3.8	SEM/EDS.....	100
4.3.9	Software	100
4.4	Surface Preparation Techniques and System Maintenance Procedures	101
4.4.1	Basis of Sample Preparation Procedures	101
4.4.1.1	Roughness	101
4.4.1.2	Engrained Stresses (Tensile and Compressive Effects, refer to sections 3.3.1.3.4 and 4.1)	101
4.4.1.3	Heat Treatment.....	102
4.4.2	Metal Sample Preparation Procedures	103

4.4.3	Experimental Procedures for Potentiodynamic and Potentiostatic Tests	104
4.4.4	Test Equipment Cleaning Procedure	105
4.4.5	Test Cell Cleaning Procedure	106
4.5	Design of Corrosion Cell and Support Equipment	108
4.5.1	Background Information	108
4.5.2	Apparatus Design	110
4.5.2.1	Maintenance Considerations	110
4.5.2.2	Geometry Considerations	113
4.5.2.3	Solution Flow Considerations	115
4.5.3	Testing and Analysis of the Corrosion Cell	117
4.5.3.1	Considerations for Testing Conditions	117
4.5.3.1.1	Distribution of the Flow across the Surface	117
4.5.3.1.2	Results across a Series of Identical Tests	118
4.5.3.1.3	Effect of Flow Rate	119
4.5.3.2	Comparison of Test Results from the Cell to Other Research Data ...	120
4.5.3.2.1	Experimental Results	120
4.5.3.3	Conclusions	122
5	RESULTS AND DISCUSSION	123
5.1	Test and Observation Information	123
5.2	SA Series Results: Potentiostatic and Potentiodynamic Analysis of 316L Stainless Steel in 1M H ₂ SO ₄	124
5.2.1	Solution and Test Properties	124
5.2.2	Changes Recorded During Initial Immersion	125
5.2.3	Polarization Data	127
5.2.3.1	Potentiodynamic Test Results	127
5.2.3.2	Potentiostatic Test Results	131
5.2.3.2.1	Aerated Tests	131
5.2.3.2.2	Deaerated Tests	133
5.2.4	Progressive Development of Etching, Pitting and Other Features during Polarization	135
5.2.5	Development of Grain Boundary Etching in 1M H ₂ SO ₄ under Potentiostatic Polarization	138
5.2.5.1	Aerated Test Results	138
5.2.5.2	Deaerated Test Results	139
5.2.6	Development of Pitting in 1M H ₂ SO ₄ under Potentiostatic Polarization	140
5.2.7	Etching and Color Change of Grains at High Anodic Potentials	140
5.2.8	Color Change on Sample's Surface due to Potentiostatic Polarization ..	142
5.2.8.1	Theoretical Explanation for this Behavior	143
5.2.9	Peeling of Thin Surface Layer	144
5.2.10	Conclusions	145
5.3	SB Series Results: Potentiostatic and Potentiodynamic Analysis of 316L Stainless Steel in Various Sulfuric Acid Based Solutions	146
5.3.1	Solution and Test Properties	146
5.3.2	Changes Recorded During Initial Immersion	148

5.3.3	Polarization Data.....	149
5.3.3.1	Potentiodynamic Test Results.....	150
5.3.3.1.1	Scan Results.....	150
5.3.3.1.2	Potentiodynamic Polarization Analysis Results	151
5.3.3.2	Potentiostatic Test Results	154
5.3.4	Observed Corrosion Behaviors.....	156
5.3.4.1	Color Change during Polarization	157
5.3.4.2	Light Spots on Metal Surface	158
5.3.4.3	Peeling of Surface Layer.....	158
5.3.4.4	Localized Detachment of Surface Layer.....	160
5.3.5	Pitting Behavior under Potentiodynamic and Potentiostatic Conditions	161
5.3.6	Pitting Behavior of 316L in Solution 4 Polarized Potentiostatically	163
5.3.6.1	Pitting Behavior Results	167
5.3.6.2	Theoretical Explanation for Observed Pitting Distribution	170
5.4	SC Series Results: Potentiodynamic Analysis of 316L Stainless Steel in Experimental Hydrometallurgy Process Fluids (EHPF).....	171
5.4.1	Solution and Test Properties	171
5.4.2	Polarization Data.....	172
5.4.3	Borderline Passivity	176
5.4.4	Color Change and Peeling of Oxide Layer during Polarization	177
5.4.5	Changes in Surface Features.....	180
5.4.6	Benefits and Limitations of the In-Situ Optical Microscopy System When Using Experimental Hydrometallurgy Process Fluids.....	182
5.5	Miscellaneous Metals Results: Behavior of Industrial Metals in 3.5% NaCl Solution.....	183
5.5.1	316L Stainless Steel in 3.5% NaCl Solution	184
5.5.1.1	Potentiodynamic Test Results.....	184
5.5.1.2	Aerated Test Results	186
5.5.1.2.1	Theoretical Explanation for Pitting Behavior.....	188
5.5.1.3	Deaerated Test Results.....	188
5.5.1.3.1	Theoretical Explanation for Pitting Behavior.....	190
5.5.1.4	Conclusions.....	191
5.5.2	Testing Magnesium in Salt Solution.....	192
5.5.2.1	Test Results.....	192
5.5.2.2	Discussion	194
5.5.2.3	Conclusions.....	194
5.5.3	Testing of 6061 Aluminum in 3.5% NaCl Solution	195
5.5.3.1	Test Results.....	195
5.5.3.2	Conclusions.....	196
5.5.4	Testing of Cu/Sn Based Electronic Trace Material in 3.5% NaCl Solution 197	
5.5.4.1	Test Results.....	197
5.5.4.2	Conclusions.....	198
5.5.5	Titanium.....	199

5.5.5.1	Salt Water Tests	199
5.5.5.2	Titanium in Sulfuric Acid Results	202
5.6	Overall Analysis of Corrosion Results	204
5.6.1	Introduction.....	204
5.6.2	Corrosion Potential for All Sulfuric Acid Solutions.....	204
5.6.3	Corrosion Rates for All Sulfuric Acid Solutions	206
5.6.3.1	Corrosion Rate Test Results.....	206
5.6.3.2	Conclusions.....	207
5.6.4	Pitting Potentials for All Sulfuric Acid Solutions	209
5.6.4.1	Pitting Potentials	209
5.6.4.2	Conclusions.....	211
5.6.4.2.1	Theoretical Explanation for Aerated vs. Deaerated Test Results .	211
5.6.4.2.2	Theoretical Explanation for Etching Behavior of SA Series Samples Polarized at 0.9 V, Aerated	212
5.6.5	Anodic Knee	213
5.6.5.1	Aerated Solutions.....	213
5.6.5.2	Deaerated Solutions	214
5.7	SEM and EDS Analysis of Corroded Samples	216
5.7.1	Chromium Carbide Inclusions	216
5.7.2	Sulfide Inclusions.....	219
5.7.2.1	CuS Inclusions	219
5.7.2.2	MnS Inclusions	220
5.7.3	Surface Oxide Composition.....	222
6	CONCLUSIONS.....	224
7	FUTURE APPLICATIONS.....	229
8	REFERENCES	231
Appendix A	235
Appendix B	239
Appendix C	240
Appendix D	243

LIST OF TABLES

Table 1: Chemical composition of 316L stainless steel (excluding iron) used in testing (43).....	69
Table 2: Enthalpy values associated with sulfide inclusions (1, 47)	78
Table 3: Solution compositions and pH for SA and SB series tests	96
Table 4: SA series solution composition and pH.....	125
Table 5: SA series potentiodynamic polarization results.....	128
Table 6: SB series solution composition and pH.....	146
Table 7: SB series potentiodynamic polarization results.....	153
Table 8: SC series solution measured pH	172
Table 9: Corrosion test data SC series	174
Table 10: Mixed corrosion potential (E_{corr}) for all potentiodynamic tests.....	204
Table 11: Corrosion rate for all potentiodynamic sulfuric acid tests.....	206
Table 12: Pitting potentials for all potentiodynamic sulfuric acid tests.....	210

LIST OF FIGURES

Figure 1: Potentiodynamic polarization curves for three deaerated solutions (1)	7
Figure 2: Extraction of i_{corr} and E_{corr} from polarization curves (5) G3 p42.....	11
Figure 3: Typical regions found on polarization curves (5) G3 p42.....	14
Figure 4: Energy spike due to metastable pitting recorded in a potentiostatic test.....	21
Figure 5: Spikes in current with and without chlorides (18) p27	23
Figure 6: Intergranular attack of 304 stainless steel (25) p321.....	32
Figure 7: Plot of corrosion rate vs testing period and volume/area ratio for nitric acid (32)	36
Figure 8: Effects of flow rate on corrosion rate and potential p93 of (4)	37
Figure 9: Potentiostatic polarization above and below pitting potential (9) p5.....	41
Figure 10: Changes to potentiodynamic polarization curves with increased temperature or pH. (4) p120.....	55
Figure 11: Standard pitting charts by ASTM standards G46-94 (5).....	66
Figure 12: Variations in cross-sectional shape of pits G46-94 (5)	66
Figure 13: EDS scan results for 316 stainless steel test samples (1)	70
Figure 14: Eh-pH or Pourbaix Diagrams of Fe, Ni and Cr for pure 1M H_2SO_4 solution (44).....	73
Figure 15: Eh-pH or Pourbaix diagrams of Fe, Ni and Cr in 1M H1M H_2SO_4 solution containing Nickel Sulfate and Nickel Chloride (44).....	74
Figure 16: Eh-pH or Pourbaix diagrams of Fe, Ni and Cr in 0.6M NaCl (44).....	75
Figure 17: Image on 1 μm polished 316L metal surface showing inclusions including $M_{23}C_6$ (larger angular inclusions) and sulfide inclusions (small rounded inclusions), the image on the left is to the same 0.5 mm tall scale as the in-situ images and was acquired using an SEM.....	77
Figure 18: Types of MnS inclusions and their pitting behavior (49).....	79
Figure 19: Pits seen forming on surface of 304 stainless steel (16).....	81
Figure 20: Schematic of lacy metal cover formation (16).....	82
Figure 21: Eh-pH diagram, $Ti-SO_4^- - H_2O$, 25°C (36).....	84
Figure 22: Eh-pH diagram, $Ti-Cl^- - H_2O$, 25°C (54)	85
Figure 23: Raman spectroscopy illustration (60).....	87
Figure 24: Illustration of a scanning probe microscope (63).....	88
Figure 25: Image of a droplet cell (64).....	89
Figure 26: Contrast enhanced microscopy and EMSI apparatus (48)	90
Figure 27: Corrosion test apparatus.....	105
Figure 28: Corrosion test cell.....	106
Figure 29: Internal schematic of corrosion test cell (right) showing the reference electrode (yellow), image of corrosion test cell (middle), image of corrosion test cell mounted to movable platform with vernier scale (68).....	111
Figure 30: Schematic of XANES in-situ cell (65).....	111

Figure 31: Figures of Raman spectroscopy cell (left) (59) and IR reactor cell (right) (69)	112
Figure 32: Cross sectional view of corrosion cell including reference electrode (68) ...	114
Figure 33: Sketch of the design principles of the flushed port cell (5).....	114
Figure 34: Cross section of corrosion cell showing acid flow path and sample mounting apparatus (68).....	116
Figure 35: Results of three potentiodynamic tests, one taken with fresh acid, two others done with the same reused acid from 2 weeks later after 8 tests.	119
Figure 36: SA3 (aerated) sample surface after 60 minutes of immersion without polarization, left image is at start, right image is after 60 minutes.	126
Figure 37: SA6 (aerated) development of a dark uneven oxide layer after 60 minutes of immersion before polarization, left image is at start, right image is after 60 minutes....	126
Figure 38: SA14 (deaerated) darkening scratches seen developing after 60 minutes of immersion before polarization, left image is at start, right image is after 60 minutes....	127
Figure 39: Aerated (green) and deaerated (blue) polarization test scans.....	130
Figure 40: Results of aerated SA series potentiostatic tests.	132
Figure 41: Image of mild etching resulting from SA11 potentiostatic polarization at 0.9 V (left is original 0.5 mm tall image, right image is magnified to show mild etching, height of right image is approximately 0.1mm).....	133
Figure 42: Results of deaerated SA series potentiostatic tests.....	134
Figure 43: Aerated test samples after polarization. a) potentiodynamic, b) potentiostatic 0.9 V, c) potentiostatic 0.925 V, d) potentiostatic 0.95 V, e) potentiostatic 0.975 V, f) potentiostatic 1.0 V, g) potentiostatic 1.25 V.	136
Figure 44: Deaerated test samples after polarization. a) potentiodynamic, b) potentiostatic 0.975 V, c) potentiostatic 1.0 V, d) potentiostatic 1.025 V, e) potentiostatic 1.05 V, f) potentiostatic 1.075 V, g) potentiostatic 1.1 V, h) potentiostatic 1.25.	137
Figure 45: Pitting and etching in aerated (left) and deaerated (right) 1M H ₂ SO ₄ at 1.25V potentiostatic (images have a height of ~0.2mm).	138
Figure 46: Surface of SA12 (deaerated) before (left) and after (right) reaching secondary passivation (note presence of contrast darkened etch pits, grain boundaries, and sub-boundaries which appear as twins, twin boundaries and dislocation slip traces).	141
Figure 47: Aerated potentiostatic test at 1.25 volts, left is before polarization, right is immediately after polarization.	142
Figure 48: Deaerated potentiostatic test at 1.025 volts, right is immediately after polarization.	142
Figure 49: Image of surface layer peeling in SA6, (0.5mm tall image on left, 4X magnified crop right).	145
Figure 50: SB12 (aerated) initial immersion creating dark gray oxide layer, start of immersion (left), end of immersion just before polarization (right).	149
Figure 51: Aerated SB series potentiodynamic scans with SA3 for comparison	150
Figure 52: Deaerated SB series potentiodynamic scans with SA12 for comparison.....	151
Figure 53: SB series corrosion potential graph.....	153
Figure 54: SB series estimated corrosion rate graph	153
Figure 55: SB series pitting potential graph	154

Figure 56: Aerated potentiostatic scans SB series at 1.13 V	155
Figure 57: Deaerated potentiostatic scans SB series at 1.13 V.....	155
Figure 58: Surface color changes upon polarization SB10 (top two images with left being before and right being after polarization), SB14 (bottom two images with left being before and right being after polarization).	157
Figure 59: Image showing light color spots forming in surface layer of Test SB9 (deaerated with 0.1M Cl ⁻), (left image is 0.5mm tall, right image is cropped to upper left corner at 4X greater magnification).....	158
Figure 60: Peeling surface layers seen in SA6 (top left), SB8 (top right), SB9 (bottom left) , SB13 (bottom right).	159
Figure 61: Localized peeling of surface layer leading to large scale peeling after polarization (progression of images over 60 minutes top left to bottom right).	160
Figure 62: Images of pit growth for SB13 (potentiodynamic) top left, SB14 (potentiostatic) top right, SB15 (potentiodynamic) bottom left, SB16 (potentiostatic) bottom right.....	162
Figure 63: Potentiostatic test results SB14 deaerated.....	164
Figure 64: Original surface (top left), first stage of pitting (top right), second stage (middle left), third stage (middle right), final surface (bottom left), resulting surface of the 7mm wide exposed sample area (bottom right).	165
Figure 65: Imperfection in material's surface prior to polarization (left), pit forming at this site after polarized (middle), overlay of pit perimeter (red) with blue circle around pre-existing surface flaw. All images are at the same magnification.	166
Figure 66: SEM image of a rounded surface feature on sample SB15 after testing, also many noticeable square structures are present on the surface.	169
Figure 67: Polarization curves for SC series solutions (SC1, SC3, SC5 are deaerated).	172
Figure 68: SC series corrosion potential graph.....	174
Figure 69: SC series estimated corrosion rate graph	174
Figure 70: SC series pitting potential graph	175
Figure 71: corrosion potential before polarization SC1.....	176
Figure 72: Corrosion potential after polarization SC1.....	177
Figure 73: SC1 peeling event sequence of photographs, 1 minute time lapse between photographs, each image height represents 0.5mm.	178
Figure 74: SC2 peeling event selection of photographs, images chosen from various times in the sequence, each image height represents 0.5mm.	179
Figure 75: Images of SC1 (top left), SC2 (top right), SC3 (mid left), SC4 (mid right), SC5 (bottom left) surfaces after testing (taken after removed from fluid)	181
Figure 76: Overlay of saltwater aerated (black) and deaerated (red) tests with SA3 aerated (green) and SA12 deaerated (blue) 1M H ₂ SO ₄ results.....	185
Figure 77: Progression of pitting for 316L stainless steel in 3.5% NaCl aerated (images 1-5, first image at top left, final image bottom left), scanned image of sample after testing was completed (bottom right)	187
Figure 78: Progression of pitting for 316L stainless steel in 3.5% NaCl deaerated (first image at top left, final image bottom left)	189
Figure 79: Magnesium potentiostatically tested in saturated table salt solution.	193

Figure 80: Pitting in aluminum as observed in test A2.....	195
Figure 81: Pitting in aluminum as observed in test A4 (first image at top left, final image bottom left).....	196
Figure 82: Photograph of signal trace metal Cu/Sn ~ 80/20 (by weight), left is circuit before solder, middle is a trace before test began, right is the same trace during testing.	197
Figure 83: Potentiodynamic polarization scan results of a titanium welding rod in saltwater	201
Figure 84: Image of the tip of a titanium rod being tested in saltwater solution at start (left) and at the end (right)	201
Figure 85: Potentiodynamic polarization data from test TiA1 (titanium in solution 4 deaerated)	202
Figure 86: Images of titanium surface before (left) and after (right) polarization in test TiA1 (titanium in solution 4 deaerated)	203
Figure 87: Corrosion potential (aerated in green, and deaerated in blue).....	205
Figure 88: Corrosion rate in mpy (aerated in green, and deaerated in blue)	207
Figure 89: Pitting potentials (V) (aerated in green, and deaerated in blue).....	210
Figure 90: Polarization curves for aerated SA and SB series solutions.....	214
Figure 91: Polarization curves for deaerated SA and SB series solutions.....	215
Figure 92: Polarization curves for SC series solutions (SC1, SC3, SC5 are deaerated).	215
Figure 93: Image of surface of sample in Test SB7 before polarization, note the presence of a few larger dark spots on the surface	217
Figure 94: SEM images of the surface of SB7, left image is at same 0.5 mm scale as previous figure, right image is a higher magnification at center of previous image showing a small inclusion inside a pit	217
Figure 95: EDS test results of the inclusion within the pit, note the high Cr content and slightly elevated carbon content.....	218
Figure 96: Images of a CuS inclusion in the surface of SC4, top left is at 0.5 mm tall, top right is at 0.02 mm tall.	219
Figure 97: EDS results for a CuS inclusion in sample SC4, see peaks for Cu and S	219
Figure 98: SEM images of sample SB3, left image is 0.5 mm tall, right image is 0.07 mm tall showing a small MnS inclusion	221
Figure 99: EDS scan results showing composition of the pit seen in previous figure as Mn, Al and S with very low Fe levels	221
Figure 100: Images of sample SC4, left image taken with a scanner is approximately 21 mm tall and shows a brown oxide layer, and the right image taken with SEM is 0.5 mm tall and shows the border between a brown section and a cleaner metal section	223
Figure 101: EDS Scan of dark brown oxide layer (green area) compared to metal composition (blue line)	223
Figure 102: Sample surface observed using SEM imaging (0.5 mm tall image)	235
Figure 103: SEM image at higher magnification at center of previous figure. Image of Cr ₂₃ C ₆ inclusion (large angular inclusion) and MnS inclusions (small inclusions) refer to EDS scans below for composition (image is 0.08136 mm wide).....	235
Figure 104: EDS Scan of 316L base metal composition	236

Figure 105: EDS Image of larger angular inclusions with high Cr content and slightly elevated carbon content presumed to be Cr_{23}C_6	236
Figure 106: MnS inclusion (small round inclusions).....	237
Figure 107: SEM image of silica rich elongated inclusion (near bottom edge of image) (image is 0.08553 mm wide)	238
Figure 108: Silica rich elongated inclusion	238
Figure 109: Potentiodynamic scans and Tafel plot with corrosion rates for all SA, SB, SC tests	248

LIST OF EQUATIONS

Equation 1	4
Equation 2	5
Equation 3	6
Equation 4	9
Equation 5	9
Equation 6	10
Equation 7	10
Equation 8	10
Equation 9	39
Equation 10	40
Equation 11	45
Equation 12	46
Equation 13	50
Equation 14	50
Equation 15	54
Equation 16	57
Equation 17	57
Equation 18	62
Equation 19	62
Equation 20	69

NOMENCLATURE

$e^{Fe^{3+}/Fe^{2+}}$ - Standard reduction potential for Fe^{3+}

e^{H^+/H_2} - Standard reduction potential for hydrogen

ρ - Density

β - Tafel Slope

a – Atomic weight

A – Surface area

ads – Adsorption

Al₂O₃ – Aluminum oxide or alumina

AlS – Aluminum sulfide

C - Conversion constant

CCS -Critical crevice solution

Cl⁻ - Chloride ion

com – Complex

CPT -critical pitting temperature

Cr - Chrome

Cr₂₃C₆ – Chromium carbide

Cr₂O₃ – Chromium Oxide

CrO₃ -Dichromate

CrS – Chromium sulfide

Cu²⁺ - Cupric

d - Definite limit on resolving power

E – Driving Potential

e⁻ - Electron

E_{corr} –Corrosion potential or mixed potential

E_{cp} – Critical protection potential or repassivation potential

EDS – Energy Dispersive x-ray Spectroscopy

E_h – Voltage Potential as Calculated by the Nernst Equation

EHPF - Experimental hydrometallurgy process fluid

EMSI - Elliptical microscopy for surface imaging

E_{pit} –Pitting Potential

E_{pp} -primary passive potential

EW – Equivalent weight

F – Faraday constant = 96,500 coulombs/equivalent

Fe²⁺ - Ferrous ion

Fe₂₃C₆ – Iron Carbide

Fe₂₃C₆ – Iron carbide

Fe₂O₃ - Ferric oxide (hematite)

Fe³⁺ - Ferric ion

Fe₃O₄ – Ferrous ferric oxide (magnetite)

FeO – Ferrous oxide (wustite)

FeS – Iron Sulfide

G – Gibbs Energy

H – Enthalpy

H⁺ - Hydrogen ions

H₂O - Water molecule

HCl – Hydrochloric acid

HF – Hydrofluoric Acid

Hg – Mercury

H₂SO₄ – Sulfuric Acid

I – Total current

i_{corr} -Open circuit current density

IGC - Intergranular corrosion

LJP – Liquid junction potential

M - Metal

M – Molar Mass

Mag - Magnification

mmpy – millimeters per year

Mn – Manganese

MnS – Manganese sulfide

Mo - Molybdenum

Mo₂₃C₆ – Molybdenum carbide

mpy – thousandths of an inch per year

N – Normal

n – Number of moles of electrons per mole of metal involved in the reaction

N.A. -the listed numerical aperture

NaCl – Sodium chloride (salt)

Ni - Nickel

Ni²⁺ - Nickel ion

NiS – Nickel Sulfide

NiS – Nickel sulfide

pas – Passive

pH – Measure of solution acidity

rds – Rate determining step

Rp – Polarization resistance

S – Entropy

SA – First test series using 1M sulfuric acid

SB – Second test series using a variety of solutions

SC – Third test series using EHPF

SCC -stress corrosion cracking

SCE –standard calomel electrode

SEM – Scanning Electron Microscope

SHE – standard hydrogen electrode

SHE – Standard Hydrogen Electrode

SO₄²⁻ - Sulfate ion

SPM -scanning probe microscopes

S.S. – Stainless steel

T – Temperature

t – Time

Ti – Titanium

TiO₂ – Titanium oxide

TiS - Titanium Sulfide

TJP – Thermal junction potential

V - Volt

w.l. - Wavelength of the light used

XANES – X-ray absorption near edge structure

α – Proportional to

ΔG = Change in Gibbs free energy

ΔH = Enthalpy or “heat of formation”

ΔS = Δ Entropy “disorder”

v -Potentiodynamic scan rate

τ – Incubation time

1 INTRODUCTION

The Faculty of Engineering and Applied Science at Memorial University of Newfoundland in collaboration with Inco Limited (Voisey's Bay Nickel Mining Co.) is conducting an ongoing research project into the corrosive properties of metals used in the Voisey's Bay hydrometallurgy process. These metals include stainless steel, and various grades of Titanium for use in autoclave lining and other process components. This testing was combined with Potentiodynamic and Potentiostatic tests that can be used to rank metals on the basis of pitting potential and the standard post testing microscopic examinations.

The properties of metals are of interest to engineers and scientists as metals are the fundamental building block of today's technological society. The corrosion properties of metals are of particular interest as almost all metals will at some point in their service be exposed to a potentially corrosive environment. Typical reasons for testing a material are to determine whether or not it will perform satisfactorily in a given environment and to compare its performance with other materials. Ranging from severe environments such as the hydrometallurgical process proposed by Inco to the more common place saltwater exposure metals must be chosen to meet both strength and longevity requirements.

The document describes an exploration of an optical technique extending the capabilities of the commonly employed electrochemical corrosion testing techniques. Through the

use of the electrochemical test cell designed by the author it is possible to achieve the real time visual examination of metal surfaces during polarization testing.

A variety of metals were examined using these modified electrochemical techniques.

These metals were tested in solutions related to two areas of interest, the hydrometallurgical process employed by Inco, and simulated seawater.

The hydrometallurgy process is modeled using a base line 1 molar sulfuric acid solution which is further modified by varying acid, chloride, nickel, and sulfate ion concentration. Additionally, aerated and deaerated acids were tested to observe their effects on pitting. A simulated saltwater was used in tests, which consisted of a 3.5% reagent grade salt in deionized water solution.

The testing of a variety of different metals was used as a demonstration to show the effect of varying types of oxide layers, pitting, and luster on the images taken of these surfaces. Various solutions were used to observe the changes in the visual and electrochemical measurements associated with pitting. Through this research patterns were demonstrated and explored with the goal of this research being to integrate conventional polarization testing techniques with in-situ optical microscopy and identify the benefits and limitations of the testing technology and the possible areas for further research based around the visual examinations.

2 OBJECTIVES

The primary objective for this research is the measurement of corrosion activity using both the standard polarization techniques and the modified capabilities of the corrosion cell allowing for in-situ image and video recording. The combination of computer recorded data along with the visual record allowed for a more complete understanding of the behavior of these metals during polarization testing.

As a secondary objective a series of different metals were tested for their compatibility with the visual components of the new electrochemical cell. A saltwater solution was also employed on some samples to allow for safe preliminary trials of the system before using sulfuric acid and as a means of comparison between the pitting behavior of 316L stainless steel in sulfuric acid solutions and saltwater solution.

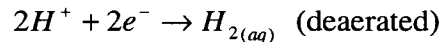
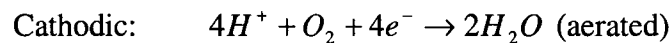
3 LITERATURE REVIEW

3.1 General Theory of Corrosion

Corrosion is an electrochemical process that is generally characterized as being degrading to a metallic substance. Different forms of corrosion are considered more or less harmful based on a variety of different criteria typically focused on the resulting loss of mechanical strength and the rate of this progression. Some corrosion byproducts such as oxide layers are considered beneficial, sometimes even enhancing a metal's mechanical properties such as in the case of aluminum which develops an alumina (Al_2O_3) oxide layer that gives the relatively soft metal a hard protective coating.

At anodic sites the metal experiences corrosion which produces electrons that flow to cathodic sites where they typically produce one of two reduction reactions depending on whether the solution is aerated or deaerated. On a chemical level the most basic reactions are:

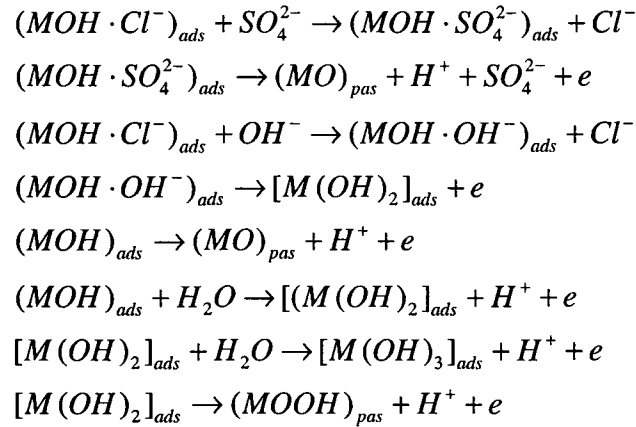
Equation 1



The cathodic oxygen reduction reaction is favored when dissolved oxygen is present in the solution, with the hydrogen reaction occurring when the solution has low levels of oxygen.

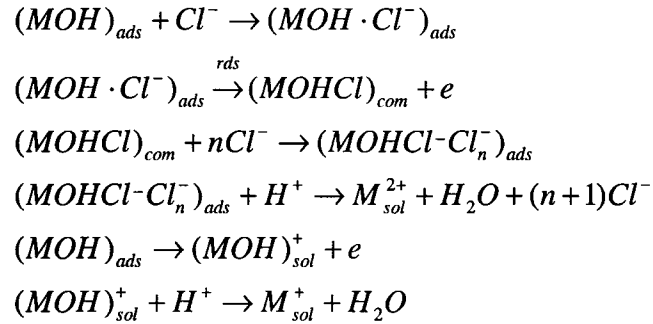
Many of the metals used in corrosive environments produce an oxide layer which acts as a diffusion barrier to reduce further corrosion; these are called active-passive metals. For austenitic stainless steels the full set of chemical reactions occurring on the metal's surface are detailed in Equation 11, however the relevant equations for the formation of oxide layer are the passivation reactions (1, 2):

Equation 2



Other reactions occur which damage the oxide layer and typically become more common only under unfavorable combinations of chemical and polarization exposures. These are called depassivation reactions (1, 2):

Equation 3



The subscript letters used in the equations mean ads (adsorption), pas (passive), com (complex), sol (solution) and rds (rate determining step).

When a metal is initially exposed to a solution without having first formed an oxide layer, it will experience a brief period of active dissolution, and under typical circumstances will form an oxide layer shortly thereafter (3). While the oxide layer is intact these metals experience a slow rate of metallic dissolution. Ideally a series of moving anodic and cathodic sites on the metal surface tend to distribute the corrosion rate evenly across the surface, however under real life circumstances this ideal behavior is rarely perfectly achieved. A variety of metallic inconsistencies across the surface may lead to preferential corrosion in a particular area. Sites with varying surface stresses, metallic and nonmetallic inclusions, precipitates, or inconsistent surface features may be preferentially corroded. Under some situational circumstances these sites may become nucleation points for pitting.

During some tests using more aggressive solutions the depassivation reactions may occur at a sufficient rate so as to create an unstable oxide layer on the metal surface leading to a

reduction in the effectiveness of this protective layer resulting in greater current density and corrosion rate during polarization testing. This behavior was observed in the work of Snow (1), showing a limited reduction in current density within the passive region of solution 4 which used increased levels of chloride ion. See Figure 1.

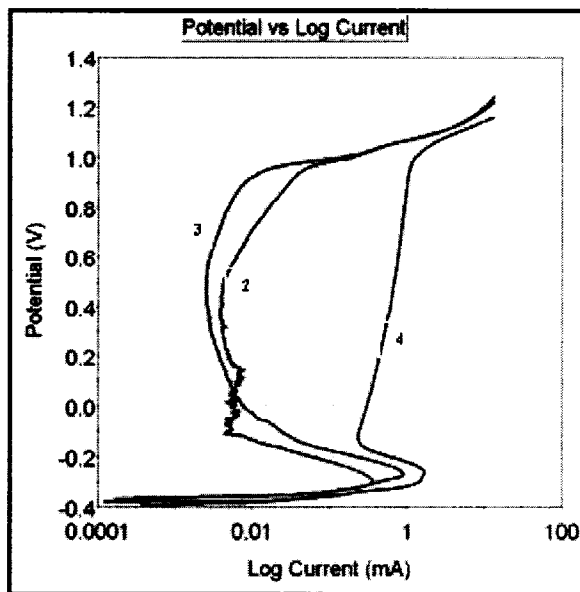
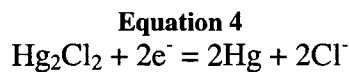


Figure 1: Potentiodynamic polarization curves for three deaerated solutions (1)

3.1.1 Open Circuit or Corrosion Potential

The open circuit potential or corrosion potential (E_{corr}) is generated by the polarization of the metal surface as it reacts with the solution and is the result of the chemical reactions resulting in the mixed potential. The open circuit potential is the potential the surface adopts, relative to the aqueous solution it is situated in when the above condition exists. It is a combination of the half cell reactions of the anodic and cathodic sites which meet at the corrosion potential (4, 5). See Figure 2. Various sites on the metal surface become anodic and cathodic in nature and generally these sites move around the uniform surface of polished samples giving the sample a uniform corrosion rate. “Open circuit” means that there is no electrical current to or from the metal, as there can be when it is in contact with a different metal or other source of current, promoting or preventing corrosion. At open circuit conditions all electrons produced by anodic reactions at the surface are consumed at cathodic reactions elsewhere on the same surface, the anodic and cathodic sites moving around.

To measure the potential of a surface a second standard corrosion or chemical reaction is needed to act as a reference point. This second reaction is built into a device called the reference electrode. The standard hydrogen electrode (SHE) is considered the most reliable reference point and is given the potential of 0.00 V. For these experiments a different, and more convenient, type of reference electrode is used which is called a saturated calomel reference electrode. This electrode is based on the chemical reaction at equilibrium:



In which the mercury chloride (calomel) solution is saturated and at 25°C.

This reaction at equilibrium has a potential listed as +0.241 V on the SHE scale. A simple addition is done within the computer to display all results relative to the SHE which is used in all computer outputs used in this document.

The actual rate of corrosion if the metal piece is corroding freely in the solution in question, not in contact with other metals or source of external electrical current, is indicated by the open circuit current density (i_{corr}), however as this current passes exclusively through the metal itself it is not possible to directly measure its magnitude under conventional means (4). It is sometimes possible to estimate i_{corr} based on potentiodynamic testing results using assumed Tafel slopes of the anodic and cathodic sections of the scan in combination with the polarization resistance (R_p) using the equation:

Equation 5

$$R_p = \frac{\beta_A \beta_C}{2.3(i_{\text{corr}})(\beta_A \beta_C)}$$

Where β_A is the slope of the anodic side, and β_C is the slope of the cathodic (6). See Figure 2 for illustration.

The rate at which the metal is corroding may be calculated based on the measured current and by the application of Faraday's first law (4):

$$\text{Equation 6}$$

$$m = \frac{(i_{\text{corr}})(t)(a)}{nF}$$

m=mass loss due to corrosion

i_{corr} = current

t = time

a = atomic weight

n = number of equivalents exchanged

F = Faraday's constant = 96,500 coulombs/equivalent

The PowerSuite PowerCORR software package calculating i_{corr} uses the model described by Stern-Geary (7) quotes the equation:

$$\text{Equation 7}$$

$$i(E) = i_{\text{CORR}} [10^{(E-E_{\text{corr}})/\beta_a} - 10^{(E_{\text{corr}}-E)/\beta_c}]$$

Where I is the net or total current that flows at any one point in time at a specific applied potential, E. i_{corr} is the open-circuit potential for the system. β_a and β_c are the Tafel proportionality constants for the anodic (oxidation) and cathodic (reduction) reactions and are defined as positive numbers (8). This may in turn be converted into a corrosion rate using:

$$\text{Equation 8}$$

$$\text{Corrosion Rate} = C (EW / d) (i_{\text{corr}} / A)$$

Where EW is the equivalent weight of the sample in g, A is the sample area in cm^2 , d is its density in g/ml, and C is a conversion constant that depends on the units being used. C

is 1.287×10^5 when i_{corr} is expressed as a current in amperes and you want the corrosion rate expressed in mils (thousandths of an inch) per year (mpy). C is 3.268×10^3 when ICORR is in amperes and you want the corrosion rate expressed in millimeters per year (mmpy). If the data being fitted are normalized with respect to Area (8). Refer to Appendix C for full documentation.

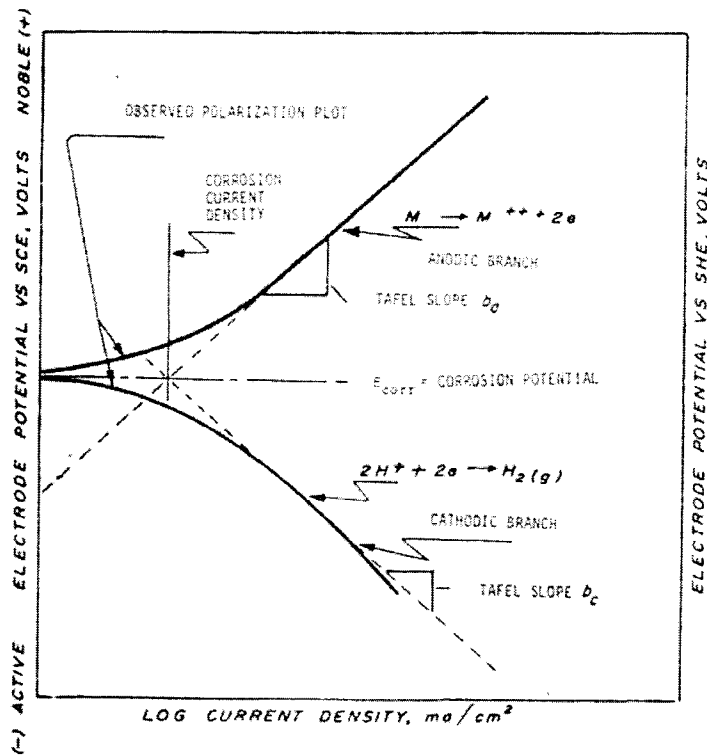


Figure 2: Extraction of i_{corr} and E_{corr} from polarization curves (5) G3 p42.

3.1.2 Natural Exposure Tests vs. Accelerated Tests

Testing samples in a realistic environment is the most conclusive means of evaluating a material's corrosion properties, however testing in a fully functional facility is not always a reasonable possibility. Naturally exposing materials through field testing is excellent for evaluating a set of materials in a single set environment; however it is difficult to test these materials for their properties in a series of different fluids as the process stream in the testing environment may not be easily changed. Field testing has some other limitations, being that it only gives an average rate and type of attack and it can not provide information on changes in corrosion rate vs. time from a single test (5). Multiple tests are required to gain adequate results to be used for maintenance and design considerations. In cases where the corrosion testing is taking place during the design stage of a plant and is using the process streams of existing plants it may become apparent that modifications to the new system will make this data irrelevant. Also of concern is the significant periods of time required to prepare, install, and wait for corrosion to occur on test samples. Some tests may require years to corrode sufficiently to give useful results, and in some cases the corrosion may be so extensive that the sample itself is lost, giving only a simple "fail" as the final test results.

Accelerated testing of samples does not offer the same realistic pitting patterns of corrosion as does natural exposure tests; in fact few accelerated tests can even claim to have produced corrosion patterns similar to those seen in real process environments (9). The benefit of accelerated testing, such as electrochemical tests, lies in its ability to

perform the rapid and cost effective testing of a variety of metals in a series of different chemical environments. The results of these tests may be used to assess the nature of the damage taken and allow the ranking of the metals (9). Ranking order is typically based on the pitting potential (E_{pit}) of the material, although in some cases the primary passive potential (E_{pp}) may be of greater interest if the material does not naturally passivate (4). By testing and comparing multiple materials in a broad series of possible environments it is possible to either choose the final materials, or to choose a set of preferred candidates for natural exposure testing.

3.1.3 General Structure of Polarization Plots for Passivating Metals

The polarization diagrams for active-passive metals will typically have three regions. These regions are called active, passive, and transpassive. Each of these will display a distinctive behavior and in polarization tests may be initiated by varying the potential imposed on the metal surface (5). These regions are illustrated in Figure 3.

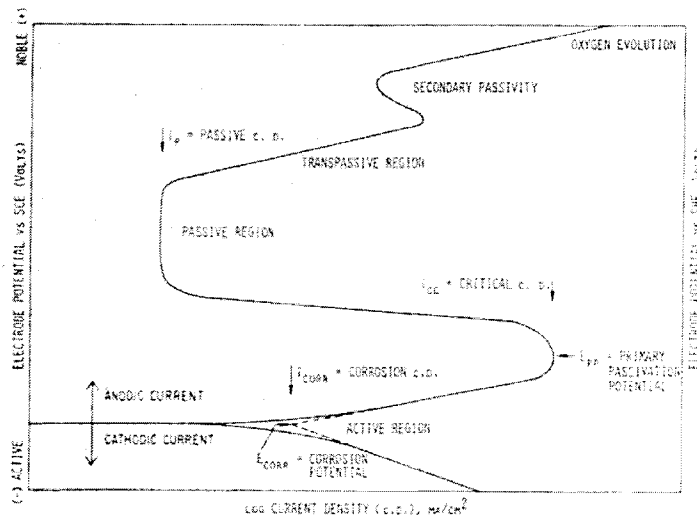


Figure 3: Typical regions found on polarization curves (5) G3 p42.

3.1.3.1 Active Region

The active region is sometimes seen at low potentials, where the hydrogen cathodic reaction is favored, and commonly found in deaerated acid solutions because it is not yet protected by a stable oxide layer. It displays a high corrosion rate due to the active dissolution of the metal and may form rough pits (10). This region is most active at the primary passive potential (E_{pp}) also known as passivation potential and is defined as the

point of maximum anodic current density of an active-passive material before passivation (4, 11).

3.1.3.2 Passive Region

The passive region is generated as the potential is increased, the oxygen cathodic reaction may play the major role, and the passive oxide film becomes stable. In this region the corrosion rate is reduced by as much as 10^6 (4, 12). It is typically the goal of engineers to keep the metal in this state at all times during the materials operating life. Although lower corrosion rates are theoretically possible for some metals at the lower end of the active region, the passive region gives a wider range of potential values in which to remain stable, and so a wider range of operating conditions which may change over time.

3.1.3.3 Transpassive Region

The transpassive region is marked by a sudden increase in current density on polarization charts. The corresponding potential is called the pitting potential (E_{pit}), at which the protective oxide layer breaks down resulting in rapid corrosion. As this region is located at a high polarization potential for stainless steels and chromium-bearing nickel alloys it is rarely seen in practice, however this region is readily reached by some aluminum alloys immersed in saltwater.

3.1.3.4 Secondary Passivity

This is a region beyond the pitting potential, located in the transpassive region where the oxide layer forms a new protective layer causing a noticeable drop in current density for some metals. The occurrence of secondary passivity on stainless steel is confirmed for sulfuric acid solutions (13). For 316L stainless steel in sulfuric acid it is attributed to the buildup of Fe in the outermost part of the oxide layer (14).

3.1.4 Passivation Principles

Passivation is the result of the creation of a stable oxide/hydroxide layer which forms a barrier between the metal and the fluid, and in particular increases the electrical resistance between the metal and the fluid in cathodic regions. Most commonly available corrosion resistant alloys depend on passive films for their resistance, which may reduce the corrosion rate by as much as 10^6 (4, 12). This increase in electrical resistance is important as the increased resistance polarization acts as a barrier to the flow of electrons and thus reducing the corrosion rate (15). The oxide layer typically forms spontaneously in air by reaction with oxygen, and also in aqueous media as metal ions bond with components of the fluid such as hydroxyl ions. In pure metals such as aluminum typically alumina is formed (Al_2O_3), or in iron, iron oxides (Fe_2O_3 , and Fe_3O_4) however some metals such as in stainless steels use added metals such as Chromium (Cr) to enhance the production of a stable oxide layer such as Cr_2O_3 , potentially resulting in a mixed oxide of all the metallic constituents, Fe, Cr, Ni. If the oxide layer is mechanically

breached the underlying metal may experience temporary corrosion, however after a short period of time and under relatively mild conditions it will regenerate. In the case of stainless steel, a buildup of chromium occurs on the surface during active dissolution of the Fe^{2+} metal ions, which is generally required before passivation occurs.

Passivation may be enhanced through the use of strong oxidizers after initial construction. The rapid and even corrosion of the surface results in a thickening of the passive layer, which makes it more effective in preventing corrosion (1, 4)

Solution composition can have a significant effect on passivation. If a solution is an extremely strong oxidizer, or the metal is anodically polarized, the oxide layer may deteriorate and be breached, resulting in a significant increase in the corrosion rate. Under controlled conditions the use of anodic polarization in a specific acid solution may be used to artificially thicken the oxide layer in a process called either pickling or electropolishing (12). Additionally, if the solution is a weak oxidizer and the oxide layer is breached, the oxide layer may not spontaneously repair itself. This loss of protection can result in the rapid localized corrosion of the metal (4). If halides are present in the solution, such as chloride ions (Cl^-), the result may be the localized deterioration of the oxide layer likely resulting in pitting. The presence of chloride ions may also trigger the thinning of the passive oxide layer according to the “thinning” model (16).

Other solution properties may effect passivation, including the aeration of the solution. If the solution is sufficiently deaerated a metal will not be able to generate the oxides required for passivation and will eventually begin to corrode.

3.1.5 Pitting Principles

Pitting is described as the “localized attack in an otherwise resistant surface” (4) and may be deep, shallow or undercut. The occurrence of pits and the very localized damage by them in materials resistant to uniform corrosion, such as stainless steels, is of great practical concern. The type and shape of a pit although not always obvious from surface analysis, is of great interest as the depth to which the penetration occurs is of great interest to designers. Pitting may be triggered by a variety of means related to the fluid properties, metal properties, and the electrochemical nature of its surroundings. While the propagation of a pit, once formed, is largely understood, the initiation of a pit is still the subject of much research.

The pitting of stainless steels shares some of the same mechanisms as crevice corrosion, itself behaving in much the same way as a self propagating crevice (4). If allowed to reach a critical depth, a pit can result in the rupture of a container or pressure vessel. This type of failure can potentially cause injury or environmental damage, making it vital that every engineer made aware of the effects and implications of this type of corrosion and that this information is stored in such a way that it is easily retrievable and ready to be used (17). Pitting may also lead to a variety of other corrosion assisted failures such as

crevice corrosion, stress corrosion cracking, corrosion fatigue, and failure of coatings (1, 16, 18).

3.1.5.1 Pitting Potential Principles

The pitting potential for a material is not a single value that can be applied to any situation; it is a complex and highly sensitive characteristic that is the primary focus of most pitting corrosion studies. The pitting potential is effected by temperature, solution characteristics and even the debatable definition of pitting potential itself. In potentiodynamic scans the pitting potential is commonly preceded by a series of energy spikes in the current density, and is generally followed by a steep rise in current density. These spikes are due to the initiation and repassivation of pits, and due to this behavior it is commonly asserted that pitting is not solely controlled by unique free energy of formation (19, 20, 21). It is also worthy to note that not all potentiodynamic scans produce a distinct pitting potential. Some can display a more gradual and less distinct change (20). The convention used to describe the pitting potential for metals says that the higher the pitting potential (more noble) is, the greater the pitting resistance of a metal to a particular solution. At higher potentials the pits begin to propagate for longer periods of time until they become self propagating pits.

If one looks at potentiostatic scans across a range of potentials close to the pitting potential it will be noted that there is an incubation period leading up to pitting. At low

potentials near the pitting potential the incubation period is substantial, and marked by numerous current spikes from metastable pits which gradually decrease, until stable pitting is initiated which is marked by a consistent increase in current density recorded in Figure 4. At higher potentials the incubation period is much shorter, with fewer distinct metastable pitting events occurring before stable pitting occurs and a rapid increase in current density is noted on the scan.

The effects of temperature are significant in that as the temperature increases the corrosion resistance of the metal generally decreases. The method of evaluating and quantifying this behavior is listed in the Annual Book of ASTM Standards section G150-99 (5).

Pitting is not a guaranteed result of increasing the potential. If the oxygen reduction potential is reached for a solution then electrolysis of the water will result generating gaseous oxygen. This directs most of the current into gas formation rather than increased corrosion of the metal removing any electrochemical driving force preferring pitting over active surface dissolution (22).

After reviewing the literature it is apparent that one can best describe the pitting potential as being a value within a range possible values which result in active stable pitting.

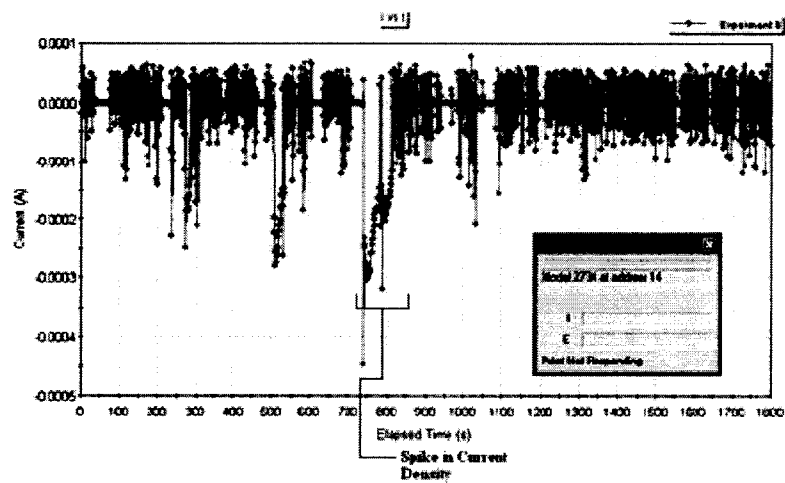


Figure 4: Energy spike due to metastable pitting recorded in a potentiostatic test.

3.1.6 Stages of Pitting

Although the later stages of pitting are generally easily located, the early stages are not as pronounced. Pits begin through nucleation which occurs on a microscopic scale and has a near instantaneous nature. The complex and sometimes unpredictable nature of pitting is considered to be stochastic (9, 23), thus the pitting potential is dependent upon the precise conditions and makeup of the solution and the metal.

3.1.6.1 Pit Nucleation

Pit nucleation is the initial breach of the protective passive layer over the metal surface. Depending on the metal, solution and polarization conditions of this event may be recorded as a series of electrical peaks near the top end of the passive region on a potentiodynamic scan, or as a series of fluctuations showing an increase in current density on potentiostatic scans, see Figure 4. These energy peaks that can be formed from an individual nucleation may be obscured by the magnitude of the passive current density due to the small size of the pit and the large size of the metal (18). It is suggested that some experiments may be performed using working electrodes with extremely small diameters mounted in epoxy resin (microelectrodes) so as to make the system more sensitive to current peaks (18). During testing of 304L stainless steel (S.S.) microelectrodes using solutions both with and without chloride ions present, it was demonstrated that metals exposed to chlorides experienced a significant number of peaks in current density during testing, illustrating the ability of Cl^- to penetrate the metal's

oxide layer (18), see Figure 5. Once a pit is nucleated it may propagate, or repassivate depending on factors such as the relative position of neighboring pits, the extent of polarization etc.

Nucleation sites typically coincide with the weakest points in the passive layer, relying on sites such as crevices and various types of inclusions and other imperfections. Areas which were stable cathodic sites before polarization began will typically be the last to nucleate pits as the corrosion of surrounding areas will protect them. As pitting along the metal surface continue to propagate the occurrence of pit nucleation will decrease due to the lowering of the overall surface current density (4).

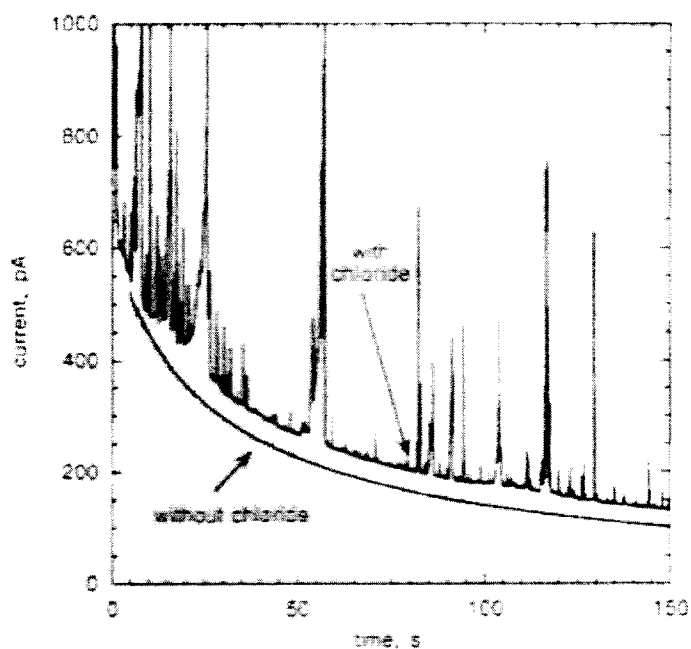


Figure 5: Spikes in current with and without chlorides (18) p27

3.1.6.2 Pitting Initiation Theories

Initiation of pits is a topic of some debate. Many theories have been proposed, however three models may be compiled to best explain the stages observed during pitting.

Absorbed ion displacement models:

These models are based on the absorption of anions such as chlorine or fluorine into the passive film. In the case of stainless steel and nickel based alloys these ions compete with oxygen in the film. The resulting damage to the oxide layer creates areas of reduced protection, which may lead to the nucleation of pits. (1, 9, 16)

Ion Migration or penetration models:

This theory states that anions such as chlorine etc. penetrate the oxide layer, reaching the underlying metal surface where it acts as a nucleation site for pits. (1, 9)

Breakdown-repair models:

This group is based on a mechanical disruption of the passive film by a chemical reaction. Various chemical reactions are described for theories in this group, including local acidification model, by which a breakdown due to mechanical or electrochemical means results in the exposure and eventual hydrolysis of the material causing a drop in the local pH. The salt film model describes the creation of a non-protective salt film over the area where the passive film breaks down, potentially resulting in pit nucleation. (1, 9)

3.1.6.3 Pit Propagation

Pit propagation theories typically focus on geometry mass transfer and reaction kinetics (9). This area is not yet fully understood due to the complex and hidden nature of corrosion in pits. A pit acts as a self propagating crevice, and encloses a small volume of fluid (4). This fluid is partially isolated from the bulk of the solution by the presence of a single small opening and a porous barrier of corrosion byproducts. The solution in the pit experiences a decrease in pH, and will commonly accumulate anions such as chlorine due to the electrical attraction of the negatively charged anions to the positively charged metal surface (1, 4, 18). These properties tend to support corrosion making these sites the preferential targets for continuing corrosion, even when the surrounding solution properties no longer favor pitting (1).

Theories on this topic may be broken down into three groups:

Metal dissolution hydrolysis:

This group considers the dissolution and hydrolysis of the metal to be a function of pH and potential, as well as the limiting current placed on the cathodic reaction. The corrosion of the metal is considered to be balanced by the reduction of hydrogen. (9)

Salt layer formation:

This theory attributes pit growth to a highly resistive film, probably a salt film that exists on a growing pits surface. It is theorized that this film is formed by the cations of the

metal and the aggressive ion (often Cl^-), and that it is poreless and that the rate of pit growth is equivalent to the rate of salt film dissolution (9).

Mass transfer control:

This group models the mass transfer of ions in and out of the pit controls the corrosion rate, and although mass transfer by migration can occur, it is assumed that for this theory mass transfer occurs by diffusion only (9).

The theory provided by Burstein, Liu, Souto and Vines (18) combines elements of all three of these theories. It states that the rapid propagation of pitting, specifically in chloride solutions, is generally attributed to two factors. The first being the presence of an ohmic potential drop between the pit interior and the cathodic reaction is so large that the potential at the pit surface is lowered to a value that is in the active region of the metal, thereby allowing the pit to propagate at the maximum rate controlled by the critical current density (18). The second is that the solution within the pit is high in Cl^- and artificially low in pH, making the solution more aggressive and so allowing the high propagation rates to be sustained (9, 18). This is attributed to the formation of an anolyte saturated with, or nearly saturated with a metal chloride salt (9, 18). Finally, limiting factor for the propagation rate of pits is the diffusion rate of metal cations out of the pit, which is limited by pit geometry (9, 18).

Stochastic models are also proposed, whereby pit initiation, growth or repassivation is of a more random nature (9, 23). Models for stochastic pitting fall into two categories, birth stochastic models which only consider pit generation events, and birth and death stochastic models which considers pit repassivation in addition to the nucleation process (23). As pitting along the metal surface continue to propagate the occurrence of pit nucleation will decrease due to the lowering of the overall surface current density (4). The drop in overall surface current density will also tend to increase the probability for small pits to repassivate as the potential applied to these sites decreases.

3.1.6.4 Metastable Pitting

Metastable pitting occurs when a nucleated pit experiences a period of corrosion, followed by repassivation. This repassivation is due to the inadequate driving force to keep the pit from regenerating a passive oxide layer. It is found over a large range of potentials, most commonly near the pitting potential (19). Some possible reasons for pit repassivation are that the solution within the pit was not sufficient to initiate stable pitting, or that other active sites in the area reduced the local anodic potential.

3.1.6.5 Stable Pitting

Pits which develop to a point where the solution within the pit is of a sufficiently aggressive nature that it is able to maintain pitting for prolonged periods of time are considered to be stable pits. Stable pits are able to remain active even if the potential of

the metal is reduced below pitting potential, and may remain active even if the outside solution becomes less aggressive. As pits develop, becoming larger and deeper the rate at which electrons can diffuse out of the pit may become restrictive, actually reducing the rate at which the pit may progress (4).

3.1.6.6 Pit Repassivation

Pit repassivation occurs when the basic requirements for a propagating pit are not met and the activity of the pit ceases. Some typical causes are a breach in the pit's cover, allowing increased ion transfer between the pit fluid and the surrounding solution, or a decrease in the applied potential. This results in the regeneration of the passive film or oxide layer within a pit.

3.1.6.7 Transpassive Pitting Characteristics

Once beyond the pitting potential heavy pitting occurs across the surface. Near the pitting potential some areas that are less predisposed to pitting will remain unaffected. These regions will often be created where less tensile stress is present in the surface, and had acted as cathodic regions of the surface before polarization began (4). As polarization increases pitting will continue to initiate and grow, often with changing patterns as pits begin to consume the metal around them, creating a greater number of open pits as they collapse. At lower potentials etch pits with jagged edges are described, and at high potentials more rounded smooth pits are observed (1, 10). As the pits

collapse they will often repassivate as the corrosive pit electrolyte is diluted, however as the potential continues to increase pits may continue to grow as open pits. Typically once the working electrode's surface potential is polarized sufficiently, bubbles of oxygen will form on the surface, consuming some of the electrons being pushed into the metal by the potentiostat (20). This state makes the relation of current measurements to metal dissolution rates inaccurate beyond this point.

3.1.7 Factors Effecting Pitting

Pitting is an event that may be substantially effected by any change in the conditions and properties of both the metal and the solution.

3.1.7.1 Metallurgical

Each of the metals and alloys offered has a different set of corrosion properties which contribute to the type, thickness and stability of the protective film. The passivation properties associated with austenitic stainless steels are attributed to the Cr_2O_3 oxide layer. The effectiveness of this protective layer is also influenced by the other elements present in the metal's composition such as nickel and manganese which help to promote repassivation and act as an austenitic stabilizer. (24)

3.1.7.1.1 Metal Type

Each metal will display different corrosion characteristics. Different alloys contain different elements to create better properties such a strength, corrosion and workability. Beyond the corrosion characteristics of the metal due to composition, the intended use of an alloy will effect the corrosion behavior as some will be cast, or extruded which develop different grain structures and different patterns of internal stress. Even the use of a metal in a facility will change its behavior as some will be under tension, compression or will be altered by processes such as welding etc. In metals such as austenitic stainless

steel increasing the alloying elements such as nickel and chromium the general corrosion resistance stainless steel may be improved, however the higher the chromium content the greater the rate at which the pH will drop in crevice solutions for a given passive current (9). Other alloying elements can also effect corrosion behavior. By increasing the molybdenum content in ferritic and austenitic stainless steel an increase the pitting potential while in chloride solutions was noted, possibly achieved by effecting the pit initiation process (19, 25, 26). The composition also has an effect on the maximum rate of corrosion, as illustrated by the higher corrosion rate for super ferritic stainless steel over a high alloy austenitic material (9).

3.1.7.1.2 Precipitates and Metallic Inclusions

Some materials experience a reaction called sensitization when held in a particular temperature range for a period of time. During this process precipitates such as chromium carbides ($Cr_{23}C_6$) may form in stainless steel, depleting surrounding areas of chromium, potentially leaving these sites vulnerable to intergranular corrosion (IGC), see Figure 6 (4, 9, 25). Generally cleaner steels with fewer inclusions and impurities have better pitting resistance as these sites often act as nucleation sites for pitting as structures such as sulfide inclusions may dissolve, leaving a small pit behind (25). Many precipitates and inclusions may be removed by electropolishing the surface, which typically reduces the corrosion rate (27).

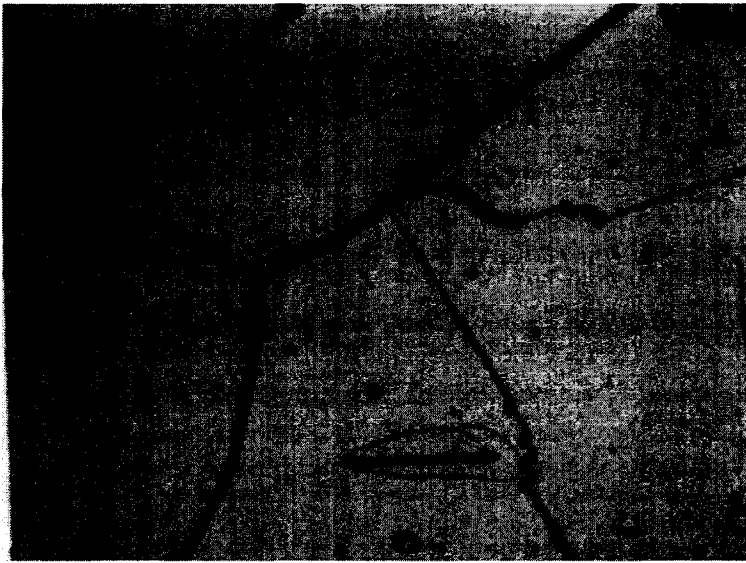


Figure 6: Intergranular attack of 304 stainless steel (25) p321

3.1.7.1.3 Surface Condition

Surface treatments due to the fabrication process create a unique set of localized corrosion properties. Features such as end grain attack in steel rods, or grain elongation and compressive/tensile stress locked into cold rolled steel plate give each material its unique corrosion behavior (9). Crevices at the surface will also have a substantial effect, as discussed in the crevice corrosion section 3.1.9. A few of the relevant properties of these materials are looked at in section 3.3.

In the case of galvanic corrosion the surface area of samples may greatly effect the corrosion rate and local severity (5). For cases where there is a large cathode and a small anode the anode will be aggressively corroded, while for the reverse case with a small

cathode and a large anode there will be a much less aggressive and less localized corrosion.

Processes such as electropolishing improve surface conditions by smoothing the surface and reducing the surface stresses (12, 27). Electropolishing removes burrs from the surface because the tip of a burr experiences a greater current density than the general metal surface and oxygen does not protect it as well as it does in the valleys (25). Under some conditions with high polarization potentials etching of the grain boundaries and dissolution of inclusions will occur during this process and may lead to a rough appearing surface with very few remaining weak points at which corrosion may nucleate (4, 22). Electropolishing also creates a surface devoid of hydrogen which cannot support bacteria, and it does not cause hydrogen embitterment.

3.1.7.1.4 Heat Treatment

Heat treating of metals is often used to reduce stresses locked into the atomic structure of the metal which in turn reduces the preferential occurrence of corrosion due to sites with locked in tensile stresses. It is also important to be aware that heat treatment of some materials may cause sensitization leading to an increase in localized corrosion.

Sensitization is a process which is caused by a material remaining at a temperature that allows the precipitation or segregation of certain compounds into the grain boundaries leading to susceptibility to intergranular corrosion (4, 9, 25). An example of this is for stainless steels containing chromium being held at 426 to 815°C which produces

chromium carbides (mainly $Cr_{23}C_6$) (4, 25). If the local chromium content goes below 10% due to this phenomenon then the grain boundaries will be preferentially corroded.

3.1.7.2 Electrochemical Reactions

Electrochemical reactions such as those caused by galvanic corrosion due to neighboring metals, changes in metal composition such as multiple phases, stresses, or several different metals segregated within the same alloy may accelerate corrosion.

3.1.7.3 Composition of Solution

Some chemicals have a powerful corrosive effect such as halide ions like chlorine, however other ions such as the concentration of sulfate ions in the fluid have been shown to have some protective effects against chloride ions (1). Solutions with varying compositions over a sample surface may effect the corrosion rate and distribution as one section of the surface becomes a cathode and the other an anode, an example of this is in the case of varying rates of oxygen reduction in crevice corrosion as explained in the crevice corrosion section (9). Other more subtle effects are known, such as the presence of precipitated corrosion products in the solution. An example of this is the case of copper ions damaging aluminum, while protecting iron (5).

Acid type and concentration has a significant effect on the corrosion behavior of a metal. While testing 304L stainless steel in nitric acid it was demonstrated that at a low acid

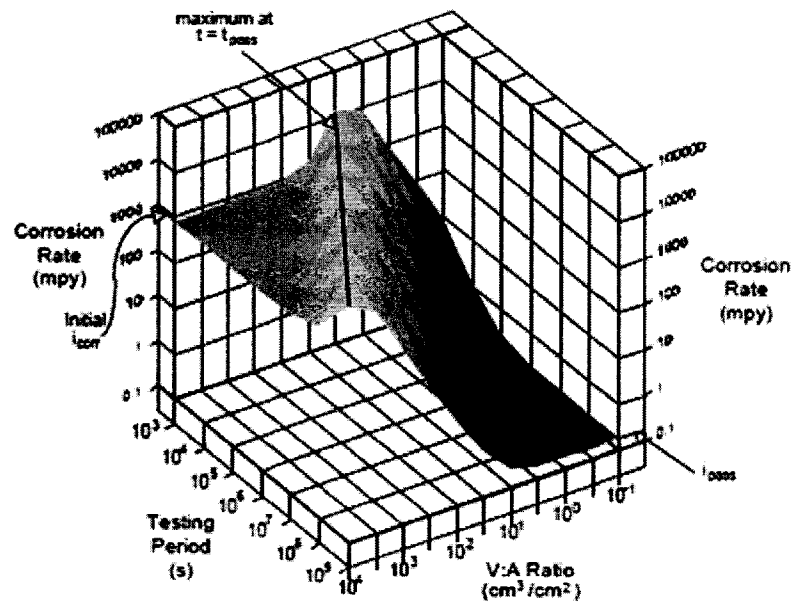
concentration (1-2N) the metal passivated immediately, while for high acid concentrations (4-10N) there was an initial phase of active dissolution before passivation (3). The passivation potential and passive current density were lower for the low acid concentrations compared to the high concentration tests.

Other types of damage may also occur from particular solutions, such as stress corrosion cracking (SCC) which may be triggered by increasing the temperature, chlorine concentration, or by decreasing the solution's pH, acting on metals under tensile stress (28). It is estimated that 32% of all SCC is caused by the presence of Cl^- (28). This type of damage may sometimes be observed as a small crack on the surface, and can propagate quickly under some conditions (29).

Volume effects may also come into play as metal ions and corrosion products often tend to effect corrosion characteristics in laboratory processes than in real operating conditions due to lesser test solution volume (9, 30). The E_{corr} of an electrochemical process is effected by the concentration of the reactants and inversely proportional to the concentration of the products (31). Therefore in a case where a disproportionately small volume of acid is used E_{corr} will drop as corrosion of the sample progresses and the acid is consumed and replaced by metal ions and oxides (31). This was shown to be the case for 304 stainless steel in nitric acid, which displayed a consistent active corrosion rate and duration at the beginning of tests however over time this value changed as the solution properties were effected by the presence of dissolved metal ions from the metal

sample itself (32). The ratio of solution to surface area should be kept constant for all tests and with a volume/area ratio exceeding 100 for tests running under 4 hours (9, 32).

See Figure 7.



Plot of calculated corrosion rates that would be obtained from weight loss measurements on 304 SS exposed to 4.1 M HNO_3 + 1 M NaCl as a function of V:A ratio and test period. The calculation assumed that the potential increased linearly with time until passivation. The maximum in corrosion rate occurs when the test period equals the time required for passivation.

Figure 7: Plot of corrosion rate vs testing period and volume/area ratio for nitric acid (32)

3.1.7.4 Mass Transport

The mass transport rate may be the controlling factor in the maximum reduction rate as demonstrated by the limiting current being at the cathode in most metals due to an easily accessible supply of metal atoms to corrode at the anode as shown in Figure 8 (4, 9). The flow rate of the solution controls this by controlling the rate of oxygen reduction.

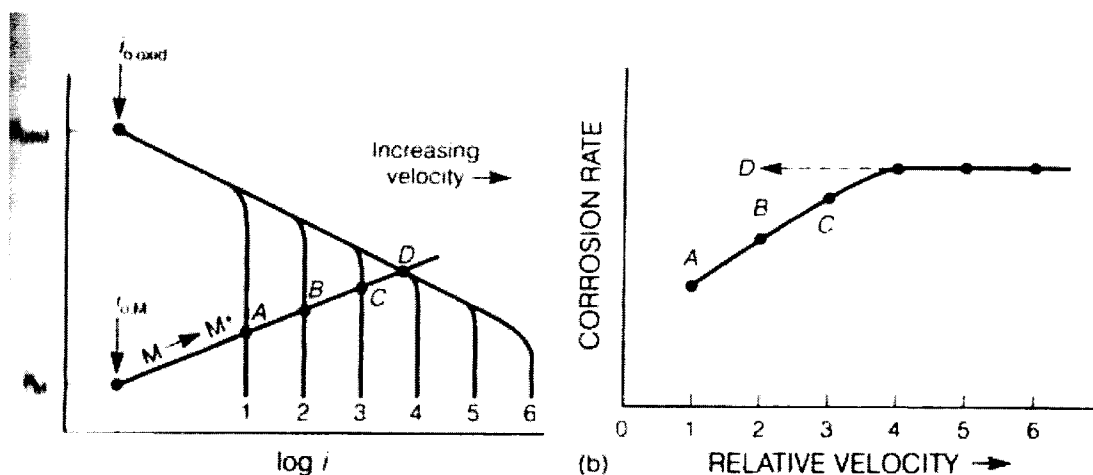


Figure 8: Effects of flow rate on corrosion rate and potential p93 of (4)

3.1.7.5 Temperature

Temperature may greatly effect the pitting behavior of a metal. For metals such as austenitic stainless steel an increase in temperature will generally move the pitting potential to a lower potential, making the metal more likely to pit in high temperature applications, although for some situations the opposite may also be true (9). In addition to decreasing the transpassive and pitting potentials, it has been shown that an increase in temperature for 304L stainless steel in nitric acid there experiences an increase in passive

current density with a profound effect at 348K causing a significant drop in pitting potential (3). This change in corrosion rate is attributed in part to the increased oxidizing power of nitric acid at increasing temperatures.

3.1.7.6 Pit Electrolyte Composition

As pits develop they isolate the fluid within from the outside solution due to their small openings and a porous oxide barrier. As corrosion continues within the pit, the solution experiences various changes in composition. These changes include the buildup of metal ions and oxides, a decrease in pH, and the absorption of anions from the bulk solution. All of these conditions result in the creation of a typically much more aggressive electrolyte within the pit than the initial solution outside, making the pit less sensitive to changes in the bulk solution and more likely to propagate rather than to repassivate (30). The limiting factor placed on the rate at which corrosion may occur inside the pit is generally attributed to the rate at which corrosion products (metal ions) may leave the pit (31).

3.1.8 Methods of Electrochemical Testing and Chemical Effects that Influence their Results

3.1.8.1 Potentiokinetic Testing

Potentiokinetic methods are based around the determination of current density as a function of potential. There are three methods of potentiokinetic testing being potentiodynamic, quasi-stationary method, and the stationary method (9). The most popular method is potentiodynamic polarization testing, which may be performed to quickly characterize a material's approximate pitting potential (E_{pit}) and its repassivation potential (E_{cp}) (9). This test produces a range of possible values which are open to interpretation and does not give an accurate indication of the incubation period (20). The resulting pitting potential value is highly dependent on scan rate and pit nucleation generally occurs at potentials where the induction period is very short (9, 20, 23). A scan rate of 0.6V/hr is recommended by ASTM standards (5), although faster scan rates are commonly used by researchers, typically near 1.2V/hr. Studies have shown that tests performed at a fast scan rate results in a pitting value that is too noble due to long induction time for pit nucleation, and a scan rate that is too slow also gives a more noble pitting potential due to the amelioration of the passive film (20, 23). Some researchers have observed that E_{pit} is proportional to the scan rate (v). Experimental relationships are (23):

Equation 9

$$E_{pit} \propto \log(v), E_{pit} \propto \log(v)^{1/2}, \text{ and } E_{pit} \propto \log(v)^{1/3}$$

Scans usually start at 0.25V below the corrosion potential (E_{corr}), and end at 1.6V vs. SHE.

3.1.8.2 Potentiostatic Testing

A more precise method is potentiostatic testing, which exposes a sample to a constant potential that allows the determination of current as a function of time. Potentiostatic is perhaps the most reliable method of determining the pitting potential and incubation period, however it is sometimes difficult to accurately attain values of E_{pit} and E_{cp} as it does not give the same overview of the material's behavior at multiple potentials without multiple tests. The determination of E_{pit} and E_{cp} each requires a different type of test. To determine E_{pit} a set of new passive samples are tested at different potentials until pitting occurs after a measured incubation period, then the incubation period (τ) data from a series of samples is used to extrapolate the pitting potential at which the incubation period is infinite (20):

Equation 10

$$\frac{1}{\tau} = 0$$

To determine E_{cp} a sample with active pits is tested at different potentials until the first potential where an upward trend in current at the end of a test is located, see Figure 9 for illustration on how to evaluate current (I) vs time (t) graphs (9). It is also able to estimate the incubation period for pits at the pitting potential, allowing for more precise characterization of a materials pitting potential. An additional test for the critical pitting

temperature (CPT) may be added onto the end of tests to locate E_{pit} by raising the temperature of unpitted samples at the end of the test until pitting occurs (9, 20). This provides a pitting potential as a function of temperature which may be of use in determining a material's behavior at elevated temperatures. A less common method of testing for E_{cp} is to remove the oxide layer by scratching the metal surface to observe if it pits at values below E_{pit} (9). The drawback for the potentiostatic method is the need for multiple samples and multiple test sessions requiring a greater investment of materials and personnel time.

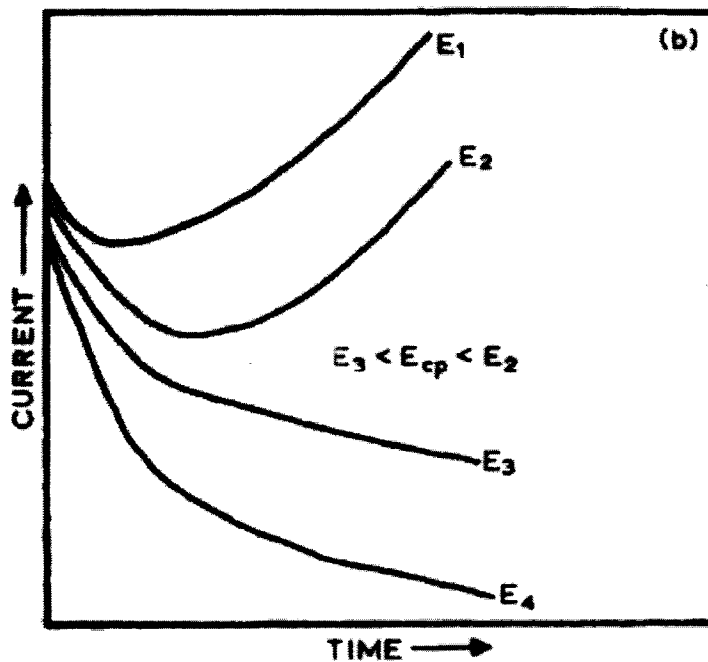


Figure 9: Potentiostatic polarization above and below pitting potential (9) p5.

3.1.8.3 Pitting Potential Interpretation and Limitations on Test Results

As pitting is an electrochemical process, it may to an extent be modeled and evaluated by electrochemical means. The application of various polarization tests may be used to rank metals for a given solution. Typically the most common point of interest regarding pitting is the Pitting Potential (E_{pit}) at which the formation of stable pits occurs.

Although pitting is commonly considered a fixed potential for a particular metal in a particular solution it is more often distorted as there are multiple stages of propagation each of which has a limited survival probability (18). This creates a question as to when does metastable pitting in the form of electrochemical noise end and stable pitting begin (9). Additionally the time required for pitting to initiate at a given pitting potential, called the incubation period, adds an additional variable into these observations.

Several authors have pointed out the limitation and inconsistencies placed on accelerated corrosion testing, stating that they do not directly relate to service experience and therefore simply provide a ranking order, and that correlations between techniques for studying alloys of similar corrosion resistance is poor (9). However it is generally accepted that the most reliable means of rapid corrosion testing are potentiostatic and potentiokinetic testing (9). These tests provide values for the free corrosion potential, the open circuit corrosion current density hence acting as an indication of uniform corrosion rate. They also provide corrosion current densities at potentials at other than the free corrosion potential providing some guidance in estimating corrosion involving mixed

potentials in galvanic couples or under imposed external current and also the potential range with passive behavior, and the potential at which pitting may occur.

An efficient means of testing samples for pitting is to use a potentiodynamic test to locate the approximate pitting potential, followed by a series of potentiostatic tests to locate the more precise pitting potential and its incubation period.

3.1.8.4 Cyclic Polarization

Cyclic polarization is based upon a standard potentiodynamic scan that is reversed once a predetermined point is reached, typically based on reaching a chosen current density in a scan (9, 20). Once the current is reversed there is commonly a deviation from the previously recorded curve due to the continued propagation of existing pits. This phenomenon is called a “hysteresis”. The increased current density is due to the ongoing dissolution of metal from the areas left without a stable oxide layer (26). Generally, the greater the hysteresis, the greater the extent of pitting as areas left without existing pits will tend to regenerate their passive layer in a brief period of time (26). As the polarization of the metal is reduced, the pits will tend to repassivate, eventually returning to the current density seen previously in the passive region.

3.1.8.5 Tests Based on Stochastic Theory of Pitting

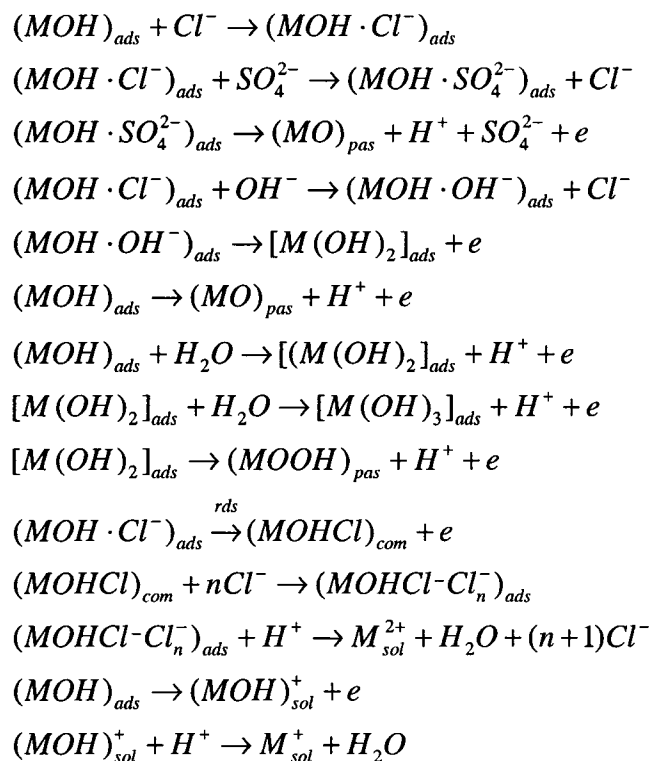
These tests focus on the electrochemical noise created by the nucleation of pits attributed to the stochastic nature of pitting. Typically during testing the operator holds the scan's potential once a trigger event occurs. According to Dr. Oldfield, there are three parameters of interest in this analysis (9):

- I. The trigger current level: A trigger event is an energy spike with sufficient magnitude to mark the initiation of a pit.
- II. The potential scan rate: the chosen scan rate for the potentiodynamic scan associated with testing will effect whether the initial events being detected are metastable or stable pitting events.
- III. The hold time: If the current falls again then the pit has repassivated and the potential scan is restarted, and if the potential continues to stay above the trigger level then there is an active pit.

3.1.8.6 Chemical Reactions

The following chemical reactions are considered to be common to many metals corroding in solutions with sulfates and chlorides. Some of these reactions are the basis of the formation of the oxide layer for austenitic stainless steels immersed in sulfuric acid solutions containing chloride ions (1, 2).

Equation 11



The subscript letters used in the equations mean ads (adsorption), pas (passive), com (complex), sol (solution) and rds (rate determining step). Although not universally compatible with all tests they are relevant to many tests performed. Refer to material specific sections for more information on oxide layers.

3.1.8.7 Explanation of Eh-pH Diagrams

The Eh-pH (Pourbaix or pH-Overpotential) diagrams as developed by Dr. Marcel Pourbaix map out the theoretically stable elements possible when a metal is at a particular potential in a solution of known pH. In the case of passivating metals such as stainless

steels these diagrams may be used to locate regions that will produce oxides favorable to forming a strong insoluble and corrosion resistant oxide layer.

The foundation for all metallic corrosion is the changes in the Gibbs free energy. For a reaction to occur the Gibbs free energy must have a negative value associated with the chemical change. The change in the Gibbs free energy is (4):

$$\text{Equation 12}$$
$$\Delta G = \Delta H - T\Delta S$$

ΔG = Δ Gibbs free energy

ΔH = Δ Enthalpy or “heat of formation”

ΔS = Δ Entropy “disorder”

T = absolute Temperature,

The subtle variations in the metal’s surface potentials complicate the use of these charts considerably as some areas will be naturally more cathodic than others. This makes it possible for compounds normally considered unstable at a particular potential to exist and form at these sites.

Pourbaix diagrams are listed for stainless steel and titanium in later chapters.

3.1.8.8 Liquid Junction Potential (LJP)

The liquid junction potential (LJP) is a chemical effect that may influence the determination of potentials within a corrosion cell. It is generated when two different solutions come into contact with each other causing an offset in measured potentials. Similarly a thermal junction potential (TJP) also exists where two solutions of different temperature comes together. Each solution used will generate a different LJP and as such would have to be calculated independently.

Using Vaughan's LJP calculator spreadsheet (33, 34) the LJP for a 1M H₂SO₄ solution is -0.0341 V. The LJP represents a significant offset from the original values however as the experimental hydrometallurgy process fluids (EHPF) used in the SC series tests is of unknown composition it is not possible to calculate this value for those tests. The SB series uses a series of different solutions each with a different LJP and varying amounts of elements such as nickel and chloride ions. As the Vaughan calculator does not include nickel concentration as a variable it may not be used for these solutions and it is not possible to determine the calculations used in the program making it difficult to verify the accuracy of the resulting values.

Due to these limitations on the LJP calculations the recorded values will be listed in all sections without any correction for this value. This is considered acceptable as the test results will not be critically skewed as the fluids are more commonly compared on an aerated vs. deaerated or potentiostatic vs. potentiodynamic basis where all tests are based

on the same solution composition. Also the corrosion behaviors shown by the metals will remain valid and the work done by Snow does not appear to correct for LJP making test result comparisons possible.

3.1.8.9 Electrode/Electrolyte Interface

Corrosion of a metal surface occurs where the metal meets the solution at the electrode/electrolyte interface. At this point a series of chemical reactions take place which determine the mixed corrosion potential, current density, and the prevailing corrosion products.

3.1.8.9.1 Limiting Current

The limiting current for a given situation is the maximum current density that may be achieved under the given conditions. This is the result of an inherent restriction to current flow, typically found at the electrode/electrolyte interface where the movement of the chemical elements in the fluid may be the limiting factor for the rate of corrosion (4). The most easily changed factor that can increase the limiting current is the flow rate.

3.1.8.9.2 Flow rate

The rate at which a given solution flows over a surface helps to carry in new solution and fresh oxidizers while carrying away corrosion byproducts. The increase in local

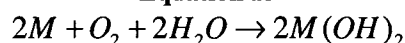
concentration of oxidizers influences corrosion rate just as much as the reduction in byproduct concentration (4). An increase in flow rate may potentially increase corrosion rate by raising the limiting current, or it may decrease it by exposing the metal to more oxygen and allowing for the rapid regeneration of the oxide layer. A decrease in the flow rate may result in a decreased limiting current, or it may allow for increased localized corrosion due to deaerated conditions or increased likelihood of localized corrosion such as crevice corrosion.

Under some conditions there may also be no appreciable effect due to flow rate. For sulfuric acid on stainless steel velocity has little effect on corrosion in the passive stage but mostly in the active state where it can cause increased corrosion (35).

3.1.9 Crevice Corrosion

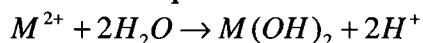
Crevice present at the surface of a sample exposed to a corrosive solution isolate a small amount of the liquid, restricting mass transfer into or out of this area (9). The geometry of the crevice, such as its depth and width will effect the severity of the corrosion as tighter crevices will trigger severe crevice corrosion (9). The process of crevice corrosion as presented by Dr. Oldfield (9) is described as taking three steps. During the first stage the typical anodic and cathodic chemical reactions take place both inside and outside the crevice, generally the overall reaction is:

Equation 13



In the second stage, after the depletion of oxygen within the crevice the inside becomes an anode with the outside surface the cathode (9, 10). This produces an increase in metal ions within the crevice which then hydrolyse causing the reduction of the pH in the solution through the reaction:

Equation 14



Additionally anions such as Cl^- are attracted to the crevice to maintain electroneutrality. The third step is the point in the process where the now more aggressive solution is able to break down the passive layer, this is called the critical crevice solution (CCS), and is a function of metal type, pH, and anion (Cl^-) concentration. The composition of the metal will also have an effect on crevice corrosion. Stainless steels with more chromium will experience a faster pH drop for a given passive current (9). The resulting electrolyte

created by crevice corrosion is very similar to that of a formed pit; however the presence of these crevices in the early stages of corrosion gives them the ability to start this process before most other sites are able to begin pitting. Crevice corrosion may result from crevices that form from either the metal's surface structure or the presence of other items being pressed against the surface (4, 9). The number of crevices is important as once corrosion begins at one location it may cathodically protect other locations nearby (9).

3.1.10 Sample Mass Loss Due to Corrosion

Corrosion is an electrochemical process, in which metal atoms at anodic sites produce free electrons by becoming positively charged ions. In the case of polarization testing, the electrons are produced at the anode, and are transferred to the cathode. In a greatly simplified case, the number of electrons being transferred is directly proportional to the number of metal atoms being consumed. If the precise chemical reaction is known and the current being transferred is known, then the amount of metal dissolution may be calculated.

The simplicity of this model is disrupted by the complexities of reality. Depending on the corroding material, solution and chemical reaction properties the system may create unanticipated results. Gas products may be created such as the case of oxygen generation at the anode in electrolysis may create a falsely high estimate of corrosion rates. Other subtle reactions may occur, such as continued cathodic activity on the anode's surface

when at low polarization potentials (4). Such reactions may cause an underestimation of corrosion rates as the electrons generated by the corroding metal do not pass through the potentiostat. Metals can potentially have several possible reactions depending on factors such as pH and implied potential as illustrated in pourbaix diagrams (4). This complexity may lead to the assumption of an inappropriate chemical reaction, leading to an inaccurate estimate as to the mass loss. Measuring the weight before and after testing is an effective method of determining metal mass loss; however an error may be created due to the addition of the mass added when creating the surface oxides, particularly while testing titanium due to the typically low corrosion rate, particularly after immersion tests (33, 36).

Accepted procedures for converting the results of electrochemical measurements to rates of uniform corrosion are presented in the Annual Book of American Society for Testing Materials (ASTM) Standards section G102-89 (5).

Although the metal mass loss is useful in corrosion evaluations, it is not always the most important factor. Evenly distributed surface corrosion may be accurately estimated, however when pitting occurs factors such as depth and distribution are of greater importance (4, 22). The phenomenon of pitting is not accurately modeled using mass loss.

3.2 Solution Chemistry and Effects

The corrosion characteristics of a metal are directly linked to the type of corrosive environment it is in. For metals exposed to a liquid there are a variety of chemical factors to be considered as there is an infinite variety of different compositions possible for testing.

3.2.1 Volume Effects on Solution Composition

In addition to the initial solution composition there are a number of changes which may occur during testing, some of which are linked to the corrosion of the metal itself. While testing a sample there is an unavoidable contamination of the solution by metal ions and corrosion products due to the dissolution of the metal surface. An extreme example of this is in the artificial pit experiments of Hakkarainen and Pohjanne, who dissolved 50g of 316L stainless steel into 200ml of 10M HCl to produce a pit solution which was injected into drilled artificial pits (30). Although this is an intentional situation it is common that tests using limited volumes of solution will potentially become sufficiently contaminated that the results of testing are inaccurate often reflecting an artificially reduced corrosion rate due to the presence of large amounts of corrosion products or a lack of remaining reactants in the solution such as chloride ions. Tests are generally performed with 250-1500mL of solution, depending on material and test properties (5, 30, 36).

3.2.2 Sulfuric Acid Solution

3.2.2.1 Specified Acid Solution Composition for Baseline Analyses

The chosen base solution for testing is 1M H₂SO₄ for testing 316 stainless steel and it is of similar concentration to that used by Snow (1). This solution has a significantly lower pH than that of actual hydrometallurgy process fluids however as these tests are performed at lower temperatures and pressures with a higher grade of sample preparation the increased corrosion resistance associated with these test conditions should be counteracted in part by the increased acidity of the solution used.

3.2.2.2 Acid Concentration Effects

Increasing the acid concentration increases the presence of H⁺ ions in the solution, thereby decreasing the pH and making the solution acidic. The theoretical pH as a measure of acidity for a given acid solution is calculated using:

$$\text{Equation 15}$$
$$pH = -\log_{10} \frac{(H^+)}{1\text{mol} / L} \quad (4, 22)$$

Where H⁺ represents the hydrogen ion concentration in moles per liter. The actual solution pH is also effected by the temperature of the fluid which increased the activity of these ions and thereby reduces the pH. Addition of other substances to an acidic solution will also change the pH and require more complicated calculations to obtain an accurate value.

A decrease in pH will typically decrease E_{pit} , and increase the potential for the active region, see Figure 10 (4, 10). This has the typical effect of reducing the range of potentials in the passive region, making the metal less likely to passivate for a given set of operating conditions. For some metals increasing the acid concentration will actually help to protect it from corrosion. Metals such as titanium will passivate only in strong oxidizers and will actively corrode in weak acids. This is due to the formation of a strong TiO_2 oxide layer in strong oxidizing solutions which protects the metal. Also the type of acid being added has the effect of increasing other chemicals in the system, which may actually have a greater effect than the decrease in pH. By adding HCl there will typically be an increase in Cl^- concentration which will most likely accelerate corrosion, and by adding H_2SO_4 the increased sulfate ion concentration may protect the metal from Cl^- attack (1).

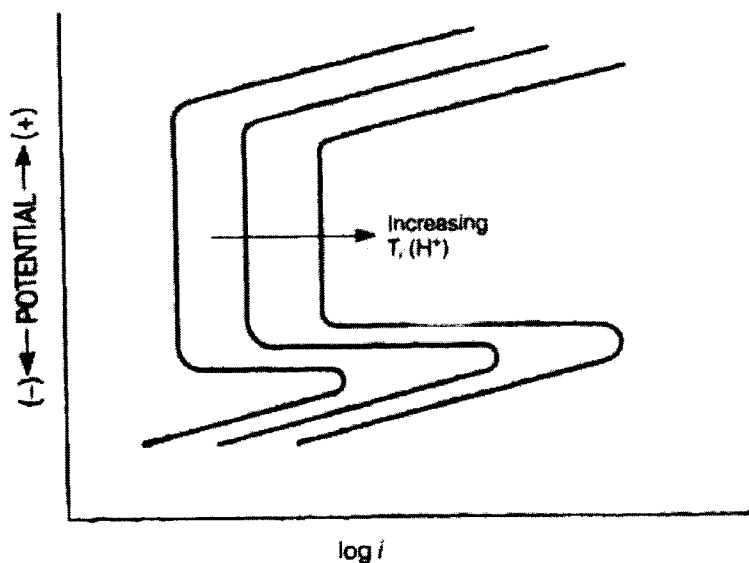


Figure 10: Changes to potentiodynamic polarization curves with increased temperature or pH. (4)
p120.

3.2.2.3 Chloride Concentration Effects

Increased chloride ion concentration has been shown to significantly increase corrosion rates and the occurrence of pitting when present in sufficient quantities (1, 4, 35). During testing of 304L stainless steel microelectrodes using solutions both with and without chloride ions present, it was demonstrated that metals exposed to chlorides experienced a significant number of peaks in current density during testing, illustrating the ability of Cl^- to penetrate the metal's oxide layer (16, 18). Chlorides have also been shown to reduce the pitting potential for stainless steels, making them more susceptible to pitting (10, 16).

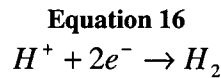
3.2.2.4 Sulfate Concentration Effects

Sulfate ions are attracted to anodically polarized surfaces just as is the case for chloride ions. Upon polarization of a given material exposed to a solution containing these ions a increase in the local concentration at the metal surface will occur with both negatively charged ions competing for space near the surface. This competition has the benefit of reducing the degree to which chloride ions can accumulate locally on the metal surface at a given polarization potential, thereby potentially preventing pitting as the critical chloride ion concentration needed to breach the oxide layer is not achieved (1, 37).

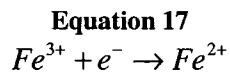
Sulfate ions when present in solutions without any more aggressive ions present may themselves cause pitting when present within certain ranges (16).

3.2.2.5 Iron, Nickel and Other Ion Effects

Test solutions using more than one oxidizer tend to have a more complex nature than those that use only one. During immersion testing there is an assumption made that the reduction of hydrogen is the only cathodic reaction taking place in the system, however as other elements are added to the water the possibility of unforeseen chemical reactions taking place on the surface of the anode and cathode increases (4). Tests adding strong oxidizers such as Fe^{3+} ions to the system create a situation where there is a mixed potential from the hydrogen reduction reaction



and the iron reduction reaction



When below $e^{Fe^{3+}/Fe^{2+}}$ and e^{H^+/H_2} , the current density is a function of both reactions, however for cases where E_{corr} is above e^{H^+/H_2} only the ferric ion reduction reaction will take place (4).

3.2.2.6 Aeration

Aeration plays a significant role in the production of the oxide layer of a metal. Without an adequate supply of oxygen present in the solution the oxide layer will tend to break down, leaving the material open to corrosion. During testing it is important to ensure that the solution is either aerated or deaerated depending on the test criteria. Deaerated tests will typically be considered the more aggressive environment, however it is also difficult to prepare the sample and place it into the corrosion cell without forming an oxide layer from exposure to the atmosphere, therefore all samples should be prepared a maximum of 1hr before testing (5, 36). The solution should be saturated with either oxygen or argon for 30 minutes before exposure to the sample; this ensures that the solution will be consistent throughout the test and that the sample's oxide layer will not be artificially thickened at the start of deaerated tests, nor allowing surface damage or unrealistically thin passive layer at the start of the aerated tests. ASTM G5 standards recommend using $150 \text{ cm}^3/\text{min}$ for a minimum of $\frac{1}{2}$ hr at the start of all tests (5).

Samples exposed to a varying degree of aeration across the surface may result in the active corrosion of areas with lower aeration. This natural polarization of the sample is the result of having two different mixed potentials connected by the conductive base metal or other connection. The aerated sections will have a more noble potential compared to the deaerated sections which results in electrons flowing to the high aeration surfaces thereby increasing the corrosion rate on deaerated areas of the surface.

3.2.3 Seawater Solution

Saltwater solutions are commonly used in experiments related to seawater simulation and for testing scientific theories. Experiments are commonly performed at a variety of concentrations, two of which are 3.5% and 5% sodium chloride (NaCl) (4, 20, 23). Some authors point out that testing a metal's resistance to calm seawater cannot be tested with any degree of confidence, and that agreement between different tests and different metals of similar composition is questionable (9). In a paper examining the effect of potential scan rate on 304L and 316L stainless steel a solution of 5% NaCl was used using a stochastic approach (23).

3.2.3.1 Specified Salt Solution Composition

The chosen solution consists of 35g of certified American Chemical Society (A.C.S.) NaCl in every 1 liter of test solution and is consistent with other sources (20, 38). This NaCl solution is considered adequate for testing despite not containing chemicals such as calcium found in real seawater which consists of only 25 g/L sodium chloride (39).

3.2.3.2 Chloride Concentration Effects

During testing of 304L stainless steel microelectrodes using solutions both with and without chloride ions present, it was demonstrated that metals exposed to chlorides experienced a significant number of peaks in current density during testing, illustrating

the ability of Cl^- to penetrate the metal's oxide layer (18). As is also the case with sulfuric acid increased salt content (and hence the chloride ion concentration) has been shown to reduce the pitting potential for stainless steels, making them more susceptible to pitting (10).

3.2.3.3 Aeration

Aeration plays a significant role in the production of the oxide layer of a metal. Without an adequate supply of oxygen present in the solution the oxide layer will tend to break down, leaving the material open to corrosion. During testing it is important to ensure that the solution is aerated at all times, as the seawater being simulated is rarely deaerated. Aerating the solution 30 minutes before exposure to the sample, ensures that the solution will be consistent throughout the test and that the sample's surface and oxide layer will not be adversely effected at the start of the test.

ASTM G5 standards recommend using $150\text{ cm}^3/\text{min}$ for a minimum of $\frac{1}{2}$ hr at the start of all tests (5)

3.2.4 Surface Analysis Equipment

3.2.4.1 Scanning Electron Microscope (SEM)

Using an electron beam to image the surface this method is able to accurately image the topography of the surface. Unlike optical microscopy the scanning electron microscopy (SEM) images produced may achieve a magnification of up to 100,000x due to the smaller wavelengths, and with improved depth of field (3 dimensional effect) (22). These images can be used to determine the extent of pitting, and to locate, image and measure small characteristics such as potential nucleation sites when employed before electrochemical testing.

3.2.4.2 Energy Dispersive Spectroscopy (EDS)

EDS is a method of determining the chemical makeup of a substance, and is useful for evaluating the composition of the oxide layer and to verify the composition of metal samples. Using the SEM to target a location the X-rays emitted by the surface are measured, and are displayed as a set of X-ray peaks that correspond to chemical elements in the periodic table. The results of these tests can help to determine the chemical elements and compounds found in the corrosion of pits and the type of oxides in the protective passive film (22).

3.2.4.3 Optical Microscopy

Optical microscopy uses the reflection of light from a material's surface and filtered through a set of lenses to create an image of a material's surface topography with a magnification of up to 1000x. The limitation on a microscope's ability to accurately magnify a surface is the optics of the microscope and the limitations of light itself, with a wavelength of about 3,000 angstroms (22). The definite limit on resolving power (d) of a microscope is:

$$\text{Equation 18}$$
$$d = w.l. / N.A.$$

Where w.l. is the wavelength of the light used, and N.A. is the listed numerical aperture for the objective lens which determines the range of angles through which it can accept or emit light (40). Typically a greater value numerical aperture will provide a greater resolution.

Magnification is based on the ability of the human eye to focus on an object 250mm away, which is considered 1x magnification. Magnification (Mag) is based on the equation (40):

$$\text{Equation 19}$$
$$Mag = Size2 / Size1$$

The ability of a microscope to magnify a surface with good resolution is controlled by the quality of the optics, and the calibrations of the user. The main calibrations are:

- (1) The radiant field diaphragm (or field diaphragm), which controls the size of the area illuminated is located near the light source. The larger the area illuminated, the greater the amount of excess light will be absorbed into the lens, potentially causing a reduction in resolution. It is best to avoid illuminating more of the surface than is seen through the microscope as light entering the objective from portions of the surface outside the area seen is likely to hit the inner walls of the lenses or microscope tube and scatter producing a “fogged” image.
- (2) The aperture diaphragm is adjusted to make the microscope compatible with the objective lens and the sample surface. Typically a setting of 90-50% is suitable. The aperture diaphragm determines the angle of the cone of light illuminating each point on the object. If the angle is smaller than that corresponding to the numerical aperture of the objective the full resolution possible with the objective is not realized and the resolution suffers. If the cone angle is bigger than that corresponding to the numerical aperture light may scatter from the inner side wall of the objective and produce a fogged image.

When light hits the surface there are a number of possible ways for it to react (40).

Absorption of light may cause the returning light rays to change colors as some wavelengths are preferentially absorbed. Refraction may occur as the light bends while passing through materials of different densities. Diffraction may occur when light bends around objects with sharp edges, and may be treated using a low aperture lens.

Dispersion may occur as light breaks up into its constituent wavelengths.

Using optical microscopy along with a digital camera attached using an adapter, a standard microscope can be used to collect high resolution images and videos of features and visible chemical processes on the surface. Using specialized techniques it is possible to image real time pitting, etching, and other corrosion events.

3.2.4.4 Metallograph

A metallograph is an advanced optical microscope, commonly equipped with high end optics, filters, image and video recording capabilities and often measuring equipment. It may be used for detailed examination of the topography of a metal surface and to characterize the features on the surface.

3.2.5 Surface Analysis Techniques

3.2.5.1 Analysis Methods Regarding Pit Morphology

Pit depth may be determined by a variety of different ASTM recommended ways. The first is to use a calibrated microscope to focus on the top surface of the material and then measure the distance the platform travels to focus on the bottom of the pit. A second method uses a probe attached to a micrometer or depth gauge. A third method is using a metallographic technique, by cutting the sample in half and polishing the edge followed by a examination under magnification to determine an accurate depth. Although very effective, and shows the shape of the pit's internal structure (see Figure 12) only a few pits will be exposed, and the deepest pit may not be found in this way. The fourth way is to machine the surface of the sample on a lathe or milling machine until the deepest pit is located and made flush with the machine surface, followed by an accurate measurement from the bottom of the pit to the top of the initial surface (5).

Pit size and density may be calculated by counting and measuring, or estimated using ASTM charts, see Figure 11 (5).

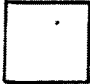








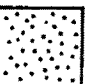





	<u>A</u> DENSITY	<u>B</u> SIZE	<u>C</u> DEPTH
1	 $2.5 \times 10^3 / m^2$	 0.5 mm^2	 0.4 mm
2	 $1 \times 10^4 / m^2$	 2.0 mm^2	 0.8 mm
3	 $5 \times 10^4 / m^2$	 8.0 mm^2	 1.6 mm
4	 $1 \times 10^5 / m^2$	 12.5 mm^2	 3.2 mm
5	 $5 \times 10^5 / m^2$	 24.5 mm^2	 6.4 mm

Figure 11: Standard pitting charts by ASTM standards G46-94 (5)

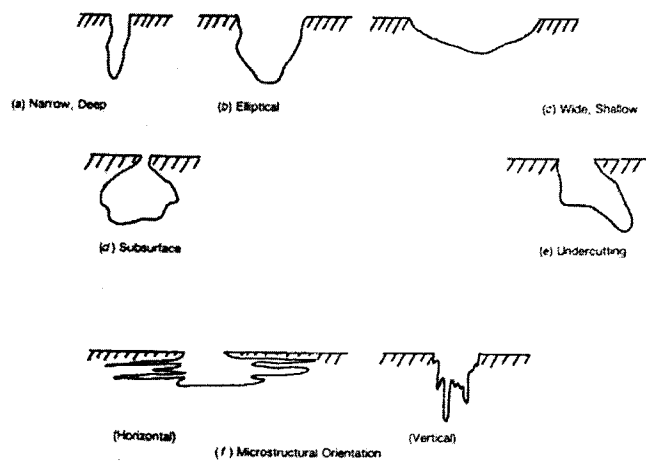


FIG. 1 Variations in the Cross-Sectional Shape of Pits

Figure 12: Variations in cross-sectional shape of pits G46-94 (5)

3.2.5.2 Low Magnification Surface Analysis

Using a microscope at low magnification features such as etching, pitting, dealloying, parting, tarnishing, filming, scaling etc. may be observed (5). After cleaning away the oxides other features such as the size, shape, and density of pits and maximum depth may be estimated (5). These details are useful for estimating the extent of the damage, particularly in the case of maximum pit depth which will give an indication of the material's susceptibility to penetration by pits, which for example could lead to dangerous pinhole leaks in pressure vessels etc.

Some surface cavities may not be pits. Some inclusions may dissolve during testing or these features may be caused by metal dropout caused by intergranular corrosion, dealloying etc. (5).

3.3 Sample Material Properties

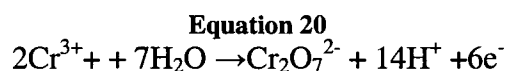
3.3.1 Stainless Steel Specific Information

316L stainless steel is a Class D austenitic stainless steel (24). It is considered to be highly resistant to corrosion and oxidation at elevated temperatures with a particularly good resistance to pitting (24). Regarding sulfuric acid environments, this grade of stainless steel is recommended for service with either weak solutions or in high concentration sulfuric acid above 93% at 40°C (35).

Stainless Steels may form iron oxides (Fe_2O_3 , and Fe_3O_4), however, stainless steels use added metals such as chromium (Cr) to enhance the production of a stable oxide layer (Cr_2O_3). If the oxide layer is mechanically breached it may experience temporary corrosion, however after a short period of time and under relatively mild conditions it will regenerate. In the case of stainless steel, an accumulation of chromium occurs on the surface during active dissolution and removal of Fe^{2+} metal ions, which is generally required before passivation occurs.

The Cr_2O_3 oxide layer is characterized as being strong and brittle in nature. The typical thickness is estimated at 1.0 nm (0.04 μin) and is generally considered to be clear in color (41). This oxide is presumed stable until the sample reaches the transpassive region. Once in the transpassive region and beyond 1.3 V in acid solutions, the chemical reaction

changes resulting in a soluble substance called dichromate ions $\text{Cr}_2\text{O}_7^{2-}$ according to the reaction (41):



316L stainless steel has an equivalent weight of 25.29 g/equivalent (42) and a density of 8 g/cm³.

Testing procedures for this metal are available from the Annual Book of ASTM Standards sections G5 and G61-86 (5).

Composition of metal samples provided by the retailer is provided below and in Appendix B (43).

Table 1: Chemical composition of 316L stainless steel (excluding iron) used in testing (43)

Elements	C%	Si%	Mn%	P%	S%	Cr%	Ni%	Cu%	Mo%	N%	Co%
Results	0.026	0.33	1.51	0.04	0.02	16.42	10.28	0.52	2.11	0.035	0.17

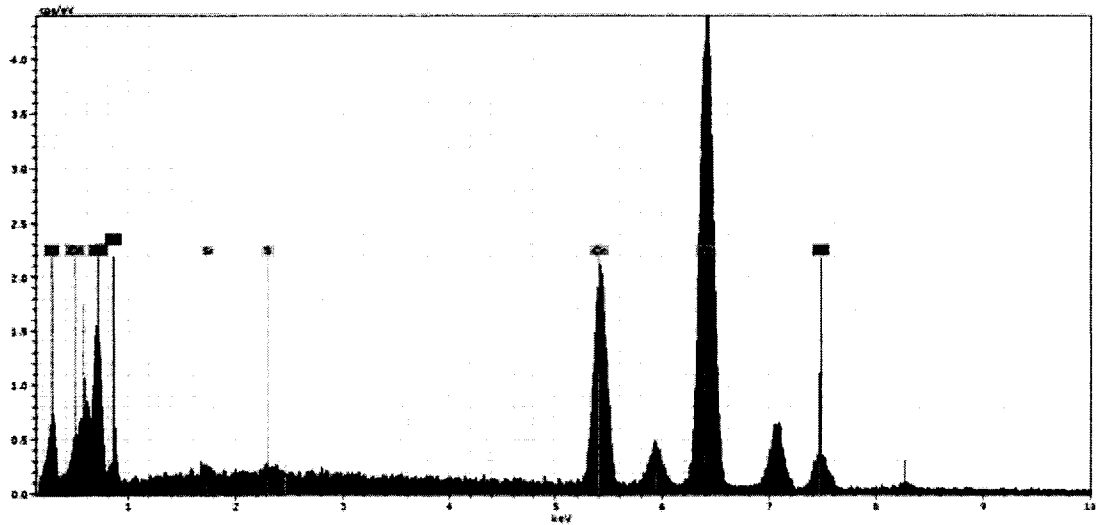


Figure 1. EDS spectra of investigated steel

Figure 13: EDS scan results for 316 stainless steel test samples (1)

3.3.1.1 Effect of Different Alloying Elements

Manganese: It is an alternative austenite stabilizer which is introduced to reduce the amount of nickel present in the metal. Its effects on corrosion properties are not well known but it has been shown to combine with sulfur to create manganese sulfides in the metal whose geometry may play some role in the corrosion behavior of the metal.

Molybdenum: By increasing the molybdenum content in ferritic and austenitic stainless steel an increase the pitting potential while in chloride solutions was noted, possibly achieved by effecting the pit initiation process (19, 24, 25, 26).

Chromium: In metals such as austenitic stainless steel increasing the alloying elements such as nickel and chromium the general corrosion resistance stainless steel may be improved, however the higher the chromium content the greater the rate at which the pH will drop in crevice solutions for a given passive current (9). Stainless steels use added metals such as chromium (Cr) to enhance the production of a stable oxide layer (Cr_2O_3). If the oxide layer is mechanically breached it may experience temporary corrosion, however after a short period of time and under relatively mild conditions it will regenerate. In the case of stainless steel, a buildup of chromium occurs on the surface during active dissolution of the Fe^{2+} metal ions, which is generally required before passivation occurs (4).

Nickel: Nickel acts as an austenitic stabilizer when introduced in sufficient quantities. It also has the benefits of helping to promote repassivation and to reduce the occurrence of stress-corrosion cracking (24).

Carbon: Although carbon doesn't seem to play a great intrinsic role in the metal's corrosion characteristics it does have a role to play in forming carbides (24). 316L has a very low carbon content reducing the risks associated with sensitization during welding.

3.3.1.2 Eh-pH Diagrams for Sulfuric Acid and Salt Solution

Diagrams are generated using HSC Chemistry 5.1. The accuracy of these diagrams were not confirmed using any other sources and are used only in minor interpretations of the test data.

For pure 1M H₂SO₄ solution, same diagrams are produced for nickel sulfate solutions:

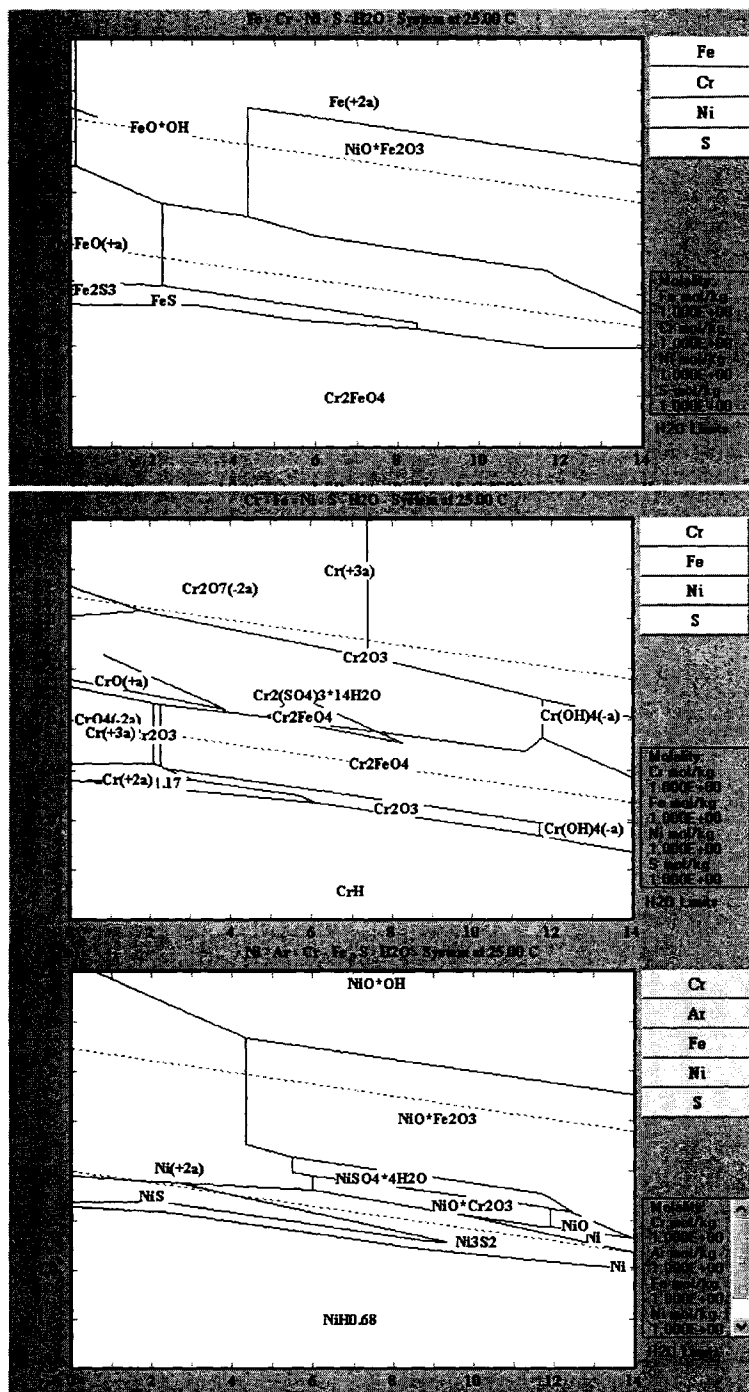


Figure 14: Eh-pH or Pourbaix Diagrams of Fe, Ni and Cr for pure 1M H₂SO₄ solution (44)

For 1M H₂SO₄ solution containing Nickel Sulfate and Nickel Chloride:

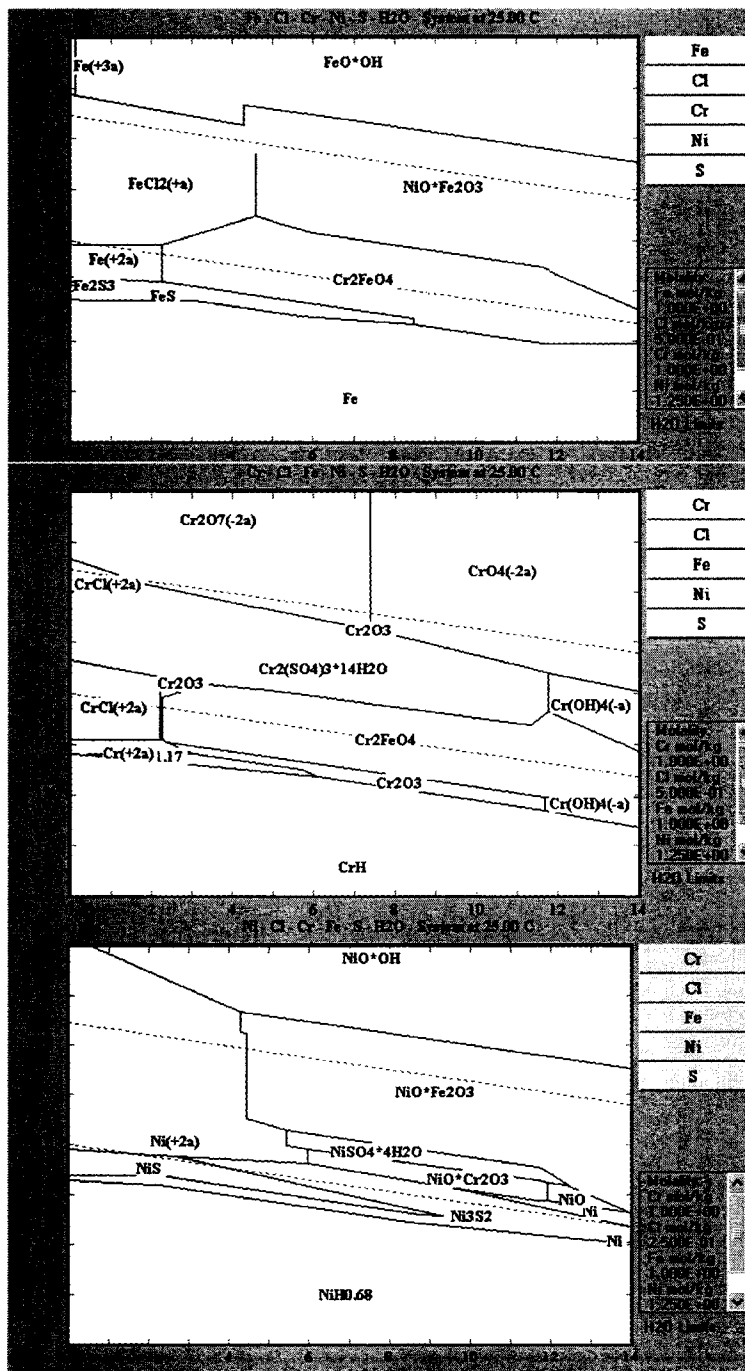


Figure 15: Eh-pH or Pourbaix diagrams of Fe, Ni and Cr in 1M H₂SO₄ solution containing Nickel Sulfate and Nickel Chloride (44)

For 0.6M (3.5%) NaCl solution:

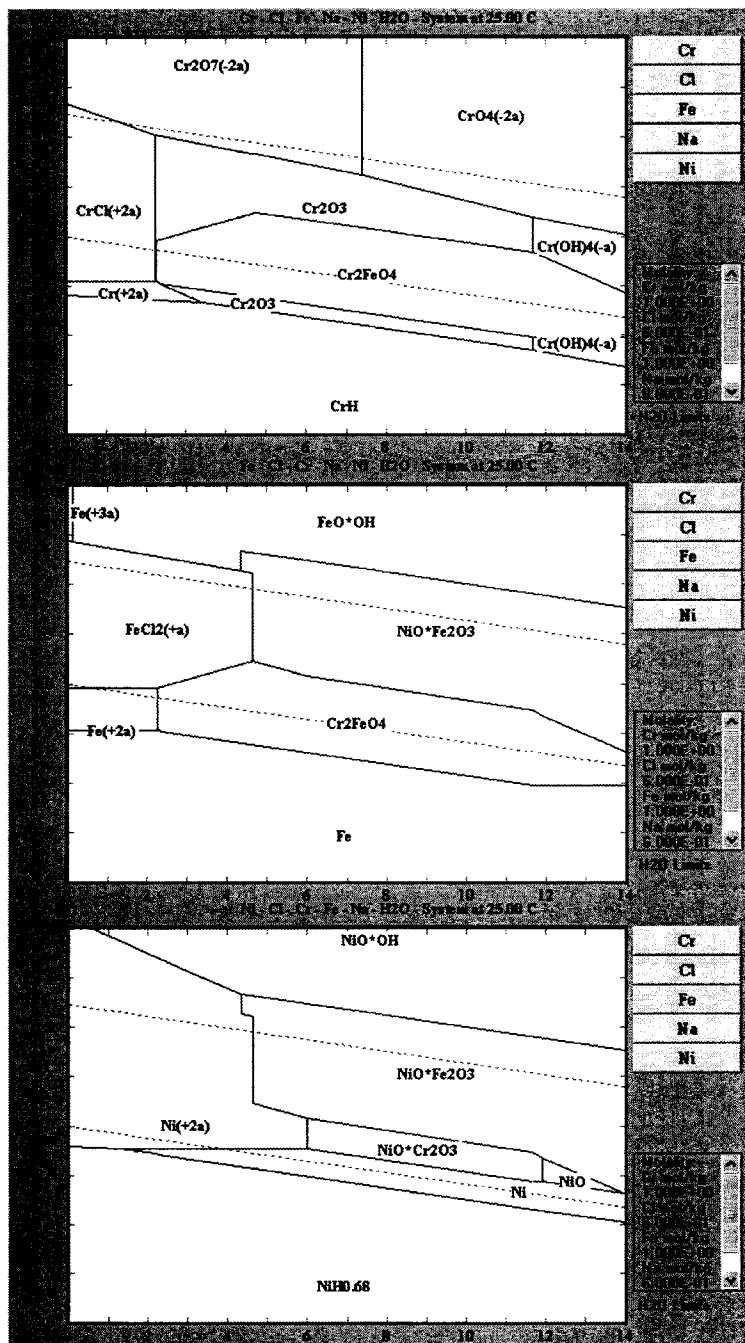


Figure 16: Eh-pH or Pourbaix diagrams of Fe, Ni and Cr in 0.6M NaCl (44)

3.3.1.3 Surface Feature and Inclusion Types, Shapes, and Effects

Images of the actual inclusions present in the 316L stainless steel samples tested are presented in (Figure 17). These images were acquired using a Scanning Electron Microscope (SEM) and the composition of these inclusions were attained using a set of Energy Dispersive Spectroscopy (EDS) tests at a variety of sites on sample surfaces that were not corroded.

The 316L sample was polished to 1 μm and is seen at the same magnification as is observed during testing Figure 17. The metal surface reveals inclusions including Cr_{23}C_6 (larger angular inclusions) and sulfide inclusions including manganese sulfide (MnS) small rounded inclusions. One silica rich inclusion was also located displaying an elongated structure; see Figure 107. The EDS results showing the composition of these inclusions is shown in Appendix A. The EDS results were used in combination with images of etched samples showing various inclusion types as seen in the American Society for Metals (ASM) Handbook (45) to confirm the type and behavior of these inclusions.

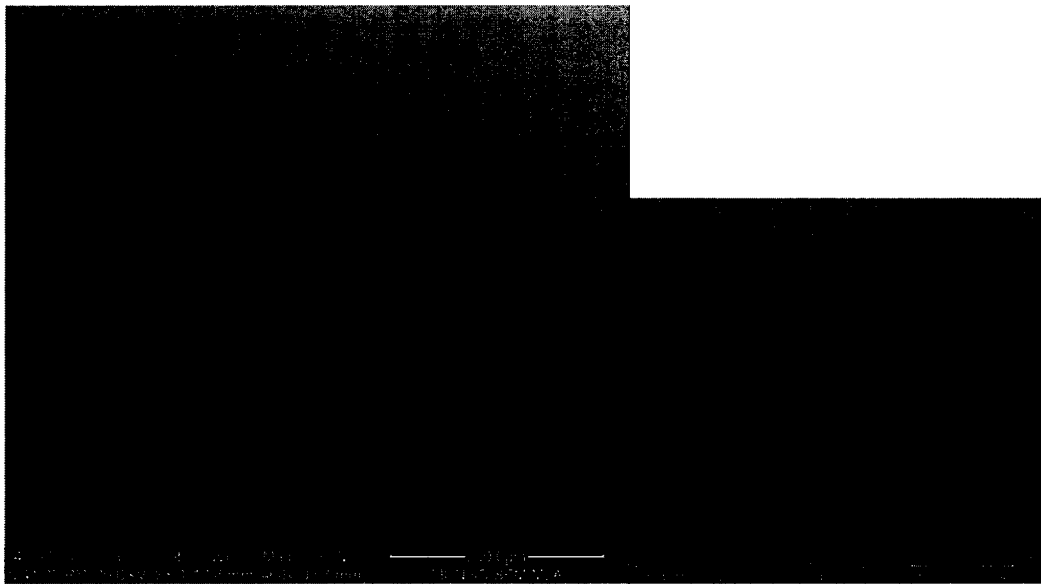


Figure 17: Image on 1 μm polished 316L metal surface showing inclusions including M_{23}C_6 (larger angular inclusions) and sulfide inclusions (small rounded inclusions), the image on the left is to the same 0.5 mm tall scale as the in-situ images and was acquired using an SEM.

3.3.1.3.1 Chromium and Iron Carbides

The 316L samples used contain high chromium content and a low carbon content reducing the risk of sensitization which typically occurs when held at 426 to 815°C. The heat treatment of the samples was also designed to avoid long exposure to this range of temperatures. This would normally produce chromium carbides (mainly Cr_{23}C_6) (4, 25), which if left to develop for a sufficient amount of time could result in the depletion of local chromium content. If the chromium content goes below 10% due to this phenomenon then the grain boundaries will be preferentially corroded (4, 9, 25). Similarly iron carbides Fe_{23}C_6 and Mo_{23}C_6 are also possible but do not have the same effects on chromium content of surrounding metals but may play a role in the formation of anodic and cathodic sites on the surface (45).

3.3.1.3.2 Sulfide Inclusions

Sulfide inclusions are common to stainless steel due to the sulfur impurity present in the metal. For stainless steels a variety of different types have been identified (Fe, Al, Cr, Mn, Ti, Ni)S and also mixed sulfide-silicate inclusions etc. (1, 16, 46, 47, 48, 49).

These inclusions have an associated negative enthalpy for the following transformations:

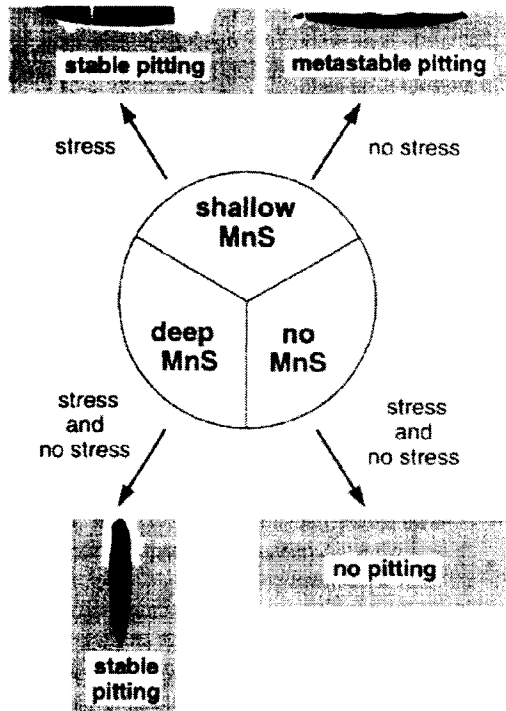
Reaction	$\Delta^{\circ}H$ (Kcal/mol)
$FeS + Cr \rightarrow CrS + Fe$	-48
$MnS + Cr \rightarrow CrS + Mn$	-50
$NiS + Cr \rightarrow CrS + Ni$	-22
$3FeS + 2Cr \rightarrow Cr_2S_3 + 3Fe$	-144
$3MnS + 2Cr \rightarrow Cr_2S_3 + 3Mn$	-150
$3NiS + 2Cr \rightarrow Cr_2S_3 + 3Ni$	-64

Table 2: Enthalpy values associated with sulfide inclusions (1, 47)

The negative enthalpy value for these reactions means that they have an autocatalytic nature and will occur spontaneously under the correct conditions.

Manganese sulfide inclusions is of particular interest as it has been found to have a negative effect on the metal's performance as it acts as a nucleation site for pitting (16, 71). This is supported by test results indicating that the highest amount of adsorbed chlorides may be found on stainless steels containing high levels of sulfur (1, 50). In other tests with NaCl it was found that when highly dispersed these inclusions generally formed smaller less dangerous pits (16). Some other tests have shown that the inclusion

often simply dissolved leaving behind a cavity in the surface (1, 49). The shape of the cavity depends largely on the shape of the original inclusion which in turn effects the initial pitting behavior (49). See Figure 18.



Types of pitting observed at MnS inclusions on 304 SS in 1 M NaCl with and without applied stress.

Figure 18: Types of MnS inclusions and their pitting behavior (49)

3.3.1.3.3 *Smaller Nucleation Sites*

Some small nucleation sites are also attributed to causing more pitting. Although little is yet known of these sites some are theorized as being caused by the presence of small iron-rich clusters (45, 16).

3.3.1.3.4 Mechanical Defects

Mechanical defects such as surface roughness, scratches, cracks and triple points at grain boundaries may act as nucleation sites due to high local stress or relative susceptibility of the metal structure to pitting (1, 4, 16). Rough surfaces also provide increased surface area as compared to a similarly exposed smooth surface. This additional surface area can lead to an increased number of pitting sites (1).

3.3.1.4 Common Pit Structures

Pitting may be seen in a variety of shapes and sizes, often with deceptively small surface area but significantly larger internal diameter. Images of pits that formed on stainless steel samples are shown. The metal type and solution is not the same as those used during testing however the pits seen are similar to those one would expect under polarization conditions (16). See Figure 12 and Figure 19.

The shape of pits seen on the surface is largely controlled by the internal geometry of the pit. A theoretical growth structure is theorized where the internal growth of the pit undercuts the surface of the metal creating the porous cap seen in many pits (16, 51). See Figure 20 (16).

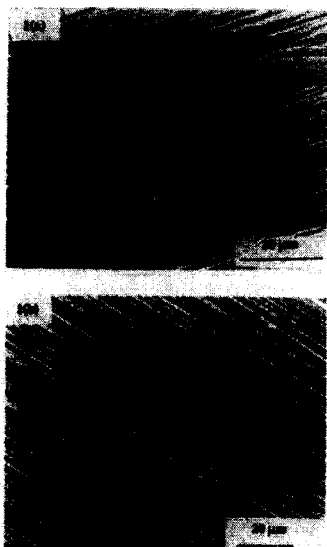


FIGURE 3.6 SEM Micrographs of covered pits on (a) type 304 stainless steel, showing a circular symmetry, with collapse of the central part of the cover into the pit, (b) type 2304 stainless steel, showing a more complete cover with many tiny perforations, and (c) the pit in (b) viewed using backscattered electron to show the underlying structure. Source: N. J. Laycock, S. P. White, J. S. Noh, P. T. Wilson, R. C. Newman, *J. Electrochem. Soc.* 145 (1998): p. 1101, reprinted with permission.

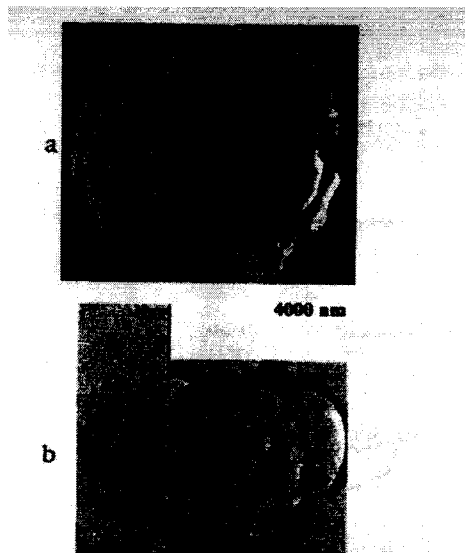


FIGURE 3.8 (a) TEM image of a pit showing a pit cover with the passive film and lacy structure. The passive film grown at 0.8 V shows a distinct tear and that the pit cover was at an angle to the surface. (b) an enlargement of the pit cover in (a) with an inset showing a further enlargement. Source: H. Isaacs, Y. Zhu, R. L. Sabian, M. P. Ryan, "Critical Factors in Localized Corrosion III," eds. R. G. Kelly, G. S. Frankel, P. Naeishan, R. C. Newman, *Electrochem. Soc. Proc.* 98-17 (1998): p. 376, reprinted with permission.

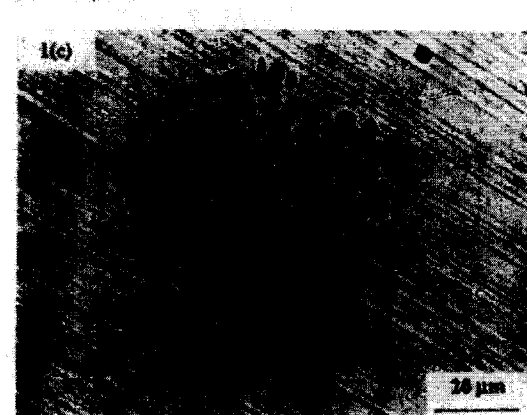


FIGURE 3.6 (Cont.)

Figure 19: Pits seen forming on surface of 304 stainless steel (16).

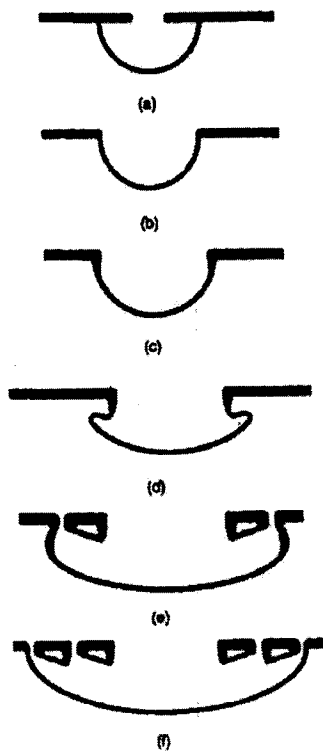


FIGURE 3.7 Schematic of lacy metallic cover formation in pitting of stainless steels. Bold lines indicate passive metals Source: R. C. Newman, *Corrosion*, 57 (2001); p. 1031.

Figure 20: Schematic of lacy metal cover formation (16).

3.3.2 Titanium Specific Information

Titanium alloys are highly corrosion resistant, have great strength, hardenability, and light weight with a density 56% that of steel. Titanium is also described as being immune to corrosion in saltwater, erosion resistant and is highly efficient at performing heat transfer (52). Titanium works well in a variety of highly oxidizing environments due to the fast forming TiO_2 oxide layer, and remain corrosion resistant throughout most temperature ranges. A limitation on this metal is that it does not readily produce a stable oxide layer in highly reducing environments, although even this limitation may be addresses through the addition of certain metal ions and chemical additives, and it does not work well in solutions containing fluorine or fluorides (52). The addition of aggressive agents such as oxygen, chlorine, bromine, nitrate, chromate, permanganate, molybdate and cationic metallic ions, such as ferric (Fe^{3+}), cupric (Cu^{2+}), nickelous (Ni^{2+}), and many precious metal ions to a reducing solutions will act as potent inhibitors even in the range of 20-100ppm (52).

For reasons of cost some autoclaves will use an explosion bonding process, fusing 6-8mm of titanium to 100mm steel, resulting in a significantly different stresses and grain structures on the material surface (34, 53). This may effect the corrosion behavior of the metal during service as apposed to most titanium testing done to date which uses standard titanium sheets and rods as material sources.

Titanium is considered extremely resistant to sulfuric acid solutions. Pitting is not reported for saturated chloride containing solutions within a sulfuric acid concentration range of 0-50% (35).

3.3.2.1 Eh-pH Diagrams for Sulfuric Acid and Salt Solution

Eh-pH diagrams (Pourbaix diagrams) for titanium in sulfuric acid and water containing chloride ions (equivalent to salt water) are presented below.

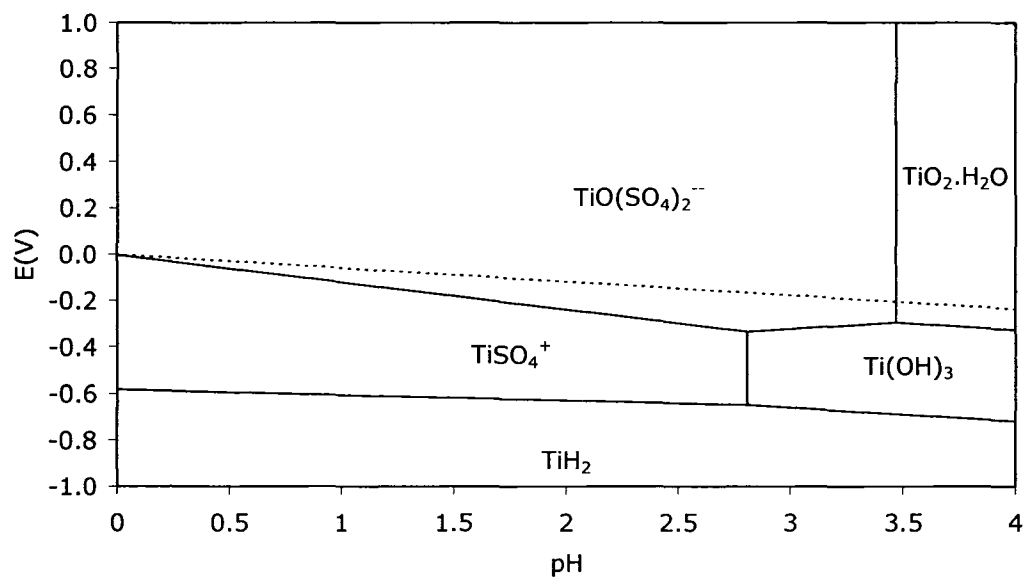


Figure 21: Eh-pH diagram, Ti-SO₄⁻-H₂O, 25°C (36)

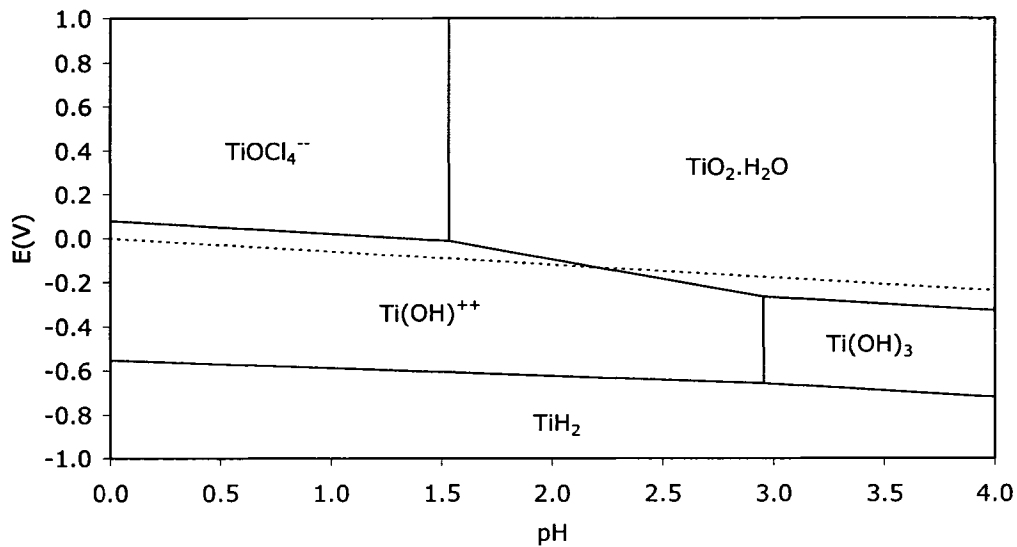


Figure 22: Eh-pH diagram, Ti-Cl⁻-H₂O, 25°C (54)

3.3.2.2 Oxide Types

The passive oxide layer is typically TiO_2 , $TiO_2 \cdot 2H_2O$, $Ti(OH)_4$, although the accuracy of the Pourbaix diagrams is a matter of some discussion (33, 34, 52). TiO_2 is highly corrosion resistant but may be susceptible to pitting when immersed in certain HCl, H_2SO_4 , NaOH and HF acid solutions (25, 55). After corrosion testing an increase in sample mass may be measured due to the addition of oxygen while generating the oxide layer, making accurate determination of mass loss during testing difficult (36). The rapid bonding of titanium to oxygen in the atmosphere makes deaerated testing of the metal difficult, potentially resulting in a result that reflects a mix of aerated and deaerated behaviors (36). This rapid bonding between titanium and oxygen is the metal's greatest asset regarding corrosion, as scratches in the oxide layer will immediately heal itself (52).

3.3.3 Aluminum Specific Information

A brief description of aluminum's basic corrosion properties is discussed in this section; however as aluminum is not a primary focus for this research it is not extensively detailed.

Aluminum is a common component of electronic devices and is commonly used as an electrical conductor resulting in natural polarization (15). These conditions make it of interest for corrosion research regarding reactions of electronic component exposure to water. Aluminum alloys are also used in various cooling systems in which corrosion due to exposure to water and ethylene glycol are of interest (56).

Testing procedures for this metal are available from the Annual Book of ASTM Standards sections G5 and G69-97 (5).

3.3.3.1 Oxide Types

Aluminum oxide Al_2O_3 is the transparent and very hard oxide which forms this metal's passive layer (4). When present in sufficient quantities may appear as a white powder on the surface of a metal (56). Although not easily pitted in aerated solutions containing most nonhalide ions it is highly reactive to halide ions including chloride ions which readily penetrate this oxide layer (57). When exposed to saltwater solutions it will typically have already reached the transpassive state (4).

3.3.4 Visual Analysis Techniques and Applications

3.3.4.1 Raman Spectroscopy and Microscopy

This technique uses a laser and a spectrograph to record data on the chemical composition, molecular structure and molecular interactions on a materials surface while immersed in a test fluid. The analysis performed may be of use in determining the nature of corrosion reactions observed within a given area of the surface (58, 59, 60, 61).

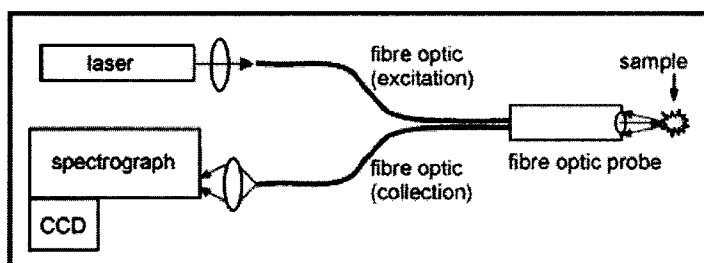


Figure 23: Raman spectroscopy illustration (60)

3.3.4.2 SPM and AFM Systems

Scanning probe microscopes (SPM) with a variant known as an Atomic Force Microscope (AFM) are developed to image a metal's surface and to potentially measure a point's open circuit potential on a surface with great accuracy (62). SPM uses a probe to map the surface topography of a sample and is capable of imaging a surface in great detail while in solution, but has limitations on imaging speed and has high associated cost (38, 63). See Figure 24.

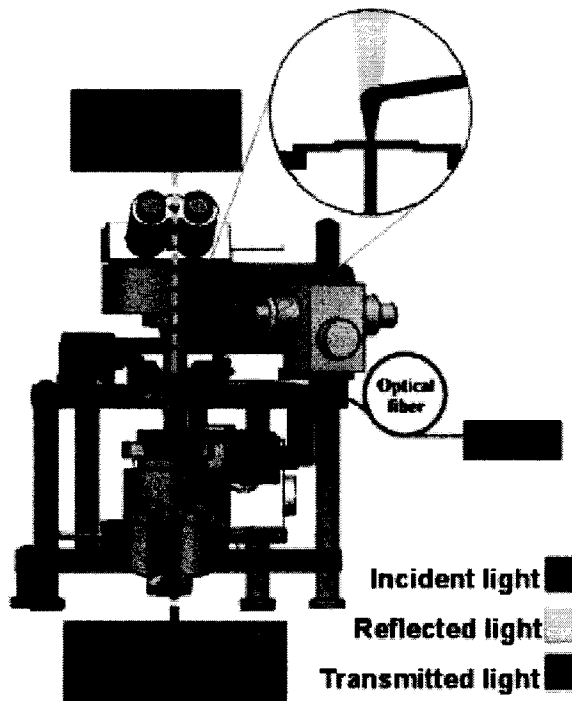


Figure 24: Illustration of a scanning probe microscope (63)

3.3.4.3 Electrochemical Droplet cells

Droplet cells are a corrosion apparatus that incorporates the typical methods of polarization testing into a form that allows its application to a small area on a material's surface using a droplet of fluid. The droplet cell may be used to observe the corrosion reactions taking place in a drop of water on a metal surface during testing by looking through a glass tube containing electrolyte at 45° (64). See Figure 25.

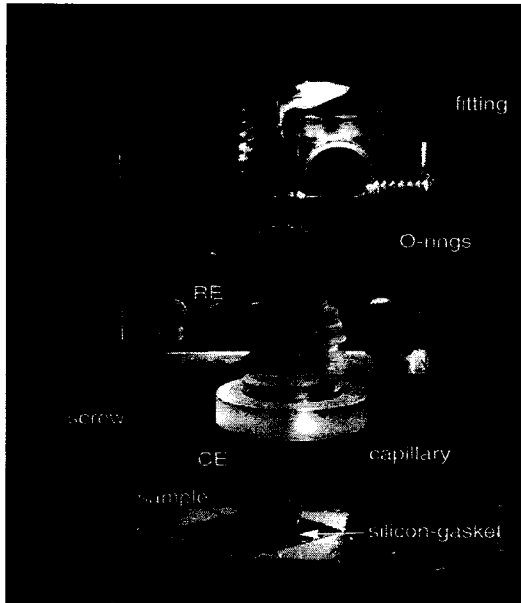


Figure 25: Image of a droplet cell (64)

3.3.4.4 XANES

X-ray absorption near edge structure (XANES) is a technique that uses x-rays to examine the oxidation state of materials being observed. The system may be used to record the changes in the atomic structures on a material's surface (65).

3.3.4.5 Contrast Enhanced Microscopy and Elliptical Microscopy for Surface Imaging (EMSI)

This is a testing technique which allows for in-situ testing of a similar nature to those conducted with the modified in-situ techniques used in the research conducted for this thesis project (48, 61). This technique may be combined with elliptical microscopy for surface imaging (EMSI) to generate images of pits and changes in surface layer

thicknesses with a resolution of $2\mu\text{m}$ for contrast enhanced microscopy (48, 61) and $12\mu\text{m}$ for EMSI (48).

This technique offers similar results to those obtained with this project's in-situ optical microscopy apparatus but appears to incorporate a more elaborate setup. See Figure 26. This would likely present a greater overall cost to construct than the process developed for testing using standard microscopes as used in this thesis.

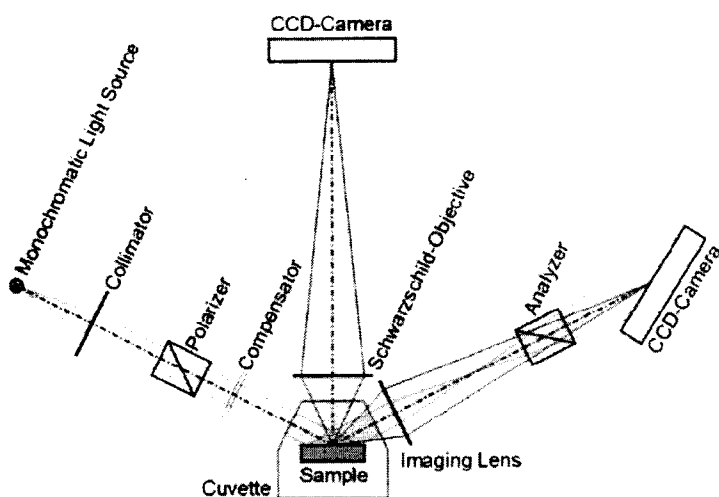


Figure 26: Contrast enhanced microscopy and EMSI apparatus (48)

3.3.5 Areas of Technical Interest in the Scientific Community

The abilities of in-situ optical microscopy present opportunities for cost effective corrosion testing and modeling. Areas and abilities that are of benefit to scientists and engineers include:

- Can pause testing at a precise point of interest in the corrosion process based on visual observations and measurements, allowing the evaluation of corrosion based on details such as gas evolution and changes in pitting characteristics. The ability to pause testing and examine in-situ would have been of great benefit to corrosion studies that examined metastable pitting and artificial pit behavior (20).
- Existing studies using in-situ techniques developed around the more complicated apparatus of Raman, XANES, SMP and EMSI may be reproduced using these techniques at a much lower cost but with similar results.
- Pit initiation studies may be conducted without the interruptions associated with conventional testing techniques and without considerable cost.
- Examination of the progression of corrosion on a specialized circumstance basis, such as the examination of scratches and other holidays in protective coatings on metals may benefit from using these techniques (4, 9).

- The process may be used to augment and record the progression of artificial pitting experiments such as those tested in the literature (30). Using this new data it would be possible to clearly identify the progression of pits and any surface changes that may be interpreted as inconsistent with natural pitting.
- In-situ studies of stress corrosion cracking and its visible surface features would benefit greatly by adopting in-situ techniques adding further details to works performed in the literature (28, 29).
- Visual studies regarding the reversibility of chemical reactions and the evenness of metal electroplating techniques may be possible.
- Evaluation of chemical corrosion inhibitors on a microscopic basis may be augmented improving existing analysis methods in the literature (6). Details such as peeling events and corrosion around inclusions may be monitored in addition to pitting and etching behaviors.
- May act as a means of measuring the depth of surface material lost during active dissolution through changes in the focus of the microscope during testing.

- Observations of unstable oxide formations on surface which would normally react with air once removed from standard corrosion test apparatus are possible using this technique.
- Evaluation of corrosion effects on soldered connections exposed to fluids. The system can be used to observe the polarizing effect of an electrical circuit on itself and add more detail to existing studies in the literature (15). It may also be used to evaluate the corrosion protective coating on a connection or connector exposed to a corrosive environment.
- The system can evaluate the presence of pitting for metals that lack a distinctive pitting potential on potentiodynamic scans. It can also give a more accurate estimate of the incubation period of pits under potentiostatic testing and more information into the etched behavior of samples during testing.
- Comparison of the pitting behavior on microelectrodes to standard size samples across a range of potentials may be performed with particularly useful results as the entire sample surface may be observed during testing. The ability to monitor the entire surface would allow the polarization data to be directly linked to individual pit formations as most or all of the pitting events and etching may be monitored.

4 Experimentation Materials and Equipment

4.1 Experimental Metals

4.1.1 Stainless Steel

Testing used a set of annealed 316L stainless steel samples with the base metal provided by Russel Metals. Precise material composition provided by Venus Wire Industries are given in Appendix B.

4.1.2 Titanium

Grade 2 titanium samples were taken from a sample provided by Inco. A second set of samples were taken from a titanium welding rod composed of Grade 2 titanium labeled as AFM ERTi-2. The composition of this material is confirmed to be within the specifications listed for Grade 2 Ti by the manufacturer American Filler Metals (66)

All test samples are polished to 1 μm , cleaned with acetone, rinsed with deionized water and quickly weighed limit exposure to air before testing reducing the degree to which the oxide layer may form before exposure to the solution (34, 36).

4.1.3 Aluminum

Samples of 6061 Aluminum were tested. They were taken from a bar of 1 inch round stock for which the heat treatment was not known. These samples were not stress relieved and most likely suffered from increased susceptibility to end grain attack.

4.1.4 Magnesium

A sample of magnesium was obtained and tested using an EDS scan to confirm its composition. The results indicated that the sample was almost pure magnesium with some minor trace elements present.

4.2 Experimental Solutions

4.2.1 Sulfuric Acid Based Solutions

4.2.1.1 Aeration

Tanks of oxygen and argon are used during testing to ensure the solution is aerated or deaerated as chosen for each test.

4.2.1.2 Base Solution

Reagent grade sulfuric acid is used in all tests, and is mixed with deionized water. Base solution is 1M H₂SO₄, which is of similar concentration to that used by Snow (1).

4.2.1.3 Various Mixes of Solution

A variety of different solutions were created and tested during the SB series.

Table 3: Solution compositions and pH for SA and SB series tests
Solution 1: SA Series

Electrolyte	Molar Concentration	Solution Composition (g/L)	Mass %	Theoretical pH:	Measured pH at 20.2°C:
Nickel Sulfate	0.00	0.00	0.00		
Nickel Chloride	0.00	0.00	0.00		
Sulfuric Acid	1.00	98.08	9.39	-0.30	0.260
Water	Remainder	946.70	90.61		
Total(s)		1044.77			

Solution 2: SB5-SB8

Electrolyte	Molar Concentration	Solution Composition (g/L)	Mass %	Theoretical pH:	Measured pH:
Nickel Sulfate	0.25	65.72	6.09		
Nickel Chloride	0.00	0.00	0.00		
Sulfuric Acid	1.00	98.08	9.09	-0.30	0.029
Water	Remainder	914.95	84.82		
Total(s)		1078.74			

Solution 3: SB9-SB12

Electrolyte	Molar Concentration	Solution Composition (g/L)	Mass %	Theoretical pH:	Measured pH:
Nickel Sulfate	0.15	39.43	3.64		
Nickel Chloride	0.10	23.77	2.20		
Sulfuric Acid	1.00	98.08	9.06	-0.30	0.102
Water	Remainder	920.95	85.10		
Total(s)		1082.23			

Solution 4: SB13-SB16

Electrolyte	Molar Concentration	Solution Composition (g/L)	Mass %	Theoretical pH:	Measured pH:
Nickel Sulfate	0.00	0.00	0.00		
Nickel Chloride	0.25	59.43	5.46		
Sulfuric Acid	1.00	98.08	9.02	-0.30	0.097
Water	Remainder	929.96	85.52		
Total(s)		1087.46			

Solution 5: SB1-SB4

Electrolyte	Molar Concentration	Solution Composition (g/L)	Mass %	Theoretical pH:	Measured pH:
Nickel Sulfate	0.25	65.72	5.54		
Nickel Chloride	0.00	0.00	0.00		
Sulfuric Acid	3.39	332.04	28.01	-0.83	-0.760
Water	Remainder	787.80	66.45		
Total(s)		1185.55			

4.2.2 Artificial Seawater Salt Solution

A test solution of 35 g/L reagent grade NaCl was mixed using deionized water.

4.2.2.1 Aeration

As most bodies of water experience considerable aeration and there is no means of accurately measuring aeration during these tests a continuous supply of oxygen is used in all tests, saturating the solution with oxygen.

4.2.2.2 Solution Composition

The solution consists of 35g of certified American Chemical Society (A.C.S.) NaCl in every 1 liter of test solution. This NaCl solution is considered adequate for testing despite not containing chemicals such as calcium found in real seawater.

4.3 Experimental Equipment

4.3.1 Test Cell (refer to other section)

4.3.2 Image and Video Capture Equipment

An Olympus Stylus 710 digital camera with a 7.1 megapixel resolution was used with a custom built microscope camera mounting arrangement equipped with a custom made electronic timing device. The timer assembly was developed to take photographs at one minute intervals, as well as to output a video image to the Centrios DVD+R Video Recorder. A model CB-MA1 adapter with an AC Adapter model D-7AC was used to power the camera and allow for a direct video feed to the DVD recorder.

4.3.3 Potentiostat

All polarization testing was conducted using a Princeton Applied Research model 273A Potentiostat/Galvanostat. This device was controlled by a IEEE-488 (GPIB) computer interface using PowerCorr Software

4.3.4 Reference Electrode

Potentials were measured with respect to an Accumet saturated calomel reference electrode with porous ceramic junction. PowerCORR Software automatically converted all values to the standard hydrogen cell potential presumably by adding 0.241 V (4).

4.3.5 pH Meter

Measurement of all real pH values is done using a SevenGo pH/ORP/Ion meter SG8 by Mettler Toledo.

4.3.6 Mechanical Polisher

Samples were prepared in part using a Minimet Polisher manufactured by Buehler Ltd. Buehler sanding discs and Aerosol spray diamond compound (1 and 6 μm).

4.3.7 Constant Temperature Bath

A NESLAB RTE-111 constant temperature bath is used to maintain a 25°C fluid temperature during testing.

4.3.8 SEM/EDS

SEM and EDS tests were performed using the Quanta 400 by FEI.

4.3.9 Software

- 1) PowerCORR software was used to record and control all potentiostatic and potentiodynamic tests. It was also used to calculate i_{corr} and the corrosion rate in mpy from potentiodynamic test results.
- 1) HSC Chemistry 5.1 was used to generate Pourbaix diagrams for all stainless steel tests. © 2001-2005 ESM Software
- 2) ANSYS was used for a thermal analysis of the corrosion cell to ensure a sample temperature of 24°C \pm 1°C was attained.

4.4 Surface Preparation Techniques and System Maintenance Procedures

4.4.1 Basis of Sample Preparation Procedures

4.4.1.1 Roughness

Surface roughness has been linked to an increase in the number of nucleation sites on a sample, although due to the increased surface area associated with rough surfaces there are actually fewer sites per square centimeter of surface area (1). The visual testing process used for experiments works best on highly polished surfaces due to the improved contrast between pits and the surrounding material. As the surface of the sample is more consistent across the surface when highly polished, the data acquired from a small area is more likely to be accurate for the majority of the sample's central surface area. For these reasons, and to reduce the role of engrained stresses in the sample, a 1 μ m polished surface is chosen as the standard for use in testing.

4.4.1.2 Engrained Stresses (Tensile and Compressive Effects, refer to sections 3.3.1.3.4 and 4.1)

During the manufacturing process, and the process of preparing metal samples for testing certain compressive and tensile stresses are created in the material. Compressive stresses in the material make the material more corrosion resistant locally, while tensile stresses

are more easily corroded (4). Ideally during testing it is best to have a consistent surface to work with, one that can be used to evaluate materials used in real world applications. Testing done on this project attempts to attain a surface with a consistent minimal stress level across the surface through sanding using a set of progressively finer silicon carbide sandpapers and diamond polishing compounds. In the case of the 316L stainless steel samples heat treatments are also used to create a uniform stress free sample surface. The treatment of the samples is described in detail in each test section.

4.4.1.3 Heat Treatment

Appropriate heat treatment relieves stresses locked inside samples, reducing the tendency of some metals to corrode in uneven and unwanted ways. The 316L stainless steel samples are annealed in air at 1100°C so as to reduce the occurrence of end grain corrosion due to the residual stresses from the steel rod manufacturing process (1, 4). This also had the effect of allowing carbide precipitates to dissolve and to create an equiaxed microstructure (1). This allowed inclusions such as sulfides to spheroidize thereby improving the overall corrosion resistance of the alloy.

Due to the small lot size used in testing other metals, and the effect of heat treating samples with unique existing heat treatments no other metal samples were heat treated.

4.4.2 Metal Sample Preparation Procedures

All different metal types prepared separately to avoid cross contamination. The preparation procedure is based on typical preparation practices used on 316L stainless steel (67) where the surface is machined, progressively sanded and polished to a 1 μ m finish then cleaned with acetone and rinsed with deionized water.

Engineering Building Performed Activities:

- Heat treat metals if required under individual test criteria.
- Remove any thick metal oxides from the back of the sample to ensure good electrical contact.
- Machine the front face of the samples on a lathe.
- Hand sand with 220 to 600 grit silicon carbide sand paper.

IIC Building Performed Activities:

- Final sample preparation is to be performed no more than 15 minutes before testing is to begin to avoid formation of oxide layer due to reaction with the atmosphere. Standard cleaning steps are taken after each step in the polishing process and are based on ASTM G1 cleaning procedures (5).
- Using Minimet Polisher sand surface with 600 grit silicon carbide sandpaper.
- Using Minimet Polisher diamond polish the surface to a 6 μ m finish.
- Using Minimet Polisher diamond polish the surface to a final 1 μ m finish

4.4.3 Experimental Procedures for Potentiodynamic and Potentiostatic Tests

- Prepared equipment by placing 300mL of fluid into the upper container and beginning aeration for 10 minutes before starting the flow. See Figure 27.
- Ran the solution through the system using the bypass loop for 20 minutes to ensure the remaining fluid in the system does not contact the sample surface in its pure form, and to ensure that the aeration of fluid in the lower tank and temperature is given time to stabilize.
- Calibrated the flow rate of fluid in the system to the chosen test rate.
- Finished preparing the sample surface no more than 15 minutes before beginning flow to reduce the formation of an oxide layer.
- Weighed the sample.
- Performed a final degreasing of the metal surface using acetone.
- Clean thoroughly with deionized water.
- Transferred the flow through the bypass line to the corrosion cell and inserted the reference electrode once the luggin probe is filled with fluid. Adjusted luggin probe to remove any trapped gas bubbles from the chamber.
- Measured the corrosion potential of the sample for 60 minutes while waiting for the stabilization of the measured mixed potential. Also began recording pictures and video at the start of this period.

- Began potentiodynamic or potentiostatic testing in accordance to chosen test criteria.
- Once test was completed stopped the video recording and took pictures of any areas of interest across the surface before stopping the fluid flow.
- Began test equipment cleaning procedure when appropriate.
- Reweighed the sample and scan the front surface as a visual reference.

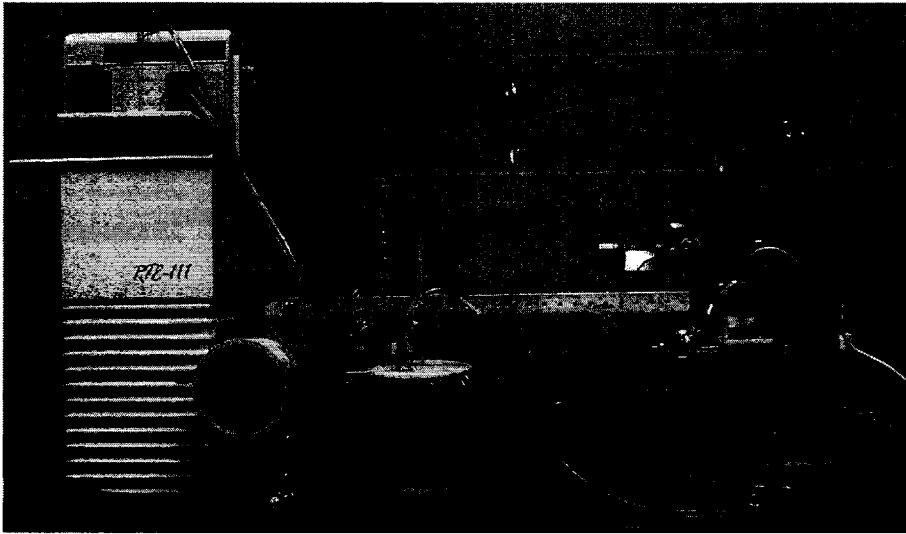


Figure 27: Corrosion test apparatus.

4.4.4 Test Equipment Cleaning Procedure

- Purged the system using 150ml of deionized water to remove any hazardous chemicals and residues.
- Remove sample from cell and remove test cell from system if required.
- Remove test beakers 1 and 2 from the system with float beaker 3.

- To clean the Tygon tubing install the cleaning beakers to replace beakers 1 and 2 in the system, and cycle 500ml of deionized water through the system for a minimum of 10 minutes using the bypass loop or through the test cell if test cell cleaning procedure is in use.
- Purge any remaining water from the tubing using a pipette bulb.
- Clean test beakers and float in tap water and paper towels, followed by cleaning with ethanol and a final rinse with deionized water.
- Clean test cell according to cleaning procedure (a), (b) or (c) as appropriate.
- Reassemble the test cell to original configuration. See Figure 28.

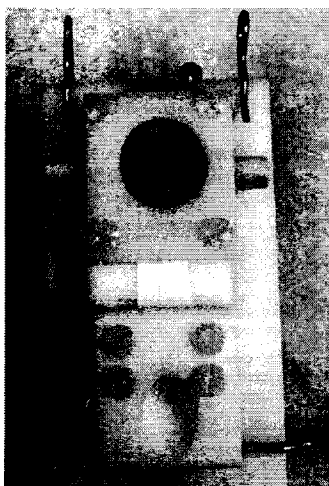


Figure 28: Corrosion test cell.

4.4.5 Test Cell Cleaning Procedure

(a) Complete Cell Rebuild

- Occasional use for cases where residue from previous experiments threatens to contaminate upcoming tests.

- Remove test cell from system and fully dismantle.
- Dispose of all used Teflon tape as well as any other disposable materials.
- Hand clean all components using paper towels water and ethanol.
- Place in Sonic Cleaner for 1 hour using deionized water.
- Reassemble the test cell to original configuration. See Figure 28.

(b) Moderate Cell Cleaning

- Used for cleaning the cell when starting a new batch of tests that does not contain chemicals that were used in previous tests. Example: Switching from chloride containing tests to a set of tests theoretically free of chloride ions.
- Remove test cell from the system.
- Clean all ports and accessible areas with ethanol and a cotton swab
- Place in Sonic Cleaner for 1 hour using deionized water.
- Reinstall into the system.

(c) Light Cell Cleaning

- Used for cleaning the cell between tests using similar fluids containing the same types of chemicals.
- Leave the cell connected to the system.
- Clean the inner surface of the glass with a cotton swab and deionized water through the access port.
- Clean any accessible surfaces with visible contamination.

4.5 Design of Corrosion Cell and Support Equipment

4.5.1 Background Information

Corrosion of metals in various environments such as microelectronics, industrial metal products and transportation etc., has been a significant engineering challenge, not only because of the challenges in developing new materials to resist these environments, but also posing the challenge of finding new ways to quantify and confirm these properties for engineering applications.

Classically, optical microscopy and scanning electron microscopy (SEM) has been the benchmark for most analysis of the surface features and characteristics of metals after exposure to these environments over the last 25 years. The appeal of this technique is that these instruments are generally the most widely available and cost effective tool available to most laboratories. In addition to this, the use of optical and scanning microscopes for some applications requires minimal preparation and a moderate skill level to produce useful results.

The development of new methods to allow for the optical examination of samples while undergoing corrosion testing, presents a valuable tool to scientists and engineers seeking to measure and understand corrosion. The design and research techniques developed represent a first step to the cost effective application of in-situ optical microscopy to both immersion and polarization tests without interfering with standard test practices. These

optical techniques augment other technologies capable of in-situ examination of materials undergoing electrochemical corrosion. Existing technologies may be used for some studies, such as a electrochemical droplet cell used to observe the corrosion reactions taking place in a drop of water on a metal surface during testing by looking through a glass tube containing electrolyte at 45° (64). Other technologies capable of in-situ surface observations are scanning probe microscopes (SPM), and Raman spectroscopy. SPM uses a probe to map the surface topography of a sample and is capable of imaging a surface in great detail, but has limitations on imaging speed and has high associated cost, see (38, 63). Raman spectroscopy uses a directed laser to image surfaces and chemical reactions (58, 60).

4.5.2 Apparatus Design

The optical corrosion test cell was developed specifically for use with standard ASTM polarization techniques. Factors such as contamination, cleaning, maintenance, geometry, flow characteristics, positioning of the auxiliary electrode wire, and temperature were taken into account during the design process. Details of the design and early testing process were published at the 2006 NECEC conference (68).

4.5.2.1 Maintenance Considerations

Contamination of the fluid was of concern in the cell design. As the corrosion cell will be used for a variety of fluids, some of which are corrosive by nature, Teflon was used as the base material for the cell as it is resistant to most acids and is easily cleaned. Teflon has been used in similar applications such as in the design of the XANES (X-ray absorption near edge structure) cell, see Figure 30 (65), the IR cell reactors for in-situ studies of metal oxide catalysts (69), and the Raman Spectroscopy cell (59), see Figure 31. All of which share several design features with the final cell design used for these experiments. To avoid unwanted leakage on top of the cell some silicone sealant is used as a backup external seal along the outer edge of the glass cover plate; however it does not come into contact with the bulk test solution, therefore cannot contaminate the solution. A glass plate is used at the top of the cell to prevent the fluid from reaching the microscope, and to prevent air from contacting the solution during deaerated testing. Ultimately the only materials in contact with the solution inside the cell are a glass plate

at the top of the cell, a reference electrode, the auxiliary electrode, Teflon, and the working electrode. These materials are common to most typical corrosion cells used in labs and are not considered to be of any risk to cause unacceptable levels of contamination.

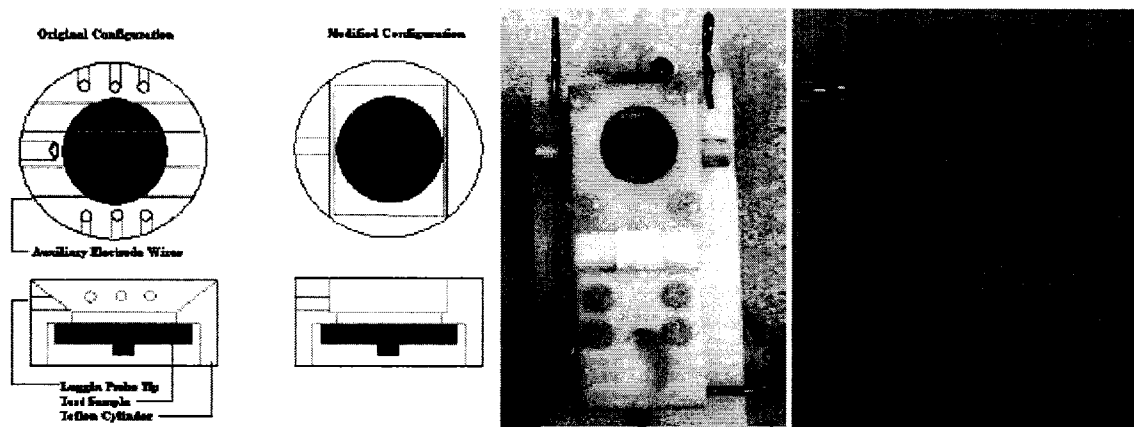
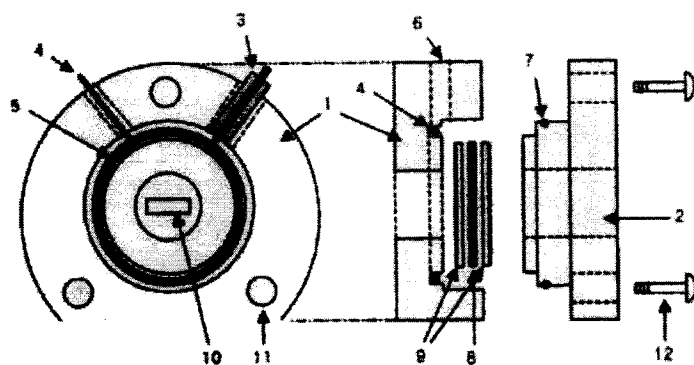


Figure 29: Internal schematic of corrosion test cell (right) showing the reference electrode (yellow), image of corrosion test cell (middle), image of corrosion test cell mounted to movable platform with vernier scale (68)



Schematic diagram of the *in situ* cell. 1: Teflon cell body 1, 2: Teflon cell body 2, 3: reference electrode, 4: Pt counter electrode, 5: groove for counter electrode, 6: hole for reference electrode and electrolyte injection, 7: O-ring, 8: carbon sheet working electrode, 9: filter paper with Kapton tape, 10: X-ray beam path, 11: screw hole, 13: screw.

Figure 30: Schematic of XANES in-situ cell (65)

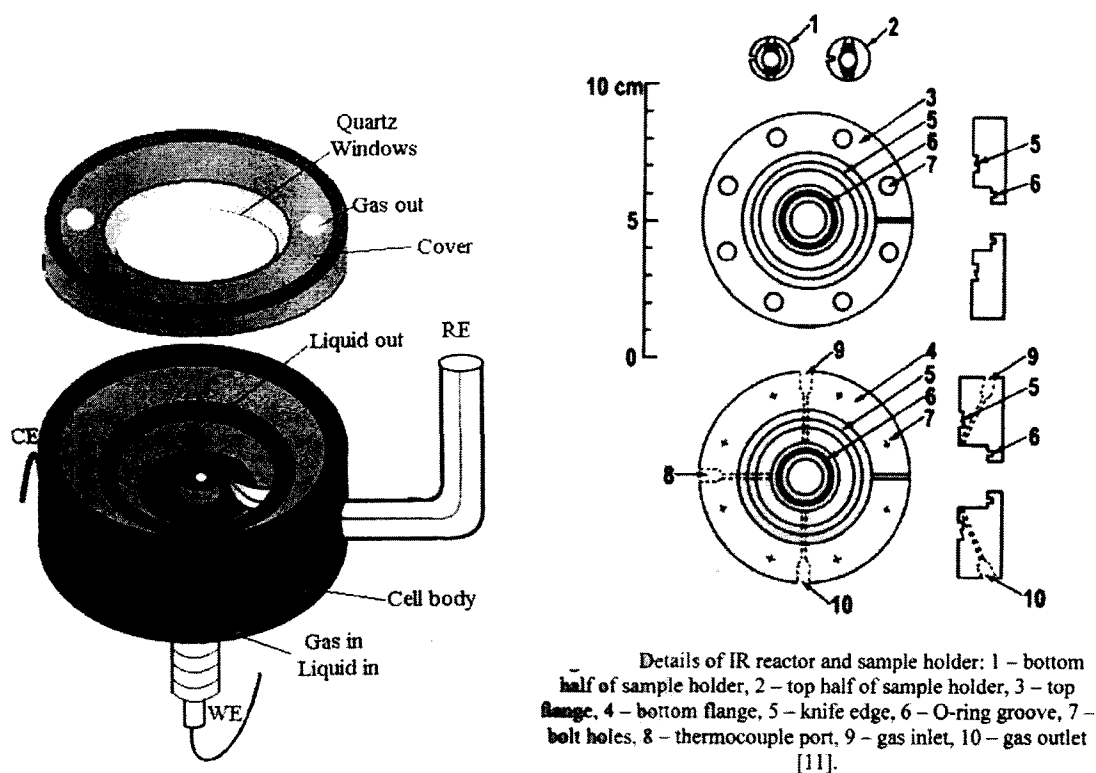


Figure 31: Figures of Raman spectroscopy cell (left) (59) and IR reactor cell (right) (69)

Contamination was also considered in the design of the pump and supporting equipment. Throughout this system materials were chosen to meet the requirements of the tests planned. Throughout the system the only materials coming in contact with the fluid is glass and Tygon R-3603 tubing. The tubing was confirmed by the manufacturer as being adequate for the task of carrying the fluid through the system (70), and to be used in a peristaltic pump which was deemed the most effective means of moving the fluid without contamination. Additionally the use of this tubing allows for the cost effective replacement of the majority of internal surfaces, which will be contaminated by various oxides and chemicals during testing.

Cleaning and maintenance is of great interest for any piece of lab equipment. The corrosion cell may be completely dismantled and cleaned thoroughly as required, however by simply running deionized water through the system followed by a thorough cleaning of the cell's internal surfaces is adequate for most tests as discussed in the test equipment cleaning procedure section. This simple cell cleaning procedure is of use for tests involving the addition of ions such as chlorine in progressively greater quantities as the series of test progresses.

4.5.2.2 Geometry Considerations

The geometry of the system is of significant importance to testing samples in accordance with the chosen standards. The system uses a built in luggin probe to connect the reference electrode to the surface so as to accurately measure the potential at the sample surface. A small tube is machined inside the Teflon block, leading from a 1mm opening 1mm above the sample surface back to the reference electrode at the rear of the device thereby meeting ASTM standards (5). See Figure 32. During all sulfuric acid tests a rubberized tape seal was used on top of the sample surface to prevent leakage due to etching under the seal and to reduce the effects of crevice corrosion. Each sample was exposed with a circular area having a 7 mm diameter. A consistent hole diameter was attained using a metal punch to make all holes consistent in size and shape. The sample mounting configuration is deemed acceptable as is similar to a cell used in ASTM G150,

called a flushed port cell, however due to limitations on time and materials the filter paper and deionized water based seal were not used on the prototype, see Figure 33 (5).

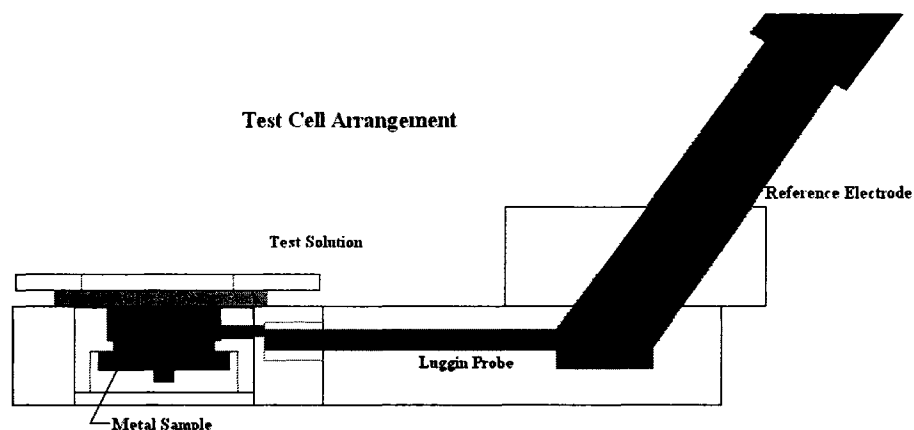


Figure 32: Cross sectional view of corrosion cell including reference electrode (68)

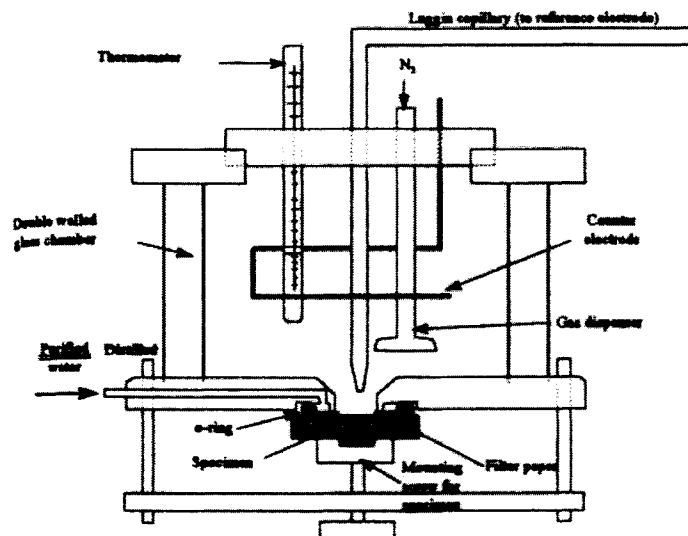


FIG. X2.1 Sketch of the Design Principles of the Flushed Port Cell

Figure 33: Sketch of the design principles of the flushed port cell (5)

The geometry of the cell surrounding the reference electrode is critical to being able to see the surface. The objective lens of the microscope will only focus within a set distance of the surface. This distance was determined before construction began. The

distance was determined to be 5.5mm, and so the combined gap between the sample surface and the top surface of the glass plate was set to this value. When filled with fluid, the optical properties change, and this minimum distance is increased to nearly 6.5 mm, giving some important extra room for maneuvering during testing as the surface may recede below it's initial surface height as the corrosion eats away at the test sample material.

4.5.2.3 Solution Flow Considerations

Some consideration was taken to maintain a uniform flow with a sustainable flow rate, see Figure 34. In an initial design the system used a series of flow tubes to evenly distribute the flow, which served to both provide a constant supply of the test fluid as well as to remove gas bubbles from the chamber. This system worked however it was replaced by the channel system (see Figure 29 for side by side images of both designs). The new design allowed for a greater flow velocity over the surface by focusing the entire flow to pass over the sample surface. This greater velocity flow helped to remove small bubbles from the area being observed so as to avoid obscuring the images taken from the microscope.

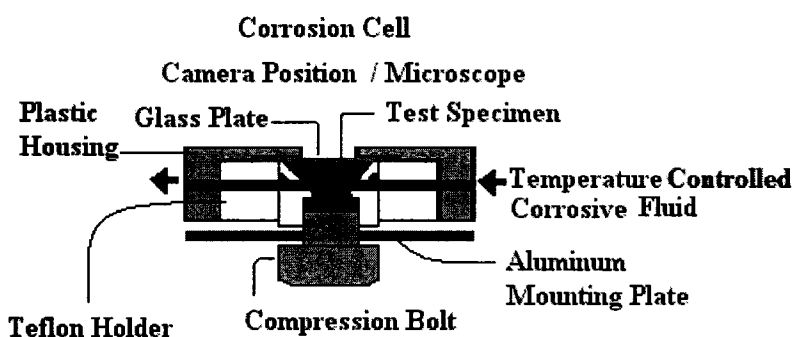


Figure 34: Cross section of corrosion cell showing acid flow path and sample mounting apparatus (68)

The position of the auxiliary electrode is a significant issue for these cells. Platinum or gold wire are the standard materials of choice (71) as it is nearly impervious to corrosion, however for this application a second option was an ITO (Indium Tin Oxide) transparent electrode which allows the transmission of light in the visible range (72). The platinum wire was chosen due to its availability and its common use in other spectroelectrochemical cells. Initially a set of four parallel wires were used perpendicular to the flow (see Figure 29), however this was found to collect bubbles and slow the flow through the system. After a set of calculations based on maintaining an even distance between any point on the surface to the two nearest wires the new channel configuration was established (see Figure 29). A set of wires are placed parallel to the flow on either side of the channel. With the wires 4mm above the surface, and 13mm apart this configuration matches the ideal spacing. This reference electrode design was then compared to other corrosion cells used for in-situ studies. The result of this comparison was that most cells of similar construction use solid platinum rings as reference electrodes to achieve a symmetric current distribution, which are very similar to the

platinum wire configuration chosen (59, 65, 73). The use of a series of wires instead of a single ring is due to material availability as well as the slight benefit of having a greater surface area on the wires rather than a flat washer.

Temperature was considered in the early stages so as to meet the required testing temperature of 25°C, which was chosen as the standard temperature for testing (5). A thermal analysis using ANSYS was conducted as well as a finite element analysis of the tubing used to construct the system. The results of the analysis provided an ideal set point temperature of 25.5°C for the system. This calculated temperature will be used in addition to measured temperatures built into the support system.

4.5.3 Testing and Analysis of the Corrosion Cell

A series of saltwater tests were conducted before the main group of sulfuric acid tests was conducted. This salt water testing reduced the risks associated with acid leakage by having an opportunity to encounter and fix problems without any serious equipment damage and operator injuries.

4.5.3.1 Considerations for Testing Conditions

4.5.3.1.1 Distribution of the Flow across the Surface

By observing the flow of bubbles and debris within the cell it is evident that there is slightly higher flow rates along the centerline of the cell with some small vortices present

near the outer edge of the flow. The vortices appear to be located above the tapered Teflon edge within the cell and so has little contact with the surface. The difference in flow velocity within the cell is most likely reduced as the flow approaches the surface however these observations led to the decision to consistently target the same spot in all tests which is along the centerline of the cell and approximately 1/3 the distance from the outgoing flow port. This location was also chosen as it had the fewest incidents of bubbles obscuring the view, and was well away from the center of the sample where machining defects may potentially still exist.

4.5.3.1.2 Results across a Series of Identical Tests

A series of potentiodynamic tests were performed using the same sample of solution 1 both new and used under deaerated conditions. This was used to determine the effects of increasing contamination from corrosion testing on the electrochemical corrosion behaviors recorded. It would also give an idea as to the consistency of test results performed under theoretically identical conditions in quick succession.

The results of the test seen in Figure 35 illustrate that there is no appreciable effect of reusing the same 300 mL of test fluid under these test conditions. This is supported by the literature (32) which demonstrated that with the sample's (solution volume)/(sample surface area) ratio being $780 \text{ cm}^3/\text{cm}^2$ for these tests it would take over 10^6 seconds (2 years) of immersion in 4.1M nitric acid for the solution to be significantly effected. Even under the aggressive conditions associated with the tests, unless pitting is achieved and

significant metal mass loss occurs it is unlikely that the dissolved metal byproducts will accumulate sufficiently to cause any significant effects. See 3.1.7.3 for more details.

Given the number of hours these metals are tested even and the observed corrosion rates and metal loss it is unlikely that the behavior will be effected in any significant way. It also demonstrated that the test results had a great degree of reproducibility within this apparatus. See Figure 35.

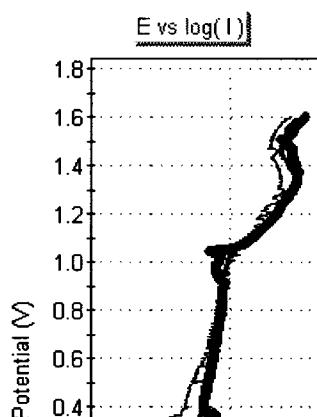


Figure 35: Results of three potentiodynamic tests, one taken with fresh acid, two others done with the same reused acid from 2 weeks later after 8 tests.

4.5.3.1.3 Effect of Flow Rate

The effect of flow rate is considered minimal during the sulfuric acid tests. As a means of testing this effect a short increase in fluid flow rate was performed by forcing 50 mL of fluid through the system under pressure. The changes recorded under these conditions were typically small with an occasional fluctuation in the readings. These results were also supported by the results of the literature review for sulfuric acid on stainless steel

which states that velocity has little effect on corrosion in the passive stage but mostly in the active-passive state where it can cause increased corrosion (35).

4.5.3.2 Comparison of Test Results from the Cell to Other Research

Data

Saltwater tests were performed on 316L stainless steel as a means of safely testing the system for leaks. These tests were also used to check the pitting potentials for the samples which were 0.38 V for aerated conditions and 0.3 V for deaerated. The current density ran up to $1\text{A}/\text{cm}^2$ for the aerated test and beyond the $1\text{A}/\text{cm}^2$ limit for the deaerated test.

These pitting potentials are consistent with pitting potentials recorded for similar materials demonstrated such as a 0.42 V pitting potential being recorded when testing 316 stainless steel in 3%NaCl (16). Both sets of test results also recorded similar current densities at the pitting potentials.

4.5.3.2.1 Experimental Results

Tests have been completed on a variety of metal surfaces including 316L stainless steel, aluminum and magnesium. The images provide indisputable evidence as to the order of progression of various features on the surface, including which pits formed first and propagated the fastest at the surface. Potentially of even greater importance is the ability

to quickly study the surface conditions at locations which produced pits both before and after pitting was initiated.

The images for stainless steel showed excellent contrast between pits and polished surfaces, as well as showing sites producing gas bubbles, electropolishing on some samples, and the real time development of pits including the transformation from an enclosed pit to an open pit. In some solutions the sample surface color was observed to change during testing and some mobile corrosion debris was shown to become attached to the surface at various points.

Metals such as magnesium, which do not maintain a high luster during testing are somewhat harder to image but did produced some unique results which would be difficult to observe using conventional means. The progressive formation of oxides on the surface in addition to the observation of fine gas bubbles being produced at sites across the surface show promise in future analyses (see Figure 79)

Many of the most unique observations through this type of analysis come from the real time video of the corrosion sites, which give an excellent look at the rate of progression as well as the behavior of a given region during the test.

4.5.3.3 Conclusions

The main limiting factor on the photographic analysis is the presence of large numbers of bubbles in the flow, as well as the tendency of some materials such as titanium to darken considerably as corrosion takes place. The current cell design is able to cope with these limitations and is able to take high quality images at optical magnifications of over 600X.

In any research area a new tool is of benefit, not only to those who use it for basic research, but for those who seek to adapt the technology to practical applications and in applied research. Future work in this field pertaining to the ranking of materials, and the search for methods to generate more realistic polarization testing methods should benefit from this cost effective and easy to use techniques and technology.

5 RESULTS AND DISCUSSION

5.1 Test and Observation Information

In-situ images may display some discoloration due to the effects of fluid color. All in-situ images are 0.5 mm in height unless otherwise stated.

The solutions tested have an approximate volume of 300 mL per test, a flow rate of 107 mL/minute and all tests are performed with a sample temperature of 25°C. Some solutions were used in multiple tests which were deemed acceptable due to the small quantity of metal dissolving in solution during these tests. Although the test record monitored which tests used fresh and reused fluids the reproducibility of tests using fresh vs. reused fluids is excellent with no clear signs of systematic error present as discussed in section 4.

Samples are machined and polished to a 1 μ m finish. All test samples were given an initial 1 hour immersion in the solution to attain a stable condition and to record the mixed potential. All samples used in the SA SB and SC series use a rubber adhesive seal with a 7 mm diameter punched hole located at the center of the sample exposing only this area to the solution. Potentiodynamic scans were performed from 0.25 V below E_{corr} to 1.6 V vs. SHE and followed up with a 30 minute recording of the mixed potential. Potentiostatic scans were performed for 1.5 hours at the stated potentials.

5.2 SA Series Results: Potentiostatic and Potentiodynamic

Analysis of 316L Stainless Steel in 1M H₂SO₄

This stage of the analysis looks at the behavior of the samples in 1M H₂SO₄ when undergoing potentiodynamic and potentiostatic testing in aerated and deaerated conditions. The results of the potentiodynamic tests are used to determine the pitting potential followed by a series of potentiostatic polarization tests near the pitting potential in an effort to observe the corrosion characteristics near the pitting potential.

5.2.1 Solution and Test Properties

The SA series was used as a means of setting a baseline for corrosion behavior of a simple sulfuric acid solution before adding elements such as nickel and chloride ions. A 1M H₂SO₄ solution was chosen so as to keep the composition of the test solutions similar to the initial work of Snow (1) for comparison purposes. The solution properties are listed in Table 4.

The solution's pH was both calculated and later measured. The measured pH is significantly higher than was calculated as for this particular solution only a small sample remained at the time the measurement was taken which was then diluted by the deionized water used to clean the tip of the probe.

Table 4: SA series solution composition and pH

Electrolyte	Molar Concentration	Solution Composition (g/L)	Mass %	Theoretical pH:	Measured pH at 20.2°C:	Comments
Nickel Sulfate	0.00	0.00	0.00			Baseline test for comparison purposes.
Nickel Chloride	0.00	0.00	0.00			
Sulfuric Acid	1.00	98.08	9.39	-0.30	0.260	
Water	Remainder	946.70	90.61			
Total(s)		1044.77				

5.2.2 Changes Recorded During Initial Immersion

All samples were immersed in the solution for 1 hour before polarization began to allow for the formation of a typical stable oxide layer. The surface characteristics of samples were all identical regarding their preparation to a 1 μ m finish however the visual characteristics of samples were not always uniform once immersed in the solution.

An uneven surface oxide appearance was seen in 4 of the 9 aerated tests and in 6 of the 8 deaerated tests. See Figure 37. Scratches were also seen to darken in their appearance due to the residual stresses of polishing. See Figure 38.

Also noted was the development of dark spots on the surface during immersion. These dark points generally began developing shortly after immersion and remained in a state of extremely slow growth until polarization began. See Figure 36. SEM and EDS tests of an uncorroded metal surface revealed that a few relatively large chromium based inclusions were present on the metal surface. The proportion and size of these inclusions

matches the number and initial size of these dark points leading to the conclusion that these dark spots are the result of metal with low chromium content corroding preferentially leaving behind a thick dark brown iron based oxide (4, 9, 25).



Figure 36: SA3 (aerated) sample surface after 60 minutes of immersion without polarization, left image is at start, right image is after 60 minutes.

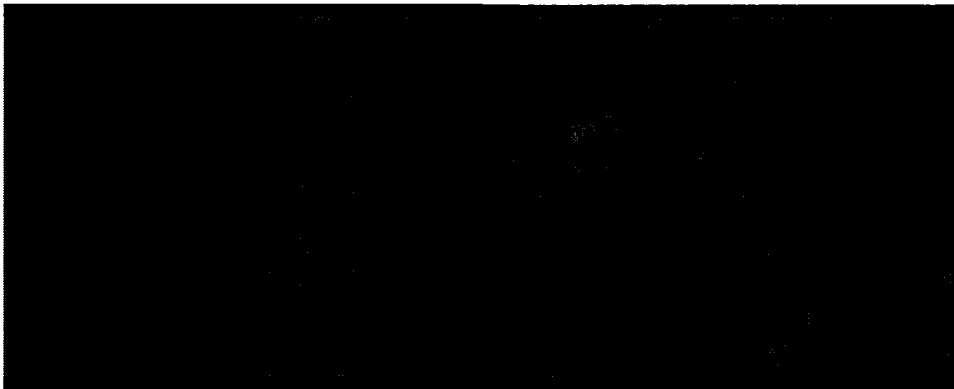


Figure 37: SA6 (aerated) development of a dark uneven oxide layer after 60 minutes of immersion before polarization, left image is at start, right image is after 60 minutes.

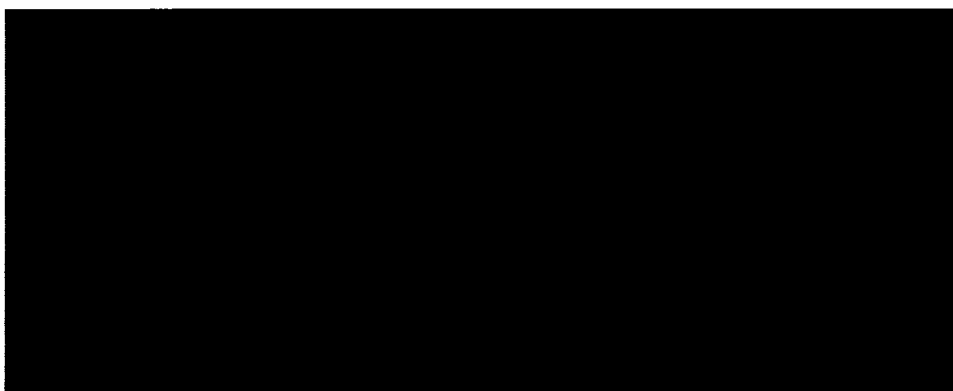


Figure 38: SA14 (deaerated) darkening scratches seen developing after 60 minutes of immersion before polarization, left image is at start, right image is after 60 minutes.

5.2.3 Polarization Data

A pair of potentiodynamic scans was performed in order to determine the approximate value of the pitting potentials. This was then followed by a series of potentiostatic tests intended to both confirm the accuracy of the pitting potential and to observe the pitting and etching behavior at and above the pitting potential.

Polarization curves including Tafel fit and associated information is provided in Appendix D for all SA, SB and SC series potentiodynamic tests.

5.2.3.1 Potentiodynamic Test Results

Aerated and deaerated potentiodynamic tests were performed using a 0.33mV/s scan rate. Although a series of these were performed at different times in the testing schedule only

two potentiodynamic scans are included in the analysis. These were chosen as they were performed without any noticeable flaws in execution and are consistent with other tests performed under the same conditions.

The following information was taken from this test data:

Table 5: SA series potentiodynamic polarization results

Test Number:	Solution	Aeration	E _{corr} (mV)	I _{corr} (μA)	Corrosion Rate (mpy)	Pitting Potential (V)	Weight Lost (g)
SA3	1		155.4	5.66E-01	5.99E-01	0.9	0.0009
SA12	1	Deaerated	-334.5	1.38E+03	1.46E+03	1.05	0.0163

The information from these scans indicated that for this solution deaerated conditions were much more aggressive than aerated with a significantly greater natural corrosion rate and a greater current density in the passive and transpassive region. It is worth mentioning that the pitting potential for the aerated solution is lower than that for the deaerated which is contradictory to some of the trends seen in the literature review for samples achieving passivation (1, 4, 5, 74). When the current density for aerated conditions is compared to deaerated conditions it is observed that there is a current density 1000 times larger in the passive region of the deaerated curve as compared to the aerated curve. It is also apparent that the aerated sample's passive region's current density is almost constant showing a relatively vertical appearance compared to the sloped section of the deaerated test. It is likely that the deaerated sample has not achieved a stable passive oxide layer within this solution which is consistent with data specific to stainless steel in this concentration of sulfuric acid (4, 35). This is further

supported by the observations showing the peeling of the oxide layer during the immersion stage of some SA series tests, see Section 5.2.9.

A curve was also observed in the work of Snow (1) which displayed a profile similar to that seen for deaerated conditions, however during these tests, this high current density passive region only appeared for an aggressive chloride containing solution. See Figure 1 Solution 4. The resulting differences between the passivating deaerated tests of Snow and other authors with this solution and the unstable passivation of these tests are attributed to the larger volume of solution tested combined with the effects of the realistic flowing solution used in these tests. The flowing solution has the effect of accelerating corrosion for metals without a strong passive layer (35) likely resulting in the increased corrosion rates observed here.

Both curves also indicate secondary passivation in the form of a reduction in current density within the transpassive region, see Figure 39. This secondary passivation coincides with the formation of a dark surface layer on some grains as seen in the upper left corner of Figure 46. This darkening of the grain's surface supports the theory that secondary passivation occurs in part due to the buildup of Fe in the surface of the oxide layer.

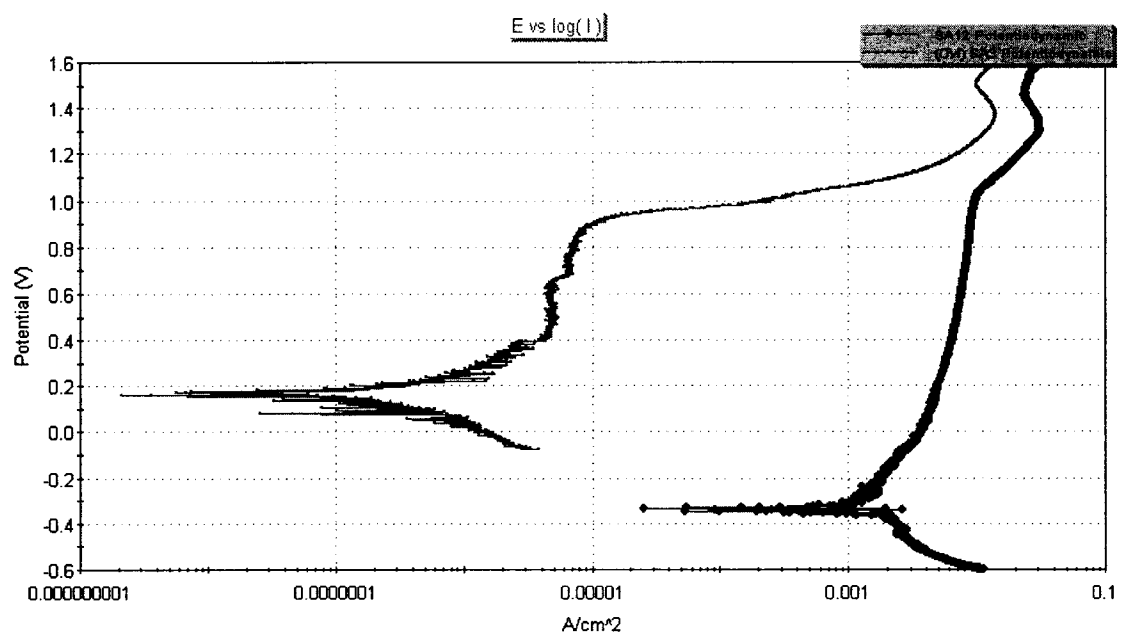


Figure 39: Aerated (green) and deaerated (blue) polarization test scans

5.2.3.2 Potentiostatic Test Results

A series of aerated and deaerated potentiostatic tests were performed around and above the measured pitting potential from the potentiodynamic tests.

5.2.3.2.1 Aerated Tests

The results from the aerated tests were largely consistent with the principles covered in the literature review (1, 4, 9, 20, 21, 35). By the end of the 1.5 hour potentiostatic polarization test each metal sample's final current density was nicely ranked in order with the lowest current of 0.0001A attributed to the lowest potential of 0.9 V and the highest current density of 0.008 A going to the greatest potential of 1.25 V.

The tests clustered at the pitting potential largely failed to encounter any etching or pitting with the exception being the lowest potential test at 0.9 V. This interesting discrepancy was present in test SA11 (potentiostatic at 0.9 V), in which the metal did not appear to passivate for most of the test as illustrated by its greater current density. Figure 40. This behavior was sufficiently active to cause some visible etching of the surface, and represented the greatest overall amount of corrosion which took place for samples polarized near the pitting potential as shown in Figure 41. To verify this result a second test was conducted at this polarization potential producing similar results. This unusual behavior is believed to be a result of the sample having barely achieved a passive

behavior in this solution which appeared to require a considerable amount of time to establish itself at this potential.

A test was later conducted at 1.25 V, producing a significant amount of surface damage and the highest current density out of the aerated test at 0.009 A.

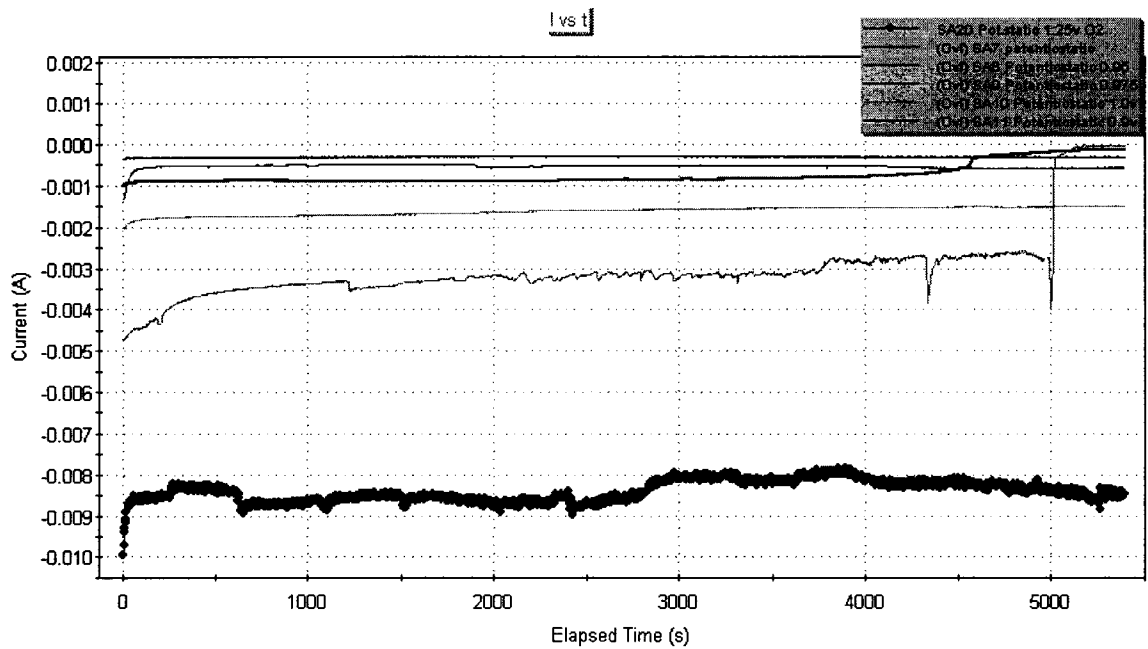


Figure 40: Results of aerated SA series potentiostatic tests.



Figure 41: Image of mild etching resulting from SA11 potentiostatic polarization at 0.9 V (left is original 0.5 mm tall image, right image is magnified to show mild etching, height of right image is approximately 0.1mm)

5.2.3.2.2 Deaerated Tests

The results from the deaerated tests were within a reasonable range of values but were not completely in sequence as was the case with the aerated test. This behavior is attributed to the smaller change in current density seen at the pitting potential in the deaerated potentiodynamic tests causing the values to be clustered into a smaller region. In this situation the random errors encountered in testing would have a greater apparent effect making some results appear out of place; see Figure 42.

Although no samples encountered true aggressive pitting there was considerable etching and relatively even surface corrosion. Etching was first noticed at 1.025 V which is consistent with the pitting potential of the potentiodynamic scan. As the potential was

subsequently increased the etching became more aggressive but no aggressive pitting occurred during these tests; see Figure 44.

These types of images may be of use and interest to those working on improving corrosion inhibitor performance.

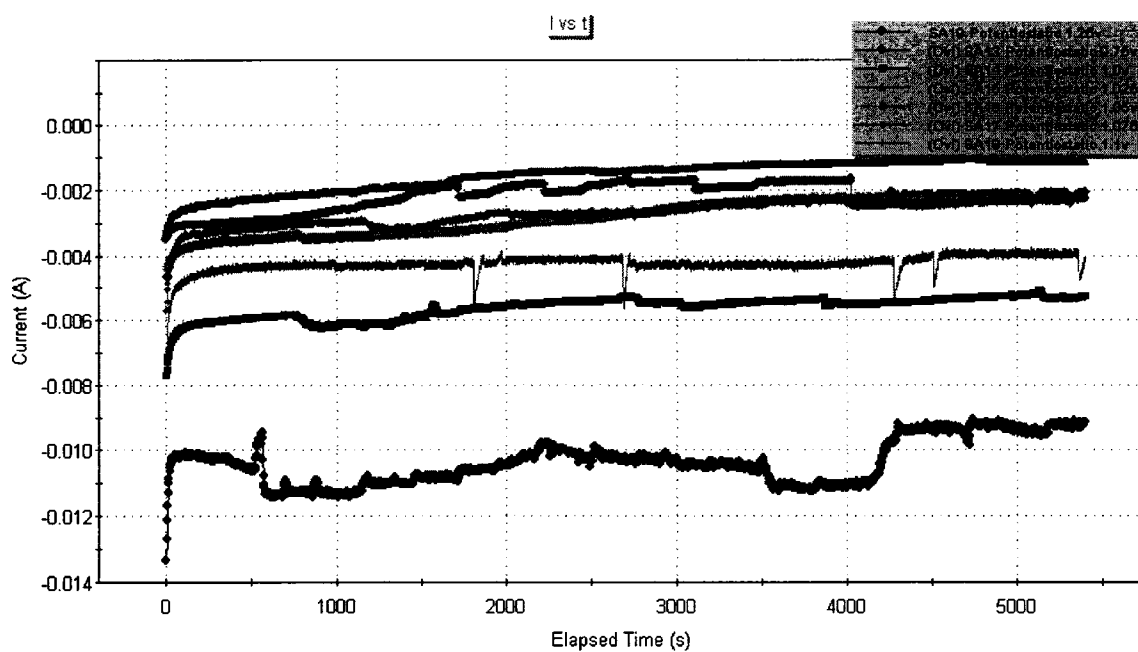


Figure 42: Results of deaerated SA series potentiostatic tests.

5.2.4 Progressive Development of Etching, Pitting and Other Features during Polarization

As discussed in section 3 one of the fastest ways to accurately locate the pitting potential for a particular metal in solution is to test samples potentiostatically over a range of potentials above and below the pitting potential. By examining the polarization charts and surface features of the sample it is possible to accurately estimate the pitting potential under a given set of conditions. The term “pitting potential” is somewhat misleading in this situation as this metal when immersed in solution has a tendency to aggressively etch rather than cause substantial pitting. Some small open pits were visible and were attributed to the dissolution of sulfide inclusions based on SEM and EDS testing. See Appendix A.

A series of tests in aerated and deaerated solutions were tested in 0.025 V increments in order to estimate the pitting potential. As this test did not involve the use of halides to initiate pits there was a strong tendency of samples to etch along the grain boundaries during test at pitting potential. Aerated tests were conducted at a range of values from 0.9 to 1.0 volts in accordance with the potentiodynamically predicted pitting potential of 0.9V. Deaerated tests were conducted at a range of values from 0.975 to 1.1 volts in accordance with the potentiodynamically predicted pitting potential of 1.0 V. At the conclusion of these tests a high potential of 1.25 V was used observe metal’s behavior in the Transpassive region. The following surface changes were recorded during testing:

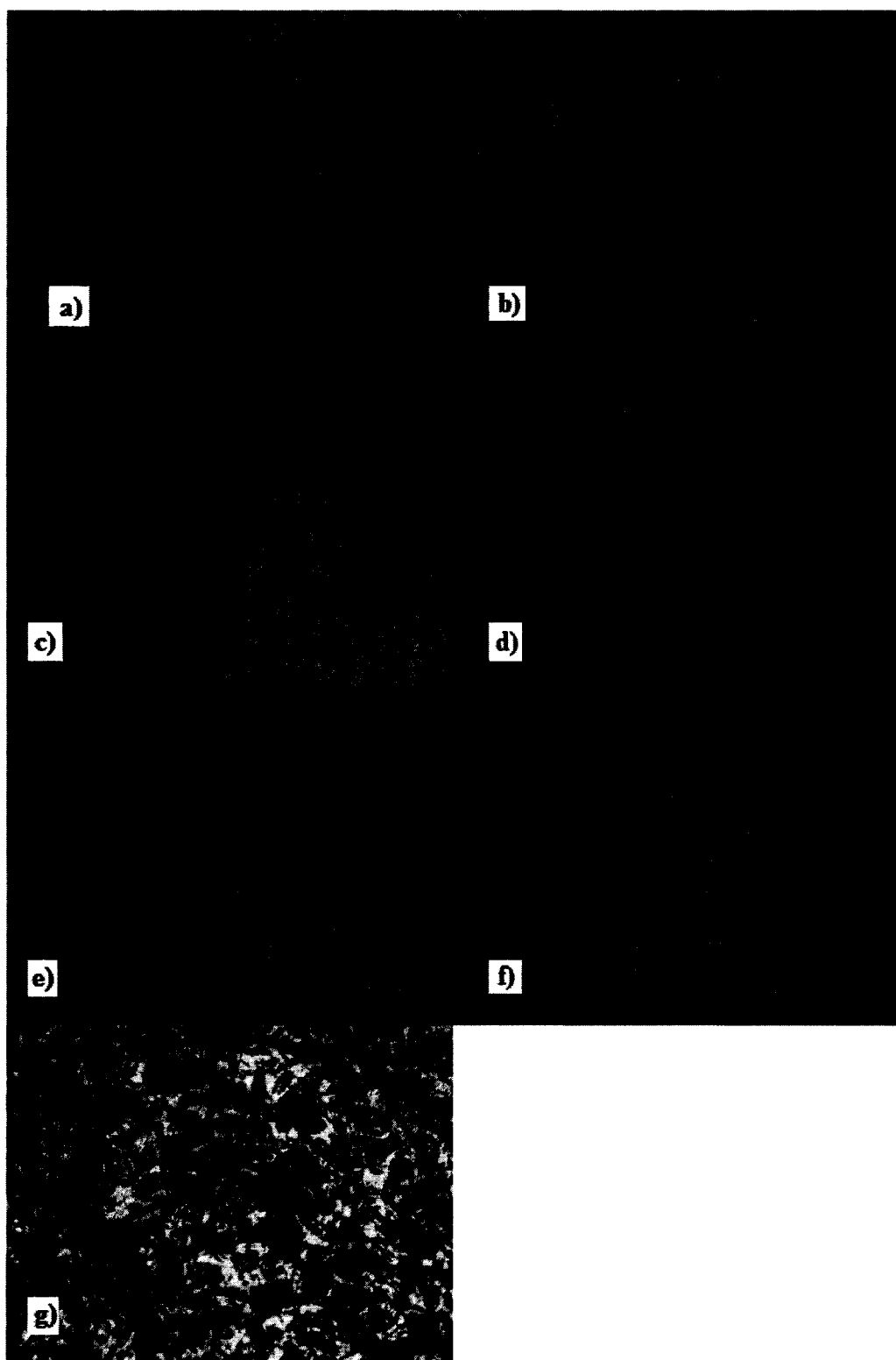


Figure 43: Aerated test samples after polarization. a) potentiodynamic, b) potentiostatic 0.9 V, c) potentiostatic 0.925 V, d) potentiostatic 0.95 V, e) potentiostatic 0.975 V, f) potentiostatic 1.0 V, g) potentiostatic 1.25 V.

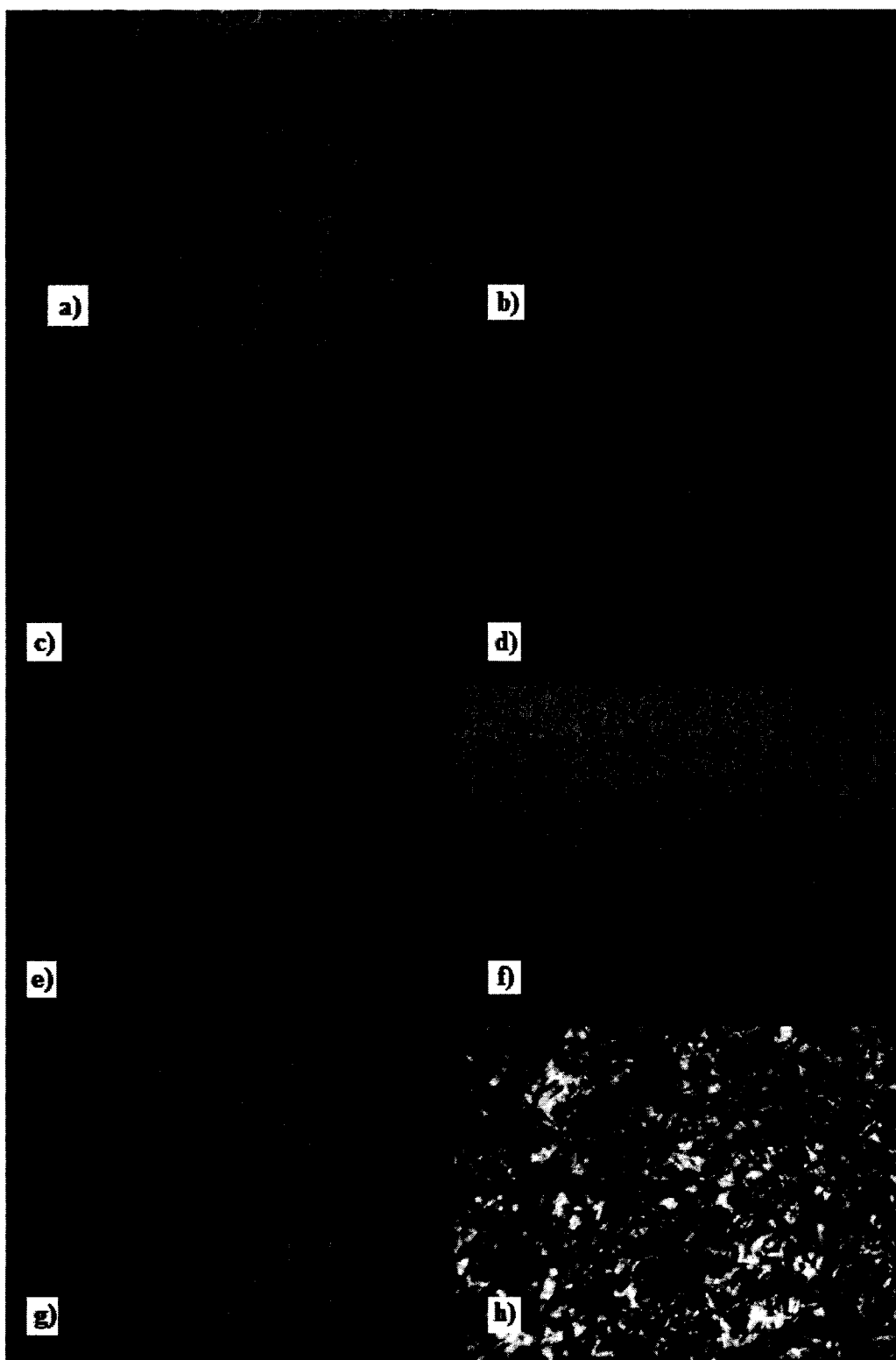


Figure 44: Deaerated test samples after polarization. a) potentiodynamic, b) potentiostatic 0.975 V, c) potentiostatic 1.0 V, d) potentiostatic 1.025 V, e) potentiostatic 1.05 V, f) potentiostatic 1.075 V, g) potentiostatic 1.1 V, h) potentiostatic 1.25.

5.2.5 Development of Grain Boundary Etching in 1M H₂SO₄ under Potentiostatic Polarization

5.2.5.1 Aerated Test Results

Although the aerated tests at pitting potential did not produce any appreciable etching or pitting the test was useful at demonstrating the significance of current density on these tests. The aerated test pitting potential had a current density of 300 times less than of the deaerated solution at the pitting potential. This means that even though it was possible that the samples were capable of being etched the progression was so slow that no reasonable duration potentiostatic test could capture it at these potentials. It was seen that etching would develop more aggressively in both potentiodynamic and potentiostatic tests when held at greater potentials as seen in the test conducted at 1.25 V; see Figure 44 and Figure 45.

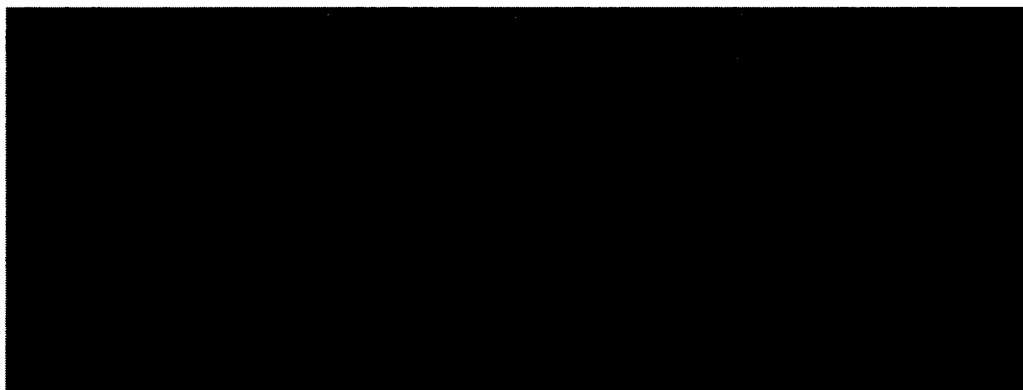


Figure 45: Pitting and etching in aerated (left) and deaerated (right) 1M H₂SO₄ at 1.25V potentiostatic (images have a height of ~0.2mm).

5.2.5.2 Deaerated Test Results

The sequence of tests produced remarkably clear images of etching and what appears to be metastable pit activity on the potentiodynamic and above pitting potential potentiostatic test surfaces. These tests illustrate the usefulness of the in-situ optical microscopy techniques as it was possible to see the development of etching in tests conducted at and above potentials above 1.025 V even though the polarization results produced by the computer did not clearly indicate that this phenomenon was occurring. The next test taken at 1.05 V had a slightly more defined current increase but still did not show any clear change due to having reached the pitting potential. See Figure 44 for images of etching and Figure 42 for polarization results.

The reason for this ambiguous behavior is that etching of grain boundaries does not necessarily share the same distinctive increase in current after initiating. In these cases pitting is not a concern however long term etching of grain boundaries may cause entire grains to fall out causing premature damage to metal components.

5.2.6 Development of Pitting in 1M H₂SO₄ under Potentiostatic Polarization

Pitting did not develop to any great extent in any tests conducted with this solution.

Images indicated that at all potentials above pitting potential etching of grains and grain boundaries were preferred rather than pitting on imperfections and existing microscopic pit sites. See Figure 45 and Figure 44 for illustrations.

Upon further examination it was found that most of the small cavities left on the surface were open with smooth clean inside walls and an apparently spherical shape. This configuration is more consistent with the dissolution of sulfide inclusions followed by crevice corrosion due to their small enclosed nature (1, 16, 46, 47) and EDS results in Appendix A.

5.2.7 Etching and Color Change of Grains at High Anodic Potentials

During the last minutes of the potentiostatic tests it was noticed that several grains develop an etched appearance with a dark colored surface layer forming near the end of the test.

The dark coloration coincided with the secondary passivation stage in the potentiodynamic polarization curves and is presumably the visible signs that a new corrosion resistant stable oxide layer is forming on these surfaces.

The presence of etching on the grain surface in the form that looks like a set of parallel scratches is due to the presence of dislocation “slip” bands (traces) which due to cold working the material (45) most likely occurring during sample machining on the lathe or sandpaper. A few large parallel etched lines are also visible as “Twin Boundaries” most likely due to mechanical twinning (See Figure 46).

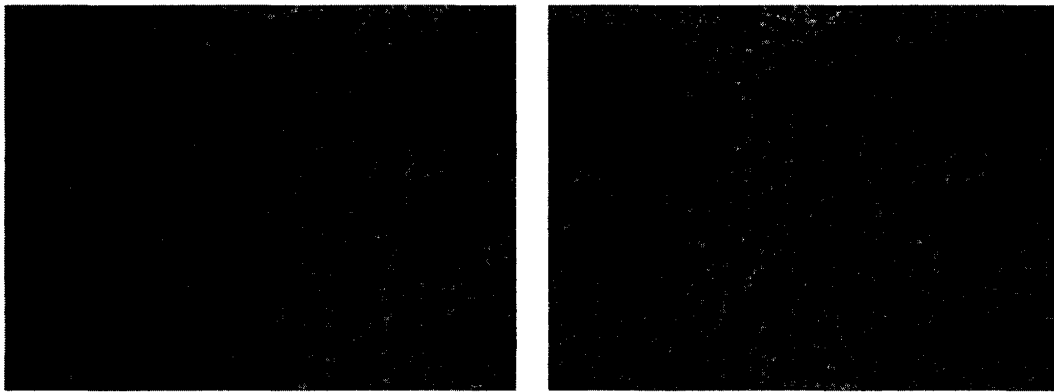


Figure 46: Surface of SA12 (deaerated) before (left) and after (right) reaching secondary passivation (note presence of contrast darkened etch pits, grain boundaries, and sub-boundaries which appear as twins, twin boundaries and dislocation slip traces).

5.2.8 Color Change on Sample's Surface due to Potentiostatic Polarization

In many polarization tests changes in surface characteristics were noted as testing was taking place. One such phenomenon was the lightening of the surface oxide layer during anodic polarization above 0.975 V (See Figure 47 and Figure 48).

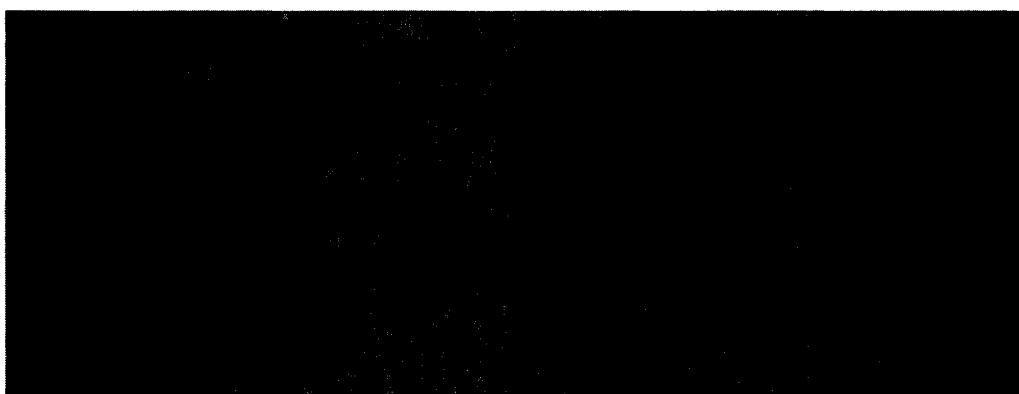


Figure 47: Aerated potentiostatic test at 1.25 volts, left is before polarization, right is immediately after polarization.

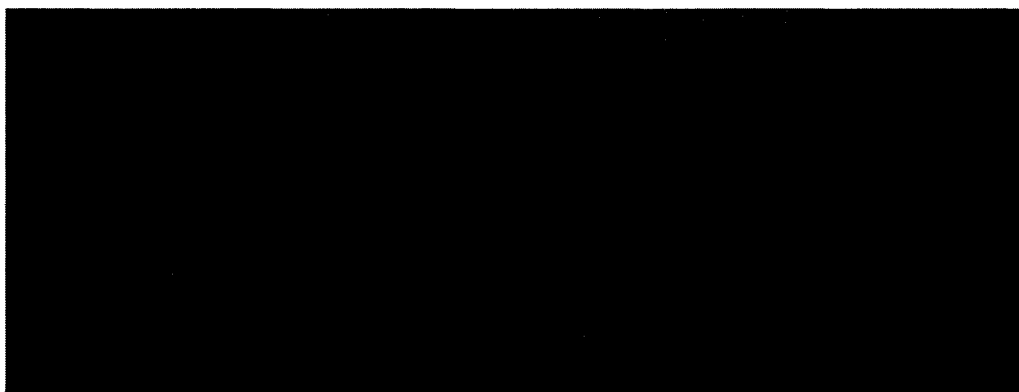


Figure 48: Deaerated potentiostatic test at 1.025 volts, right is immediately after polarization.

The reduction of the brown coloration is generally slightly more pronounced in deaerated solutions rather than aerated however during potentiostatic polarization tests run with a potential of 0.975 V or more a significant reduction in the brown surface color was noticed in all solutions. This occurred within a fraction of a second of polarization and this behavior was not seen in the initial seconds of potentiodynamic testing as it begins with cathodic polarization. The changes also became more prominent in the later test cases with increased polarization potentials of up to 1.25 V.

Further support was given by observing potentiodynamic tests and noting a similar lightening behavior in SA3, an aerated solution beginning 56 minutes from the start of the test. This corresponded to a potential of 1.03 V and a current density of 0.002 A/cm^2 .

5.2.8.1 Theoretical Explanation for this Behavior

Based on the Pourbaix diagram from HSC Chemistry 5.1 software package the suggested cause for this change is a destabilization from $\text{FeO}(+a)$ to $\text{Fe}(+2a)$ as marked at 0.75V in the chart (44) (see Figure 14). Upon further examination of the oxide layer it is possible to see a limited reduction in the brown surface oxide in test potentials of 0.9 V. This is consistent with the theory that the FeO oxide becomes unstable and dissolves into the solution at a potential of approximately 0.75 V. It may also be attributed to the partial dissolution of the oxide layer which contains a variety of iron oxides from the earlier

corrosion process, thereby releasing the substances which normally give the surface a dark color.

5.2.9 Peeling of Thin Surface Layer

Peeling of a brown surface layer occurred during the immersion stage of a test before polarization had begun. Peeling is first seen 25 minutes from when the first images were taken of aerated test SA6 and finished approximately 27 minutes later.

The peeling was first visible around a series of medium size dark spots each with a diameter less than 0.025 mm in the form of a minor discoloration of the surface. Peeling began almost simultaneously in several locations including some that did not coincide with any obviously visible imperfections. After this point the peeling continued until the majority of the surface had this layer removed. An image of an early stage of peeling is shown in Figure 49; notice the triangular flap in the middle of the magnified right side image.

The color of the surface did lighten significantly for a brief period after the peeling had begun, however the surface once exposed began developing a brown oxide layer shortly after exposure.

The observed peeling behavior supports the theory that the passive layer is unstable as this layer is most likely the passive layer composed primarily of Cr_2O_3 which allows for increased corrosion rates as peeling continues across the surface.

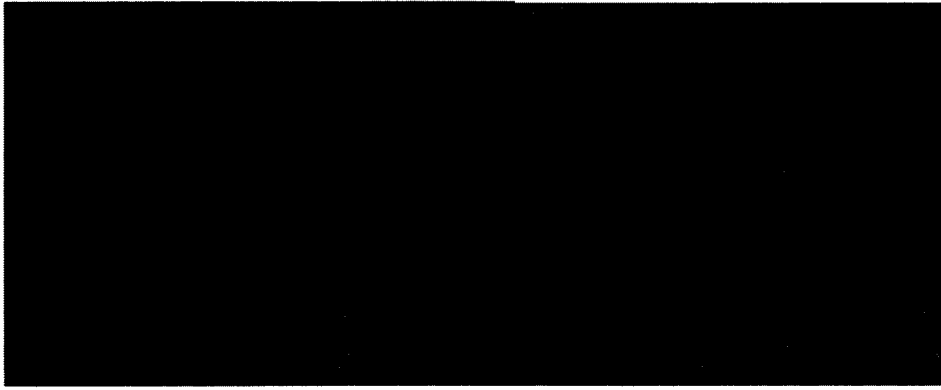


Figure 49: Image of surface layer peeling in SA6, (0.5mm tall image on left, 4X magnified crop right).

5.2.10 Conclusions

In-situ optical microscopy is capable of observing and identifying events such as etching, gas generation, and pitting that are not necessarily recorded by conventional means.

5.3 SB Series Results: Potentiostatic and Potentiodynamic Analysis of 316L Stainless Steel in Various Sulfuric Acid Based Solutions

5.3.1 Solution and Test Properties

The SB series uses various different solutions to test the behavior of the samples when exposed to various different ions in a variety of concentrations. Solutions 2 through Solution 4 contain 1M H₂SO₄ with a constant 0.25M Ni⁺ component which is maintained through all four solutions. A set of solutions based on the addition of compounds such as sulfate and chloride ions was created by using nickel sulfate and nickel chloride chemical reagents. The compositions used in these tests are comparable but not identical to those used in the work of Snow (1) for comparison purposes.

**Table 6: SB series solution composition and pH
Solution 2: SB5-
SB8**

Electrolyte	Molar Concentration	Solution Composition (g/L)	Mass %	Theoretical pH:	Measured pH:
Nickel Sulfate	0.25	65.72	6.09		
Nickel Chloride	0.00	0.00	0.00		
Sulfuric Acid	1.00	98.08	9.09	-0.30	0.029
Water	Remainder	914.95	84.82		
Total(s)		1078.74			

**Solution 3: SB9-
SB12**

Electrolyte	Molar Concentration	Solution Composition (g/L)	Mass %	Theoretical pH:	Measured pH:
Nickel Sulfate	0.15	39.43	3.64		
Nickel Chloride	0.10	23.77	2.20		
Sulfuric Acid	1.00	98.08	9.06	-0.30	0.102
Water	Remainder	920.95	85.10		
Total(s)		1082.23			

**Solution 4: SB13-
SB16**

Electrolyte	Molar Concentration	Solution Composition (g/L)	Mass %	Theoretical pH:	Measured pH:
Nickel Sulfate	0.00	0.00	0.00		
Nickel Chloride	0.25	59.43	5.46		
Sulfuric Acid	1.00	98.08	9.02	-0.30	0.097
Water	Remainder	929.96	85.52		
Total(s)		1087.46			

**Solution 5: SB1-
SB4**

Electrolyte	Molar Concentration	Solution Composition (g/L)	Mass %	Theoretical pH:	Measured pH:
Nickel Sulfate	0.25	65.72	5.54		
Nickel Chloride	0.00	0.00	0.00		
Sulfuric Acid	3.39	332.04	28.01	-0.83	-0.760
Water	Remainder	787.80	66.45		
Total(s)		1185.55			

5.3.2 Changes Recorded During Initial Immersion

All samples were immersed in the solution for 1 hour before polarization began to allow for the formation of a typical stable oxide layer. The surface characteristics of samples were all identical regarding their preparation to a 1 μ m finish however the visual characteristics of samples were not always uniform once immersed in the solution.

Similar surface behaviors were seen in the SA Series including the formation of an uneven brown surface oxide; however some tests created different colors. During tests that incorporated chloride ions a grey surface color formed. This may be the result of the destruction of some sections of the oxide layer or the removal of some unstable oxides that would ordinarily remain stable until reaching a higher potential and is consistent with the “thinning” theory in which aggressive halides are able to penetrate and partially break down the protective surface layer (16); see Figure 50 for optical microscope images.

These tests also saw similar patterns of scratches and the development of dark spots on the surface during immersion. For a closer examination of this phenomenon see SA series results section.



Figure 50: SB12 (aerated) initial immersion creating dark gray oxide layer, start of immersion (left), end of immersion just before polarization (right).

5.3.3 Polarization Data

A set of aerated and deaerated potentiodynamic and potentiostatic scans were performed. A potentiodynamic scan was first performed in order to determine the approximate value of the pitting potentials, the corrosion rate, etc. This was then followed by a potentiostatic test intended to examine the pitting behavior under potentiostatic polarization.

Polarization curves including Tafel fit and associated information is provided in Appendix D for all SA, SB and SC series potentiodynamic tests.

5.3.3.1 Potentiodynamic Test Results

5.3.3.1.1 Scan Results

Aerated and deaerated potentiodynamic tests were performed for each solution using a 0.33mV/s scan rate. This data was used to isolate the pitting potential, corrosion potential, and the corrosion rate. Overlays of the test data are shown in Figure 51 and Figure 52.

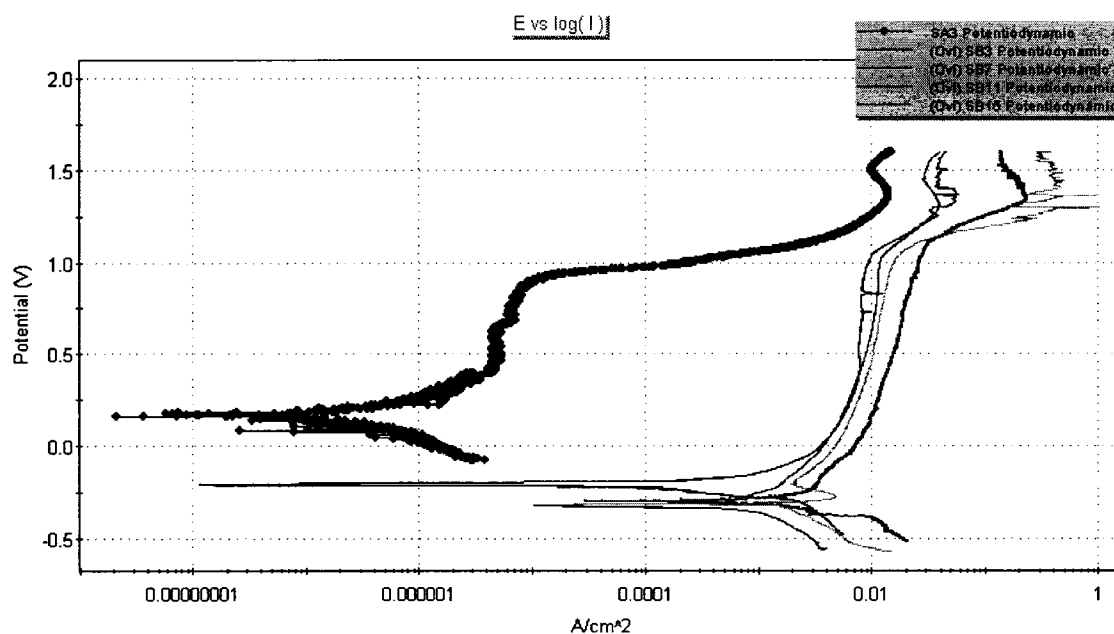


Figure 51: Aerated SB series potentiodynamic scans with SA3 for comparison

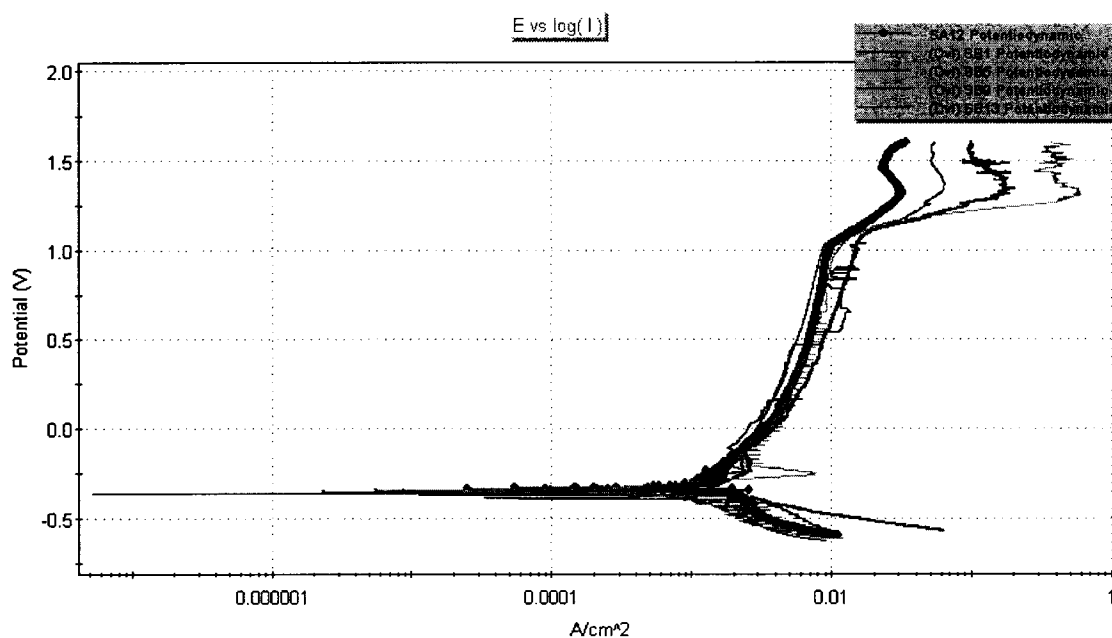


Figure 52: Deaerated SB series potentiodynamic scans with SA12 for comparison

5.3.3.1.2 Potentiodynamic Polarization Analysis Results

Several important correlations are seen in these test results:

- The current density of the transpassive region increased based on increased acidity.
 - The current density of the transpassive region increased based on increased chloride ion concentrations.
 - Deaerated SB series solutions tend to have a corrosion potential in the active region and appear to experience unstable passivation within the passive region.
- See section 5.2.3 for more information on this topic.

- Aerated SB series solutions do not appear to generate a stable oxide layer as was observed during the SA series tests. See section 5.2.3 for more information on this topic.
- Deaerated SB series solutions tend to have a more negative corrosion potential compared to aerated solutions which is consistent with the work by Snow (1). This is because oxygen is a stronger oxidizer than the typical hydrogen based reduction taking place in the deaerated solution thereby raising the mixed potential (4, 22).
- Solutions with high chloride ion concentrations have a greater anodic knee visible and an increased tendency to experience active corrosion when not polarized.
- No clear correlation showing a decrease in pitting potential for deaerated solutions compared to aerated is possible as the tests show this behavior in only two of the four tests. This may be due to the combined effects of the flowing solution used during this test with the presence of an apparently unstable passive layer. It is interesting to note that the two most aggressive corrosion solutions (low pH and high Cl^-) displayed the conventionally accepted behavior of higher pitting potentials for aerated solutions. Theories regarding this behavior are presented in section 5.6.4.2.1 Theoretical Explanation for Aerated vs. Deaerated Test Results.

The following information was taken from this test data:

Table 7: SB series potentiodynamic polarization results

Test Number:	Solution	Aeration	Ecorr (mV)	Icorr (μ A)	Corrosion Rate (mpy)	Pitting Potential (V)	Weight Lost (g)
		Deaerated	-353.4	7.83E+02	7.75E+02	-1.07	0.0237
		Aerated	-299	1.88E+03	1.99E+03	-1.03	0.0242
		Deaerated	-383.9	7.45E+02	7.87E+02	-1.03	0.0059
		Aerated	-219.5	4.49E+02	4.74E+02	-1.04	0.0102
		Deaerated	-360.6	1.04E+03	1.10E+03	-1.04	0.0078
		Aerated	-313	2.20E+03	2.32E+03	-1.02	0.0086
		Deaerated	-345.9	1.57E+03	1.66E+03	-1.03	0.0413
		Aerated	-303.9	1.75E+03	1.85E+03	-1.04	0.0416

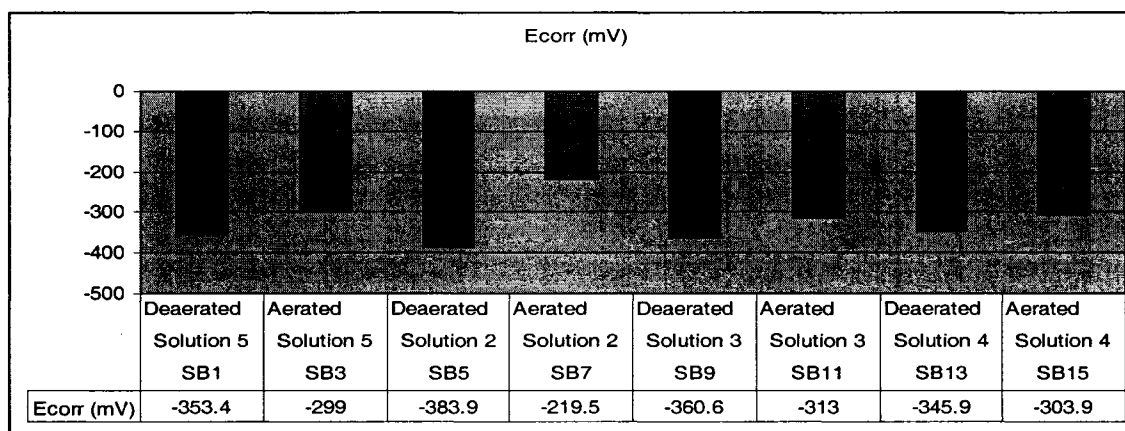


Figure 53: SB series corrosion potential graph

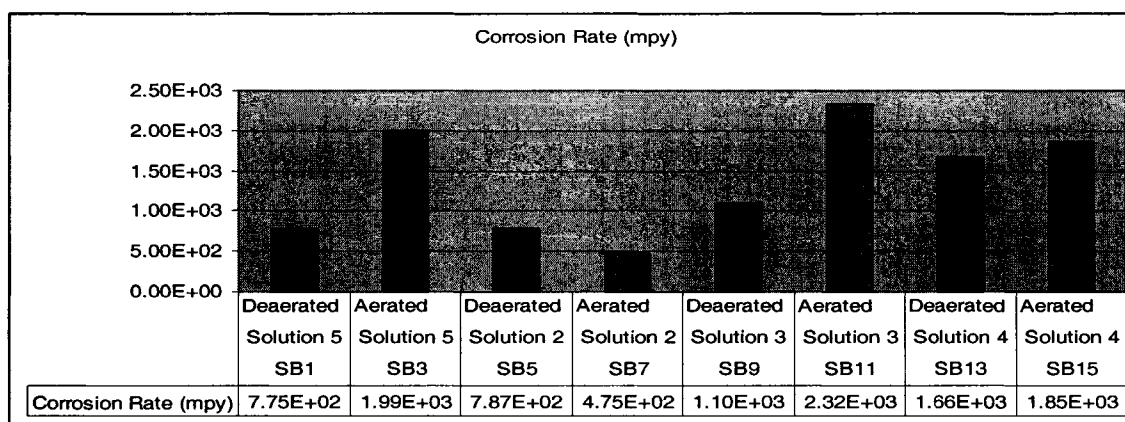


Figure 54: SB series estimated corrosion rate graph

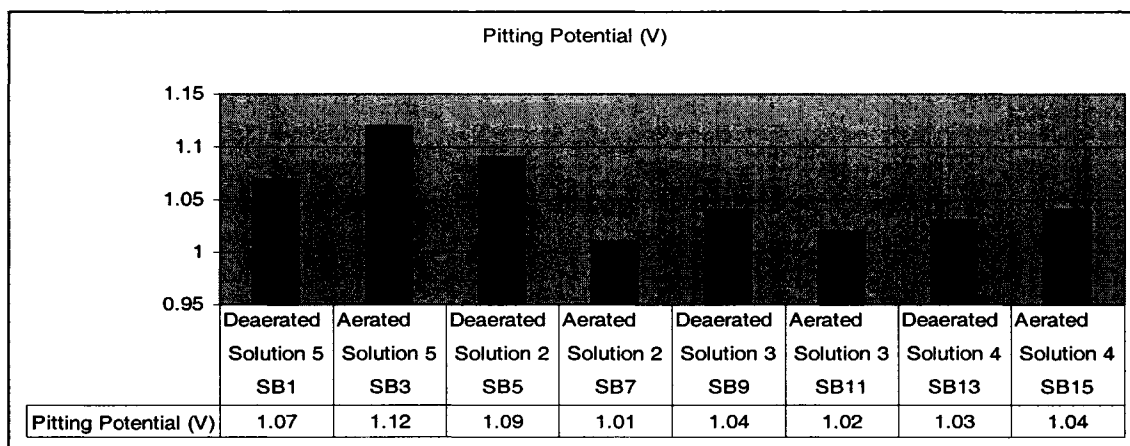


Figure 55: SB series pitting potential graph

5.3.3.2 Potentiostatic Test Results

A series of potentiostatic scans were performed at 1.13 V to observe the surface behavior of the samples when polarized to a value above the pitting potentials. A consistent 1.13 V was chosen as it above the pitting potential but below the secondary passivation section of the potentiodynamic tests; see Figure 56 and Figure 57.

Solutions with high chloride ion concentration produced the greatest current density of all solutions tested at this potential, with solution 5's low pH tests a distant second.

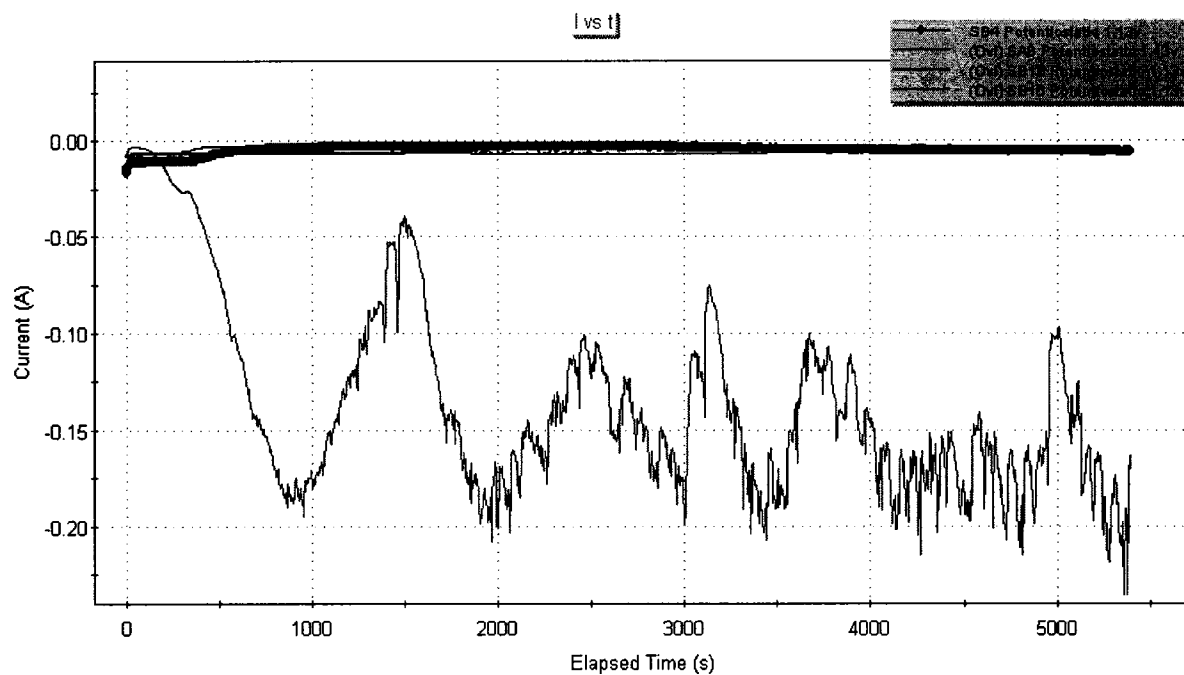


Figure 56: Aerated potentiostatic scans SB series at 1.13 V.

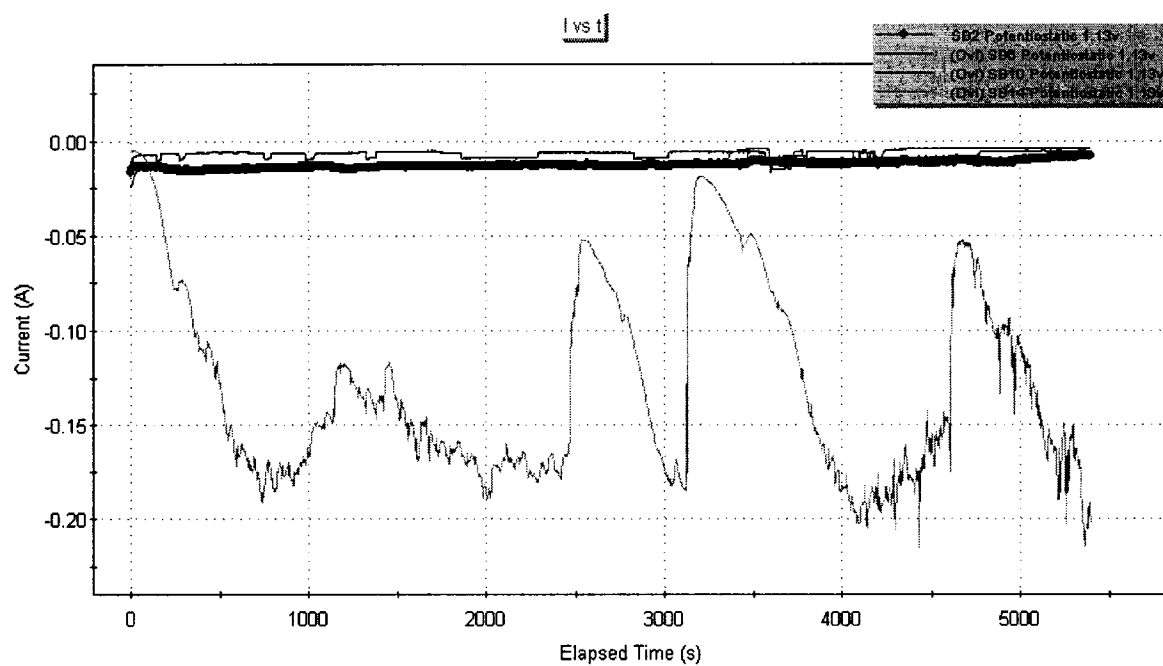


Figure 57: Deaerated potentiostatic scans SB series at 1.13 V.

5.3.4 Observed Corrosion Behaviors

Through the visual analysis of these samples under various polarization test conditions it is noted that in low chloride ion tests etching is predominant with active dissolution of the metal surface noticed in many potentiodynamic tests. These behaviors were consistent with those observed in the SA series tests performed at higher potentials. Once the chloride ions concentrations sufficiently increased aggressive pitting becomes the more prominent means of metal attack (1, 4, 10, 16, 18).

Multiple unique corrosion behaviors were visually captured during testing including changes in surface color, surface layer peeling and unique stages of pit progression observed in the high chloride tests.

5.3.4.1 Color Change during Polarization

Lightening of the overall oxide color during potentiostatic polarization was observed and imaged as seen under optical in-situ corrosion cell. This phenomenon was first observed in the SA series of tests and has continued for all SB series test solutions. The surface layer typically lightens considerably, presumably due to the presence of a Fe^+ based corrosion product (i.e. oxide, hydroxide etc.) that is unstable at higher potentials. See Figure 15. In cases where the layer is already loose it may quickly disintegrate as was the case in SB14. Examples are seen in Figure 58.



Figure 58: Surface color changes upon polarization SB10 (top two images with left being before and right being after polarization), SB14 (bottom two images with left being before and right being after polarization).

5.3.4.2 Light Spots on Metal Surface

During test SB9 small light points were seen on the surface which was already covered with a dark brown presumably of corrosion product-oxide layer, (see Figure 59). It is theorized that the chloride ions in the solution were attacking certain weak spots in the surface but were not there in sufficient quantity to break through to trigger pitting at these locations. A similar behavior was seen during a stainless steel test in saltwater, (see Figure 77). This behavior may be explained by either the absorbed ion displacement models or the ion migration or penetration models described in the literature review (1, 9, 16).

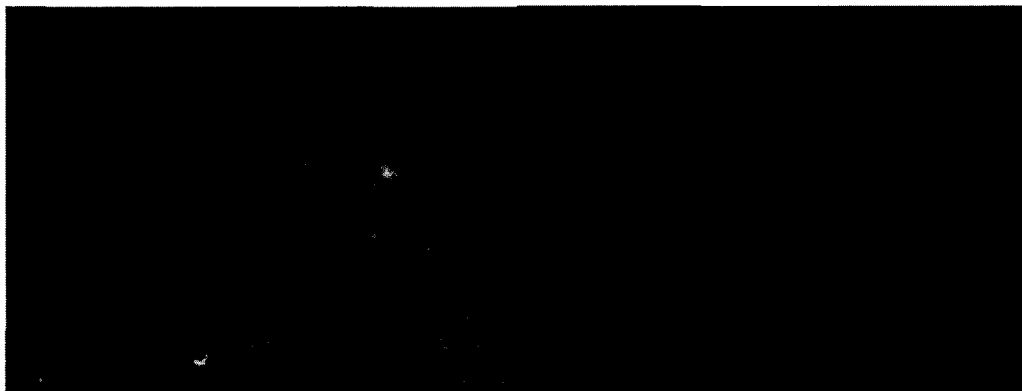


Figure 59: Image showing light color spots forming in surface layer of Test SB9 (deaerated with 0.1M Cl⁻), (left image is 0.5mm tall, right image is cropped to upper left corner at 4X greater magnification)

5.3.4.3 Peeling of Surface Layer

These peeling events are believed to be the removal of large sections of the metal's surface layer rather than the removal of surface debris during testing. This theory is

based on the observations taken during test SB11 which shed its surface twice, once at the beginning of testing and a second time during a later stage of the test.

Peeling of thin layers (refer to SA series analysis) is theorized so that it will generally occur without any significant visible changes in color. This phenomenon is seen in Figure 60 showing the peeling of test SA6. As the thickness increases the peeling process changes and often tends to occur in larger sheets with fewer visible tears as it detaches. A scattering of light also occurs more as the thickness increases, causing thin film interference colors seen in tests SB9 and SB13.



Figure 60: Peeling surface layers seen in SA6 (top left), SB8 (top right), SB9 (bottom left) , SB13 (bottom right).

5.3.4.4 Localized Detachment of Surface Layer

Color changes are also observed on a smaller scale where the surface layer becomes detached from the metal at a single point. This damage to the detached layer generally coincides with a dark spot upon which there is presumably considerably increased corrosion activity. This local damage may eventually expand triggering the peeling of large areas of the sample surface. See Figure 61 for illustration.



Figure 61: Localized peeling of surface layer leading to large scale peeling after polarization (progression of images over 60 minutes top left to bottom right).

5.3.5 Pitting Behavior under Potentiodynamic and Potentiostatic Conditions

Aggressive pitting seen developing in the high chloride tests SB13-SB16 both under potentiostatic and potentiodynamic test conditions followed the same basic patterns of behavior similar to some pitting patterns seen in the literature review (5, 72); see Figure 12 and Figure 20. Similar circular pits with dark caps formed in all four developing rough uneven growth patterns later in their progression leading to the eventual consumption and removal of the original metal surface. A detailed description of this progression is in the following sections.

There is one noticeable difference between potentiodynamic and potentiostatic pits being that a second ring of corrosion develops around the pits, (see Figure 62). This ring appears to be a deformed and cracked metal surface that is reasonably consistent with the descriptions of pit cap growth theories reported in literature (16). See Figure 12 (horizontal) and Figure 20 for theoretical cross section and see images below for actual growth patterns.

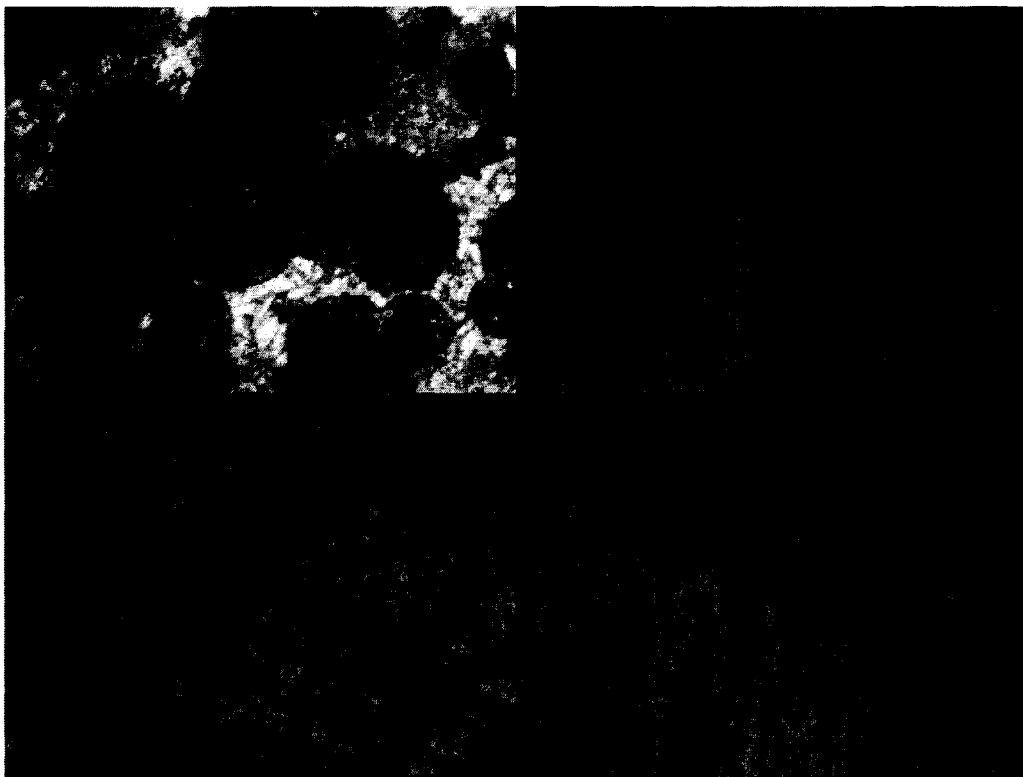


Figure 62: Images of pit growth for SB13 (potentiodynamic) top left, SB14 (potentiostatic) top right, SB15 (potentiodynamic) bottom left, SB16 (potentiostatic) bottom right.

5.3.6 Pitting Behavior of 316L in Solution 4 Polarized

Potentiostatically

This test involved polarizing the sample potentiostatically for 1.5 hours at 1.13 volts in a solution containing 1M H₂SO₄ and 0.25M nickel chloride using oxygen and argon as a means of attaining a deaerated state. The resulting corrosion behavior was only partially encountered in the literature review where the initial stages of this type of pitting is described regarding the formation of a lacy metal cover (16); see Figure 20.

Unlike previous tests where etching developed rather than pitting these tests produced virtually no detectable etching at any point in the corrosion process. This behavior is consistent with the work of Snow (1) who tested a similar fluid producing a similar pitting pattern. The corrosion pattern observed during testing was one of repeated destruction of the surface by aggressive pitting followed by the deterioration of the visible surface thereby exposing new unpitted metal. This behavior was seen in the two tests (aerated and deaerated) conducted with this solution, however only the deaerated test results are presented here.

Computer recorded polarization data experienced several current spikes as seen in Figure 63 which likely correspond to times when multiple pits developed simultaneously. As the techniques employed to observe the surface are not able to monitor the entire surface

it is not possible to confirm any direct link between the spikes and the stage of pitting exhibited on the surface.

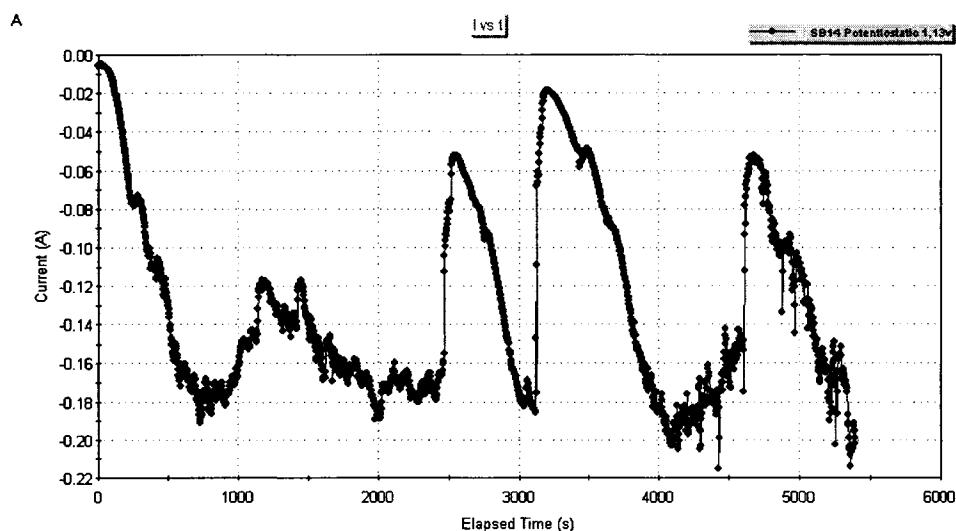


Figure 63: Potentiostatic test results SB14 deaerated

During the analysis of this sample computer image editing software was used to both locate and count the number of pits that occurred during the test in a similar fashion to that observed in the literature (48, 75); see Figure 64.

Features of interest at each stage are marked with a different color:

- Initial dark features are red
- First stage pits are green
- Second stage pits are blue
- Third stage pits are orange
- Fourth stage pits and surface features are purple.

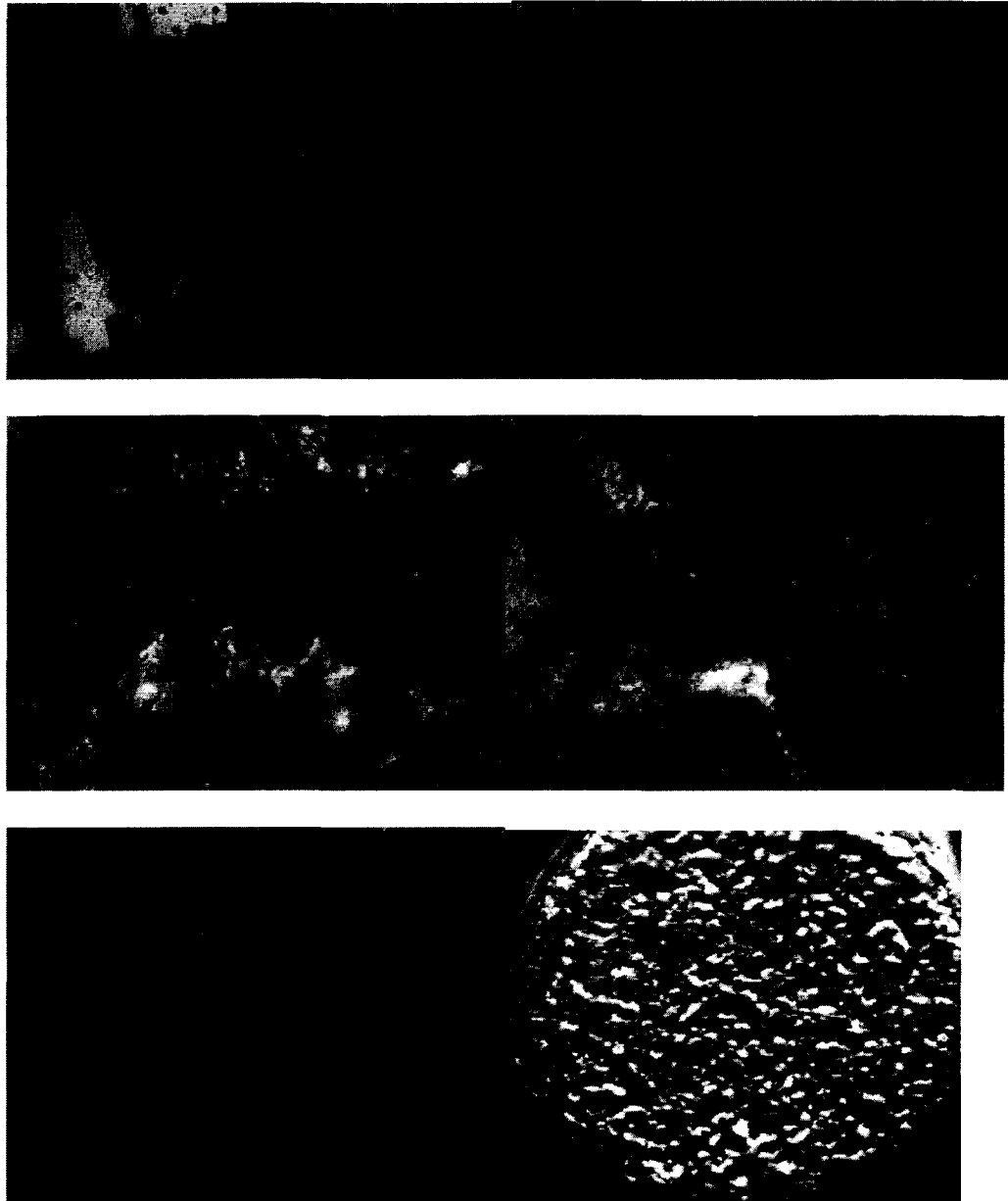


Figure 64: Original surface (top left), first stage of pitting (top right), second stage (middle left), third stage (middle right), final surface (bottom left), resulting surface of the 7mm wide exposed sample area (bottom right).

Interesting images of pit formation were also collected including before and after images of sites on which pits nucleated and grew. Seen in Figure 65 is a developing pit with an image of the site on which it formed. A small dark spot is visible and is estimated to be less than 1 μ m in diameter. Interestingly the larger dark points on the surface did not develop into pits with a tendency for small points such as the one shown to become stable pits. Using the results from the SEM and EDS analysis the small inclusions were identified as being sulfide inclusions, mostly MnS inclusions which have a tendency to dissolve leaving behind craters which commonly act as nucleation points for pits (1, 16, 46, 47, 50, 48)

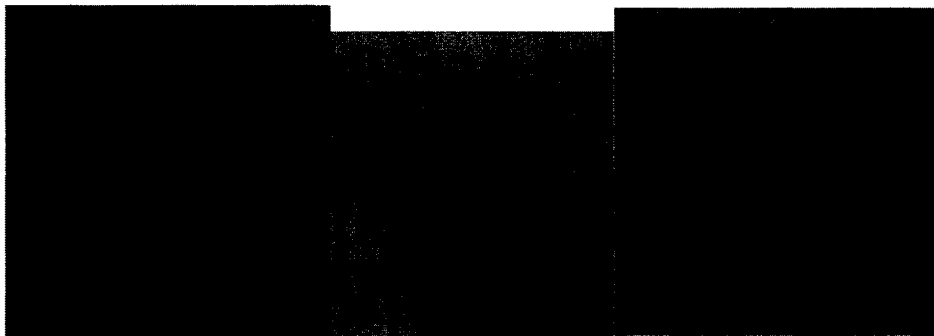


Figure 65: Imperfection in material's surface prior to polarization (left), pit forming at this site after polarized (middle), overlay of pit perimeter (red) with blue circle around pre-existing surface flaw. All images are at the same magnification.

5.3.6.1 Pitting Behavior Results

The unique pitting behavior allowed for the opportunity to track the progression, position and number of pits forming at each stage. The results are as follows:

- (1) Pitting showed a tendency to occur at what would appear to be different locations on the surface at each stage as they did not appear to nucleate at sites which were directly below the original pits. This lends some support to the assumption that most pits are forming on susceptible sites on the metal surface caused by defects such as inclusions and engrained stresses and not a continuation of previous pits.
- (2) Pits did not tend to occur on sites which had already developed large dark spots seen in the images taken at the end of immersion; rather they generally nucleated on minute dark spots which were barely imaged at this magnification. These were identified using SEM and EDS results as being most likely sulfide inclusions such as MnS inclusions, see Appendix A. These sites were best found by marking the locations in later photographs and looking back at previous images to confirm the nature of that site prior to polarization. See Figure 64 for illustration.
- (3) Pits appear to have a set growth behavior involving a first stage of being relatively round in appearance followed by a second growth stage that is more random in appearance and a third in which their progression brings them in contact with other pits. During the first step the pit grows down into the surface of the metal

and begins to expand horizontally (5, 16) as the slow removal rate of corrosion byproducts and slow flow of electrons to the base of the pit most likely reduce the rate of corrosion at the base of the pit. The second apparently random growth pattern in pit development is attributed to the progression of pits under the surface in a lateral direction parallel to the surface thereby undermining the surface before and working its way up to the surface before being exposed (16). During this test a dark porous cap appears to be present on the surface characterized by a shiny surface sparkle mixed in with a dark corrosion product.

- (4) Due to the progressive growth of the pits beneath the surface and at the same depth the surface layer eventually fails due to undermining. The force of the solution flowing over the surface causes the loose corroded metal to be pulled away exposing a relatively smooth surface beneath consisting mainly of fresh metal. After a brief incubation period this surface then begins to pit.
- (5) The final surface seen in the test results is a set of rounded peaks and valleys which appear to be uniquely resistant to pitting. An examination with the SEM failed to locate any inclusions or the typically large number of small pits left behind from the dissolution of sulfide inclusions instead only imaging unique square structures on the surface, see Figure 66. This behavior is unique to the potentiostatic samples tested in this solution under both aerated and deaerated conditions. There are no clear indications of preexisting features on the surface

present before this final step that would contribute to the position or depth of surface features in the final surface.

- (6) The number of pits on each new surface was not constant, with a tendency towards reduced numbers and larger individual pits in the last two stages with the final visible pit size increased accordingly.

The number of pits after each stage of experiential in-situ surface image observations was:

- Initial pitting: 42 pits visible
- Second surface: 69 pits visible
- Third surface: 33 pits visible
- Fourth surface: 6 pits visible.

This displays a tendency towards increased pitting resistance with ongoing exposure.



Figure 66: SEM image of a rounded surface feature on sample SB15 after testing, also many noticeable square structures are present on the surface.

5.3.6.2 Theoretical Explanation for Observed Pitting Distribution

A theoretical explanation for the observed pitting distribution in the tests is that the initial surface had relatively few sites as it was carefully polished, however there were undoubtedly surface stresses, and features such as inclusions which promoted pitting at certain locations. The second surface had experienced rapid and relatively even corrosion prior to exposure as the initial corrosion surface was perfectly flat, however it is likely that there were still numerous locked-in stresses from machining and the initial corrosion may not have consumed many of the more susceptible sites. The third surface had experienced a more thorough dissolution of the surface, possibly with fewer mechanical stresses remaining from machining thereby reducing the number of sites suitable for pitting. Finally the last stage had virtually no remaining weak spots on which pits could nucleate due to the prolonged corrosion of the surface which dissolved and rounded inclusions and would also provide a significant supply of accumulated chromium and so behaved as would an electropolished surface (27). The relatively inclusion free and uniform surface characteristics along with the surface displaying a relatively large radius of curvature makes the metal less susceptible to localized corrosion while avoiding any highly confined conditions that would cause crevice corrosion.

5.4 SC Series Results: Potentiodynamic Analysis of 316L Stainless Steel in Experimental Hydrometallurgy Process Fluids (EHPF)

The purpose of these tests beyond the acquisition of standard pitting potential and corrosion rate data is to determine the feasibility of using the in-situ optical microscopy corrosion cell for testing using real life industrial fluids.

These tests demonstrate not only that it is possible to obtain detailed pictures but that the data they provide is invaluable to the analysis of the corrosion behavior of metals in a complex chemical solution.

5.4.1 Solution and Test Properties

At the request of Inco the precise composition of the test fluids and their uses are not disclosed outside of the statement that the solutions are actual process fluids and contains sulfuric acid with various nickel and chloride concentrations.

Three test solutions were used, with the first two containing significant concentrations of nickel and sediment. The first two fluids had a dark green color which absorbed most of the light as it passed through it making imaging challenging but ultimately possible.

Table 8: SC series solution measured pH

Test Number:	Solution	Aeration	Solution pH Measured at 20.2°C
SC1	EHPF 1	Deaerated	2.865
SC2	EHPF 1		2.865
SC3	EHPF 2	Deaerated	4.829
SC4	EHPF 2		4.829
SC5	EHPF 3	Deaerated	9.496

5.4.2 Polarization Data

A series of potentiodynamic polarization tests were conducted on three solutions. This data was used to isolate the pitting potential, corrosion potential, and the corrosion rate. Polarization curves including Tafel fit and associated information is provided in Appendix D for all SA, SB and SC series potentiodynamic tests. An overlay of the test data is as follows:

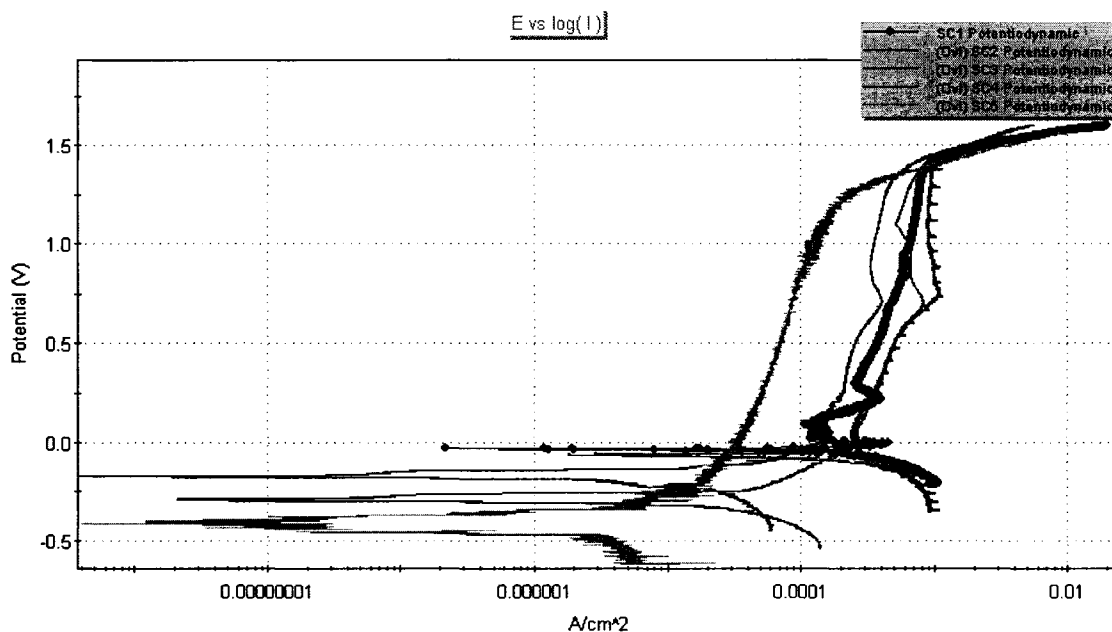


Figure 67: Polarization curves for SC series solutions (SC1, SC3, SC5 are deaerated)

An anodic knee was present in all scans except SC4 and SC5. This means that only SC4 and SC5 were in the passive state during the initial immersion at corrosion potential. The corrosion rate is calculated in Table 9. Regardless of the increased corrosion rates from active corrosion the SC series still experienced a corrosion rate that is a fraction of that found in most tests of the SB series; see Figure 69.

Surprisingly aerated solutions experienced a lower mixed potential compared to deaerated, the reverse on the results seen in the previous sections; see Figure 68.

By examining the videos recorded from the camera during testing it is observed that gas bubbles form on the metal surface at the same time the pitting potential is recorded. This makes it likely that the pitting potential for Inco Solutions 1 and 2 is potentially due to gas generation rather than pitting. See Figure 70.

Examination of the shape of the curves indicates that they may not be experiencing stable passivation as was observed in SA3, see section 5.2.3. In the case of Solution 1 and 2 this is most likely due to a combination of the presence of a flow rate and an aggressive solution. Solution 3 does not contain any substantial quantity of aggressive chemicals and has a high pH (basic solution) therefore it displays this curve most likely because of on 316L stainless steel's inability to form a passive layer in this type of solution.

Table 9: Corrosion test data SC series

Test Number:	Solution	Aeration	E _{corr} (mV)	I _{corr} (μA)	Corrosion Rate (mpy)	Pitting Potential (V)	Solution pH Measured at 20.2°C
SC1	EHPF 1	Deaerated	-20.288	1.96E+02	2.07E+02	1.4	2.865
SC2	EHPF 1	Aerated	-59.8	3.86E+02	4.08E+02	1.4	2.865
SC3	EHPF 2	Deaerated	-179.5	1.08E+02	1.14E+02	1.36	4.829
SC4	EHPF 2	Aerated	-292.94	3.69E+02	3.90E+02	1.36	4.829
SC5	EHPF 3	Deaerated	-362.3	2.55	2.695	1.23	9.496

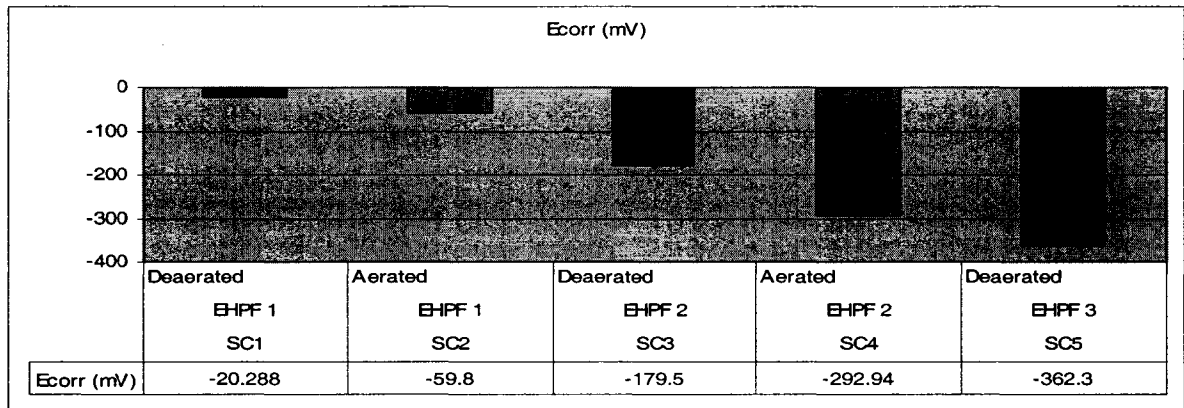


Figure 68: SC series corrosion potential graph

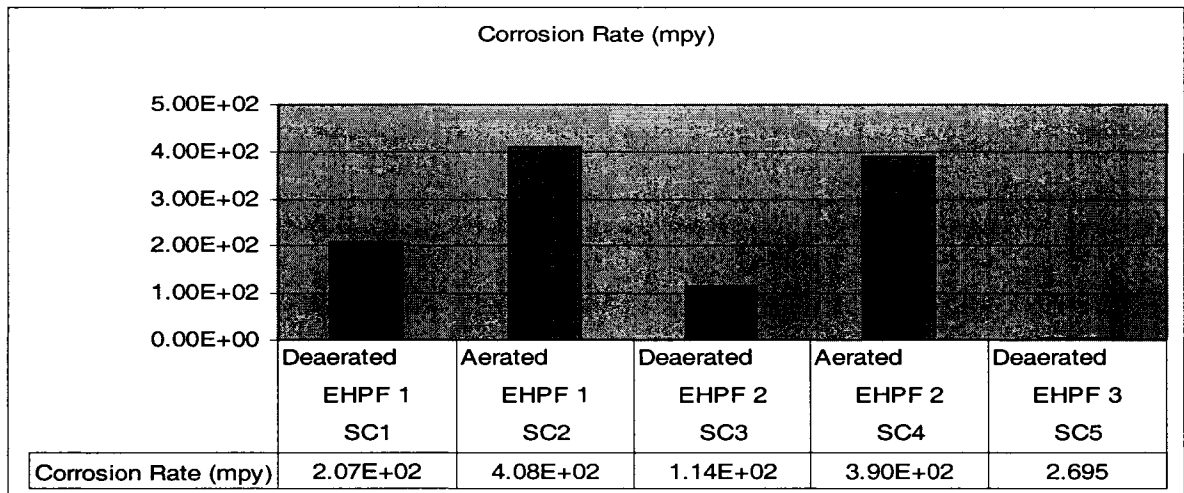


Figure 69: SC series estimated corrosion rate graph

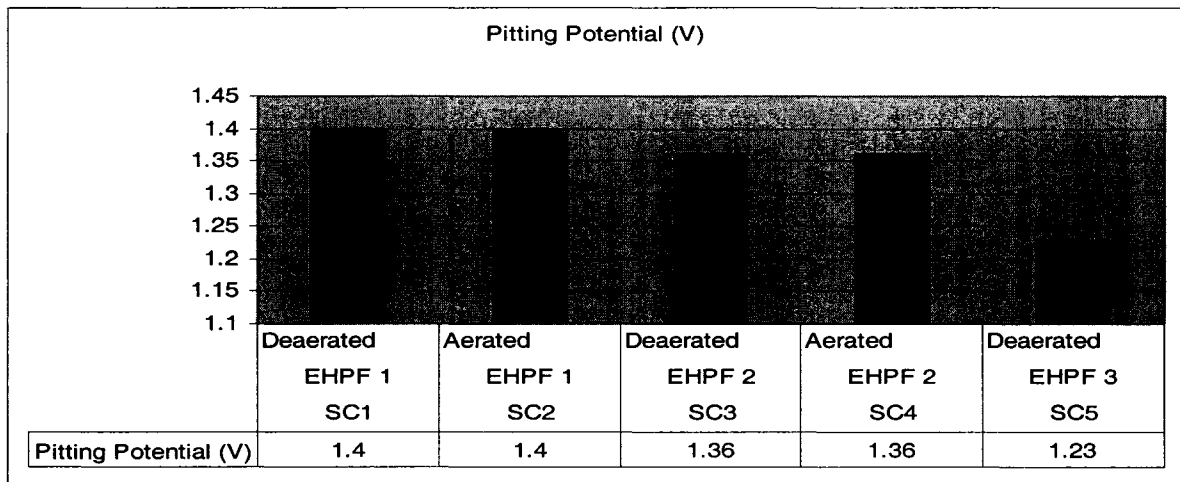


Figure 70: SC series pitting potential graph

5.4.3 Borderline Passivity

While recording the corrosion potential there was a single case of borderline passivity recorded (4). In the initial corrosion potential record of test SC1 the potential repeatedly fluctuated from -0.1 V to 0.02 V. After the test had been completed the behavior continued to fluctuate within the range of -0.016 V to 0.01 V. Further support for this conclusion came from an examination of the potentiodynamic polarization chart on which it appears that the curve has a pronounced anodic knee very close to the corrosion potential causing the metal to repeatedly go from an active to passive state and back as illustrated in the scan results below.

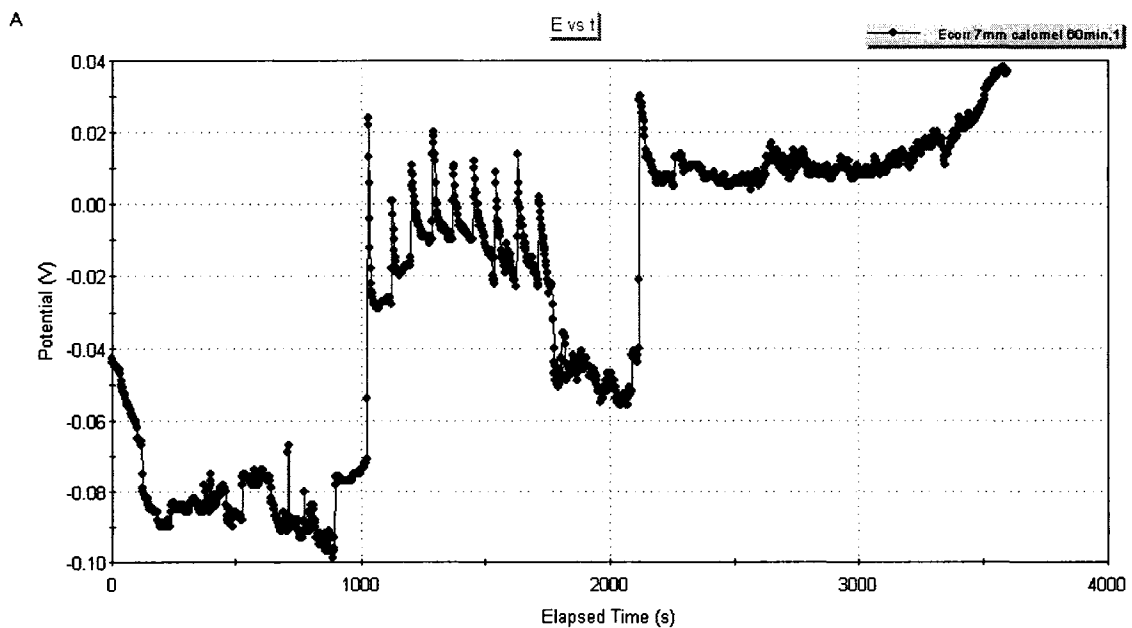


Figure 71: corrosion potential before polarization SC1

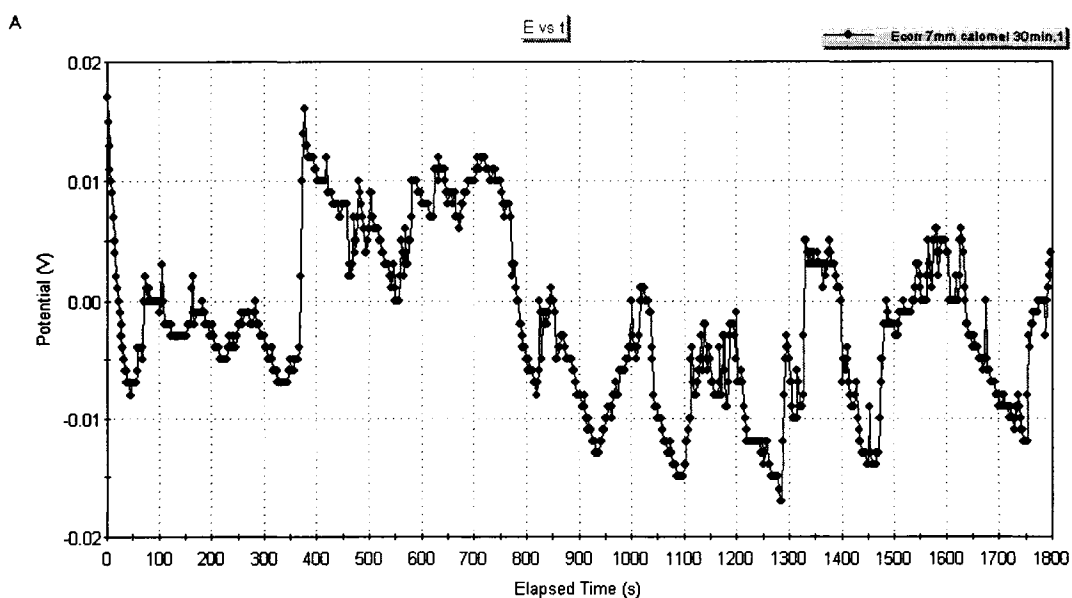


Figure 72: Corrosion potential after polarization SC1

5.4.4 Color Change and Peeling of Oxide Layer during Polarization

While undergoing polarization a number of unique color changes occurred in the surface layer of all samples tested in these three solutions. SC1-SC4 experienced a color change just before peeling. These events begin at or just before the pitting potential are reached in all four tests. See Figure 73 and Figure 74.

The following consistent sequence of events took place for SC1-SC4 tests:

- (1) A significant change in surface appearance and color occurred
- (2) Peeling began shortly thereafter
- (3) When given sufficient time to complete, the surface would be revealed again with a lighter colored appearance.

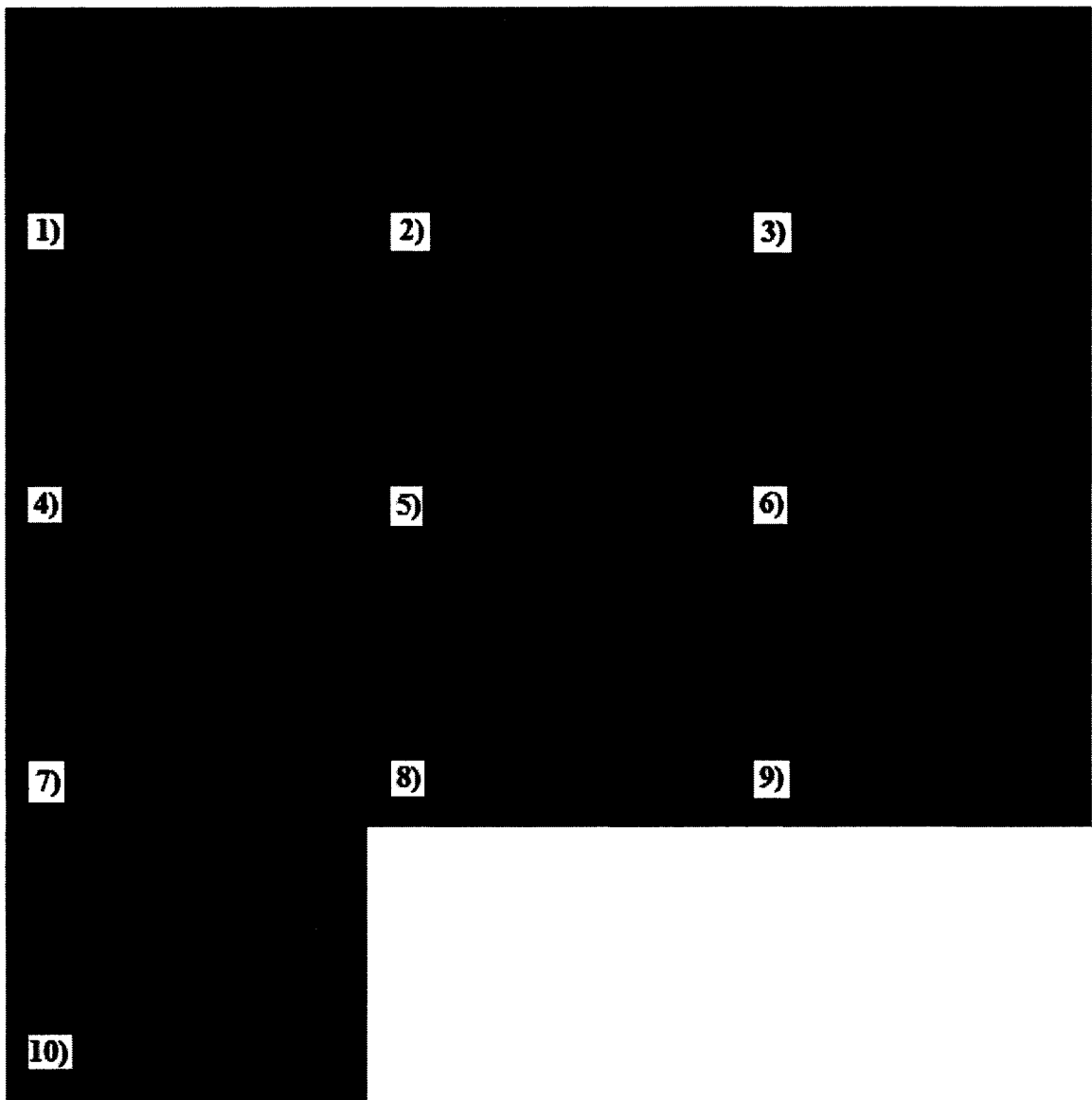


Figure 73: SC1 peeling event sequence of photographs, 1 minute time lapse between photographs, each image height represents 0.5mm.

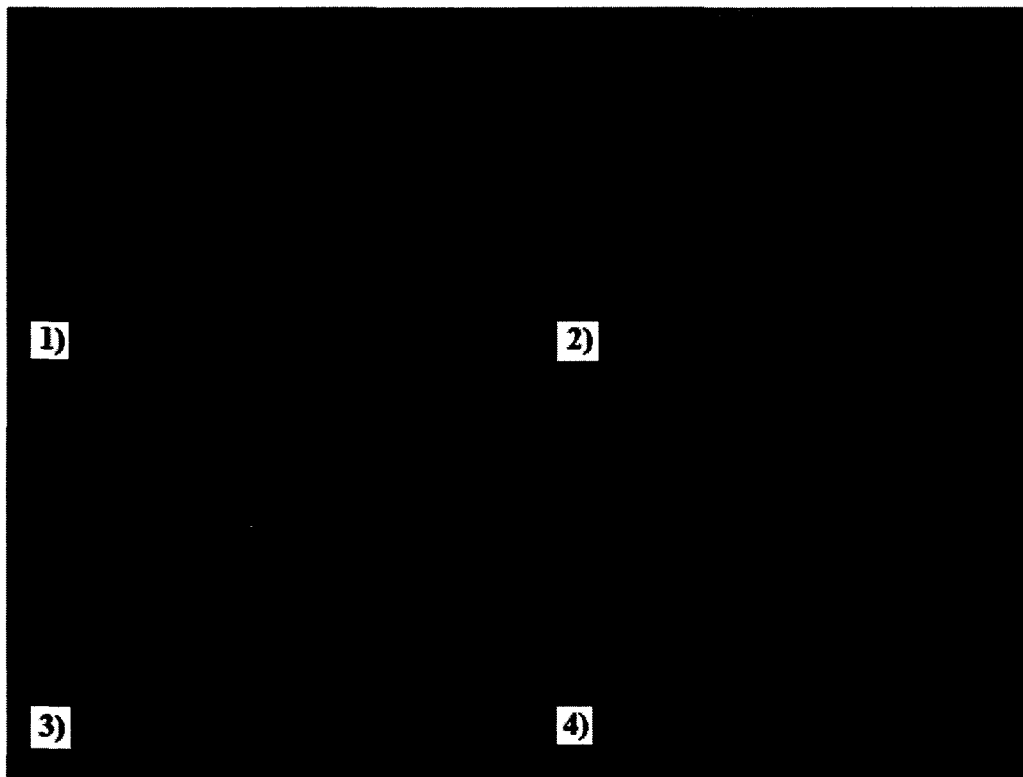


Figure 74: SC2 peeling event selection of photographs, images chosen from various times in the sequence, each image height represents 0.5mm.

5.4.5 Changes in Surface Features

A series of dark surface layers formed during testing including several which peeled off as seen in the previous section. No significant pitting or etching was ever observed either before or after testing however a thick dark oxide was found to be loosely adhered to the surface after testing and some samples displayed a slightly rougher surface after testing, (see Figure 75).

The destruction of the oxide layer may be due to the formation of dichromate instead of the stable oxide layer of chromium oxide. This may explain the common loss of color and surface cohesion at high potentials beyond 1.3 V in SC series (41).

SEM and EDS testing performed after completion of these tests revealed that the dark brown surface layer has almost the same composition of all other surface layers present on the metal samples with the exception of a slightly elevated concentration of carbon, (see section 5.7.3).

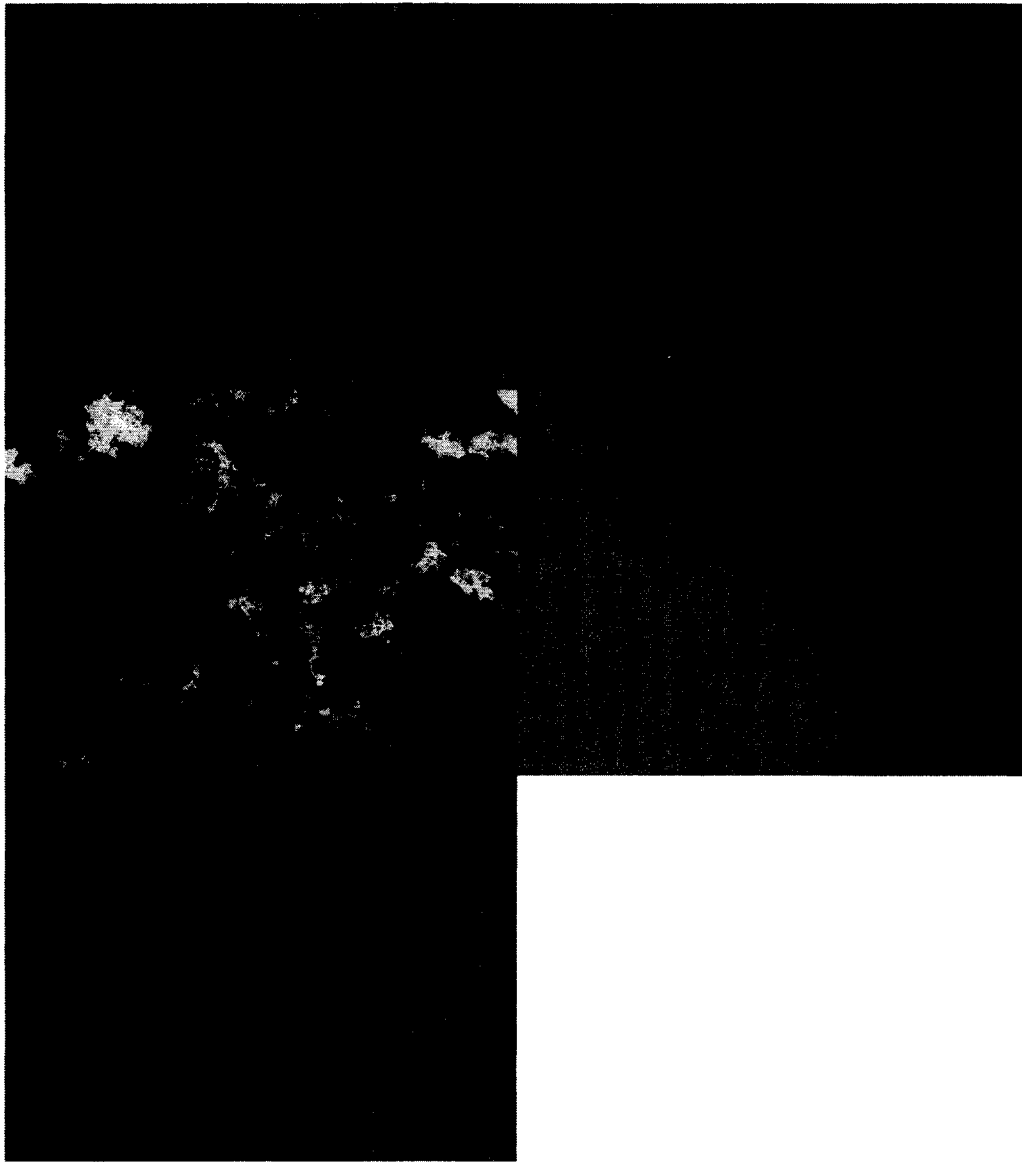


Figure 75: Images of SC1 (top left), SC2 (top right), SC3 (mid left), SC4 (mid right), SC5 (bottom left) surfaces after testing (taken after removed from fluid)

5.4.6 Benefits and Limitations of the In-Situ Optical Microscopy System When Using Experimental Hydrometallurgy Process Fluids

It is possible to see the surface through even heavily tinted and cloudy solutions but the color produced may not be filtered out by the camera optics. In the case of tests SC1-SC4 a dark green tinge is seen making it difficult to positively identify the color of i.e. oxides forming on the surface.

The strong green color makes it more difficult to accurately focus the microscope causing some minor reduction in image quality.

The reduced penetration of light into the fluid would suggest that darker pits and surfaces may be less clearly imaged.

All three of these issues may be addressed by using a high quality microscope with a powerful light source and filter system.

5.5 Miscellaneous Metals Results: Behavior of Industrial Metals in 3.5% NaCl Solution

Salt water tests were undertaken early in the testing process to act as a means of safely testing the equipment and perfecting testing procedures without the dangers associated with working with acidic solutions. These tests were conducted using a variety of metals sometimes with highly unique results.

Tests were conducted using a consistent solution of 3.5% NaCl at 25°C and samples of 316L stainless steel, magnesium, 6061 aluminum and Cu/Sn based electronic trace material. As the corrosion behavior of metals differs significantly both on the basis of each metal's composition and the solution properties, a wide variety of corrosion behaviors were imaged.

Although the standard polarization records were recorded they are not the focus of this section. This section only displays images resulting from testing and uses them to illustrate key concepts specific to illustrating the benefits of in-situ optical microscopy.

5.5.1 316L Stainless Steel in 3.5% NaCl Solution

Potentiodynamic testing on 316L stainless steel in 3.5% NaCl solution at 25°C was performed under standard aerated and deaerated testing conditions. The samples were prepared under similar degree as were those used in sulfuric acid tests; however a different pitting behavior was recorded in this solution than that seen in sulfuric acid based tests.

5.5.1.1 Potentiodynamic Test Results

The pitting potential recorded for these tests were significantly lower than those of the sulfuric acid tests. Pitting potential for aerated conditions was 0.38 V, and for deaerated it was 0.3 V. The current density in the transpassive region was much higher than was achieved in any sulfuric acid test running up to 1 A/cm^2 for the aerated test and beyond the 1 A/cm^2 limit for the deaerated test.

These pitting potentials are consistent with pitting potentials recorded for similar materials demonstrated such as a 0.42 V pitting potential being recorded when testing 316 stainless steel in 3%NaCl (16). These outside test results also recorded a comparable current density for the pitting potentials however it is noted that the curves recorded during testing show a sloped appearance within the passive region rather than the vertical one would expect for a passivating metal. This behavior is most likely due to the flowing

solution used during testing which is not present for most tests conducted using conventional cells.

The pitting potential for deaerated solutions is found to be lower than that for aerated solutions in these two tests making it more prone to pitting at lower potentials. This behavior is consistent with the literature (1, 4, 22).

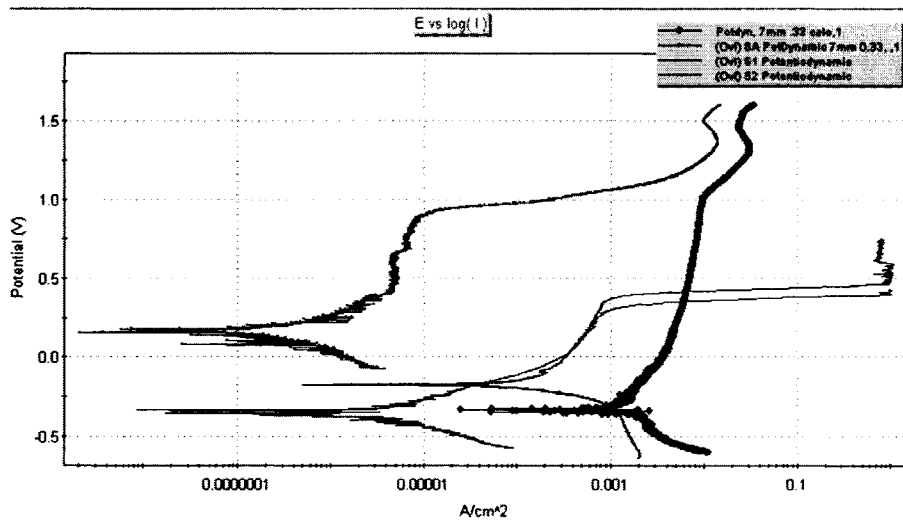


Figure 76: Overlay of saltwater aerated (black) and deaerated (red) tests with SA3 aerated (green) and SA12 deaerated (blue) 1M H₂SO₄ results.

5.5.1.2 Aerated Test Results

Under these test conditions a brown oxide layer presumably formed on the surface. As the potential approached the pitting potential a series of lightly colored spots formed on the surface. Once pitting potential was reached these areas acted as the initiation sites for aggressive pitting, as illustrated in the pit analysis images in Figure 77. It is not possible to conclusively identify the surface features which cause the light spots based solely on these test results however SEM and EDS testing of the metal surface seen in Appendix A combined with initial images from the immersion stage showing small dark spots on the metal surface where the light spots form support the assumption that these may be sulfide inclusions. The test results from sulfuric acid tests also support this conclusion.

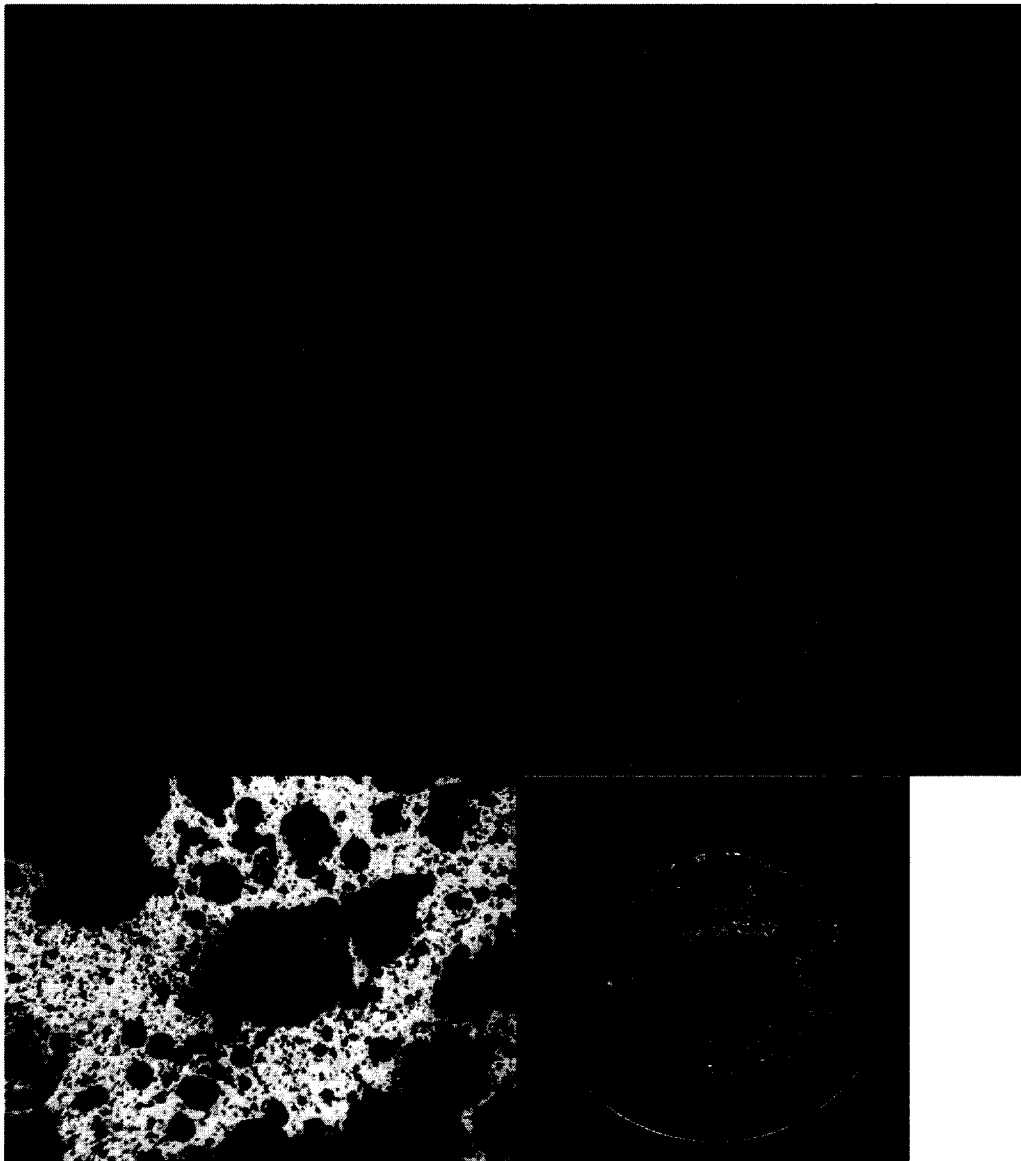


Figure 77: Progression of pitting for 316L stainless steel in 3.5% NaCl aerated (images 1-5, first image at top left, final image bottom left), scanned image of sample after testing was completed (bottom right)

5.5.1.2.1 Theoretical Explanation for Pitting Behavior

Using a graphics package it was confirmed that these pits all formed on top of a preexisting lightly colored point at which the oxide layer was presumably at its weakest due to the partial dissolution of sulfide inclusions. The literature review points to the presence of chloride ions in the solution as the most likely cause of damage and hence lightening of the oxide layer (4, 10, 16, 18).

The conclusion taken from this test is that thin points in the oxide layer coinciding with sites of particular vulnerability such as sulfide inclusions may sometimes be visually recorded in their formation as well as the progression of pit development. Although the information provided by this test is compelling further study would be required to support any conclusion on precise mechanism behind this type of pitting activity.

5.5.1.3 Deaerated Test Results

During the deaerated tests a lightly colored surface layer formed on the sample making any identification of weak points in the oxide layer such as those seen in the aerated tests difficult. Despite this limitation unique images were taken of the process by which these pits develop and it was possible to see some preexisting flaws in the surface on which some of the pits develop. A significant difference in pitting behavior between aerated and deaerated tests was also noted.



Figure 78: Progression of pitting for 316L stainless steel in 3.5% NaCl deaerated (first image at top left, final image bottom left)

5.5.1.3.1 Theoretical Explanation for Pitting Behavior

The images produced showed that the pitting behavior was deferent for 3.5%NaCl solutions under aerated and deaerated conditions. As discussed in the aerated section the small dark points on the surface which acted as nucleation points are attributed to sulfide inclusions. The deaerated tests produced rough looking capped pits seen above rather than the well rounded pits seen to develop early in the aerated test. Although both samples ultimately developed large open pits, traces of the pitting behavior which produced them are still clearly visible on the surrounding metal surface. The development of the pit structure seen in the deaerated tests is consistent with the pit cap growth theories listed in the literature (16).

The differences in surface color and pitting behavior is consistent with present known corrosion theories regarding oxide layer formation and pitting behavior (4, 16, 22).

5.5.1.4 Conclusions

In-situ optical microscopy is capable of recording the corrosion behavior of stainless steel with sufficient detail to make observations on key corrosion phenomenon possible.

These phenomenon included:

- Assessment of original surface characteristics such as inclusion shapes and sizes;
- Localized changes in oxide formation before pitting occurred;
- Observation of fine details during the early stages of pitting including shape, growth rate and distribution;
- The progression of pitting during all stages of its progression.

5.5.2 Testing Magnesium in Salt Solution

5.5.2.1 Test Results

A sample of high purity magnesium was tested potentiostatically during an early stage of testing using a saturated solution of table salt in tap water. The results demonstrate both the benefits and limitations on the system.

The test produced what appears to have been an unstable black “tentacle like” corrosion byproduct resulting from the test being done under deaerated conditions. The images obtained from testing took place within the first 30 seconds of the test as all images after that time were completely black due to the light absorbing properties of the then completely black surface.

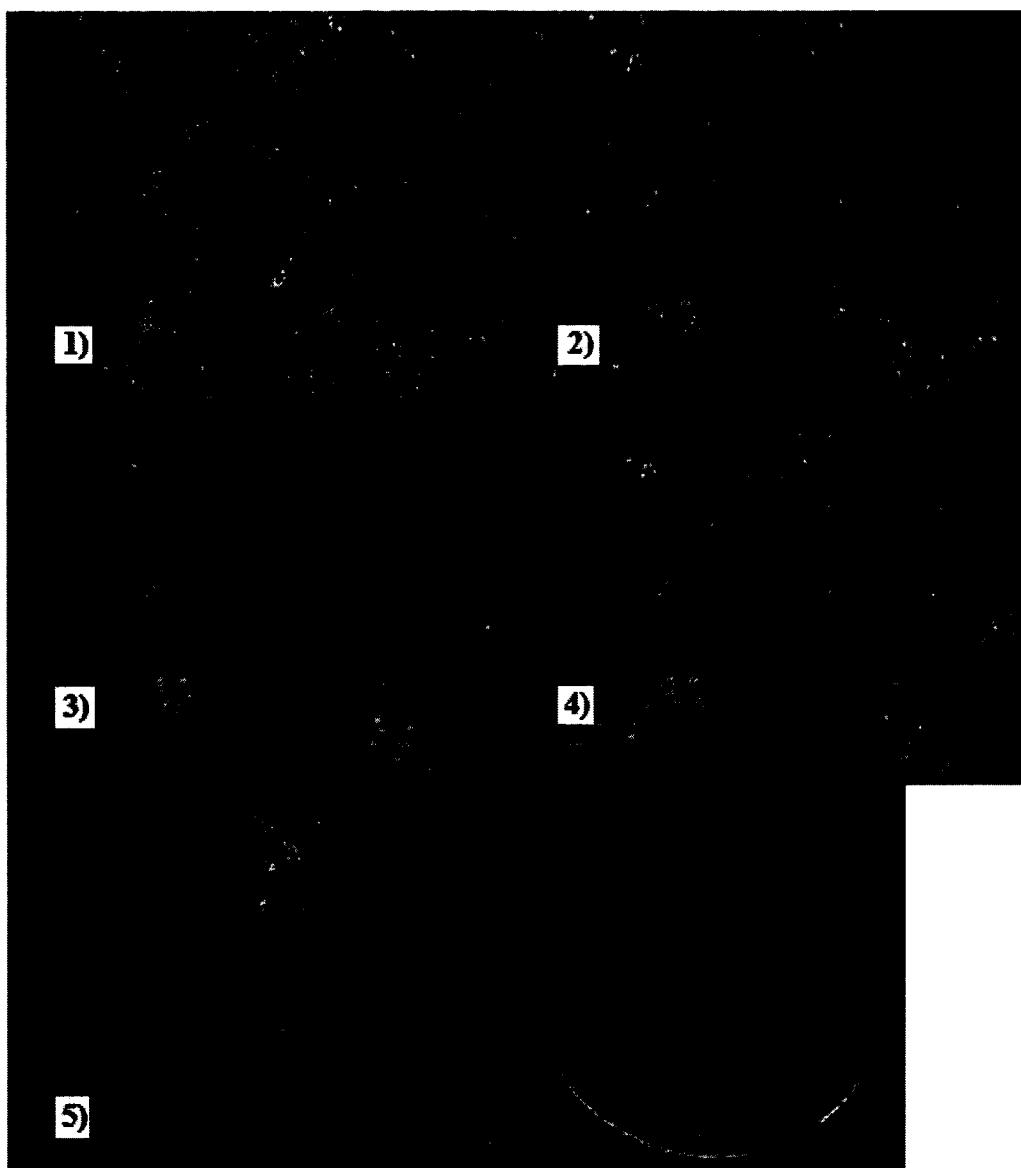


Figure 79: Magnesium potentiostatically tested in saturated table salt solution.

5.5.2.2 Discussion

It was possible to record clear images of a fast forming dark “tentacle like” corrosion product extending over the surface. Under normal testing conditions these details would have been difficult to obtain as the corrosion product was both delicate and reactive to oxygen. Once removed from the test chamber the corrosion product began to crack and bubble with gas, eventually turning the black substance bright white resembling i.e. a phase transformation. Also the byproduct separated during cleaning.

5.5.2.3 Conclusions

The system can produce good images of surface detail along with valuable video images of fast forming phenomenon that can be used for later analysis. Substances and delicate surface details that are normally not recorded during conventional testing are clearly visible without any damage

A limitation on this system is that it is difficult to image uneven or heavily darkened surfaces due to the limitations of optical microscopy.

5.5.3 Testing of 6061 Aluminum in 3.5% NaCl Solution

5.5.3.1 Test Results

A limited number of potentiodynamic tests were conducted on 6061 aluminum in a 3.5% NaCl solution. The scan results indicated that the material had naturally passed its pitting potential when immersed in the solution.

Two tests results are displayed below. These tests were both conducted under aerated conditions with similar surface conditions. The images recorded confirmed that this was the case and were able to document the progression of corrosion under both E_{corr} and polarized conditions with similar visible results from both tests.

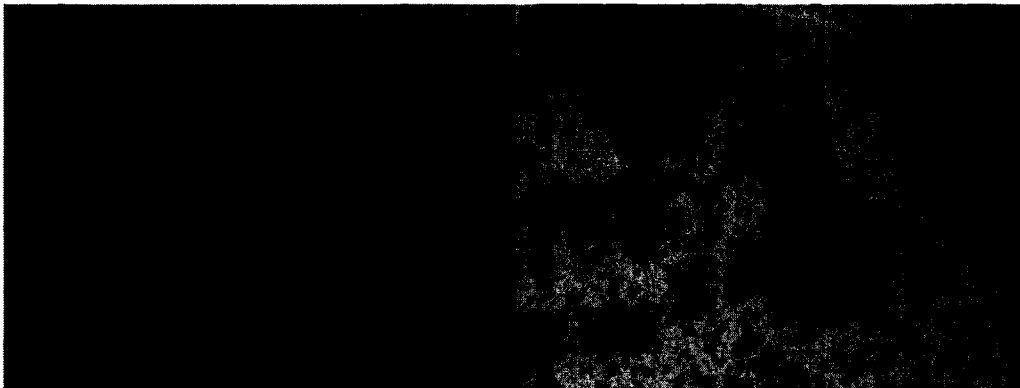


Figure 80: Pitting in aluminum as observed in test A2



Figure 81: Pitting in aluminum as observed in test A4 (first image at top left, final image bottom left)

5.5.3.2 Conclusions

The system is clearly able to take clear images with good contrast of highly complicated patterns of corrosion present around the edges of the pits. These corrosion patterns are once again unique to this metal under these conditions.

The imaging of the initial immersion stage of the test demonstrates the possibility of using these techniques in long term immersion tests to allow for observation of corrosion and pitting under realistic unpolarized immersion tests.

5.5.4 Testing of Cu/Sn Based Electronic Trace Material in 3.5% NaCl Solution

5.5.4.1 Test Results

A test was performed with the intension of demonstrating this technique's ability to image small scale components in electronic devices. Using the results of such tests it may be possible to locate weak points in corrosion resistant coatings under realistic operating conditions in which the traces and components are electrically active and hence naturally polarized.

In Figure 82 a section of circuit board was cut into a circular piece and covered with clear tape. A hole was then cut in the tape exposing the Cu/Sn ~(80/20 by weight) metal to the solution and electric current was passed through that section using the existing electrical connections of the board.

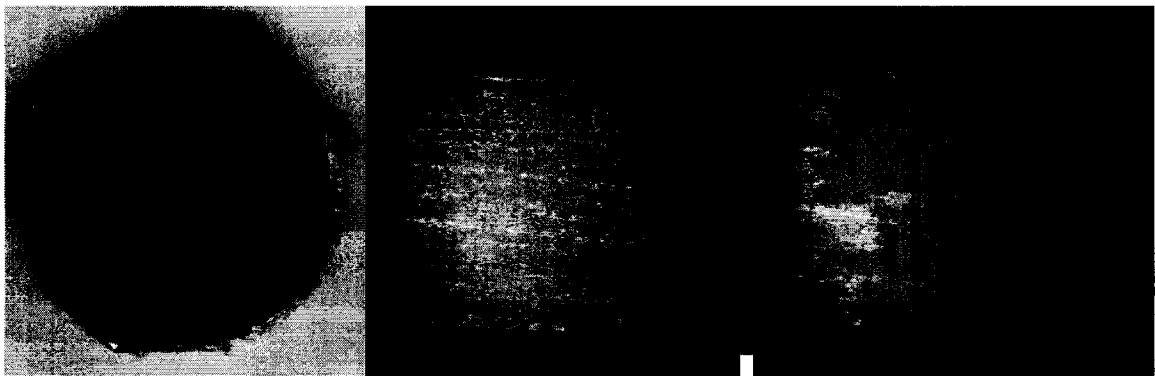


Figure 82: Photograph of signal trace metal Cu/Sn ~ 80/20 (by weight), left is circuit before solder, middle is a trace before test began, right is the same trace during testing.

5.5.4.2 Conclusions

It is possible to get high quality images of flat surfaces on electronic components undergoing polarization. A depth of field limit is present regarding imaging surfaces not in a flat plane perpendicular to the axis of the microscope. As the microscope is not able to easily image these surfaces components that are not flat such as resistors and transistors may not always be viewed clearly.

5.5.5 Titanium

Two grade 2 titanium samples were taken from materials provided by Inco. A second set of samples were taken from a titanium welding rod composed of Grade 2 titanium labeled as AFM ERTi-2. The composition of this material is confirmed to be within the specifications listed for Grade 2 Ti by the manufacturer American Filler Metals (66)

Samples of titanium were tested using saltwater and sulfuric acid solutions. Although it was possible to image the surface, the test solutions used were not able to cause pitting within the range of potentials tested which ran up to 1.6 V. These results are not surprising as according to the literature search titanium has a remarkably resilient oxide layer which unlike Cr_2O_3 does not break down at high potentials. Pitting is not reported for saturated chloride containing solutions within a sulfuric acid concentration range of 0-50% (35). Titanium is also described as being immune to corrosion in saltwater and erosion resistant (52).

5.5.5.1 Salt Water Tests

The welding rod tested in the saltwater environment is shown in Figure 83 and Figure 84. The heavy scratch pattern is from the tool marks of the lathe. Although polishing was attempted on samples such as this it was not easy to attain a proper finish and the test was performed on this rough piece of metal. Some small changes are apparent during the test such as the darkening patch on the surface.

Although the test was not successful in achieving pitting of titanium it was able to prove that the system can attain high quality images of surface features on titanium samples. It also demonstrated the ability of the system to be used with small area samples so as to be able to image most of a sample's surface while recording useful polarization data. This sort of sample with a small cross sectional area is nearly ideal for in-situ optical microscopy allowing for the observation of most of the materials surface. If a small wire is used it is possible to observe all pit nucleation events on a small sample area and directly link them to the computer recorded polarization data. Some drawbacks as seen are that samples tend to be difficult to prepare and may have high engrained stresses. Also reference electrodes may have greater difficulty detecting the fluctuations in current and potential and even small changes in exposed surface area may create a sloped appearance for the passive region in some scans.

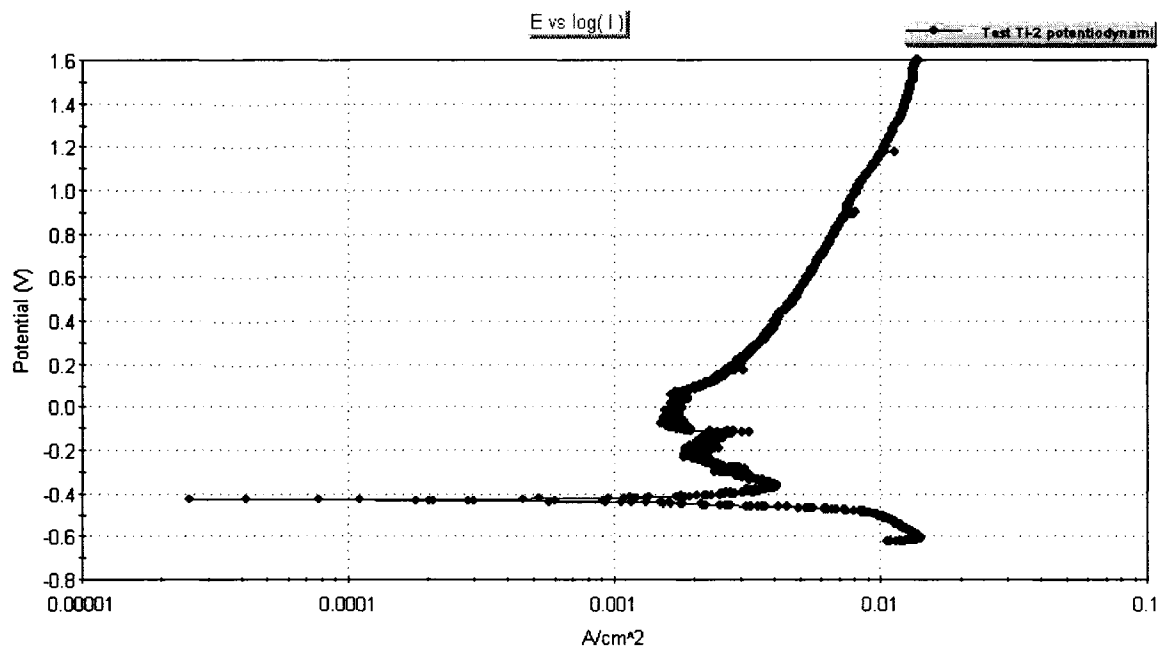


Figure 83: Potentiodynamic polarization scan results of a titanium welding rod in saltwater

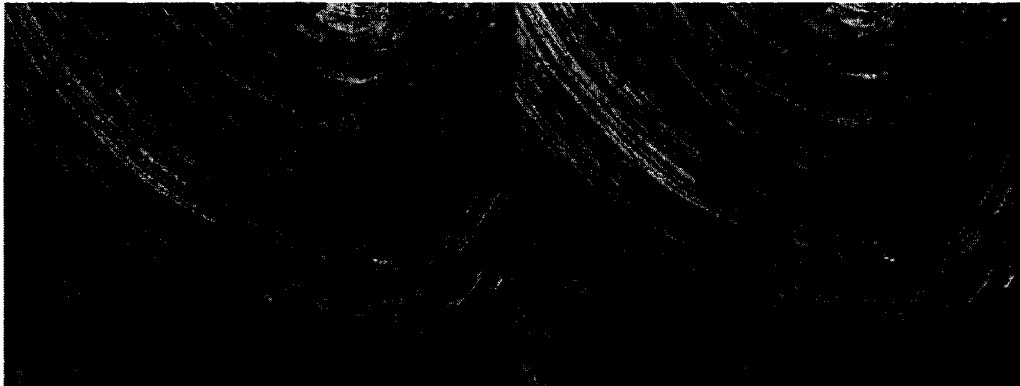


Figure 84: Image of the tip of a titanium rod being tested in saltwater solution at start (left) and at the end (right)

5.5.5.2 Titanium in Sulfuric Acid Results

Two samples were machined out of a piece of grade 2 titanium provided by Inco. These samples were machined to a $1\mu\text{m}$ finish and tested in the same manner as the stainless steel samples.

Two potentiodynamic tests were performed. The first test used Solution 4, a $1\text{M H}_2\text{SO}_4$ solution and the second used a $3.3\text{M H}_2\text{SO}_4$ saturated with nickel chloride. Neither test achieved any pitting or significant changes in surface appearance as a result of the scan, but clear images of the metal surface were taken and if tested under the correct conditions any severe forms of corrosion should be clearly visible.

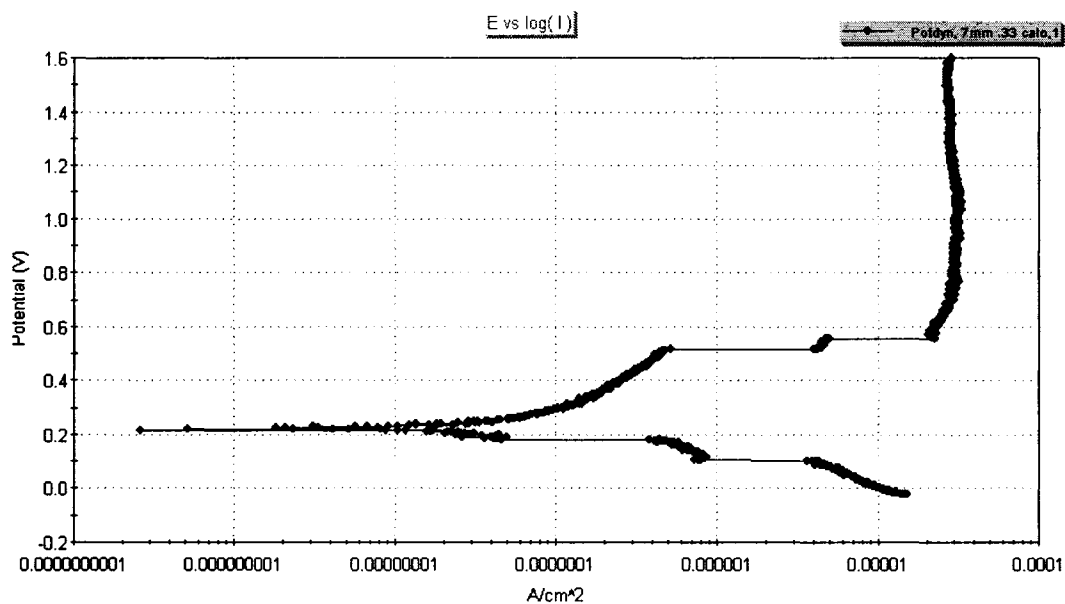


Figure 85: Potentiodynamic polarization data from test TiA1 (titanium in solution 4 deaerated)



**Figure 86: Images of titanium surface before (left) and after (right) polarization in test TiA1
(titanium in solution 4 deaerated)**

5.6 Overall Analysis of Corrosion Results

5.6.1 Introduction

Polarization curves including Tafel fit and associated information are provided in Appendix D for all SA, SB and SC series potentiodynamic tests.

5.6.2 Corrosion Potential for All Sulfuric Acid Solutions

The surface potential of a corroding metal can be measured experimentally in a cell with respect to a reference electrode and described as a corrosion potential according to mixed potential theory (4). The corrosion potential (E_{corr}) or mixed potential as it is sometimes called is a combination of both cathodic and anodic reaction potentials on a surface and provides evidence of the chemical reactions occurring on that surface. The results are as follows:

Table 10: Mixed corrosion potential (E_{corr}) for all potentiodynamic tests

Test Number:	Solution	Aeration	E_{corr} (mV)
SA3	Soln. 1		155.4
SA12	Soln. 1	Deaerated	-334.5
	Soln. 5	Deaerated	-353.4
	Soln. 5	Deaerated	-329.9
	Soln. 5	Deaerated	-386.9
	Soln. 5	Deaerated	-219.5
	Soln. 5	Deaerated	-360.6
	Soln. 5	Deaerated	-313
	Soln. 5	Deaerated	-345.9
	Soln. 5	Deaerated	-302.9
SC1	EHPF 1	Deaerated	-20.288
SC2	EHPF 1		-59.8
SC3	EHPF 2	Deaerated	-179.5
SC4	EHPF 2		-292.94
SC5	EHPF 3	Deaerated	-362.3

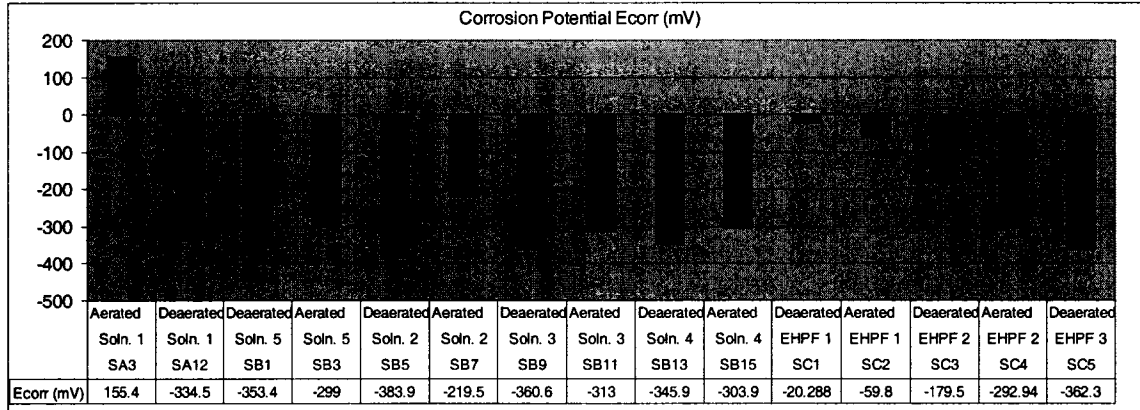


Figure 87: Corrosion potential (aerated in green, and deaerated in blue)

The corrosion potential values are consistent with the previous research work of Snow (1) with particular emphasis on the increase in potential into the positive side of the chart for Solution 1 which was also seen in the above referenced work. The correspondingly more noble mixed potentials match the theoretical behavior for samples exposed to an increased concentration of a stronger oxidizer (1, 4, 16, 22, 35).

The principles associated with the addition of a stronger oxidizer to a given solution describe a tendency towards typically increasing the overall mixed potential. When oxygen is added to the solution the potential for all solutions increases as oxygen is a stronger oxidizer in this fluid than the typical electrolysis based reactions seen in deaerated solutions.

5.6.3 Corrosion Rates for All Sulfuric Acid Solutions

5.6.3.1 Corrosion Rate Test Results

Using the PowerCORR software package's calculations based on the potentiodynamic test results the following corrosion rates are estimated for all tested solutions when naturally corroding with a corrosion potential. These results are displayed in Figure 88.

Table 11: Corrosion rate for all potentiodynamic sulfuric acid tests

Test Number:	Solution	Aeration	Corrosion Rate (mpy)
SA3	Soln. 1		5.99E-01
SA12	Soln. 1	Deaerated	1.46E+03
SA1	Soln. 5	Deaerated	7.75E+02
SA2	Soln. 5		1.99E+03
SA5	Soln. 2	Deaerated	7.87E+02
SA22	Soln. 2		4.75E+02
SA8	Soln. 3	Deaerated	1.70E+03
SA13	Soln. 3		2.32E+03
SA14	Soln. 3	Deaerated	1.66E+03
SA15	Soln. 3		1.85E+03
SC1	EHPF 1	Deaerated	2.07E+02
SC2	EHPF 1		4.08E+02
SC3	EHPF 2	Deaerated	1.14E+02
SC4	EHPF 2		3.90E+02
SC5	EHPF 3	Deaerated	2.695

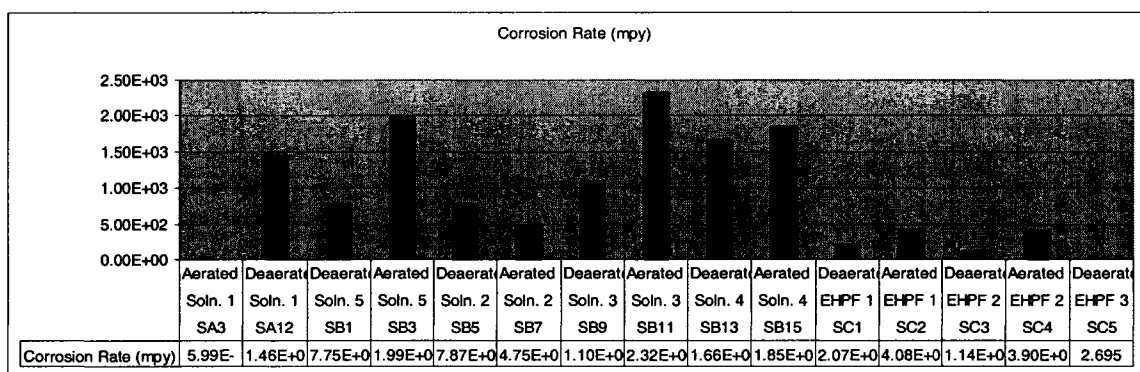


Figure 88: Corrosion rate in mpy (aerated in green, and deaerated in blue)

For most cases there was only one test performed for each unique set of testing conditions and the actual interpretation was performed using computer software. As a result a certain degree of error should be considered in interpreting these results; however the overall trends seen in these tests appear accurate.

5.6.3.2 Conclusions

The effects of decreasing pH were illustrated in Solution 5 where the composition was 3.3M H₂SO₄ rather than the standard 1M H₂SO₄ which showed a great increase in the corrosion rate of aerated solutions. The high pH solutions of the EHPF solution tests also demonstrated this effect showing a tendency for low acidity solutions to produce low corrosion rates as compared to the 1M H₂SO₄ tests.

The presence of chloride ions in high concentration also had a great effect on corrosion rates. The increase in chloride ion concentration in Solutions 3 and 4 produced the greatest corrosion rates of any 1M H₂SO₄ solution.

It appears that 1M sulfuric acid solutions do not produce a stable passive layer on 316L stainless steel. This is supported by the high corrosion rate present in all tests with the exception of SA3 and the visible phenomenon of peeling surface layers observed in a variety of tests. This result is interesting as tests by Snow (1) showed typical passivation behaviors in most solutions. The change may be related to the increased volume of acid present in the system and the presence of a constant fluid flow across the sample surface. These tests point out the possible shortcomings of standard polarization experiments using stagnant fluids as they may produce unrealistic results under certain conditions.

5.6.4 Pitting Potentials for All Sulfuric Acid Solutions

5.6.4.1 Pitting Potentials

The pitting potential is illustrated in Figure 89. In the majority of these tests there are few pits with a tendency for the pitting potential to indicate the beginning of active etching in Solutions 1, 2, 3 and 5. Solution 4 had a high Cl^- concentration causing pitting to become dominant over all other forms of corrosion once the pitting potential had been reached.

The individual pitting potentials recorded were consistent in their magnitude with the test results from the work done by Snow (1); however several tests displayed a higher pitting potential for deaerated solutions which is considered unusual. This behavior may theoretically be attributed to the lack of aggressive pitting in most solutions where corrosion rates were mostly determined by the rate of etching along grain boundaries combined with the effects of a flowing fluid over a surface with an unstable passive oxide layer. The stainless steel samples may have had trouble establishing a stable oxide layer in 1M sulfuric acid in accordance with statements made by (4, 35) which describes the difficulties associated with establishing a stable oxide layer in solutions other than very strong or very weak sulfuric acids. This topic is discussed in Section 5.2.3.

Table 12: Pitting potentials for all potentiodynamic sulfuric acid tests

Test Number:	Solution	Aeration	Pitting Potential (V)
SA3	Soln. 1		0.9
SA12	Soln. 1	Deaerated	1.05
		Deaerated	1.07
		Deaerated	1.02
		Deaerated	1.09
		Deaerated	1.01
		Deaerated	1.04
		Deaerated	1.02
		Deaerated	1.03
		Deaerated	1.04
SC1	EHPF 1	Deaerated	1.4
SC2	EHPF 1		1.4
SC3	EHPF 2	Deaerated	1.36
SC4	EHPF 2		1.36
SC5	EHPF 3	Deaerated	1.23

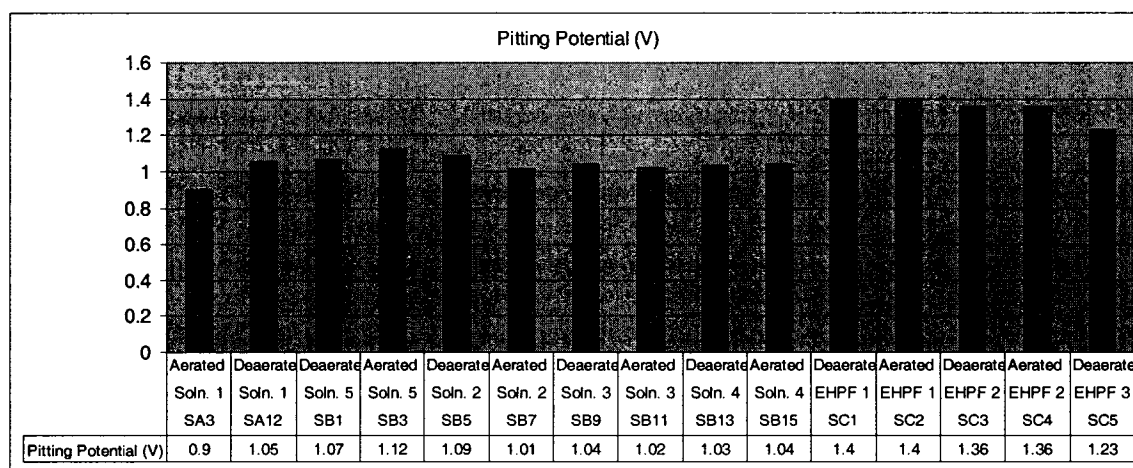


Figure 89: Pitting potentials (V) (aerated in green, and deaerated in blue)

5.6.4.2 Conclusions

5.6.4.2.1 Theoretical Explanation for Aerated vs. Deaerated Test Results

The commonly lower pitting potentials for aerated solutions are attributed to the unstable behavior of the passive layer on austenitic stainless steels in moderate strength sulfuric acid solutions (4, 35) leading to greater corrosion rates potentially being effected by fluid flow velocity. The following theory was developed to explain the observed behaviors:

Unstable Passive Layer Theory:

In deaerated tests or highly aggressive solutions tested many parts of the surface may naturally lack a stable oxide layer generating a greater current density and potentially generating a more complicated surface behavior which has not been thoroughly studied in the literature. The unstable oxide layer would not offer the same degree of protection against pitting and etching even with high levels of oxygen, resulting in the lack of any consistent difference in pitting potentials for aerated and deaerated solutions.

Solutions 4 and 5 displayed a greater pitting potential for aerated conditions in accordance with typical behaviors (1, 4, 5, 74). This may also be consistent with the theory of an unstable passive layer as these are more aggressive solutions that normally penetrate the oxide layer and could conceivably have greater effects on pitting than the instability of the oxide layer.

5.6.4.2.2 Theoretical Explanation for Etching Behavior of SA Series Samples

Polarized at 0.9 V, Aerated

Samples tested in the 1M sulfuric acid solutions showed signs of unstable oxide layers as predicted by the literature (4, 35). The unstable passive regions may have lead to greater corrosion rates potentially being effected by fluid flow velocity.

In the case of Solution 1 tested under aerated conditions a unique behavior was observed where a high corrosion rate (as marked by a high current density) was observed in the form of etching along grain boundaries when polarized potentiostatically at 0.9 V then passivating near the end of the test. This behavior may be explained by theorizing that this sample was barely experiencing the conditions necessary for passivation on the grains during testing at 0.9 V but not at the grain boundaries where inconsistencies in the metal structure made it temporarily more active in nature resulting in preferential corrosion similar to that observed in pits. The resulting naturally increased polarization of these areas and the increased current flow caused these areas to corrode at an increased rate. During later tests the surface of the grains may not have passivated resulting in a more evenly distributed corrosion process at a slower rate as the potential and current was more evenly distributed.

5.6.5 Anodic Knee

5.6.5.1 Aerated Solutions

For aerated solutions the anodic knee only appeared in the cases of EHPF Solution 1 (SC2) and Solution 4 (Test SB15). Solution 4 had a high Cl^- concentration making test sample metals more vulnerable to active corrosion and the EHPF solution was a relatively weak solution making them less likely to passivate. See Figure 90 and Figure 67 for SC. This indicates that these metals were in a state of active dissolution before polarization began. All anodic knees observed during testing were relatively small in size however using the results of Snow (1) for comparison between stable and unstable passivation for these solutions it is apparent that these small curves are indeed anodic knees; see Figure 1.

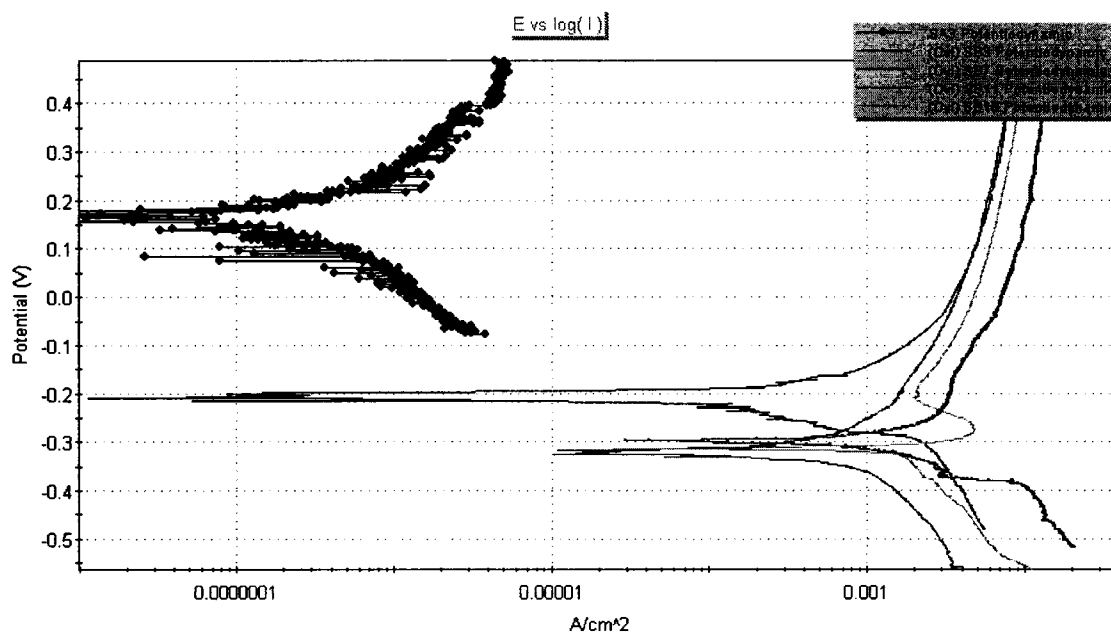


Figure 90: Polarization curves for aerated SA and SB series solutions

5.6.5.2 Deaerated Solutions

All deaerated solutions across all three series (SA, SB, and SC) displayed signs of an anodic knee with the only exceptions being Solution 1 (SA12) and EHPF Solution 5 (SC5); see Figure 91 and Figure 92. All anodic knees observed during testing were relatively small in size however using the results of Snow (1) for comparison between stable and unstable passivation for these solutions it is apparent that these small curves are indeed anodic knees (see Figure 1).

This indicated that with exception of these two tests all were in a state of active dissolution before polarization began.

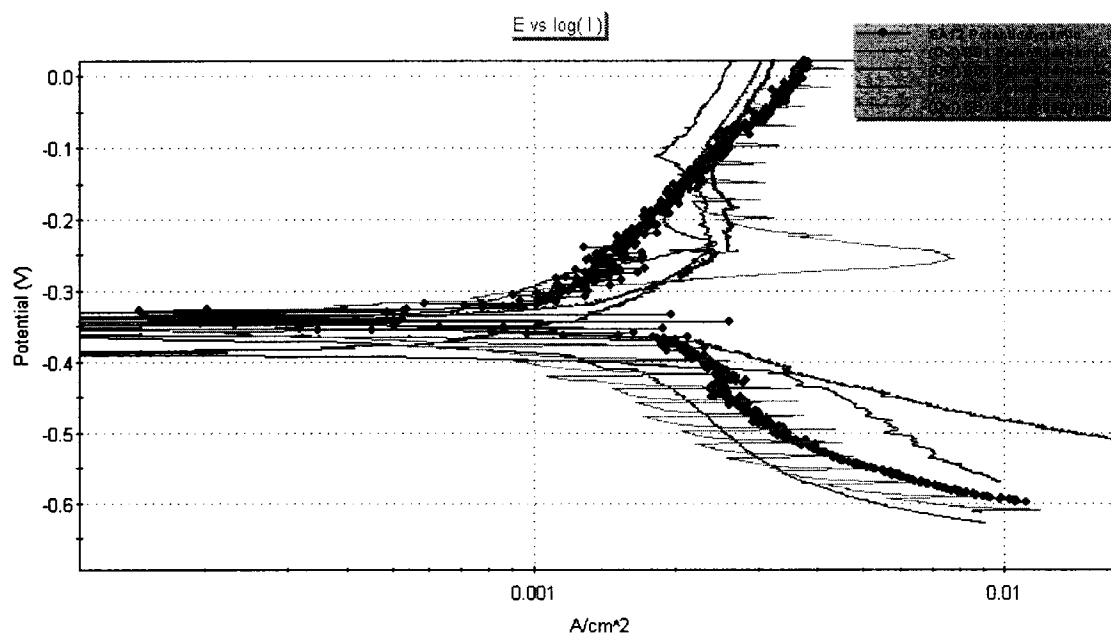


Figure 91: Polarization curves for deaerated SA and SB series solutions

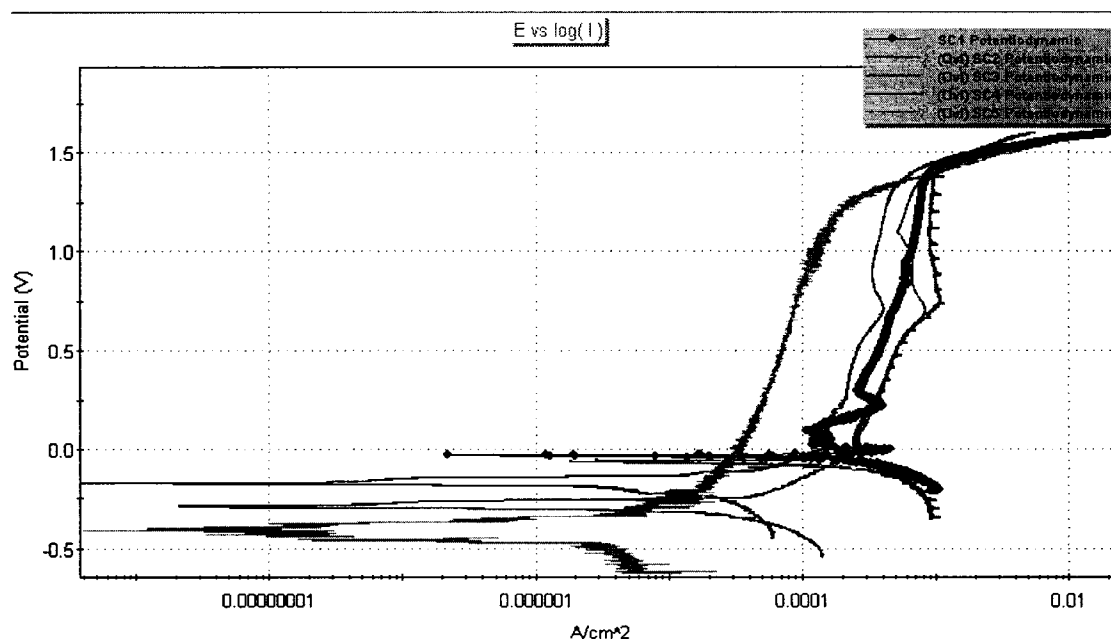


Figure 92: Polarization curves for SC series solutions (SC1, SC3, SC5 are deaerated)

5.7 SEM and EDS Analysis of Corroded Samples

All SEM and EDS tests were performed on samples exposed to Solutions 1-4 and EHPPF Solution 2 under deaerated conditions for reasons of consistency and the lack of equipment access time to check aerated samples.

5.7.1 Chromium Carbide Inclusions

Using SEM images it was possible to target individual inclusions and determine their approximate composition. Samples tested after corrosion testing in the SA and SB series displayed only larger inclusions with an apparent composition primarily being Cr_{23}C_6 . The size, shape and number of these sites along with the descriptions found in the literature review indicates that they are most likely responsible for the dark spots which formed on the metal surface (4, 9, 25, 45). The formation of Cr_{23}C_6 depletes the surrounding metal of chromium leaving it vulnerable to corrosion which would release greater amounts of iron creating the dark appearance around the site (see Figure 94).

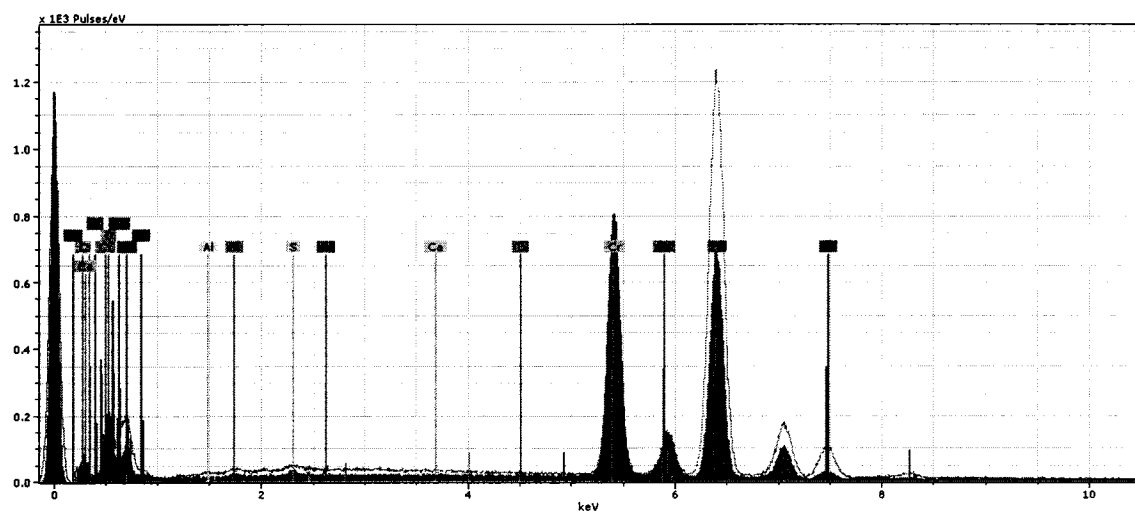
The nature of this type of site would not necessarily make it the most favorable starting point for pits as it will result in an open pit with a relatively low depth to width ratio (1, 4, 22) as compared to the deeper pits seen nearby which presumably resulted from the dissolution of manganese sulfide inclusions (MnS) which were present in the EDS scans of the polished metal surface seen in Appendix A.



Figure 93: Image of surface of sample in Test SB7 before polarization, note the presence of a few larger dark spots on the surface



Figure 94: SEM images of the surface of SB7, left image is at same 0.5 mm scale as previous figure, right image is a higher magnification at center of previous image showing a small inclusion inside a pit



5.7.2 Sulfide Inclusions

5.7.2.1 CuS Inclusions

Examination of a sample from the SC series gave the opportunity to image a sulfide inclusion which had not yet fully dissolved during testing. It was found that these sites were the only signs of pitting found on the surface. The composition of the inclusion was confirmed using an EDS scan which found this particular inclusion it to be CuS. See Figure 96 and Figure 97.

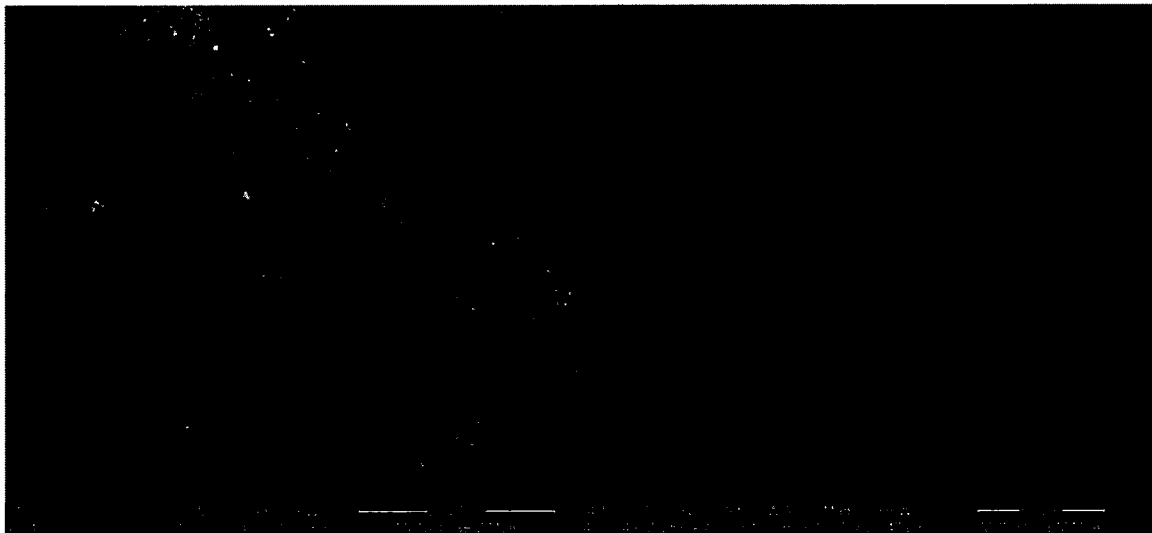


Figure 96: Images of a CuS inclusion in the surface of SC4, top left is at 0.5 mm tall, top right is at 0.02 mm tall.

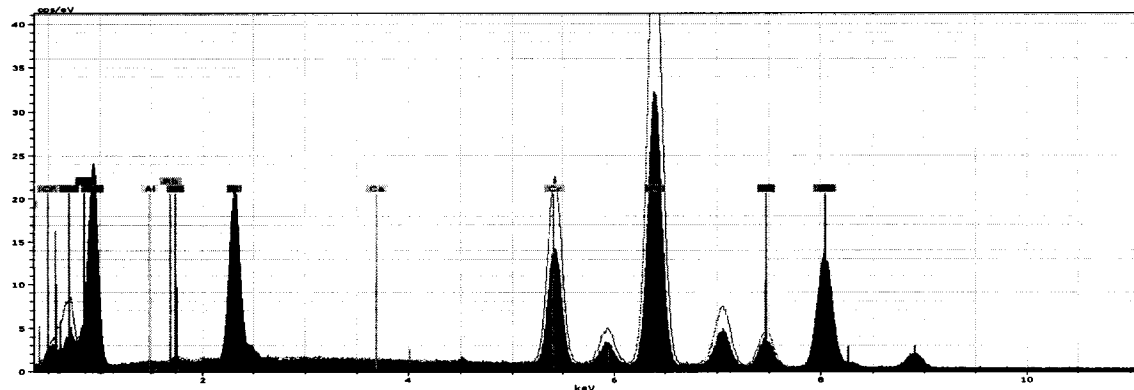


Figure 97: EDS results for a CuS inclusion in sample SC4, see peaks for Cu and S

5.7.2.2 MnS Inclusions

During the initial SEM and EDS testing of the surface a large number of small MnS inclusions were discovered. After examining the surfaces of the SA and SB series it was determined that these inclusions had dissolved leaving behind most of the small pits present on the metal surface. This was based on the in-situ images of the corrosion process showed many tiny dark spots acting as initiation points for pitting, and the literature which confirms their tendency to dissolve (1, 16, 50). This hypothesis was greatly supported by images of partially dissolved MnS inclusions taken from sample SB3. The SEM images reveal a different shape in the surrounding metal compared to the carbide inclusions. The sulfide inclusion is dissolving leaving a crisp edge on the surrounding metal rather than the chromium carbide inclusion which left an actively dissolving open pit with a jagged inclusion present in the middle. This more enclosed structure is much more likely to form crevice corrosion or pitting (see Figure 98 and Figure 99). See Appendix A for test results on uncorroded metal.

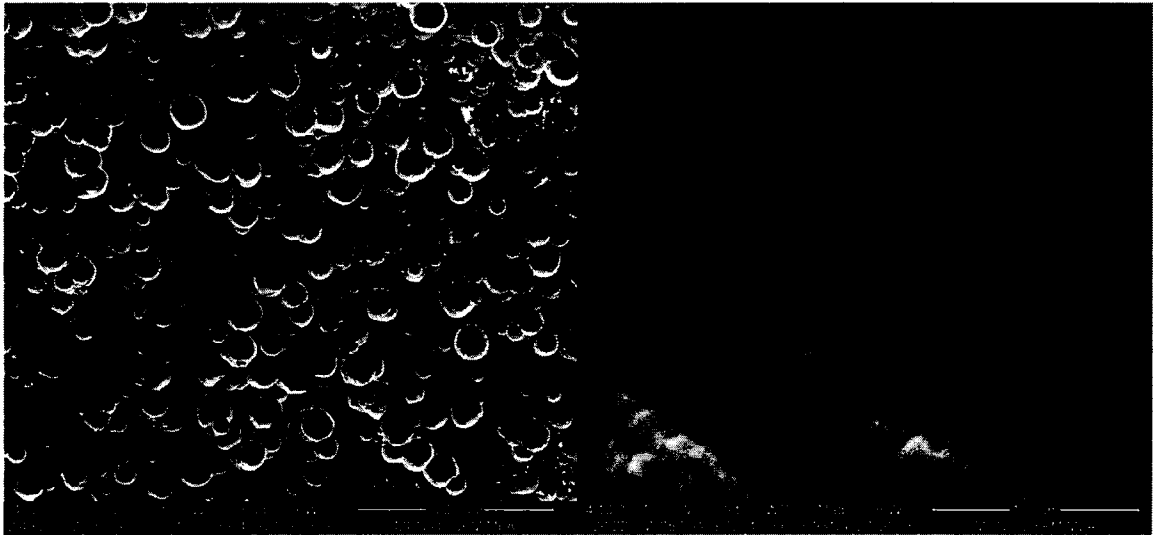


Figure 98: SEM images of sample SB3, left image is 0.5 mm tall, right image is 0.07 mm tall showing a small MnS inclusion

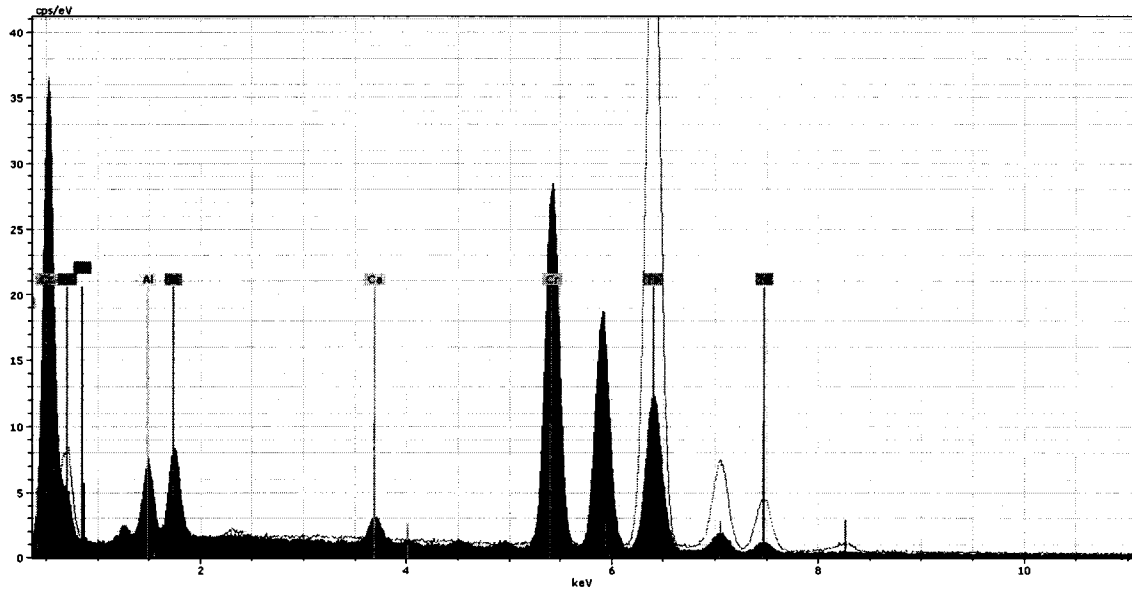


Figure 99: EDS scan results showing composition of the pit seen in previous figure as Mn, Al and S with very low Fe levels

5.7.3 Surface Oxide Composition

EDS scans of the overall surface layer composition did not reveal any significant changes between each sample type despite different surface conditions and colors. Sample SC4 possessed the thickest visible surface layer in the form of a loose brown substance. The EDS scans show a slight difference in composition between the regular base metal surfaces and this darkened area, showing a slightly higher carbon content in this section of the surface layer, see Figure 100 and Figure 101. Presumably the composition of the overall protective surface layers in all tests samples exposed to all solutions is of similar composition despite the varying exposure to different substances during testing. It is also interesting to note that no EDS test revealed any significant amounts of Cl^- present in the surface layer of any sample tested or in any inclusion or other surface feature tested. According to the literature chloride ions are attracted to pits which absorb them (1, 4, 16, 18). This explanation is feasible here as the EDS scans attempted were not done inside pits due to the effects of the narrow openings disrupting the results.



Figure 100: Images of sample SC4, left image taken with a scanner is approximately 21 mm tall and shows a brown oxide layer, and the right image taken with SEM is 0.5 mm tall and shows the border between a brown section and a cleaner metal section

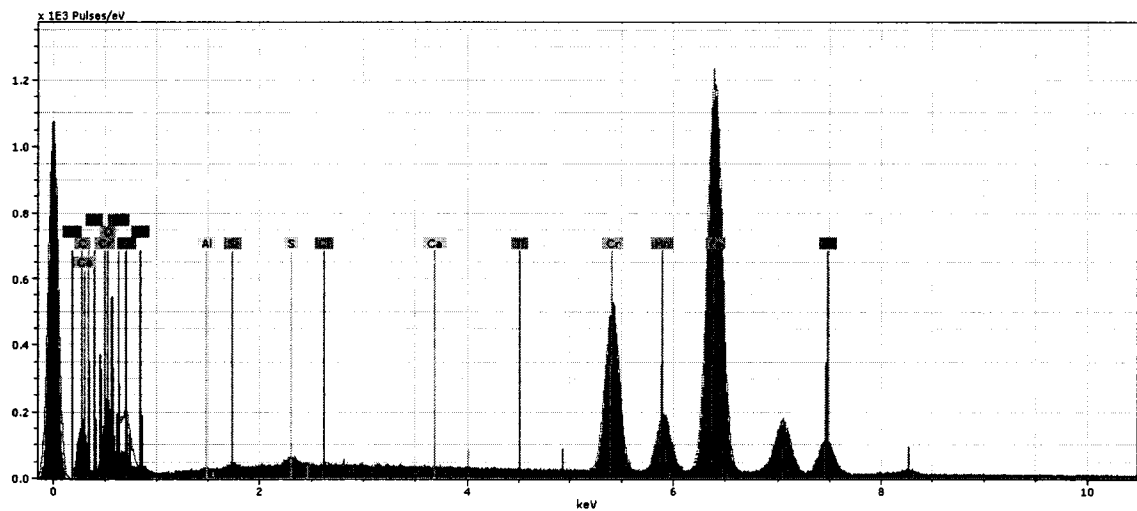


Figure 101: EDS Scan of dark brown oxide layer (green area) compared to metal composition (blue line)

6 CONCLUSIONS

It has been confirmed that initial surface conditions and changes in the surface features may be recorded using in-situ optical microscopy. These changes were recorded both during the initial immersion stages of testing and during polarization. The following surface events may be recorded:

(i) During Initial Immersion:

- 1) Initial formation of the metal's protective surface layer including details about the distribution, color, weak points and points of anodic and cathodic behavior. Evidence of loose or peeling sections of the oxide layer may also be observed.
- 2) Dissolution of the metal surrounding chromium carbide inclusions may be observed. This is due to the buildup of iron based corrosion products in these areas due to the reduced protection from the chromium oxide layer as the metal is partially depleted of chromium.
- 3) Dissolution of sulfide inclusions resulting in small enclosed cavities.

(ii) During Polarization Testing:

- 4) Changes in surface color upon exposure to high anodic polarization due to the destruction of unstable corrosion products and oxides on the metal surface at certain potentials. These include the dissolution of iron based oxides and the

destruction of the protective Cr_2O_3 oxide layer in favor of dichromate which forms at higher potentials of about 1.3 V for acidic solutions (41).

- 5) The development of etching along grain boundaries and grain structures.
- 6) The formation and growth of pits which may be observed throughout their development.
- 7) Images of the surface before pitting may be observed so as to locate any pre-existing features which may have attributed to the formation of the pit.
- 8) Loosening and peeling of oxide layer may be recorded indicating the strength of the bond to the surface. This may also provide information regarding the thickness of the oxide layer based on the color changes during its removal.

The effects of different types of inclusions on the corrosion behavior of stainless steel vary based on their composition. Two common types of inclusions were examined during this analysis with the following conclusions:

- 9) Chromium carbide inclusions present weak points at which aggressive dissolution of the surrounding metal may be observed in the form of a dark localized oxide formation. These sites may result in significant local corrosion when immersed in corrosive solutions however the resulting small open indentations in the metal does not typically trigger pitting at these sites.
- 10) Sulfide inclusions present points of high vulnerability on which pits may nucleate and develop once the inclusion has dissolved. Aggressive pitting may occur when

exposed to aggressive chloride containing solutions such as sulfuric acid and saltwater however they may still act as sites for slowly developing pits when in solutions containing sulfate ions.

Conclusions regarding the differences in pitting behavior for different solutions and different polarization schemes exist including:

- 11) Pits developing in solutions with low or no chloride ions present tend to develop at a very small size and are generally attributed to the dissolution of sulfide inclusions and the subsequent crevice corrosion occurring at these sites during the later stages of polarization. Under these conditions etching is the predominantly visible method of corrosion. Pits developing in chloride rich solutions develop much more aggressively and do not generally allow for any significant etching to occur on the metal surface.
- 12) A noticeable difference between the behavior of potentiodynamic and potentiostatically generated pits in sulfuric acid solutions containing high levels of chloride ions exists being that a second ring of corrosion develops around the pits when polarized potentiodynamically. This ring appears to be a deformed and cracked metal surface that is reasonably consistent with the descriptions of pit cap growth theories listed in the literature (16).

13) Pitting behaviors for stainless steel in sulfuric acid differs significantly from those found in saltwater samples. The difference exists in both the luster and color of the surrounding metal surface and in the black oxides which commonly form at the center of pits forming in sulfuric acid.

14) Pitting patterns found in sulfuric acid containing 0.25M nickel sulfate at 1.13 V illustrated that under some conditions unique corrosion behaviors may be recorded including the removal of corroded metal surfaces to expose fresh metal surfaces. These new surfaces were found in some cases to be more corrosion resistant than the original surfaces displaying both a reduction in the number of pits and the rate at which pits appear to develop.

The results taken from polarization test results lead to the following conclusions:

15) The corrosion potential E_{corr} typically increases in the noble direction when oxygen is added to the solution which is consistent with theories regarding the addition of stronger oxidizers to solutions (4, 22).

16) Solutions with a low pH or high level of chloride ions tend to generate greater corrosion rates.

17) Deaerated solutions tend to generate a greater current density when polarized above the pitting potential.

18) Deaerated solutions tend to have lower pitting potentials compared to aerated when tested using aggressive solutions with either a high pH or high chloride ion

concentrations. When tested using less aggressive 1M sulfuric acid solutions the opposite was often observed leading to the theory presented in Section 5.6.4.2.1 “Theoretical Explanation for Aerated vs. Deaerated Test Results”.

19) Based on the SA series tests and sources in the literature review it is concluded that 316L stainless steel produces an unstable oxide layer when exposed to 1M sulfuric acid (4, 35). This is supported by the failure to easily passivate when polarized to 0.9 V under aerated conditions.

7 FUTURE APPLICATIONS

In addition to providing a cost effective means of furthering the scientific understanding of corrosion mechanisms these techniques may also be adapted for examining the effectiveness of corrosion inhibitors and coatings in both immersion and polarization testing.

Testing involving studies of specific areas of a sample's surface could be performed using these techniques. An area may be chosen and tested using SEM and EDS scans to identify all inclusions and features visible on the surface, followed by polarization testing where images are recorded of this same area. This type of test procedure would provide indisputable evidence as to the nature of sites at which pits tend to nucleate and the fashion in which they grow.

The in-situ optical microscopy corrosion cell developed to date has the primary application of being used for corrosion tests under polarized conditions. However the concept may be extended to immersion tests. A block of Teflon may be machined to hold a series of samples in line with a constant fluid flow running across the set. Using a similar glass mounting technique to that used in the corrosion cell used in this document and an appropriate mounting arrangement under a microscope a set of time lapse images may be compiled over a period of months. If a set of auxiliary electrode wires are

introduced to the system, the sample may be tested using a long term potentiostatic polarization test.

If successful, the results from the immersion tests, the polarization tests and samples from real environmental corrosion may potentially be combined to produce a more realistic modeling technique for various suitable metals and alloys. This in turn could act as a new basis for a ranking technique to be used in combination with pitting potential ranking data for future projects.

Another type of test suitable for use with this system are tests using samples with a small cross sectional area such as wires or rods as it allows the observation of most of the materials surface. If a small wire were used it is possible to observe all pit nucleation events on a sample's surface and directly link them to the computer recorded polarization data. Although the substantial effect of the mechanical stresses within the sample would make using these test results for real world applications problematic it would provide valuable insights from an academic perspective.

8 REFERENCES

- (1) G. Snow, "Evaluation of Corrosion Performance of 316L Stainless Steel for Hydrometallurgical Processing of Voisey's Bay nickel Concentrate", M.Eng. Thesis, *Memorial University of Newfoundland*, Oct. (2005).
- (2) P. Q. Zhang, J. X. Wu, W. Q. Zhang, X. Y. Lu, K. Wang, "A Pitting Mechanism for Passive 304 Stainless Steel in Sulfuric Acid Media Containing Chloride Ions", *Corrosion Science*, Vol.34, (1993), pp. 1343-1354.
- (3) G. Suresh, V.R. Raju, U. K. Mudali and R.K. Dayal., "Corrosion assessment of type 304L stainless steel in nitric acid.", *Corrosion Engineering, Science and Technology*, Vol. 38, No. 4, (2003), pp. 309-312.
- (4) D. A. Jones, "Principles and Prevention of Corrosion Second Edition", Prentice Hall, (1996).
- (5) ASTM, " Annual Book of ASTM Standards 2004", ASTM, (2004).
- (6) M. Rothstein, "Electrochemical Corrosion Measurements for the Metal Finishing Industry", *American Electroplaters and Surface Finishers Society*, Vol. 73, No 11, (1986), pp. 44-51.
- (7) Stern, M. and A.L. Geary, *Journal of the Electrochemical Society*, Vol.104, No.56, (1957).
- (8) "PowerSuite's PowerCORR Manual v2.56", (©2001-2005)
- (9) Dr. J. Oldfield, "Test techniques for pitting and crevice corrosion resistance of stainless steels and nickel-based alloys in chloride-containing environments.", *NiDi Nickel Development Institute*, (1987).
- (10) N. Sato, "The Stability of Localized Corrosion", *Corrosion Science*, Vol.37, No.12, (1995), pp. 1947-1967.
- (11) Manyang Technological University, Online: www.ntu.edu.sg.
- (12) H. Hocheng, P.S. Kao, and Y.F. Chen, "Electropolishing of 316L Stainless Steel for Anticorrosion Passivation", *Journal of Materials Engineering and Performance*, Vol.10, No.4, August (2001).
- (13) M. Bojinov, I. Betova, R. Raicheff, G. Fabricius, T. Laitinen, T. Saario, L. Bonora, F. Deflorian, "Mechanism of the transpassive dissolution and secondary passivation of chromium in sulfuric acid solutions", *Materials Science Forum*, Vol. 289-292, No.2, 1984, pp. 1019-1028.
- (14) I Betova, M. Bojinov, T. Laitinen, K. Makela, P. Pohjanne, T. Saario, "The transpassive dissolution mechanism of highly alloyed stainless steels. I. Experimental results and modeling procedure", *Corrosion Science*, Vol. 44, No.12, 2002, pp. 2675-2697.
- (15) C. Xu, "Corrosion in Microelectronics", (2003).
- (16) Z. Szklarska-Smialowska, "Pitting and Crevice Corrosion", NACE International, (2005).
- (17) E. Mattsson, "Basic Corrosion Technology for Scientists and Engineers, Second Edition", Institute of Materials, Minerals and Mining, (1997).
- (18) G. T. Burstein, C. Liu, R. M. Souto and S.P.Vines, "Origins of pitting corrosion.", *Corrosion Engineering, Science and Technology*, Vol. 39, No. 1, (2004), pp. 25-30.
- (19) M. Kaneko and H. S. Isaacs, "Effect of Molybdenum on Pitting Corrosion Resistance of Stainless Steel in Chloride and Bromide Solutions.", *Corrosion Engineering*, Vol.50, (2001), pp. 329-338
- (20) N. Alonso-Falleiros, A. Hakim, and S. Wolynec, "Comparison Between Potentiodynamic and Potentiostatic Tests for Pitting Potential Measurement of Duplex Stainless Steels.", *Corrosion*, Vol.55, No.5, (1999), pp. 443-448

- (21) R.K. Dayal, N. Parvathavarthini, and J. B. Gnanamoorthy, "A Study of Various Critical Pitting Potentials for Type 316 Stainless Steel in Sulfuric Acid Containing Chloride Ions", *Corrosion*, Vol.36, No. 8, (1980), pp. 433-436
- (22) Dr. J. Shirokoff, "Engineering 8962/9989 Course Notes", (2005).
- (23) J.M. Bastidas, J.L. Polo, C.L. Torres and E.Cano, "A Stochastic Approach to Study Localized Corrosion of AISI 304L and AISI 316L Stainless Steels as a Function of Potential Scan Rate", *Corrosion*, Vol.57, No.8, (2001), pp. 666-669.
- (24) B. Craig, D. Anderson, V. Flint, D. Levicki, "Handbook of Corrosion Data 2nd Edition", ASM International, (1995).
- (25) W. Smith, "Materials Science & Engineering Series, Structure and Properties of Engineering Alloys, Second Edition", McGraw-Hill, (1993).
- (26) V. Cojocaru, V. Dascalescu and M. V. Popa, "The Corrosion of Some Stainless Steels in Sulfuric Acid Media", *Revue Roumaine de Chimie*, Vol.41, No.5-6, (1996), pp. 437-443.
- (27) K. B. Hensel, "Electropolishing, Surface Treatments", *Electro Polish Systems Inc.*, Milwaukee, pp. 371-378.
- (28) M. Nakahara, "Preventing Stress Corrosion Cracking of Austenitic Stainless Steels in Chemical Plants.", *NiDi Nickel Development Institute*, June (1993).
- (29) A. Turnbull and B. Nimmo, "Stress Corrosion Testing of Welded Supermartensitic Stainless Steels for Oil and gas Pipelines.", *Corrosion Engineering, Science and Technology*, Vol. 40, No.2, (2005), pp. 103-109.
- (30) T. J. Hakkarainen, P. Pohjenne, "Artificial Pit Experiments to Investigate the Growth and Repassivation of Macroscopic Corrosion Pits In Stainless Steels", *VTT Manufacturing Technology*, Finland, (1996).
- (31) W. Masterton and C. Hurley, "Chemistry, Principles and Reactions", Saunders College Publishing, (1997).
- (32) D.G. Kolman, D.K. Ford, D.P. Butt, and T.O. Nelson, "Corrosion of 304 Stainless Steel Exposed To Nitric Acid - Chloride Environments", *Materials Corrosion and Environmental Effects Laboratory*, Los Alamos National Laboratory, Los Alamos, NM 87545
- (33) J. Vaughan and A. Alfantazi, "The Thermodynamics of Titanium Corrosion in Acidic Systems", *Pressure Hydrometallurgy Conference, Banf*, www.mmat.ubc.ca, (2004).
- (34) J. Vaughan, P. Reid, A. Alfantazi, D. Dreisinger and D. Tromans , "Corrosion of Titanium and Ti-Alloys at High Temperature and Pressures", *Conference of Metallurgists, Vancouver*, www.mmat.ubc.ca, (2003).
- (35) S. Cramer, B. Covino Jr., "ASM Handbook, Volume 13C, Corrosion: Environments and Industries", ASM, (2004).
- (36) J. Vaughan, "Corrosion of Titanium and its Alloys in Sulfuric Acid at High Temperature and Pressures", *University of British Columbia*, (2001).
- (37) A. Rossi, R. Tulifero, B. Elsener, "Surface Analytical and Electrochemical Study on the Role of Adsorbed Chloride Ions in Corrosion of Stainless Steel", *Materials and Corrosion*, Vol.52, (2001), pp. 175-180.
- (38) "Wikipedia Online Encyclopedia", www.wikipedia.org.
- (39) "Crevice Corrosion of Nickel-Based Alloys in Seawater", *The Hendrix Group Reporter*, Vol. 8, No.1, March 22 (1998).
- (40) R. F. Smith, "Microscopy and Photomicrography, A Working Manual, Second Edition.", CRC Press, (1994).
- (41) S.L. Chawla, R.K. Gupta, "Materials Selection for Corrosion Control", ASM International, (1993).

- (42) Y.-M. Pan, C.S. Brossia, G.A. Cragnolino, D.S. Dunn, V. Jain, and N. Sridhar, "Evolution of Solution Chemistry through Interactions with Waste Package Internal Structural Components", *Mat. Res. Soc. Symp. Proc. Vol. 713*, Materials Research Society, (2002).
- (43) "Venus Wire Industries Limited Inspection/Mill/Quality Certificate", (2003).
- (44) "HSC Chemistry 5.1", *ESM Software*, (©2001-2005).
- (45) G. Vander Voort, "ASM Handbook, Volume 9, Metallography and Microstructures", (2004).
- (46) G. Riedel, C. Voigt, H. Werner, K. P. Erkel, M. Gunzel, "The Influence of Acid Soluble Sulfide Inclusions on the Passivation Behavior of Austenitic Cr-Ni Stainless Steel", *Corrosion Science*, Vol.27, (1987), pp. 533-544.
- (47) G. T. Burstein, S.P. Vines, "Repetitive Nucleation of Corrosion Pits on Stainless and the Effects of Surface Roughness", *Journal of the Electrochemical Society*, Vol.148, (2001), B504-B516.
- (48) C. Punckt, M. Bölscher, H. H. Rotermund, A. S. Mikhailov, L. Organ, N. Budiansky, J. R. Scully, J. L. Hudson, "Sudden Onset of Pitting Corrosion on Stainless Steel as a Critical Phenomenon", *Science*, Vol. 305, no. 5687, (2004), pp. 1133 - 1136.
- (49) T. Suter, E. Webb, H. Bohni, R. Alkire, "Pit Initiation on Stainless Steels in 1 M NaCl With and Without Mechanical Stress", *Journal of the Electrochemical Society*, Vol. 148, No.5, (2001), B174-B185.
- (50) J. Mankowski, Z. Szklarska-Smialowska, "Studies on Accumulation of Chloride Ions in Pits Growing During Anodic Polarization", *Corrosion Science*, Vol.15, (1975), pp. 493-501.
- (51) P. Ernst, N. Laycock, M. Moayed and R. Newman, "The Mechanism of Lacy Cover Formation in Pitting", *Corrosion Science*, Vol. 39, No. 6, (1997), pp. 113-1136.
- (52) "REMBAR Titanium Technical Information", REMBAR.
- (53) J. S. Grauman and T. Say, "Titanium for Hydrometallurgical Extraction Equipment", *Advanced Materials & Processes*, March (2000).
- (54) J. Vaughan and A. Alfantazi, "Corrosion of Titanium and Its Alloys in Sulfuric Acid in the Presence of Chlorides", *Journal of The Electrochemical Society* 153, No.1, (2006), B6-B12.
- (55) ASM International, "Metals Handbook, Ninth Edition, Volume 13, Corrosion", ASM International, (1987).
- (56) "Inhibition of Heavy Metal Ion Corrosion on Aluminum in Fresh Water Cooling Systems Using Propylene Glycol Anti-Freeze", *NACE International*, (1998), Online: www.corrosionlab.com
- (57) "Corrosion of Aluminum and Aluminum Alloys", Online: www.key-to-metals.com.
- (58) W. Plieth, G.S. Wilson, and C. Gutierrez de la fe., "Spectroelectrochemistry: A Survey of In Situ Spectroscopic Techniques", *Pure and Applied Chemistry*, Vol. 70, No. 7, pp.1395-1414, (1998).
- (59) B. Ran, J.L. Yao, C.X. She, Q.J. Huang, Z.Q. Tian., "Surface Raman Spectroscopy on Transitional Metal Surfaces.", *The Internet Journal of Vibrational Spectroscopy*, Vol. 4, Edition 2.
- (60) NRC-CNRC, "Raman", Online: http://www.ibd.nrc-cnrc.gc.ca/ibd_external/research/spectroscopy/2_raman_e.html, January 16, (2006).
- (61) Recent Developments in the Department of Physical Chemistry (2005), Online: <http://w3.rz-berlin.mpg.de/pc/PCarchive.html>
- (62) P. Schutz, G.S. Frankel, F.M. Serry., "Corrosion Studies with the Atomic Force Microscope, Part 1: Characterization of Potential Inhomogeneities on Passive Surfaces by Surface Potential Imaging.", *Veeco Instruments Inc.*, (2005), Online: www.veeco.com
- (63) "The MultiView 1000", Online: <http://www.microphotronics.com/multiview1000.html>.
- (64) Dr. M.M. Lohrengel, "Electrochemical Droplet Cell and Capillary Cell", Online: <http://agef.uni-duesseldorf.de/service/dropletcell.htm>.

- (65) G. Xuan, S. Jang, G. Kwag, and S. Kim., "Simple and Convenient Design of a Spectroelectrochemical Cell for In Situ XANES Measurements of Adsorbed Species in Transmission Mode", *Bull. Korean Chem. Soc.* Vol. 26, No.4, (2005), pp. 672-674.
- (66) "American Filler Metals Titanium Alloys Specification Sheet.", Online: <http://amfiller.com>
- (67) K. Prabakaran, T.V. Thamaraiselvi and S. Rajeswari, "Electrochemical Evaluation of Hydroxyapatite Reinforced Phosphoric Acid Treated 316L Stainless Steel", *Trends Biomater. Artif. Organs*, Vol 19, No.2, (2006), pp 84-87.
- (68) R. Power, J. Shirokoff, J. Molgaard, "New Techniques for Studying the Corrosion of Metals Extending Optical Microscopy to In-situ Studies of Corrosion", *The Sixteenth Annual Newfoundland Electrical and Computer Engineering Conference*, Nov. 9, 2006
- (69) J. Ryzkowski, "IR Cell Reactors for In-Situ Studies", *The Internet Journal of Vibrational Spectroscopy*, Vol. 6, Edition 2, section 1.
- (70) VWR International, "The VWR Catalog", VWR International (2003-2004).
- (71) J.P. Busalmen and S.R. Sanchez, "Adhesion of *Pseudomonas fluorescens* (ATCC 17552) to Nonpolarized and Polarized Thin Films of Gold", *Applied and Environmental Microbiology*, Vol. 67, No. 7, (2001), pp. 3188-3194.
- (72) AS ALS Japan Ltd., "Electrochemical , Electrode & Accessories", Online: http://www.ijcambria.com/ALS_BROCHURE.pdf.
- (73) D. Lampner, "In-Situ investigations of Corrosion Via SPM", *Molecular Imaging Corporation*, Online: www.molec.com.
- (74) Z. Szklarska-Smialowska, "Pitting Corrosion of Metals", *NACE*, Houston, (1986), pp.377
- (75) R. Huang, C. Lin, and H. Isaacs, "A difference-Imaging Technique Used to Study Streaking Corrosion of Aluminum Alloys AA7075 and AA8006 in Chloride Solution", *Electrochemical and Solid-State Letters*, Vol. 9, (2006), B11-B14.

Appendix A:

SEM and EDS test results on 316L metal surface.

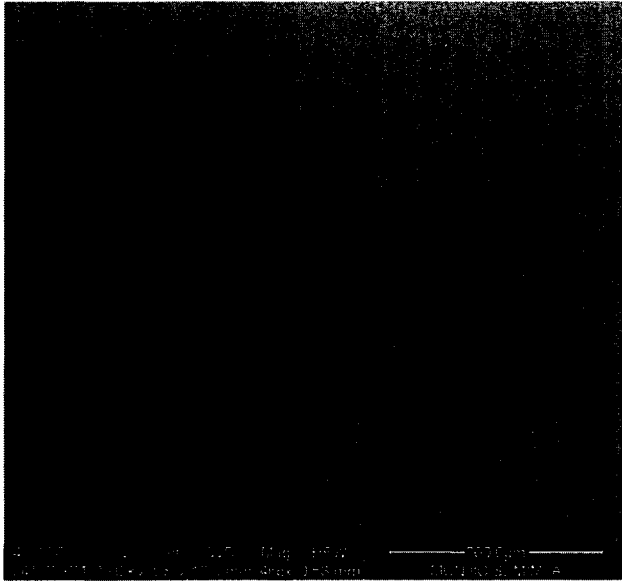


Figure 102: Sample surface observed using SEM imaging (0.5 mm tall image)

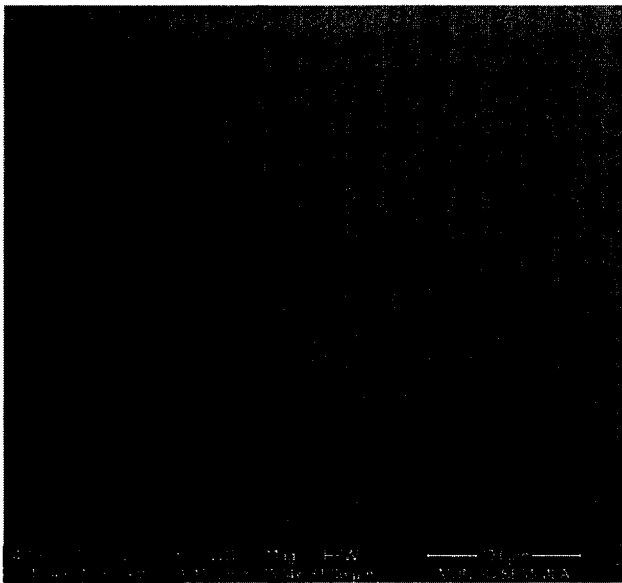


Figure 103: SEM image at higher magnification at center of previous figure. Image of Cr_{23}C_6 inclusion (large angular inclusion) and MnS inclusions (small inclusions) refer to EDS scans below for composition (image is 0.08136 mm wide)

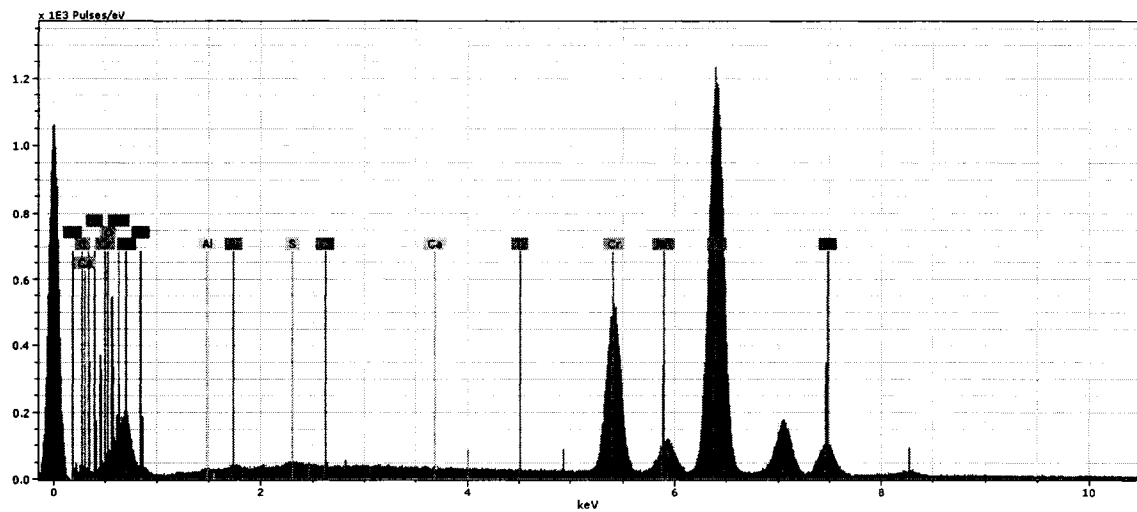


Figure 104: EDS Scan of 316L base metal composition

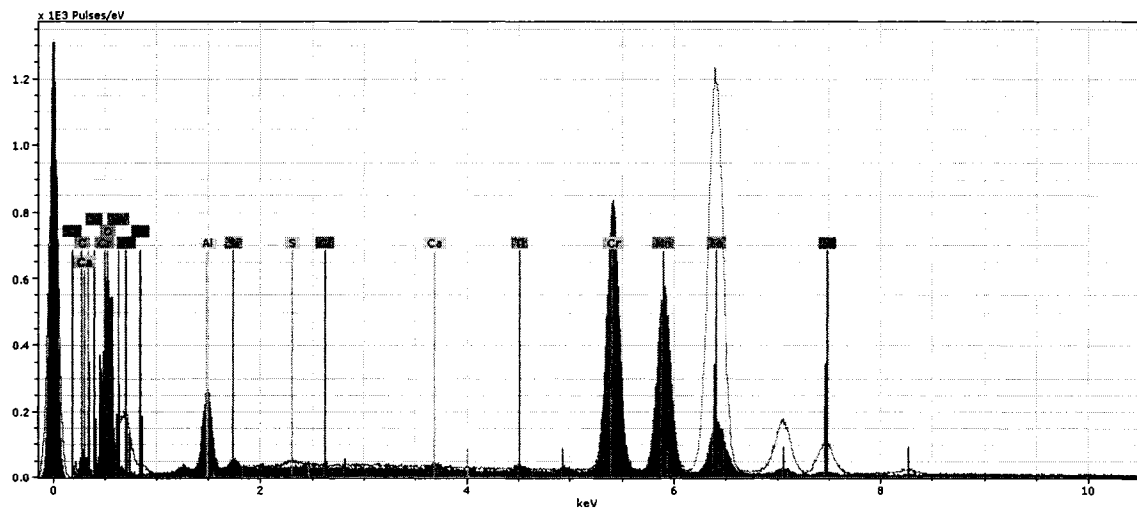


Figure 105: EDS Image of larger angular inclusions with high Cr content and slightly elevated carbon content presumed to be Cr_{23}C_6 .

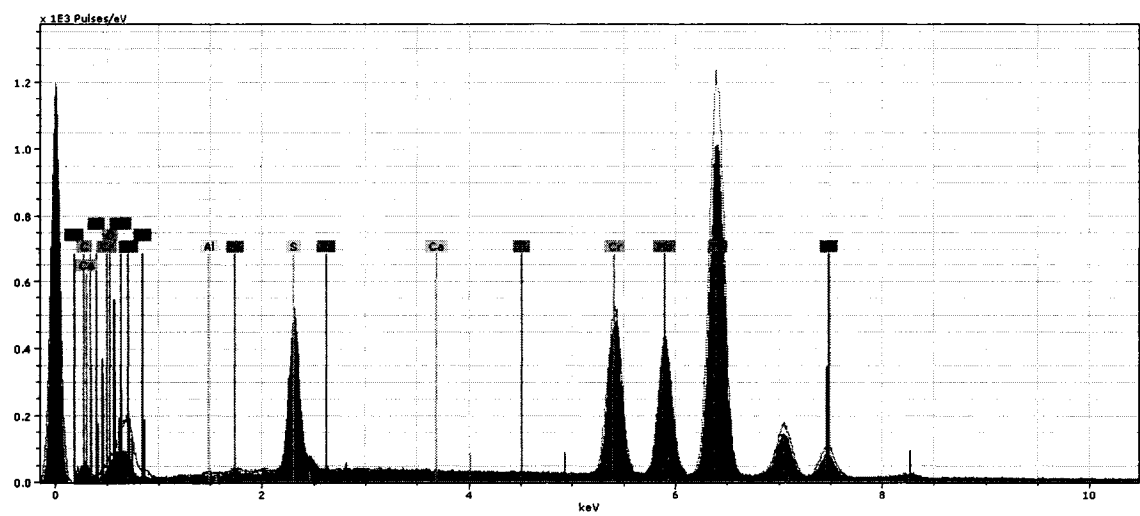


Figure 106: MnS inclusion (small round inclusions)

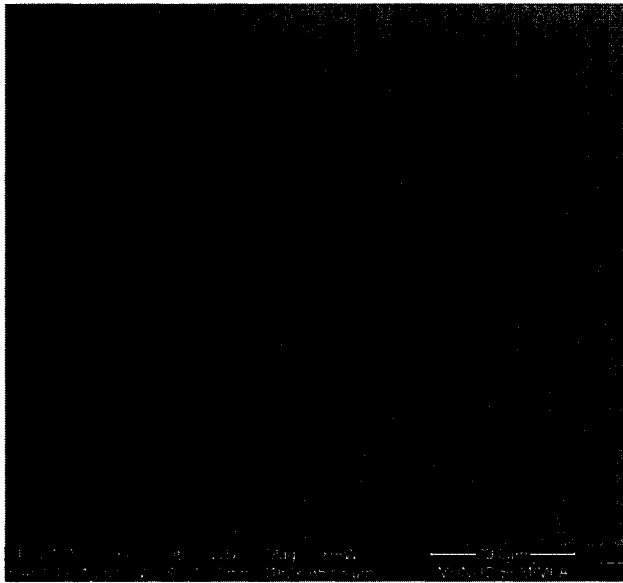


Figure 107: SEM image of silica rich elongated inclusion (near bottom edge of image) (image is 0.08553 mm wide)

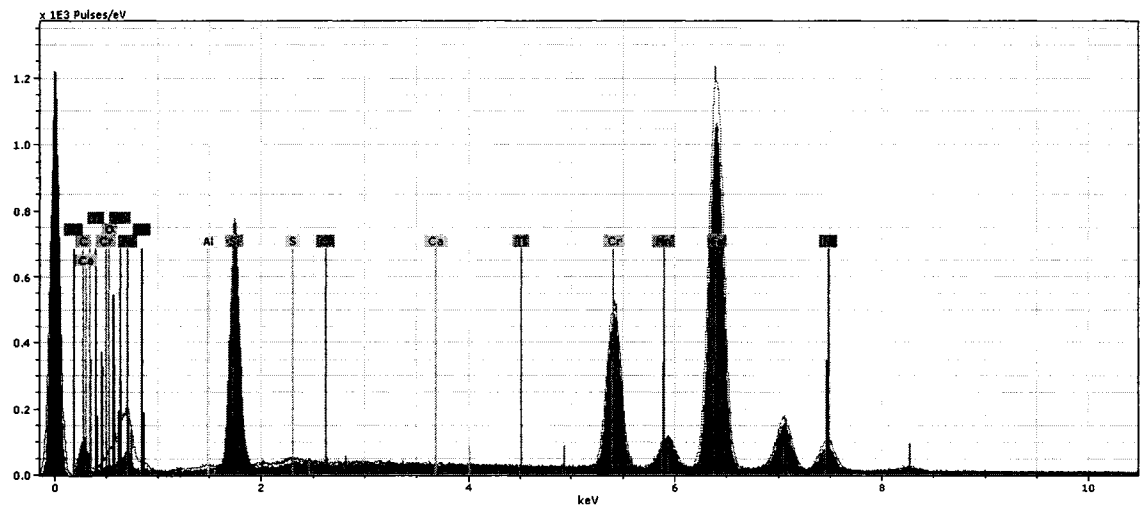


Figure 108: Silica rich elongated inclusion

Appendix B:

316L Composition Data Sheet from Venus Wire Industries Limited (43).

VENUS WIRE INDUSTRIES LIMITED												VENUS	
HEAD OFFICE : 19, Paghurshahi Mill Compound, S. B. Marg, Lower Parel, Mumbai-400 013. (INDIA) Tel : 91-22-64678940 • Fax : 91-22-64678945 • E-MAIL : info@venuswire.com • Website : www.venuswire.com													
ISO: 9002		INSPECTION / MILL / QUALITY CERTIFICATE										No. SB/VR/2003-2004/2121	
PRODUCT INFORMATION	CUSTOMER : UNALLOY-TWNC										GRADE : AISI-316/316L		
	INVOICE NO. : VR/387/EXP/2003-2004										HEAT NO. : V 3218		
	PRODUCT FORM : STAINLESS STEEL BOUND BAR												
	DIMENSION : 0.75" TOL. : ASTM A484										QUANTITY : 5242.50 LBS.		
	IDENTIFICATION : WA 384,825,626,676,677												
CHEMICAL ANALYSIS	CONDITION : ANNEALED+COLD DRAWN+CENTERSLESS GROUND+POLISHED												
	Elements	C%	Si%	Mn%	P%	S%	Cr%	NI%	Cu%	Mo%	N%	Nb%	Cu%
	RESULTS	0.025	0.330	1.510	0.040	0.020	16.42	10.26	0.520	2.110	0.035	—	0.170
MECHANICAL TESTS	UTS		YS		R.A. %		ELONGATION %		HARDNESS		GRAIN SIZE		
	RESULTS 106 KSI		78 KSI		66.10		41.00		216 HB		5		
REMARKS	HEAT TREATMENT: 1050°C-SOLUTION ANNEALED, 45 MINUTES WATER COOLING.												
	REMARKS : MATERIAL IS FREE FROM MERCURY CONTAMINATION. MICRO & MACRO TEST WAS FOUND SATISFACTORY. NO WELDING PERFORMED. MELTING PROCESSING UNIT CONVERTER VOD, HOT ROLLED. I.G.C. TEST FOUND OK.												
	MATERIAL CONFORMS TO ASTM A276-SEPT. 10, 2000; A479/A479M-MAR 10 2000; AISI/AISIN-89, A332 PRACTICE E, A314-SEPT. 10-97; A484/A484 M-JUNE 10-2000; AISI-90A HEN CLASS1; AISI/AISIN CLASS1 HEN AISI A479/A479M-88, SA192-01 SECTION II, SA192-01 SECTION II CLASS 1 HEN; SA192/200M-88 CLASS1 HEN; 925 7037 COND.A, AMS 8833 REV. E/0448 REV J; MIL-2882B; MIL-S-7720A COMP 316, NACE MR0 175; UNSM031800, S31803 												
	REFERENCE ORDER NO: 13441-000 CP, 13677-000 CP												
	<div style="display: flex; justify-content: space-between; align-items: flex-start;"> <div style="border: 1px solid black; padding: 5px; width: 30%;"> BANK OF BARODA <small>BARODA FIRST BRANCH, KARNATAKA</small> NO 11 83185 03 HARD/NA. P NARC/NARC </div> <div style="width: 60%;"> <p style="font-size: x-small;">This report is a copy of original mill certificate and verifies that the product meets the requirements as originally ordered by Unalloy/TWNC.</p> <p style="text-align: right; font-weight: bold;">98/03 98/07</p> </div> </div>												
<div style="display: flex; justify-content: space-between;"> <div style="width: 60%;"> <p style="font-size: x-small;">We hereby certify that the material described herein have been manufactured and tested with satisfactory results in accordance with the customers requirements, needs and expectations.</p> <p>DATE : 06/11/2003</p> </div> <div style="width: 35%; text-align: center;"> AUTHORIZED SIGNATORY </div> </div>													

ISO: No. 7079:1 Rev. 1

PLANT : ATKARGAON, TAKAI ADOOSH ROAD, KHALAPUR, KNOPOU-618 282.

Appendix C:

Program Data from PowerSuite's PowerCORR (8)

New Tafel Fit

New Tafel Fit, also on the right-mouse-button menu, statistically fits the experimental data to the Stern-Geary model for a corroding system, then calculates the corrosion current and the corrosion rate in either millimeters per year (mpy) or milli-inches per year (mmpy) and overlays the cathodic and anodic beta lines on the graph. The beta lines have "grab boxes" on each end that allow you to override the calculations and manually position the beta lines on the graph. Tafel data should ideally be ± 250 mV with respect to ECORR. Before analysis, you may wish to hide one or more points in the data set to exclude them from the analysis. Multiple fits can be performed on a single data set. See the Fits tab on the Experiment Bar for your module for a description of the fit parameters.

This command is only available for graphs of E vs. log I (y-axis scaling must be linear, x-axis logarithmic).

Tafel Fit Data

E(I=0) (mV)	The potential with the lowest current reading in the Rp fit analysis.
ICORR (μ A)	Corrosion current.
Cathodic Beta (mV)	The cathodic beta (β) constant as determined in this Tafel analysis, in mV per decade.
Anodic Beta (mV)	The anodic beta constant, in mV per decade.
Corrosion Rate	Corrosion rate in <u>mpy</u> or <u>mmpy</u> .
Chi-Square	Goodness of fit.
Fit Range (mV)	The range of the data points selected for this fit.
Fit Mode	Auto (software-calculated) or Manual (indicating the software-calculated beta lines have been manually repositioned).

The corrosion rate calculation requires working electrode Area, Density, and Equivalent Weight.

Introduction

The main advantage of electrochemical techniques for studying corrosion over traditional coupon testing is that it allows the rapid determination of the corrosion rate of a sample without requiring long-term testing. Corrosion rate itself can vary with time under a given set of conditions, so electrochemical corrosion measurements only give you a snapshot of how the system behaved under those conditions at that point in time. Long-term testing is still required if you need to know how a metal reacts after 12 months in a given test environment. But short-term electrochemical measurements are more than sufficient in

many cases, as they allow you to compare the performance of inhibitors or to decide that a given metal is corroding too rapidly under those conditions to be a valid candidate for the application.

The New Tafel Fit routine statistically fits the experimental data to the Stern-Geary model for a corroding system. Using the mouse, you select the data lying within the Tafel region (ideally ± 250 mV with respect to the corrosion potential). The New Tafel Fit analysis then calculates the corrosion current and the corrosion rate (in either millimeters per year or milli-inches per year) and overlays the beta lines on the graph of experimental data (which you can then manipulate manually if you wish).

The New Rp Fit routine uses a linear regression analysis to calculate the polarization resistance, then uses this value to determine the corrosion current and corrosion rate. Using the mouse, you select the data within 20 mV of the corrosion potential. The New Rp Fit analysis then performs the calculations and overlays the results on the graph of experimental data.

The calculations that occur in New RP Fit and New Tafel Fit are oriented toward finding the corrosion rate of a system and are related to a theoretical approach first proposed by Stern and Geary in 1957 [ref 1]. This approach assumes that a typical corroding system involves only two electrochemical reactions, an oxidation process and a reduction process. It is based on the Tafel equation that predicts that the logarithm of current observed in an electrochemical process is directly related to the difference in the applied potential and the redox potential for an electrochemical reaction. The proportionality constants involved are termed Tafel constants and are usually abbreviated as "beta" (β) in standard corrosion notation.

The equation proposed by Stern-Geary describes a corroding system with just two electroactive redox couples:

$$I(E) = ICORR [10(E-E_{corr}) / \beta_a - 10(E_{corr}-E) / \beta_c] \quad (1)$$

where I is the net or total current that flows at any one point in time at a specific applied potential, E . $ICORR$ is the open-circuit potential for the system. β_a and β_c are the Tafel proportionality constants for the anodic (oxidation) and cathodic (reduction) reactions and are defined as positive numbers.

If $E = E_{CORR}$, this equation predicts that I will be zero, as it should be. Just because the net current is zero at E_{CORR} does not mean that the system cannot actively corrode. It merely means that the anodic current must exactly balance the cathodic current at E_{CORR} . $ICORR$ is the size of the current that flows in equal but opposite directions at E_{CORR} .

The Stern-Geary equation also predicts that at potentials greater than E_{CORR} the anodic reaction predominates, while at potentials less than E_{CORR} the cathodic reaction predominates. This can be seen by examining the exponential terms in the equation. The β_a term is positive when $E > E_{CORR}$. Thus the first exponential dominates the expression and the net current is positive. The opposite is true when $E < E_{CORR}$ in that the second exponential dominates and the current becomes negative. ____

Corrosion Rate

For both calculations, once, I_{CORR} is known one can obtain a corrosion rate from it by using the following conversion formula (for the derivation of this conversion formula, see Princeton Applied Research Application Note CORR 1, Basics of Corrosion Measurements):

$$\text{Corrosion rate} = C (EW / d) (I_{CORR} / A) \quad (8)$$

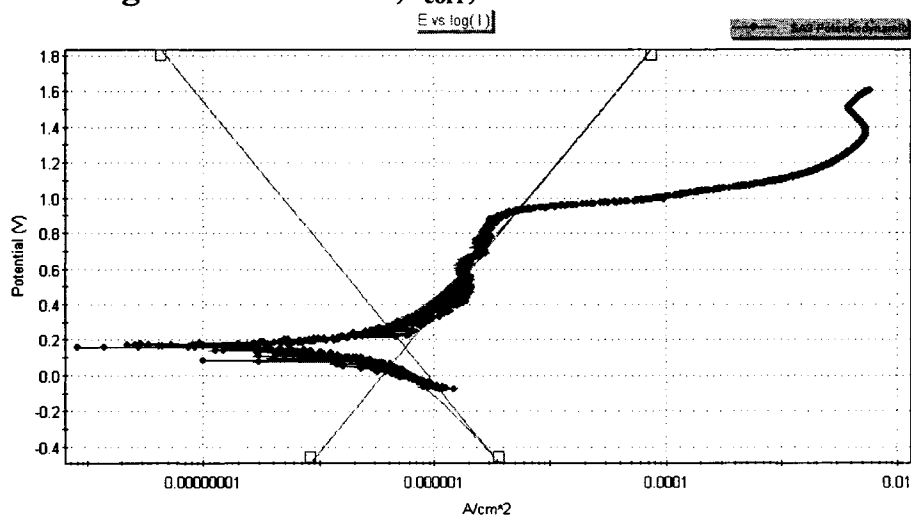
where EW is the equivalent weight of the sample in g, A is the sample area in cm^2 , d is its density in g/ml , and C is a conversion constant that depends on the units being used. C is 1.287×10^5 when I_{CORR} is expressed as a current in amperes and you want the corrosion rate expressed in milli-inches per year (mpy). C is 3.268×10^3 when I_{CORR} is in amperes and you want the corrosion rate expressed in millimeters per year (mmpy). If the data being fitted are normalized with respect to Area (see Experiment/Properties...), the I_{CORR}/A term is just replaced by I_{CORR} . ____

References

- 1 Stern, M. and A.L. Geary. J. Electrochem. Soc., 104 (56), 1957.
- 2 Pourbaix, M. Lectures on Electrochemical Corrosion, Plenum Press, New York, 1973.
- 3 Press, W.H., B.P. Flannery, S.A. Teukolsky, and W.T. Vetterling. Numerical Recipes in C, Cambridge University Press, Cambridge, MA, 1988. See Section 14.4.

Appendix D:

Tafel fit for Potentiodynamic Scans of the SA, SB and SC Series Including Corrosion Rate, i_{corr} , and E_{corr} Results



Run Fits

Tafel Fit Minimizing X Error

E(=0) (mV): 155.365
 i_{corr} (μA): 5.862e-001
 Ca. Beta (mV): 795.075
 An. Beta (mV): 786.491
 Co. Rate (mpy): 5.986e-001
 Chi-Square: 129.16
 Fit Range (mV): (-75), (780)
 Fit Mode: Auto

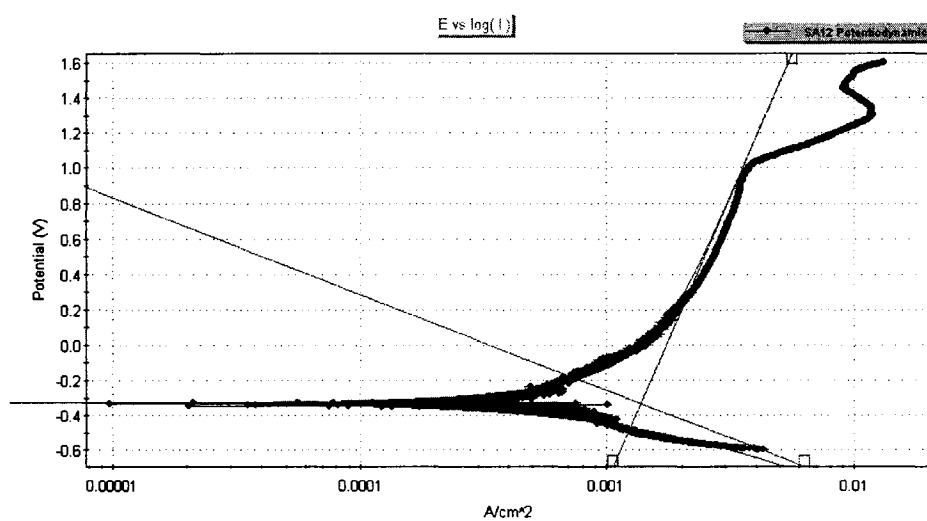
◀ Previous Next ▶

Add Selected Points

Remove Selected Points

Remove Fit

Model 273A at address 14



Run Fits

Tafel Fit Minimizing X Error

E(=0) (mV): -334.534
 i_{corr} (μA): 1.378e+003
 Ca. Beta (mV): 543.691
 An. Beta (mV): 3254.410
 Co. Rate (mpy): 1.457e+003
 Chi-Square: 136.38
 Fit Range (mV): (-599), (298)
 Fit Mode: Auto

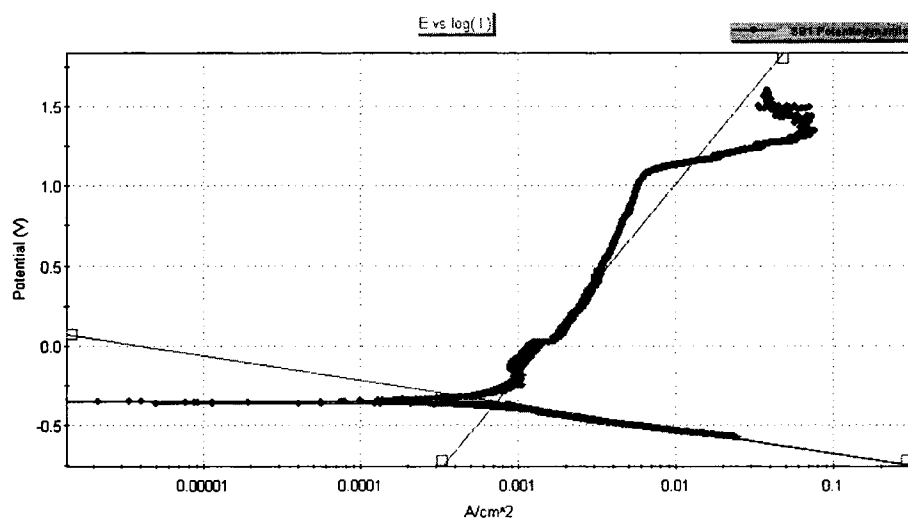
◀ Previous Next ▶

Add Selected Points

Remove Selected Points

Remove Fit

Model 273A at address 14



Run Fits

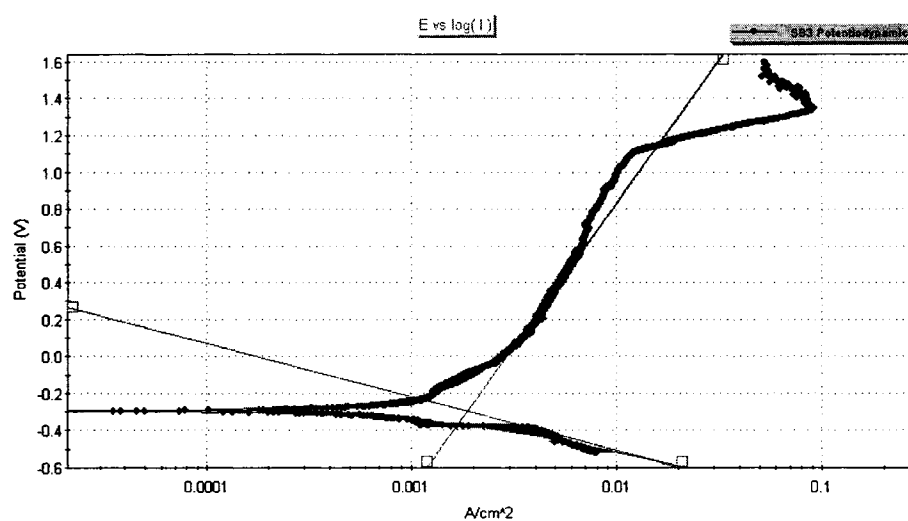
Tafel Fit Minimizing X Error

E(=0) (mV): -353.398
 Icorr (μA): 7.331e+002
 Ca. Beta(mV): 152.865
 An. Beta (mV): 1197.289
 Co. Rate(mpy): 7.751e+002
 Chi-Square: 73.09
 Fit Range(mV): (-574), (482)
 Fit Mode: Auto

Model 273A at address 14

Model 273A at address 14

Model 273A at address 14



Run Fits

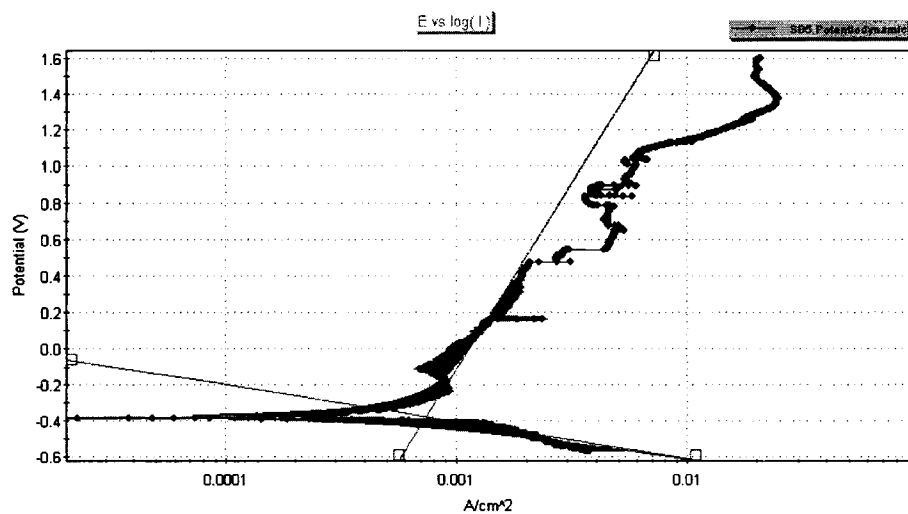
Tafel Fit Minimizing X Error

E(=0) (mV): -299.000
 Icorr (μA): 1.881e+003
 Ca. Beta(mV): 286.704
 An. Beta (mV): 1552.283
 Co. Rate(mpy): 1.989e+003
 Chi-Square: 45.05
 Fit Range(mV): (-519), (591)
 Fit Mode: Auto

Model 273A at address 14

Model 273A at address 14

Model 273A at address 14



Run Fits

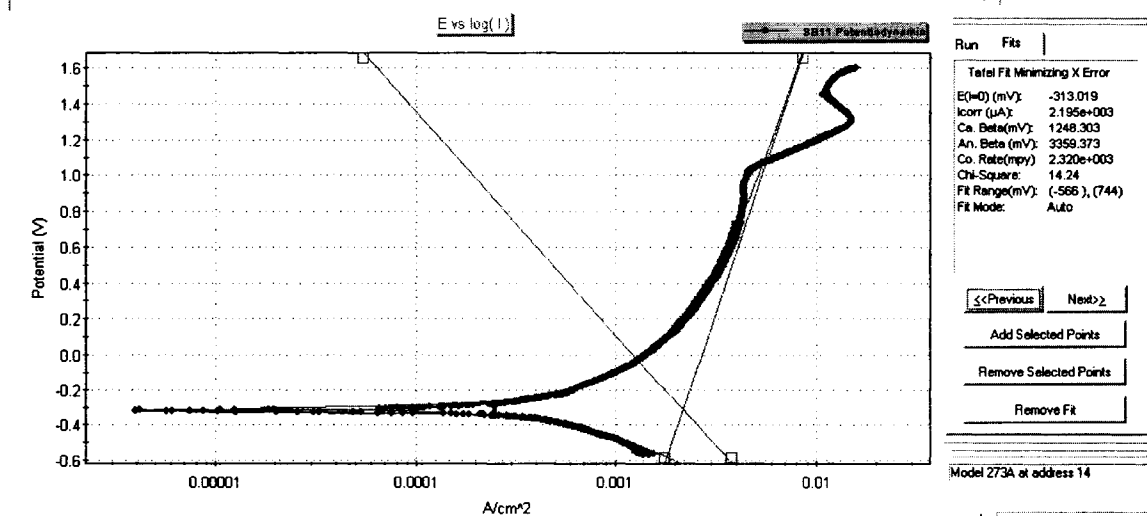
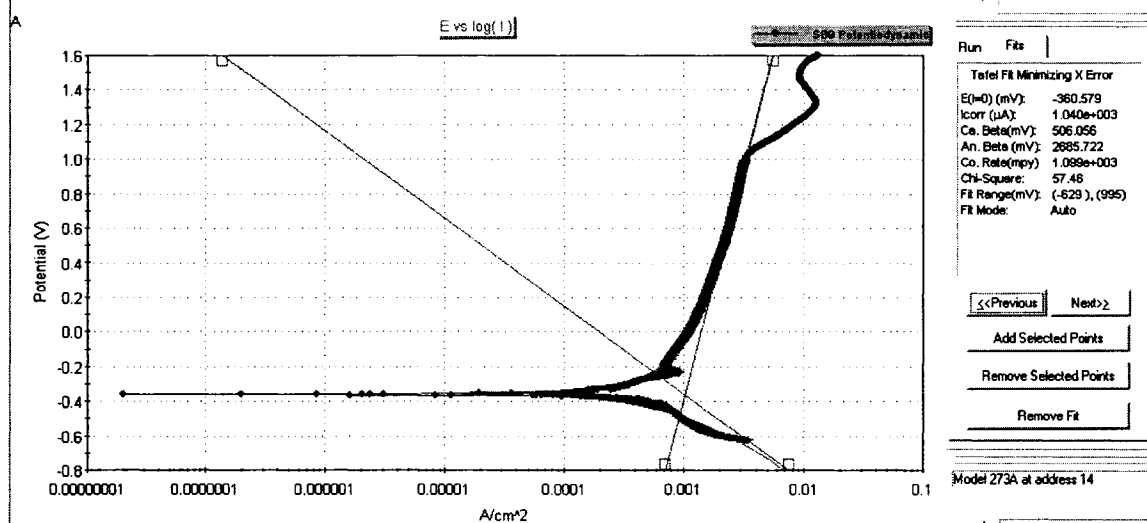
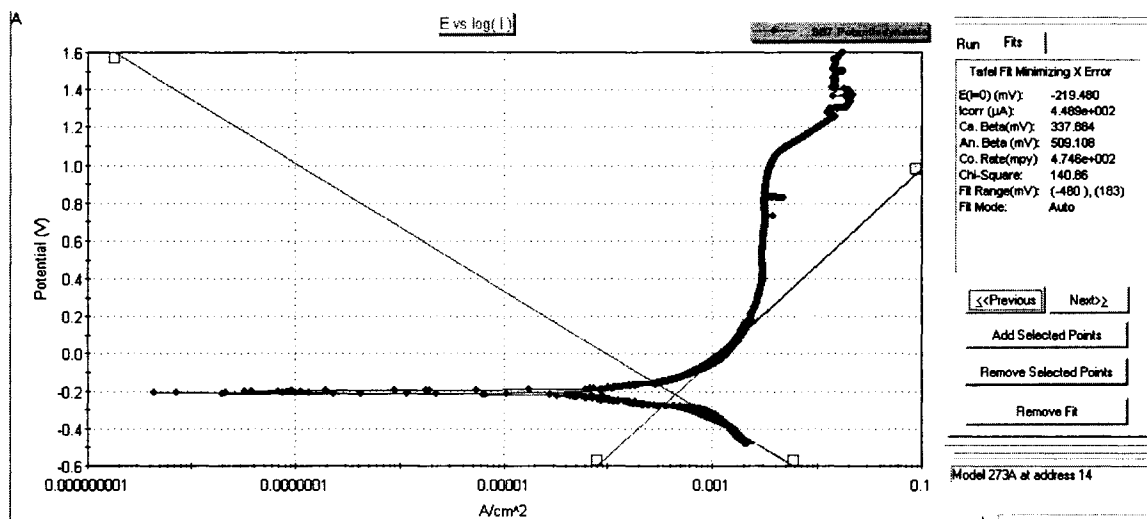
Tafel Fit Minimizing X Error

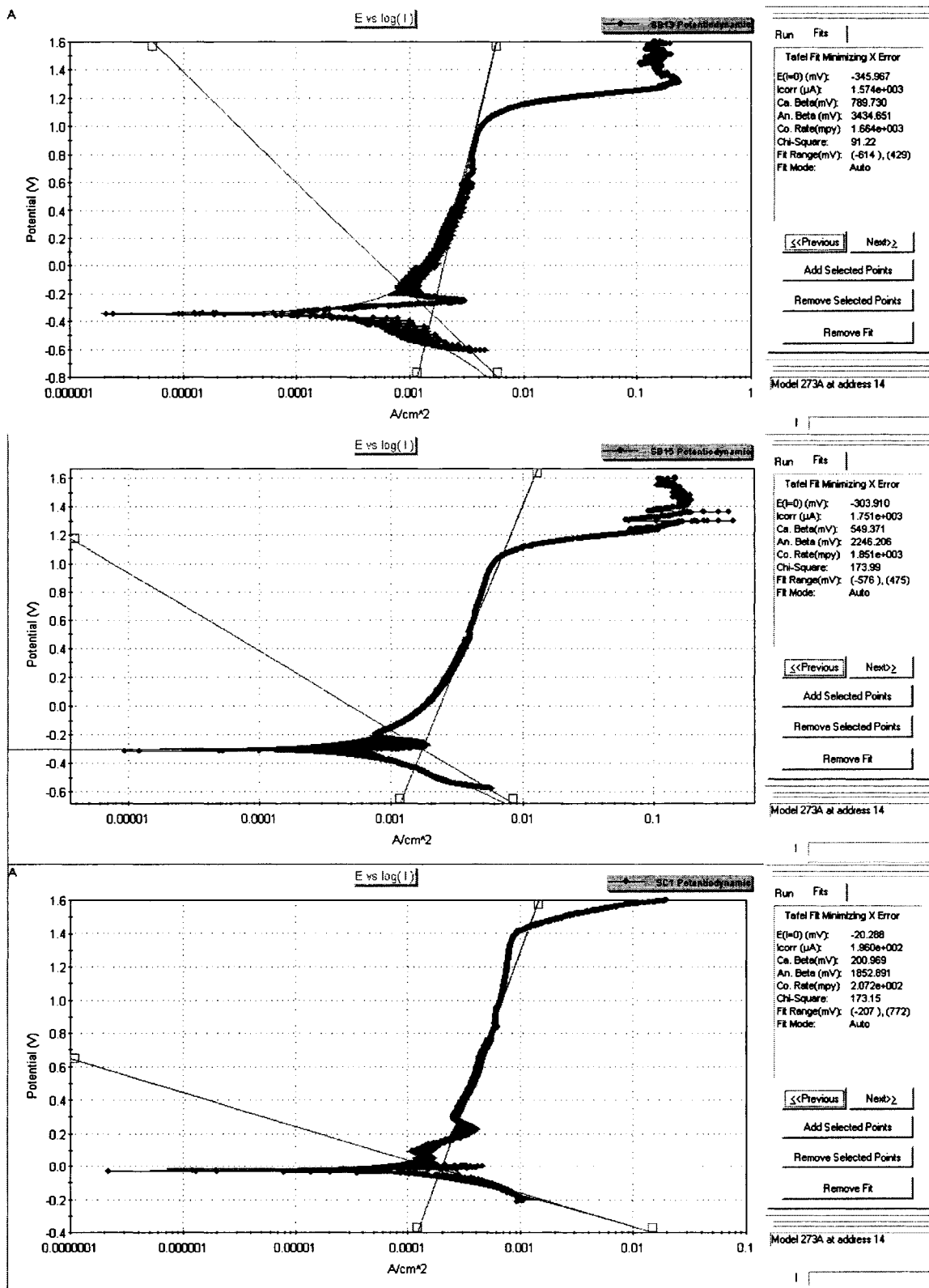
E(=0) (mV): -383.940
 Icorr (μA): 7.445e+002
 Ca. Beta(mV): 205.533
 An. Beta (mV): 2051.982
 Co. Rate(mpy): 7.871e+002
 Chi-Square: 155.32
 Fit Range(mV): (-570), (375)
 Fit Mode: Auto

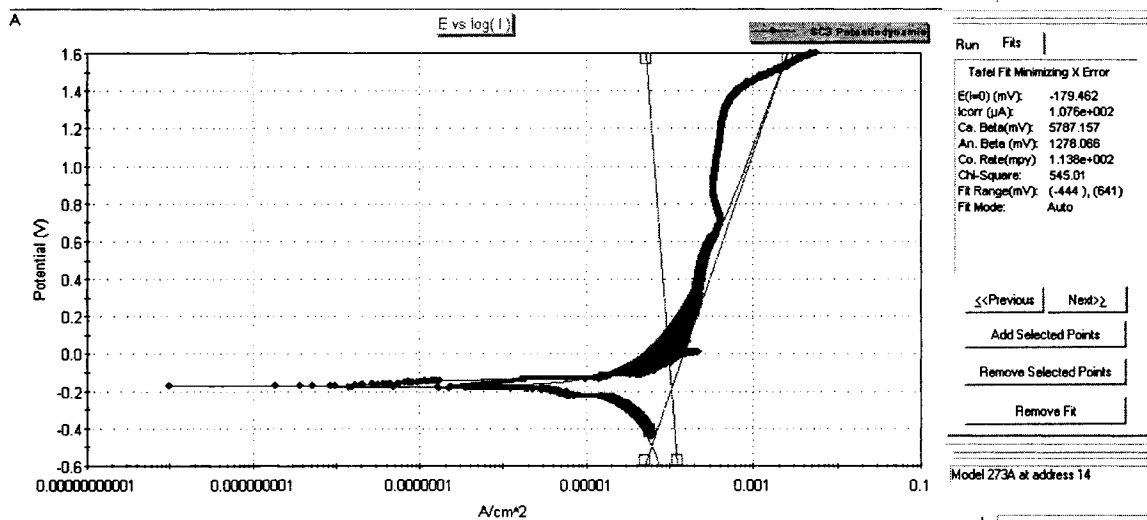
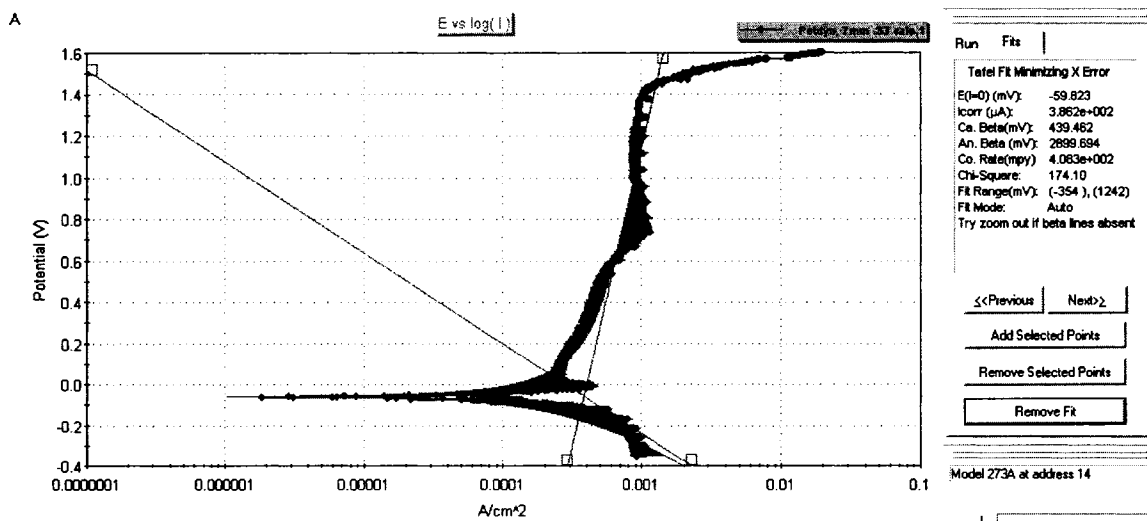
Model 273A at address 14

Model 273A at address 14

Model 273A at address 14







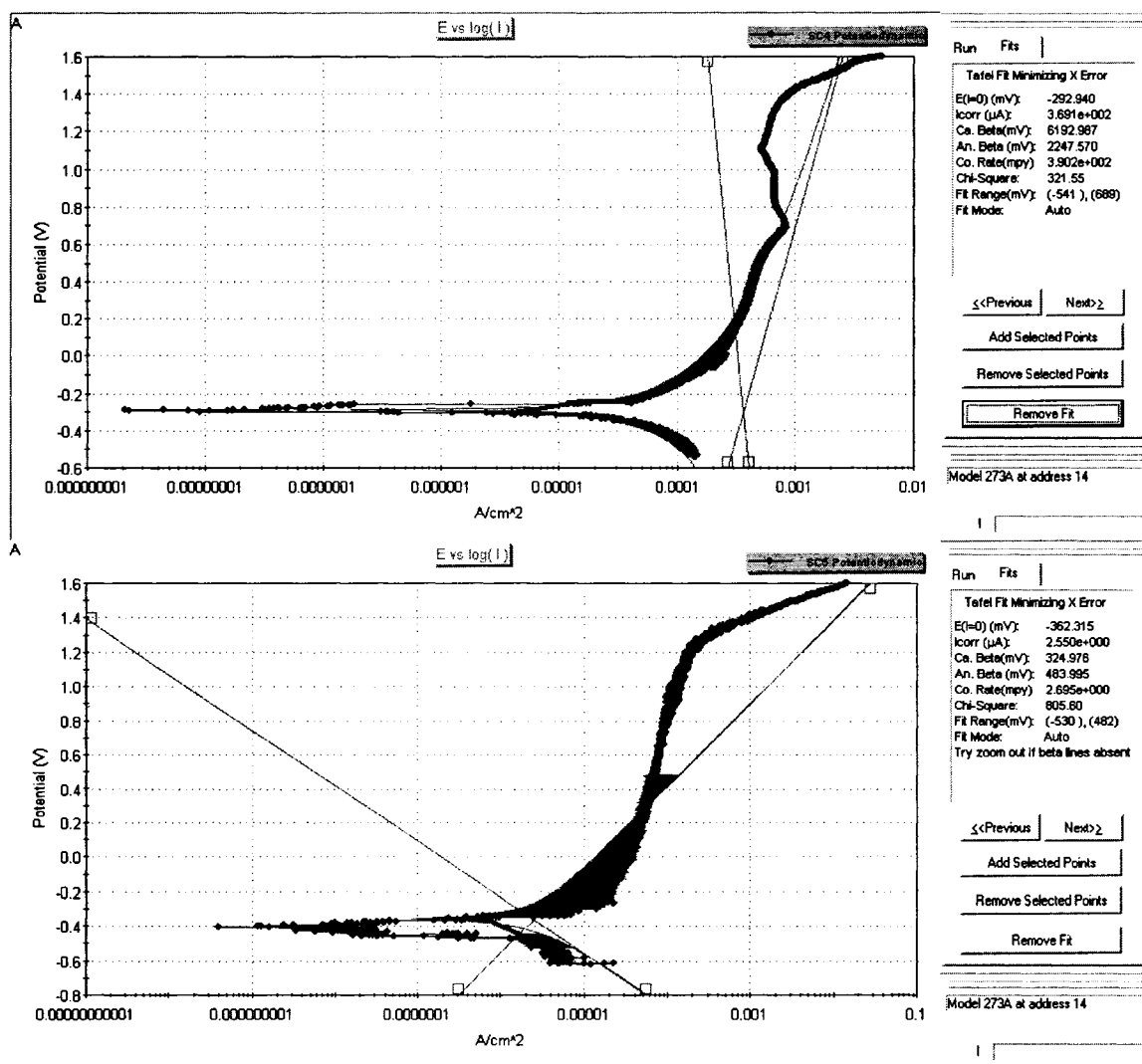


Figure 109: Potentiodynamic scans and Tafel plot with corrosion rates for all SA, SB, SC tests



